134e
S-68-6

CONTRACT REPORT S-68-6

FINITE ELEMENT ANALYSES OF SLOPES IN SOIL

by

P. Dunlop

J. M. Duncan

H. B. Seed

May 1968

Sponsored by

Office, Chief of Engineers

U. S. Army

Conducted for

U. S. Army Engineer Waterways Experiment Station

CORPS OF ENGINEERS

Vicksburg, Mississippi

under

Contract No. DA-22-079-civeng-62-47

by

College of Engineering

Office of Research Services

University of California

Berkeley, California

THIS DOCUMENT HAS BEEN APPROVED FOR PUBLIC RELEASE AND SALE; ITS DISTRIBUTION IS UNLIMITED

Property of the United States Government

RESEARCH CENTER LIBRARY
US ARMY ENGINEER WATERWAYS EXPERIMENT STATION
VICKSBURG, MISSISSIPPI

Contract Report S-68-6

FINITE ELEMENT ANALYSES OF SLOPES IN SOIL

A Report of an Investigation by

Peter Dunlop, J. M. Duncan and H. Bolton Seed

Sponsored by
OFFICE, CHIEF OF ENGINEERS
U. S. ARMY
Conducted for
U. S. ARMY ENGINEER WATERWAYS EXPERIMENT STATION
CORPS OF ENGINEERS
Vicksburg, Mississippi
under
Contract No. DA-22-079-CIVENG-62-47

College of Engineering
Office of Research Services
University of California
Berkeley, California

Report No. TE 68-3

May 1968

THIS DOCUMENT HAS BEEN APPROVED FOR PUBLIC RELEASE
AND SALE; ITS DISTRIBUTION IS UNLIMITED

TA7
W34c
No. S-68-6

SUMMARY

The study described in this report was conducted to investigate the behavior of excavated slopes and embankments using the finite element method of analysis. The aspects of slope behavior considered include stresses, strains, displacements, pore pressures, and progressive development of failure zones. Analyses have been performed using non-linear stress-strain characteristics as well as linear elastic stress-strain behavior.

A method has been developed for simulating analytically the excavation of a slope in a clay layer with arbitrary initial stress conditions. Analyses performed using this procedure have shown that the behavior of an excavated slope depends on the initial horizontal stresses in the soil layer and the variation of strength with depth. Analyses performed using initial stresses and strength profiles representative of normally consolidated clays indicate behavior which is compatible with the results of short-term ($\phi = 0$) stability analyses; the failure zones determined strongly suggest development of a curved surface of sliding, and the factors of safety calculated by the $\phi = 0$ method were close to unity at the final stage of the analysis when the failure zone encompassed a large zone between the crest and the toe of the slope. Similar analyses performed using initial stresses and strength profiles representative of overconsolidated clays indicated quite different behavior; failure zones developed which intersected the bottom of the excavations and the lower portions of the slopes while the factors of safety were still about 2. These failure zones did not resemble the usual curved failure surfaces used in equilibrium analyses of slope stability, but instead suggest the development of the condition of "loss of ground" wherein the soil in the bottom of the excavation bulges up slowly as additional soil is excavated.

Detailed consideration was given to the stress-strain characteristics of soft, saturated clays under undrained loading conditions. Using the results of horizontal and vertical plane strain tests on San Francisco Bay Mud, an empirical stress-strain relationship was developed for this material. The relationship developed was nonlinear, anisotropic, and

62151

dependent on the consolidation pressure. In spite of its complexity, the relationship can be represented in a reasonably simple form and could be conveniently employed in finite element analyses. Using this relationship, analyses were performed to predict the behavior of San Francisco Bay Mud under simple shear loading conditions, and the predicted behavior was found to agree quite well with experimental results.

Analyses were performed to calculate pore pressures around excavated slopes and in embankment foundations using a variety of possible assumptions regarding the stress-strain behavior and the pore pressure coefficients of clay soils. The most significant factor affecting the calculated distributions were found to be anisotropy with respect to both stress-strain behavior and development of pore-water pressures.

Using the finite element method it is possible to include realistic soil properties in analyses of slope performance. Nonlinear, anisotropic stress-strain relationships and anisotropic pore pressure coefficients may be incorporated in analyses in a logical and straight-forward manner, providing a means of making more accurate evaluations of stress distribution and pore pressure distributions in soil masses.

FOREWORD

The work described in this report was performed under Contract No. DA-22-079-CIVENG-62-47, "Shear Properties of Undisturbed Weak Clays," between the U. S. Army Engineer Waterways Experiment Station (WES) and the University of California. The contract was sponsored by the Office, Chief of Engineers, under Engineering Studies Item ES 525, "Shear Properties of Undisturbed Weak Clays."

The general objective of this research, which was begun in February, 1962, is to investigate the influence of pore-water pressure on the strength characteristics of undisturbed weak clays. Work on this project is conducted under the supervision of H. Bolton Seed, Professor of Civil Engineering, J. M. Duncan, Assistant Professor of Civil Engineering, and C. K. Chan, Associate Research Engineer. The project is administered by the Office of Research Services of the College of Engineering.

The phase of the investigation described in this report was performed by P. Dunlop, who is now an Assistant Research Engineer, and the report was prepared by P. Dunlop, J. M. Duncan and H. Bolton Seed. This is the sixth report on investigations performed under this contract. The previous reports are "The Effects of Sampling and Disturbance on the Strength of Soft Clays," Report No. TE 64-1, February, 1964; "The Effect of Anisotropy and Reorientation of Principal Stresses on the Shear Strength of Saturated Clay," Report No. TE 65-3 (Contact Report No. 3-132) November, 1965; "Errors in Strength Tests and Recommended Corrections," Report No. TE 64-4, (Contract Report No. 3-133) November, 1965; "The Effects of Temperature Changes During Undrained Tests," Report No. TE 65-10 (Contract Report No. 3-134) November, 1965; and "The Significance of Cap and Base Restraint in Strength Tests on Soils," Report No. TE 66-5 (Contract Report No. 3-159) August, 1966.

The contract was monitored by Mr. W. E. Strohm, Jr., Chief, Engineering Studies Section, and Mr. B. N. McIver, Chief, Laboratory Research Section, Embankment and Foundation Branch, under the general supervision of Mr. W. J. Turnbull, Chief, Soils Division, WES. Contract officers were COL A. G. Sutton, Jr., CE; COL J. R. Oswalt, Jr., CE; and COL L. A. Brown, CE.

TABLE OF CONTENTS

LIST OF FIGURES

LIST OF TABLES

LIST OF SYMBOLS

ENGLISH LETTERS

$\bar{A}$	pore pressure parameter
A	area
a	as a subscript indicates axial
B	pore pressure parameter, or
B	as a subscript indicates below the toe of the slope
b	as a subscript indicates buoyant
C	as a subscript indicates consolidation, or
C	a soil index of volume change
c	shear strength
c'	shear stress intercept of the effective stress failure envelope
E	elastic modulus
f	as a subscript indicates failure
G	shear modulus; or
G	specific gravity
H	as a subscript indicates horizontal, or
H	total slope height or total layer depth
HPS	horizontal plane strain test
h	depth below the soil surface
i	as a subscript indicates an instantaneous or tangent value
k	coefficient of total earth pressure at rest
k_o	coefficient of earth pressure at rest
[K]	total structure stiffness matrix
L	designates a test performed with lubricated cap and base; or
L	length, or
L	as a subscript indicates below slope toe
LL	liquid limit
l	distance along the failure surface from the toe, or
l	as a subscript means lateral
m	as a subscript indicates membrane
n	as a subscript indicates normal to the membrane
o	as a subscript indicates original or initial value

P load

PL plastic limit

p as a subscript indicates perimetral; or

p major principal consolidation pressure

{p} applied load vector

St sensitivity

SS simple shear test

s as a subscript indicates specimen; or

s as a subscript indicates swelling

S_u undrained shear strength

T as a subscript indicates above slope crest

t thickness; or

t time

{u} displacement vector

u pore pressure

VPS vertical plane strain test

V as a subscript indicates vertical

W length

w water content, or

w as a subscript indicates water

x as a subscript indicates x-ordinate direction (horizontal)

xy as a subscript indicate shear directions

y as a subscript indicates y-ordinate direction (vertical)

z depth below the horizontal soil surface; or

z as a subscript indicates z-ordinate or vertical direction

GREEK LETTERS

β	angle between the major principal stress and the horizontal
β_i	angle between the major principal change in stress and the horizontal
β_i	as a subscript indicates a value in the β_i direction
γ	total unit weight; or
γ	shear strain
Δ	as a prescript indicates a change in the quantity appended
ε	strain
μ	viscosity
ν	poisson's ratio
σ	normal stress
τ	shear stress
ϕ'	angle of inclination of the effective stress failure surface

CHAPTER 1

INTRODUCTION

Equilibrium methods of slope stability analysis have been widely used and have been found to be satisfactory in many respects for slope analysis and design. These methods are sufficiently simple to be employed routinely for practical problems, and are capable of accurately predicting the likelihood of catastrophic failure of many types of slopes. Satisfactory slope design, however, should preclude excessive deformation as well as catastrophic failure. It would therefore be desirable to develop methods for predicting slope deformations under design conditions, as well as the degree of safety against sliding. In order to determine in what portions of slopes failure may occur first, and how it would progress, it would also be desirable to be able to predict stresses and strains within slopes.

In order to predict stresses, strains, and displacements within slopes, it is necessary to employ analytical procedures other than the equilibrium methods. Several such procedures have already been applied to slope analyses, including mathematical analyses, photoelastic analyses, and finite difference numerical techniques. Because of the limitations of these methods, and the difficulties associated with their application to practical problems, not many such analyses have been performed. The availability of high-speed digital computers, however, coupled with the development of the finite element method of analysis, has made it feasible to analyze problems involving much greater degrees of complexity than was formerly possible, while at the same time reducing the effort required. Thus it is now feasible to analyze slope problems involving complex boundary conditions, heterogeneous material distribution, and nonlinear material properties.

The investigation described in this report was conducted to examine the usefulness of finite element techniques for slope analyses. In the following pages the factors affecting the behavior of excavated and embankment slopes are discussed, and the finite element method of analysis is described briefly.

Factors Influencing Slope Behavior

A comprehensive list of the factors affecting the behavior of embankments and excavated slopes would include slope height, slope angle, unit weights, pore pressures, initial stress conditions (prior to construction), stress-strain and strength characteristics of the soils, creep characteristics of the soils, drainage conditions, time, and perhaps more. While it may some day be feasible to include a wide variety of factors within an integrated approach to slope design, the class of problems analyzed in this investigation is restricted to short-term (undrained) analyses of slopes in clay. The effects of time on both creep movements and drainage are neglected. The stress-strain relationships used are either linear or non-linear time-independent relationships expressed in terms of total stresses. The factors considered in these analyses are described in the following pages.

Initial Stresses

In a soil deposit with a horizontal surface, the principal stress directions will be horizontal and vertical. At a depth Z below the surface of a soil deposit with a unit weight γ, the effective stresses may be expressed as

$$\sigma'_y = \gamma Z - u \qquad (1a)$$

$$\sigma'_x = K_o \sigma'_y \qquad (1b)$$

in which σ'_y and σ'_x are the effective vertical and horizontal stresses, u is the pore-water pressure, and K_o is the coefficient of earth pressure at rest.

Brooker and Ireland (1965) have measured values of K_o for five different soils of varying degrees of plasticity under a wide variety of stress conditions. They found that for normally consolidated soils, values of K_o may range from about 0.4 to 0.6, the higher values of K_o being associated with more highly plastic clays. The value of K_o of all the soils tested was found to increase during unloading to values greater than one. For unloading corresponding to an overconsolidation ratio of 32, the values of K_o range from about 1.8 for highly plastic Bearpaw shale to about 3 for clay of low plasticity.

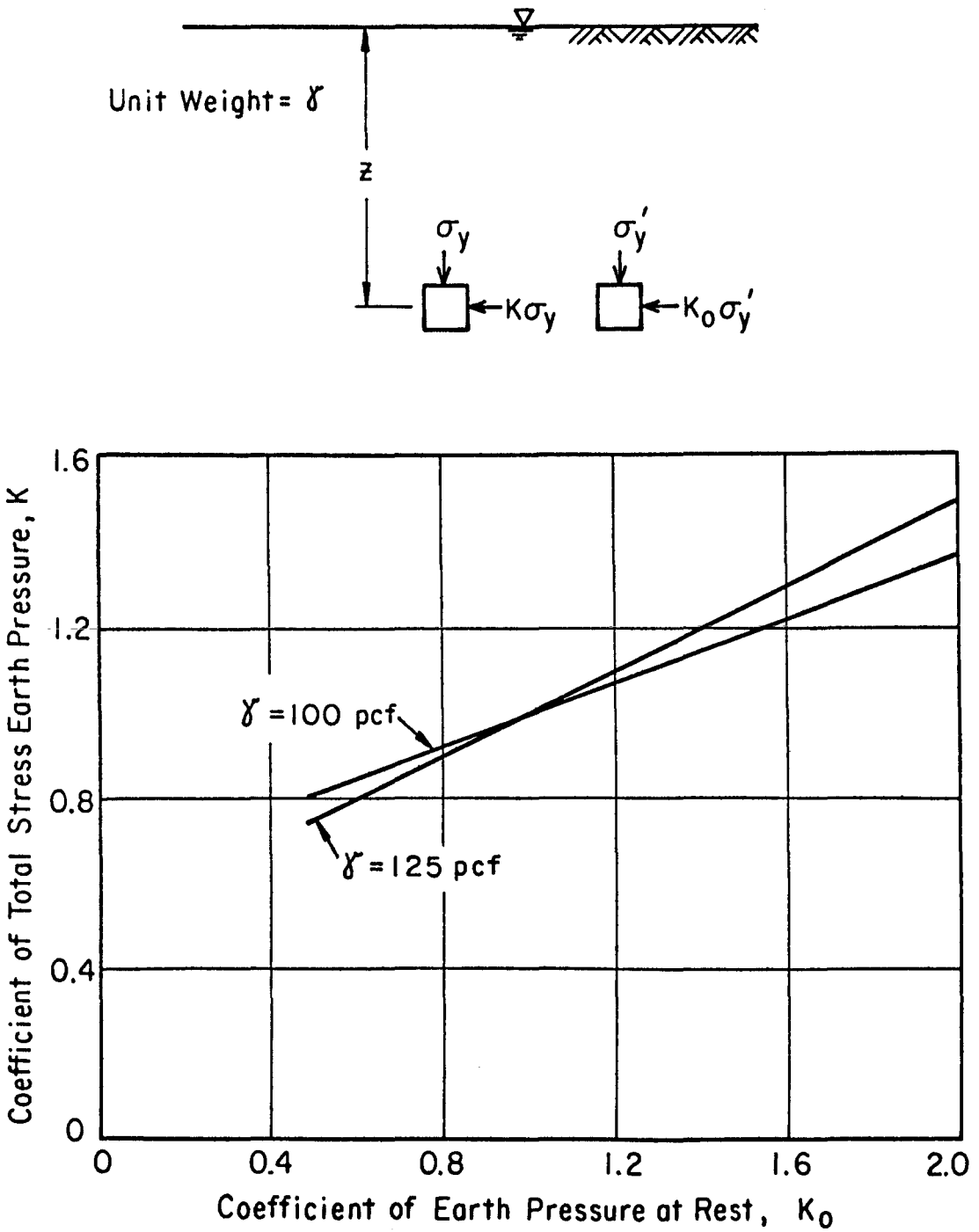

FIG. 1 RELATIONSHIP BETWEEN EFFECTIVE STRESS AND TOTAL STRESS COEFFICIENTS OF EARTH PRESSURE AT REST.

These results indicate that a wide range of in-situ stress conditions may be possible for soils, even where the ground surface is horizontal; the value of the effective horizontal stress may range from about 40% of the effective overburden pressure to about 300%, depending on the soil type and its stress history.

It may also be noted that the ratio of horizontal to vertical effective stress would not necessarily be the same at all depths throughout a soil deposit: In overconsolidated soils, the overconsolidation ratio decreases with depth, since the amount of unloading is the same for all depths, but the effective stress after unloading increases with depth. Therefore, since the overconsolidation ratio would be expected to increase toward the surface, the coefficient of earth pressure at rest would logically increase toward the surface. Even in normally consolidated clay deposits which have a desiccated upper crust, the earth pressure coefficient for the crust may be different from that of the softer clay beneath; and in layered soil deposits, the earth pressure coefficient may vary from layer to layer.

For a slope excavated in the dry, both the earth and water pressures would be reduced to zero on the excavated surface. For analysis of such slopes, it is necessary to consider both the changes in earth and water pressures during construction. This may be done conveniently by expressing the total horizontal stress, σ_x, in terms of the total vertical stress, σ_y, as

$$\sigma_x = K\sigma_y \tag{2}$$

in which K is a total stress earth pressure coefficient. If the unit weight of the soil deposit is the same at any depth and the water table is at the ground surface, both the overburden pressure and water pressure will increase linearly with depth beneath the surface. Under these conditions, the total stress earth pressure coefficient, K, may be expressed in terms of K_o, as

$$K = K_o + (1-K_o)\frac{\gamma_w}{\gamma} \tag{3}$$

in which γ and γ_w are the unit weights of soil and water. This relationship is illustrated in Fig. 1 for two values of soil unit weight. It may

62151

be noted that K is always closer to unity than K_o; thus while K_o may range from 0.4 to 3.0, K would range from about 0.7 to about 2.0.

Simulation of Excavation

The initial stress conditions would be expected to have a considerable influence on the magnitudes of the changes in stress during construction and the stresses after construction. The initial stresses along a surface to be exposed by excavation are shown in Fig. 2. During excavation the stresses on this surface will be reduced to zero, which is equivalent to subjecting the slope to an equal but opposite stress change along the surface shown. Thus the larger the initial stresses, the greater will be the changes in stress during construction. Also, since the stresses following construction are the sum of the initial stresses and the changes in stress, it would be expected that the postconstruction stresses would be influenced to a considerable degree by the initial stress conditions.

In the analyses described herein, excavation of slopes was simulated analytically in the manner illustrated in Fig. 2. Changes in stress, equal in magnitude but opposite in sign to the initial stresses, were applied to the slope along the excavated surface. Simultaneously the modulus value of the material excavated was reduced to a very small value, so that the applied loads induced stress changes only in the remaining material. The stresses induced by these loads were calculated and added to the initial stresses to determine the post-construction stresses. The strains and displacements induced by the changes in loading were also calculated.

Stress-Strain Behavior

Because of the complexity of soil behavior, constitutive laws for soil involve many factors and are difficult to determine. Recent attempts along these lines have been made by Ko and Scott (1967) for Ottawa sand, and Chang, et. al. (1967) have shown that these relations may be used in conjunction with finite element techniques. Various other investigators, including Tan (1957), Roscoe and Poorooshasb (1963), and Rowe (1962) have formulated stress-strain relationships for soils.

The most straightforward approach for developing stress-strain relations for soils for use in analyses is to test the soil under conditions closely simulating the anticipated conditions, and to derive empirical stress-strain relations directly from the results of these tests. Considering the

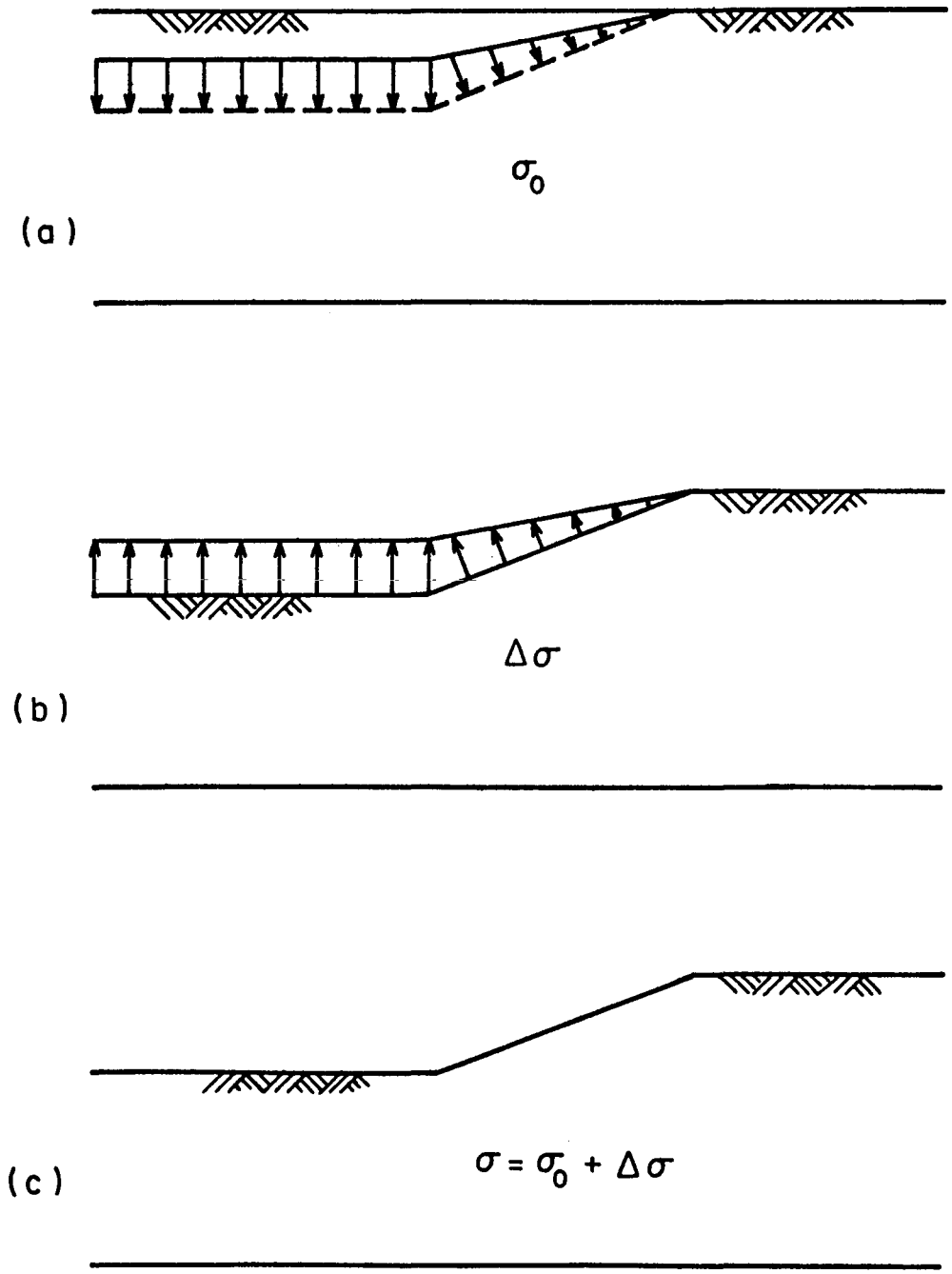

FIG. 2 ANALYTIC SIMULATION OF EXCAVATION

fact that many types of soil mechanics problems including slope behavior, have not been studied thoroughly using even the simplest stress-strain relationships, it seems reasonable to adopt a rational, empirical approach to determination of stress-strain relations for the purpose of preliminary analyses. Consistent with this philosophy, slope analyses have been conducted during the course of this investigation using three successively more complex types of stress-strain behavior: (1) Linearly elastic isotropic behavior, (2) bilinear, isotropic behavior closely approximating elastic-perfectly plastic behavior, and (3) multilinear, anisotropic stress-strain behavior based on laboratory test results for a soft normally consolidated marine clay. The stress-strain relations employed are discussed in detail in conjunction with the various analyses.

Finite Element Method

As mentioned earlier in this chapter, the finite element method, coupled with the use of high-speed digital computers, has made possible the analysis of highly complex stress-deformation problems. The fact that the finite element method may be used for analysis of inhomogeneous structures makes it possible to approximate nonlinear behavior by adjusting modulus values in accord with stress or strain levels. Therefore the method appears to have a wide variety of applications in soil mechanics problems. The basic concepts of the finite element method, and some of its previous applications in soil mechanics are described in the following pages.

The basic concept of the finite element technique is that a continuous structure may be represented as an assemblage of elements interconnected at a finite number of nodal points. The elements may be triangles, groups of triangles, or rectangles for two-dimensional plane strain or plane stress analyses. Within each element displacements are assumed to vary in such a way that compatibility within the element and along its boundaries is maintained. For triangular elements with three nodal points this may be accomplished by specifying displacements which vary linearly in two mutually perpendicular directions within the element. For elements with more nodal points, higher order displacement variations are employed.

The finite element analysis of an elastic continuum consists of 4 basic steps:

(1) The structural idealization of the continuum so that the finite element assemblage simulates the continuum.

(2) The determination of the stiffness characteristics of each element to obtain a total structural stiffness matrix [K].

(3) Analysis of the structure by standard structural methods once the prescribed forces and displacements are obtained. The equilibrium equations expressing the relationship between the applied nodal point forces {P} and the nodal point displacements {u} may be represented as

$$\{P\} = [K] \cdot \{u\} \qquad (4)$$

(4) The determination of the element stresses from the nodal point displacements {u}.

Because each element in the assemblage may have a different modulus value from its neighbors, the method is well-suited to problems involving heterogeneity. Approximate analyses of non-linear structures are possible either by incremental loading procedures or iterative procedures. The finite element method is also capable of handling virtually any boundary conditions specified in terms of forces, stresses (resolved into forces) and displacements; mixed boundary value problems may be handled as easily as problems involving only force or displacement boundary conditions.

The finite element method ensures nodal point force equilibrium and the assumed element displacement patterns ensure continuity of material, but equilibrium of stresses along the element boundaries is not ensured. Wilson (1963) has shown that if the size of elements is reduced to infinitesimal proportions the error introduced by approximating stresses by stress resultants is reduced and the finite element method will converge to the exact solution. Thus accuracy is increased by the use of smaller elements in any problem.

(1) Clough (1965) presented plane, linear elastic analyses of a thick walled cylinder, a plate with an elliptical hole, and a distributed load on a half space. These analyses were in each case compared to the theoretical solutions and indicated very close agreement. Also presented were an elasto-plastic plate analysis of a plate with bilinear stress-strain properties.

(2) Clough and Rashid (1965) analyzed the stress distribution produced by a point load on an elastic half-space and compared the stresses and displacements to those computed by the Boussinesq theory.

(3) Wilson (1965) analyzed the steady-state and transient temperature distribution in plane and axisymmetric bodies.

(4) King (1965) analyzed two-dimensional time dependent stress problems, and illustrated the use of the analysis for a concrete gravity dam.

(5) Zienkiewicz, Mayer and Cheung (1966) analyzed seepage through anisotropic materials.

(6) Idriss, I. M. and Seed, H B., Response of Earth Banks During Earthquakes (1967).

(7) Duncan, Monismith and Wilson (1967) analyzed layered pavement structures using linear and nonlinear material properties. The linear finite element analyses results were compared with theoretical layered system solutions, and the approximate nonlinear analyses were compared to the behavior of actual pavements.

Because of the large number of simultaneous equations resulting from finite element formulations, solutions by the finite element method require large, high-speed digital computers.

In the finite element analyses of slopes conducted during this investigation, plane strain deformation was assumed. If a slope is excavated in a horizontal deposit, as shown in Fig. 3a, and the longitudinal extent of the slope is sufficiently great, the deformation of a section far from the end will closely approximate plane strain. A plane strain analysis may be carried out on a unit width of slope (shown dashed in Fig. 3a). For analyses by means of the computer programs employed in this study, slopes were subdivided into triangles, or quadrilaterals consisting of four constant strain triangles, as shown in Fig. 3b. It may be noted that rectangular elements were used everywhere except along the face of the slope where trapezoids and triangles were used alternately. Whenever possible quadrilateral elements should be employed rather than triangular elements; it has been shown by Wilson (1963) that the stresses obtained

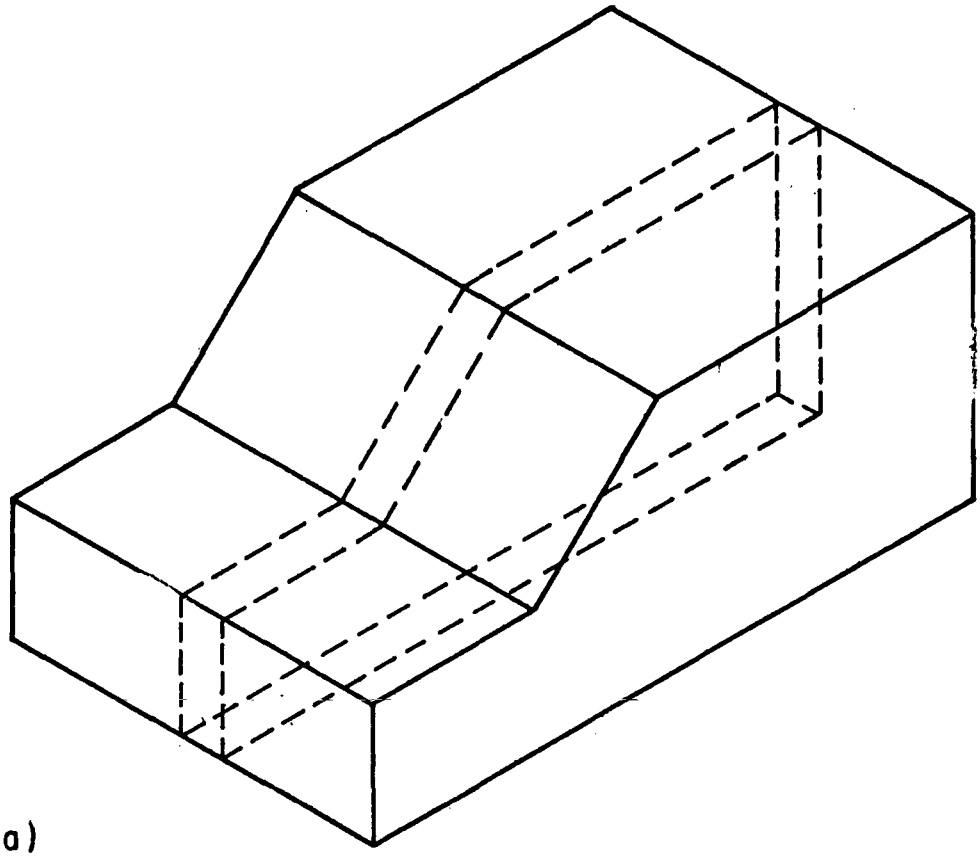

(a)

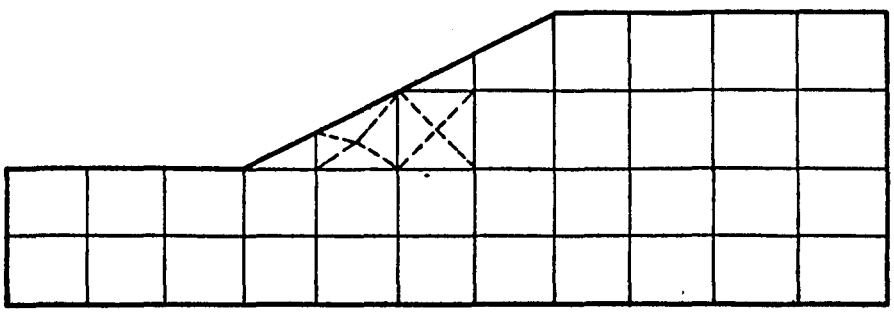

(b)

FIG. 3 (a) CONSTRUCTED SLOPE SHOWING THE SECTION TO BE ANALYZED, (b) FINITE ELEMENT IDEALIZATION OF SLOPE CROSS-SECTION.

for a triangular element do not represent stresses at any one point in the element, and therefore triangular element stresses are less accurate than quadrilateral element stresses, which are rationally associated with the center of the elements.

Excavation or embankment construction may be incorporated in analyses by simulating the addition or removal of elements. Figure 4 shows a typical finite element idealization of a soil deposit and the method of simulating excavation by the removal of elements. At each stage of construction a layer of elements is "removed" by applying stresses to the boundary in the manner previously described in the section on construction sequence. The only difference in respect to the finite element construction simulation and the true behavior of the slope is an approximation that the stresses are replaced in the analysis by equivalent nodal point forces. The stresses acting across the boundary are found by an averaging technique because stresses are calculated within elements and not at the element edges, which form the boundary. An incremental construction sequence may be followed if each succeeding removal of material is based on the stresses resulting from the initial stresses and any previous stress changes due to construction. A convenient check may be made of the errors incurred in this technique: Brown and King (1966) have shown that for a homogeneous isotropic linear elastic material the resulting stresses are independent of the construction sequence; thus analyses involving a single step or a number of steps should give the same results if the material is homogeneous, isotropic and linearly elastic. Comparisons of this type have shown that the stress obtained by single-step and multiple step analyses are nearly identical (a maximum difference of about 6% for triangular elements, less for quadrilaterals). The small differences in stress are believed to arise from errors associated with averaging stresses and computing nodal point forces for simulation of the excavation process. Since the differences in stress calculated using single-step and multiple-step analyses were very small, it is considered that the technique for simulating excavation provides an adequate degree of accuracy.

Two different approaches are possible for the solution of problems involving nonlinear stress-strain behavior. These are incremental (step-by-step) construction or loading and the iterative procedure. The

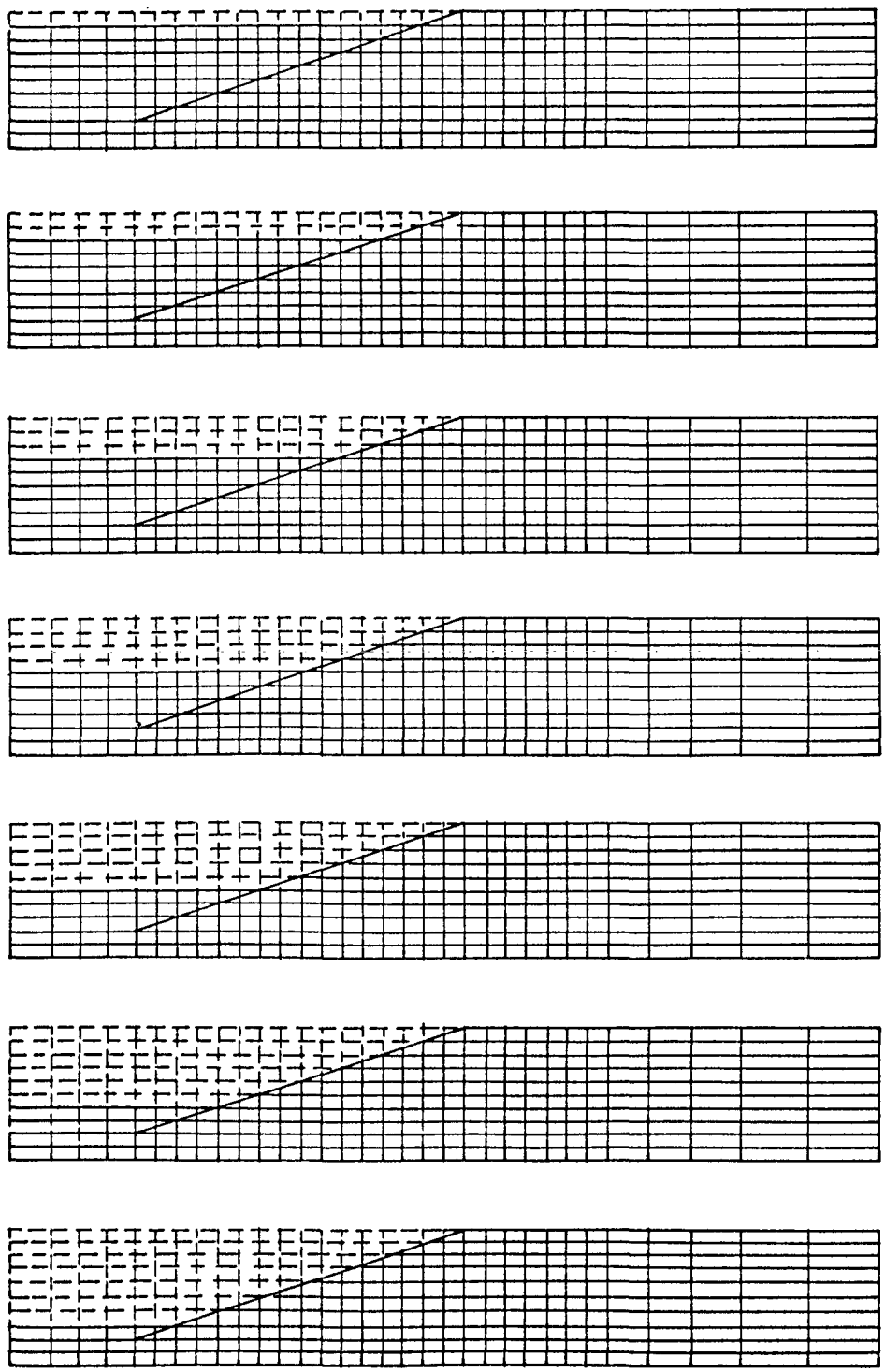

FIG. 4 TYPICAL FINITE ELEMENT CONFIGURATION OF A SLOPE SHOWING THE CONSTRUCTION SEQUENCE.

incremental method is better adapted to slope analysis problems, in which the loads are applied gradually. Simulating the load application by a series of steps makes it possible to modify material properties after each step with little extra effort. It was therefore decided to use the incremental technique in the nonlinear slope analyses conducted for this investigation.

The nonlinearity of material properties may be incorporated by evaluating the material properties of each element prior to each step of the construction procedure. If the construction steps are large, or if the material properties undergo large changes during a single step, an iterative procedure may be used to obtain more accurate material properties for any construction step. Non-linearities resulting from changes in the configuration of the structure may be accounted for by changing the geometry of the finite element idealization to the deformed shape prior to commencing a subsequent construction step. Although Clough and Woodward (1967) note that for low strains (5% to 10%) these nonlinearities are probably not significant, the refinement requires little extra effort, and in most of the analyses conducted in this investigation, the geometry of the structure was changed before each new step in accord with the previously computed displacements.

Summary

The stresses, strains, and displacements of excavated slopes during construction and at the end of construction are influenced by a number of factors, including the initial stress conditions in the soil, the stress-strain characteristics of the soil, and the construction procedure. The finite element method appears to be readily adaptable to take account of these factors, and thus may provide a means for more thorough consideration of slope behavior than was possible previously. Studies conducted to explore the usefulness of the finite element method for slope analyses are described in the remaining chapters of this report.

CHAPTER 2

ANALYSES OF SLOPES USING LINEAR ELASTIC STRESS-STRAIN BEHAVIOR

The results of slope analyses based on the assumption of linear elastic stress-strain characteristics provide information which may be useful for consideration of the behavior of stable slopes. For example, using linear elastic analyses it is possible to study the influence of various initial stress conditions, and the influence of variations in modulus values with depth on the stress distribution within the slope. The stresses calculated in this way may be useful for determining where, within a slope, failure would be expected to occur first, and through correlations with the equilibrium method of stability analysis it is possible to determine the value of the factor of safety corresponding to the beginning of failure.

Elastic stress distribution theory has frequently been used to estimate the magnitude of stresses in embankment foundations, by representing the embankment as a surface loading, but only a few previous analyses have been performed to calculate stresses within slopes. Perhaps the first such analysis was performed by Bishop (1952) using a finite difference technique. This method is restricted to slopes in completely homogeneous material, however, and has not found wide application. Middlebrooks (1936) and LaRochelle (1960) have used photoelastic techniques for analysis of stresses within slopes. Goodman and Brown (1963) obtained a closed-form solution for the stresses in an infinitely high elastic wedge constructed in a series of layers; this solution was the first in which the construction method was simulated in the analysis, and demonstrated the importance of incremental loading.

More recently Brown and King (1966) and Clough and Woodward (1967) have employed the finite element method for analyses of excavated slopes and embankments. On the basis of the experience obtained with this method up to the present time (1968) it seems likely that almost any analysis which may be performed by finite difference methods, photoelastic techniques, or mathematical analyses may also be accomplished using finite element techniques, often with much less effort. Because

of its extremely general formulation, the finite element method appears to provide the best means of performing stress analyses of complex slope problems which is available at the present time.

Stress-Strain Relationships

A number of different factors influence the stress-strain behavior of soils in laboratory tests and the correspondence between laboratory and field behavior. Ladd (1964) has shown that sample disturbance, consolidation pressure, stress ratio during consolidation, stress orientations, thixotropy, and strain rate all influence the stress-strain behavior of clays in laboratory undrained tests. If laboratory tests could be performed which simulated accurately all of the important factors controlling stress-strain behavior under field conditions, it would be expected that laboratory stress-strain relationships would correspond well to the field behavior. Precise duplication of field conditions with regard to loading time and stress orientation is seldom if ever feasible, however, and complete elimination or prevention of disturbance is nearly impossible. Therefore determination of stress-strain relationships applicable for field loading conditions requires considerable care and judgment.

Furthermore, if nonlinear stress-strain behavior is to be represented by linear behavior for purposes of analysis, consideration must be given to the anticipated stress level or percentage of strength mobilized. Typical stress-strain curves for a series of three isotropically consolidated-undrained triaxial tests performed on San Francisco Bay Mud, a soft, normally consolidated highly plastic marine clay, are shown in Fig. 5a. Depending on the stress level involved, various modulus values might be selected to represent any one of these stress strain curves. For example, if the percentage of strength mobilized in the problem analyzed was very low, it might be appropriate to use an initial tangent modulus value; for the upper curve in Fig. 5a, the initial tangent modulus, E_i is approximately 320 kg/cm^2. If the average percentage of strength mobilized was 50%, corresponding to a factor of safety of 2, it would be appropriate to use a 50% secant modulus; for the upper curve in Fig. 5a, the 50% secant modulus, E_{50}, is approximately 180 kg/cm^2. For

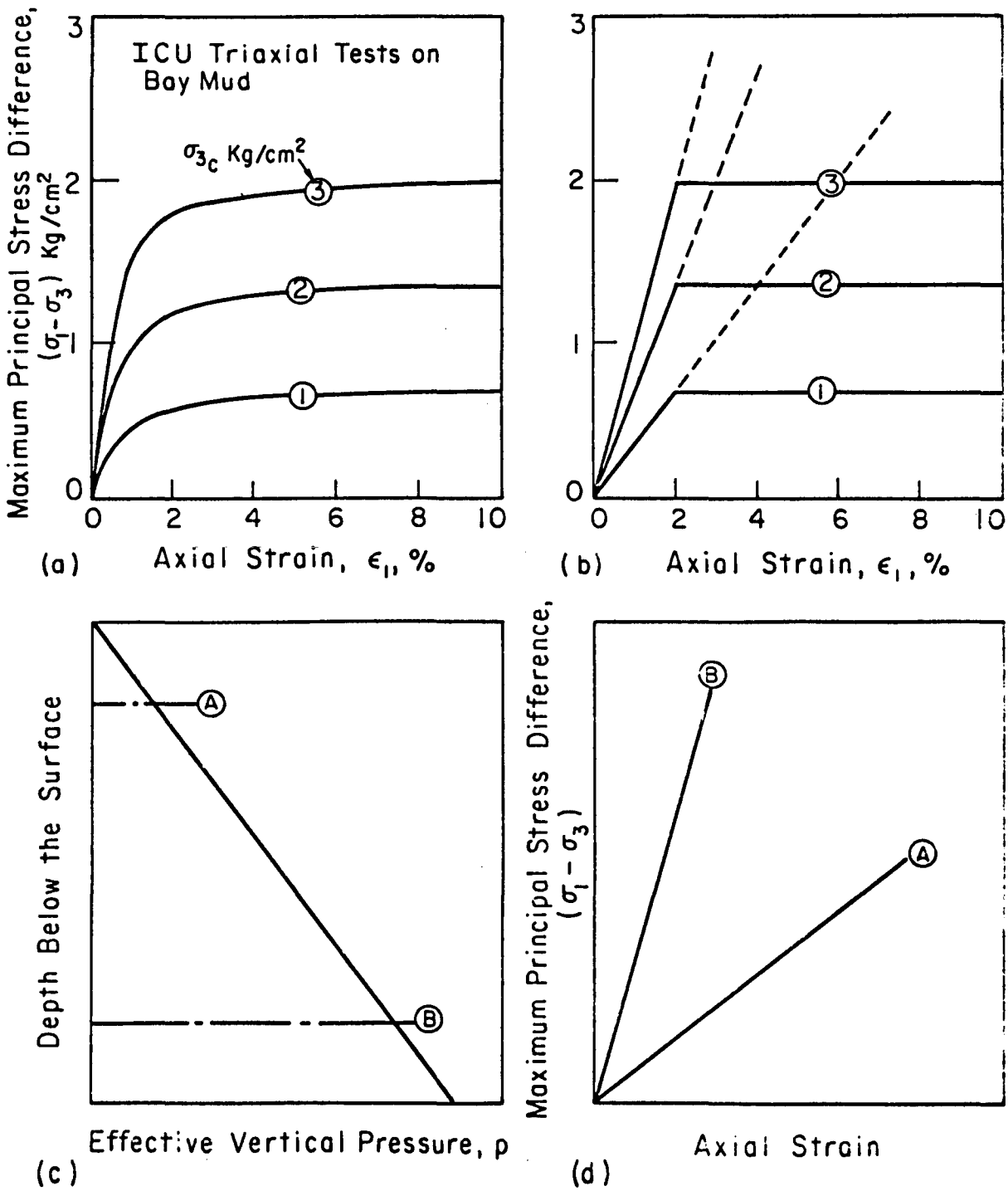

FIG. 5 UNDRAINED STRESS-STRAIN BEHAVIOR OF A NORMALLY CONSOLIDATED CLAY.

higher stress levels and smaller factors of safety, smaller values of modulus would be more appropriate. For conditions where the factor of safety is 1.18, an 85% secant modulus would be appropriate, since a factor of safety of 1.18 corresponds to mobilization of 85% of the ultimate strength. For the upper curve in Fig. 5a, the value of the 85% secant modulus, E_{85}, is approximately 100 kg/cm^2. Thus, as the factor of safety decreases from high values (10 or more) to a low value (1.18), the appropriate modulus value to represent the upper curve in Fig. 5a decreases from 320 kg/cm^2 to 100 kg/cm^2.

For purposes of analyses in which the percentage of strength mobilized is large, the stress-strain curves shown in Fig. 5a could be represented by the bilinear approximations shown in Fig. 5b. The slopes of the initial portions of these curves correspond to 85% secant modulus values. It is interesting to note that both the modulus values and the undrained strengths determined in these undrained tests are proportional to consolidation pressure. The ratio S_u/p, in which S_u is the undrained strength and p is the consolidation pressure, is equal to 0.33 for each of the three tests, and the ratio E_o/p, where E_o is the initial tangent modulus is equal to 107. Similarly, the 50% and 85% secant modulus values are proportional to consolidation pressure, the values being $E_{50}/p = 60$, and $E_{85}/p = 33$. Modulus values may also be related to undrained strength, by means of a ratio E/S_u. For the data shown in Fig. 5, $E_o/S_u = 320$, $E_{50}/S_u = 180$, and $E_{85}/S_u = 100$. Bjerrum and Eide (1956) have noted that quite a wide range of values of E_o/S_u are possible for different clays and they found that those for Norwegian marine clays generally range between 50 and 200.

An interesting consequence of the proportionality between consolidation pressure and modulus is the fact that the modulus of normally consolidated clay would be expected to increase with depth. For a normally consolidated clay deposit with constant unit weight and water table at the ground surface, consolidation pressure would increase linearly with depth as shown in Fig. 5c, and therefore the modulus values would also increase linearly with depth. Thus at a shallow level such as A where the consolidation pressure is relatively low, the modulus value would be smaller than at B where the consolidation pressure is

relatively high, and the stress-strain curves appropriate for these depths would be related as shown in Fig. 5d. Thus, for analyses of slopes in normally consolidated clay, it would be appropriate to use modulus values increasing with depth.

It should be noted that while modulus values may be selected to represent a given stress level or factor of safety, strains calculated using linear approximations for nonlinear behavior cannot be expected to represent strains in actual slopes to a high degree of accuracy. The percentage of strength mobilized will inevitably vary from point to point within a slope, and no single interpretation will be appropriate for an entire slope within which various zones are stressed to different portions of the ultimate strength.

With regard to the influence of the values of modulus on the results of linear elastic slope analyses, it may be noted that both strains and displacements vary inversely with the value of modulus used in the analyses, but stresses are completely independent of the modulus values used. Even where the slope contains zones having different modulus values, or where the modulus increases with depth, reducing each modulus value by a factor of one-half would result in displacement values twice as large but the same values of stress. The same relationship would hold for any problem in which loads are applied. (For problems in which displacements were imposed instead of loads, the stresses would be proportional to the modulus values, and strains and displacements would be independent of modulus values.)

Initial Values of Stress and Strain

For analyses of stresses around excavated slopes, and of strains and displacements resulting from excavation, it is important to consider carefully the conditions before excavation. The strains and displacements of interest to an engineer considering the behavior of a soil mass under the action of external loads are those which are induced by the loading. For this reason it is convenient to consider the initial strains and displacements, before application of loads, as being zero. The stresses of interest, however, are the sum of the initial stresses

and changes due to application of loads. Therefore typical initial conditions consist of zero values of strain and displacement, but non-zero values of stress.

The stress-strain relationships employed in stress analyses relate changes in stress with changes in strain, as shown in Fig. 6a. An element of soil acted on by initial stresses σ_a and σ_ℓ is shown in Fig. 6b. Unless these stresses are equal, the stress difference $\sigma_a - \sigma_\ell$ corresponding to zero strain will not be zero, but could be either positive or negative, as illustrated by curves A and C in Fig. 6c. If subjected to changes in stress $\Delta\sigma_a$ and $\Delta\sigma_\ell$, the soil element would undergo strains, which might be either positive or negative. Thus while a linear stress-strain relationship may be represented by a straight line relationship between change in stress and strain or a single modulus value, the final stress values and the load of the stress-strain curve for the element depend on the initial stresses in the element, as shown in Fig. 6c.

Effects of Initial Stresses and Variation of Modulus Values with Depth

For the purpose of investigating the influence of variations in initial stress conditions and variations of modulus values with depth a number of finite element analyses have been performed using linear elastic stress-strain behavior. These analyses were conducted using two values of the total stress earth pressure coefficient, K, which were considered to be representative of a normally consolidated clay (K = 0.75) and an overconsolidated clay (K = 1.25). Two modulus variations were also considered, one in which the modulus value was constant throughout the depth, and one in which the modulus values increased linearly with depth, as shown in Fig. 7. The latter variation was approximated in the analyses using the step-wise variation shown by the dashed lines in Fig. 7.

Using these variations of modulus and values of initial stress, analyses have been made of a 3:1 slope excavated in a clay layer with an initially horizontal surface. The finite element mesh used in these analyses has been described previously; a typical mesh is shown in Fig. 4. Care was exercised to insure that the lateral boundaries used

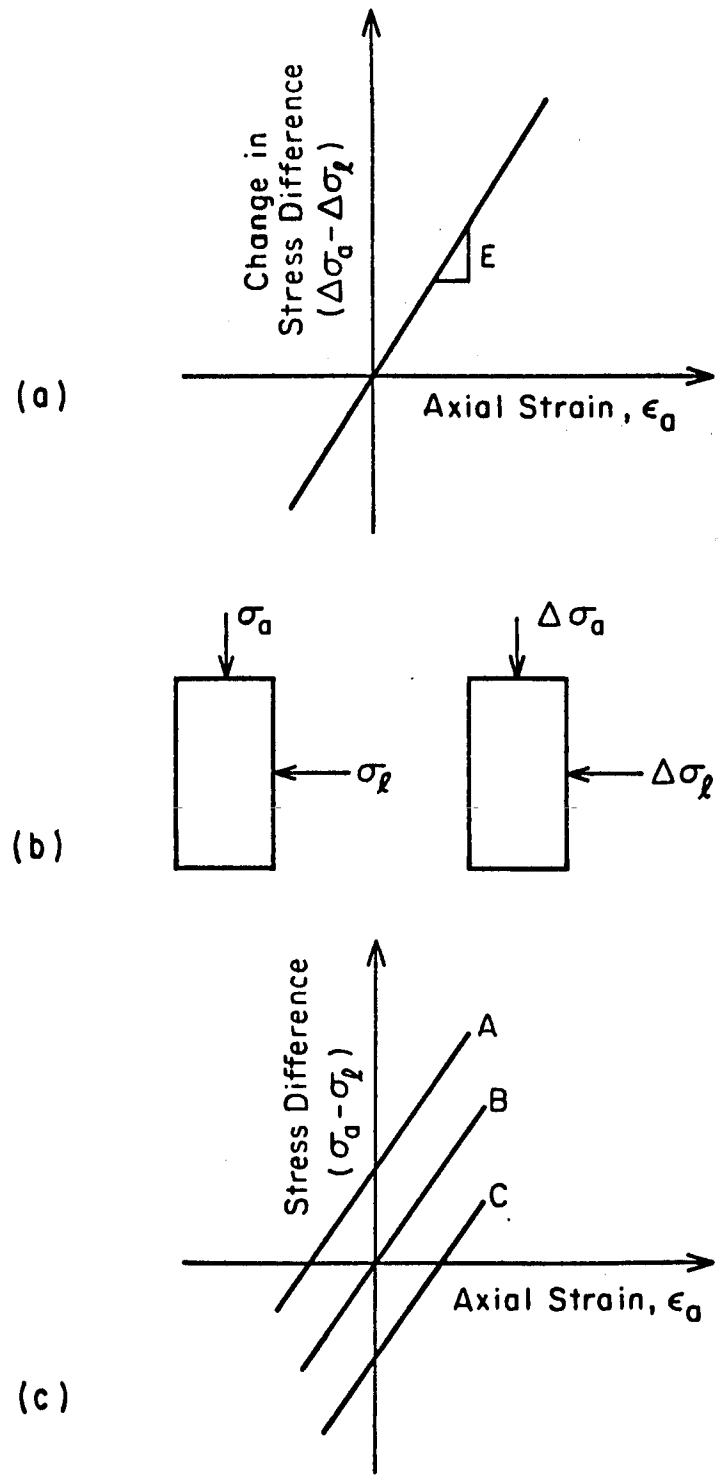

FIG. 6. IDEALIZED STRESS - STRAIN RESPONSE OF SOIL ELEMENTS

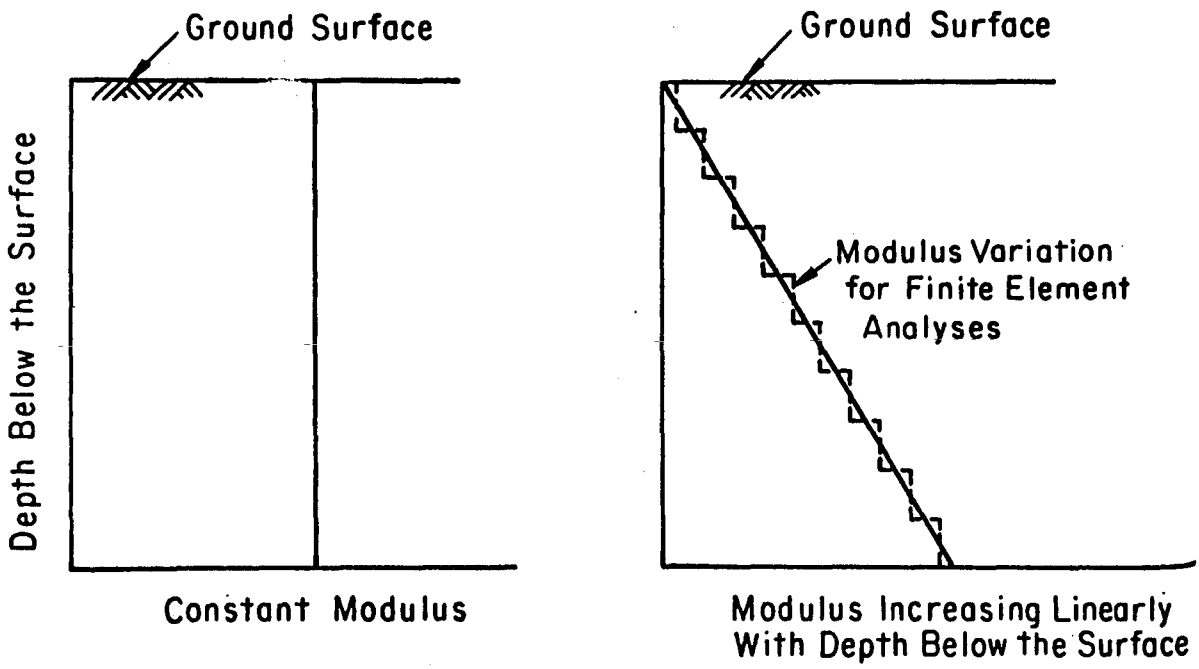

FIG. 7. MODULUS VARIATIONS FOR LINEAR ELASTIC ANALYSES

in these analyses were sufficiently distant from the slopes so that they did not influence the results; the results are thus representative of slopes excavated in a layer of very large lateral extent. The investigations conducted to determine the influence of various boundary locations, and the criteria developed, are described in Appendix A. Although the bottom boundary also influences the results of the analyses, no effort has been made to minimize or eliminate this boundary effect. It is considered that the clay layers in which the slopes are excavated are underlain by a much harder layer of soil or rock at a depth equal to twice the height of the slope. The nodal points along this bottom boundary were constrained from moving either horizontally or vertically, simulating full adhesion between the clay and the harder layer of rock beneath.

The principal stress orientations determined in these analyses are shown in Fig. 8, where the major principal stress orientations are indicated by the longer of the two crossed lines; each of the crosses is the same size, and the lengths of the lines do not indicate the relative magnitudes of the principal stresses. The finite element mesh used in conducting these analyses extended further to the right and left of the slopes than do the regions shown in Fig. 8. However, the stress conditions in the region immediately adjacent to the slope are considered to be of primary interest, and only the results for this region are shown in Fig. 8 and subsequent figures.

The four cases shown in Fig. 8 illustrate that the initial stress conditions have a large influence on the stress orientations after excavation, but the modulus variation has a relatively minor effect. For initial stress conditions representative of normally consolidated clays ($K = 0.75$) the initial major principal stresses were vertical everywhere, whereas for conditions representative of overconsolidated clays ($K = 1.25$), the initial major principal stresses were horizontal everywhere. Similarly, it may be noted that the final stress orientations shown in Fig. 8 are in both cases closer to horizontal for high initial horizontal stresses ($K = 1.25$) than for low initial horizontal stresses ($K = 0.75$).

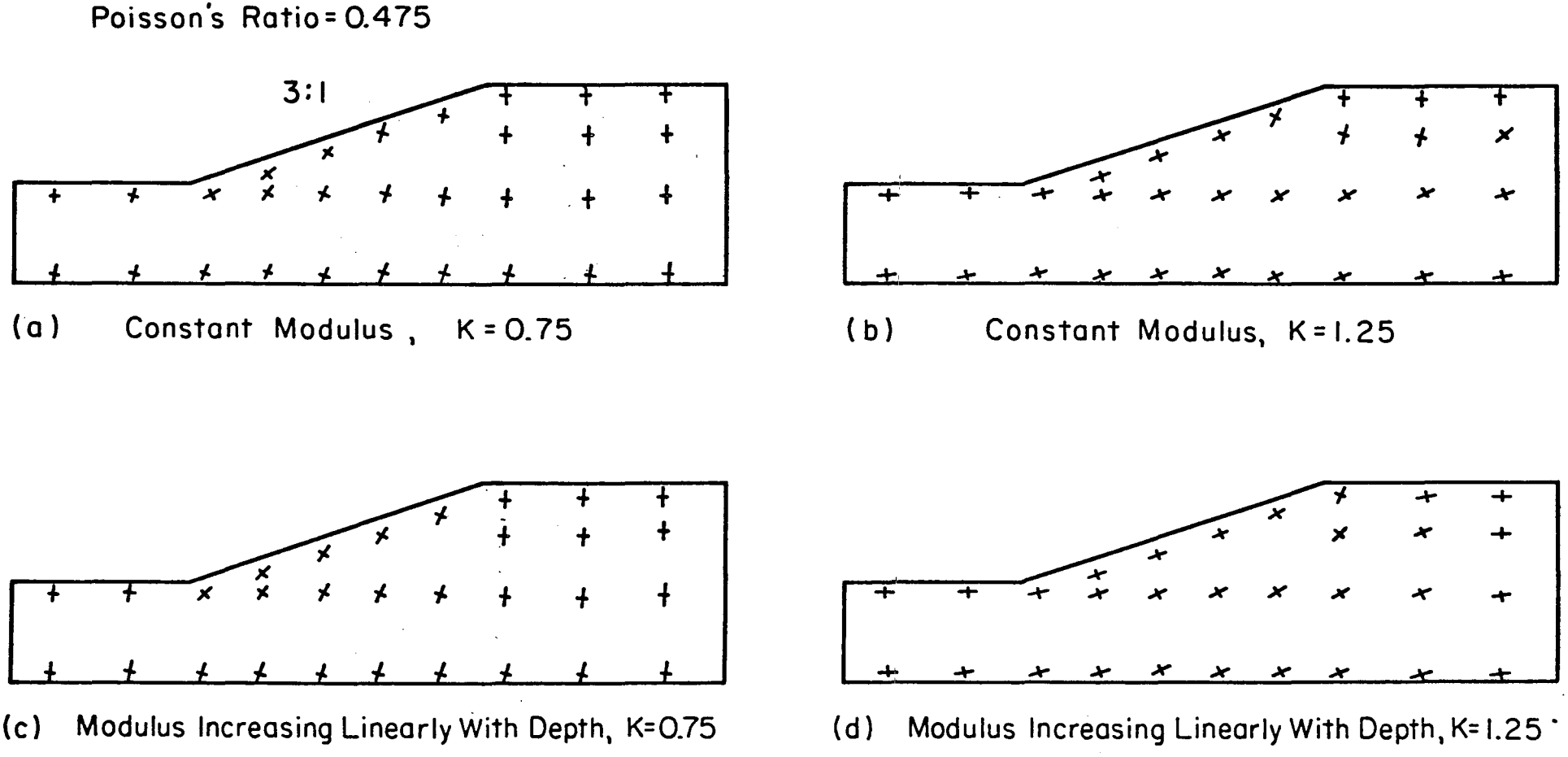

FIG. 8 EFFECTS OF INITIAL STRESSES AND MODULUS VARIATION ON PRINCIPAL STRESS ORIENTATIONS.

Near the surface behind the crest and below the toe of the slopes, the principal stresses are oriented approximately vertical and horizontal, and near the sloping surface the principal stresses tend to be roughly aligned with the surface of the slope. It would be expected that the stress orientations at these surfaces would coincide with the surface orientations because these stress-free boundaries are principal planes. The orientations shown do not coincide exactly with the boundaries because they represent conditions at the centroids of the first rows of elements within the slope, and not at the surface.

Comparing the analyses conducted using the same initial stress conditions but different modulus variations with depth, it may be seen that the stress orientations are almost identical, whether the modulus is constant or increases linearly with depth. Only in the area behind the crest of the slope with high initial horizontal stresses is there a significant difference: In the case where the modulus is constant, the major principal stress is approximately vertical, whereas for modulus increasing with depth, the major principal stress is approximately horizontal. In all other regions of the slopes, the stress orientations are influenced to a negligible extent by the modulus variation with depth.

The influence of initial stresses and modulus variation on the shear stresses around excavated slopes are shown in Fig. 9. The calculated values of maximum shear stress, τ_{max}, have been divided by the product of the clay unit weight and the slope height, γH. In an excavated slope, all stress values are proportional to the body forces. Thus the stresses calculated are equally applicable to slopes of any size, provided they are considered in terms of dimensionless coefficients such as $\tau_{max}/\gamma H$.

The contours of $\tau_{max}/\gamma H$ shown in Fig. 9 indicate that the initial stress conditions have a marked effect on the maximum shear stresses, whereas the effect of modulus variation with depth is relatively small. For low initial horizontal stresses representative of normally consolidated clay ($K = 0.75$), the shear stress contours are very nearly parallel to the surface of the slopes and the shear stresses increase with depth to a maximum at the base of the clay layer. For higher initial horizontal stresses representative of overconsolidated clays ($K = 1.25$) the shear

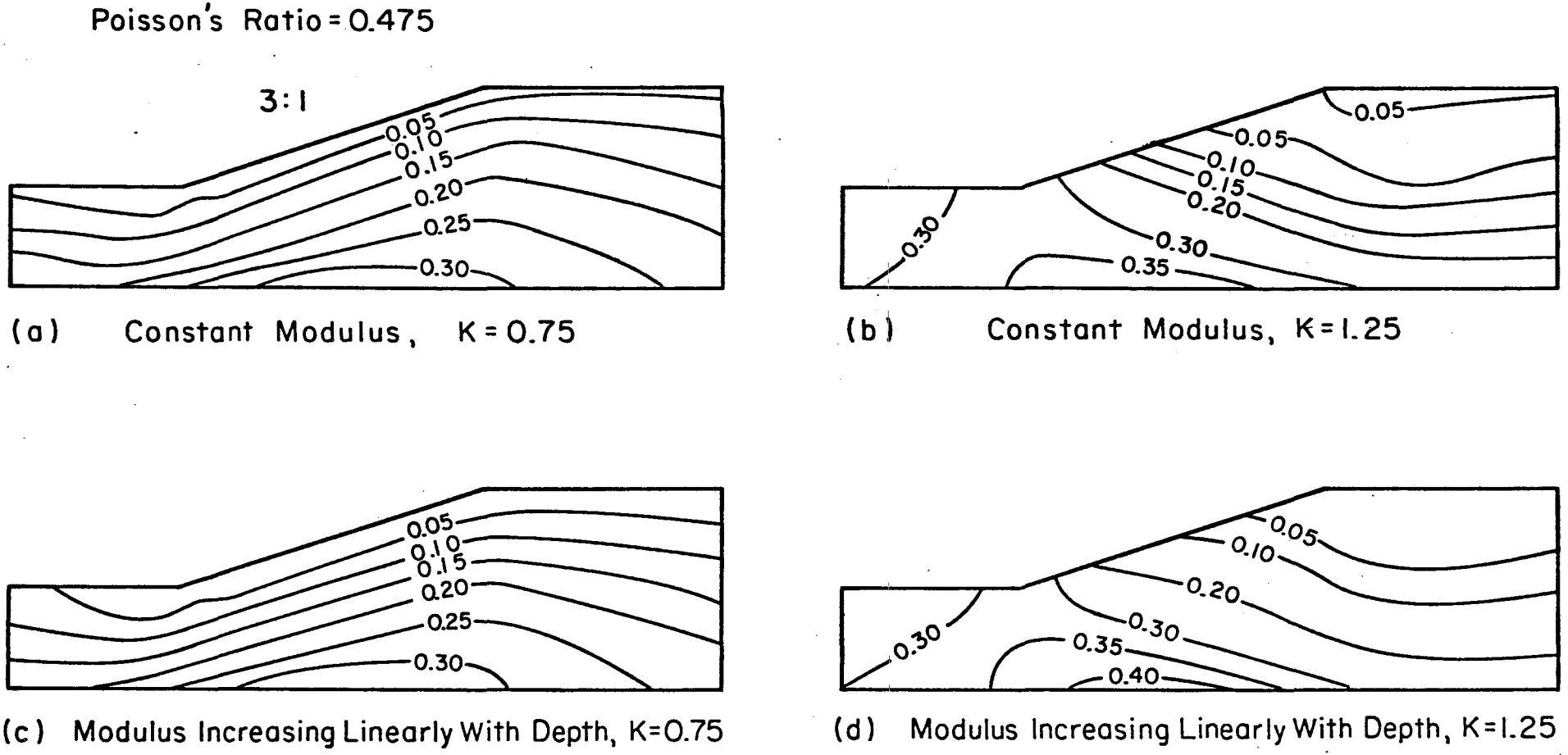

FIG. 9 EFFECTS OF INITIAL STRESSES AND MODULUS VARIATION ON VALUES OF $\tau_{max} / \gamma H$.

stress values increase progressively down the slope, to a value higher than 0.3 γH at the toe of the slope. The magnitude of the shear stresses also increases with depth, to a maximum at the base of the clay layer. The largest values of shear stresses are somewhat higher for the cases with high initial horizontal stress than for the cases with lower initial stress values, and the values of shear stress at the base of the clay layer are slightly higher for the cases in which modulus increases with depth.

Perhaps the most significant influence of initial horizontal stress values is their effect on the values of maximum shear stress around the toe of the slope. It may be noted that for conditions representative of normally consolidated clays ($K = 0.75$), the shear stress values at the toe of the slopes are very small, being less than 0.05 γH for both cases studied. On the other hand, for conditions representative of overconsolidated clays ($K = 1.25$), the toe of the slope is one of the most critical locations with regard to shear stress values; the shear stresses near the toes of these slopes are larger than 0.3 γH, and are almost as high as the largest values at the base of the clay layer. For normally consolidated conditions the largest value of shear stress occurs at the base somewhat toward the crest (to the right) from the center of the slope, whereas for overconsolidated conditions the largest shear stress occurs at the base somewhat toward the toe (to the left) from the center of the slope. Thus the higher horizontal initial stresses appear to cause increased shear stresses in the region around the toe of the slope and the base of the excavation. Similar results have been determined for slopes of steeper inclinations than the 3:1 slopes shown in Fig. 9.

Besides the shear stresses, tensile stresses around slopes are also of interest because many soils are very weak in tension and many slope failures have been preceded by development of cracks, believed to be caused by tension, behind the crest of the slopes. The zones of tension, and the locations and magnitudes of the maximum tensile stress values are shown in Fig. 10. Like the shear stresses discussed previously, these tensile stresses have been nondimensionalized by dividing the calculated values by γH. It may be noted that the size of the tension zones and the magnitudes of the tensile stresses are both much larger for

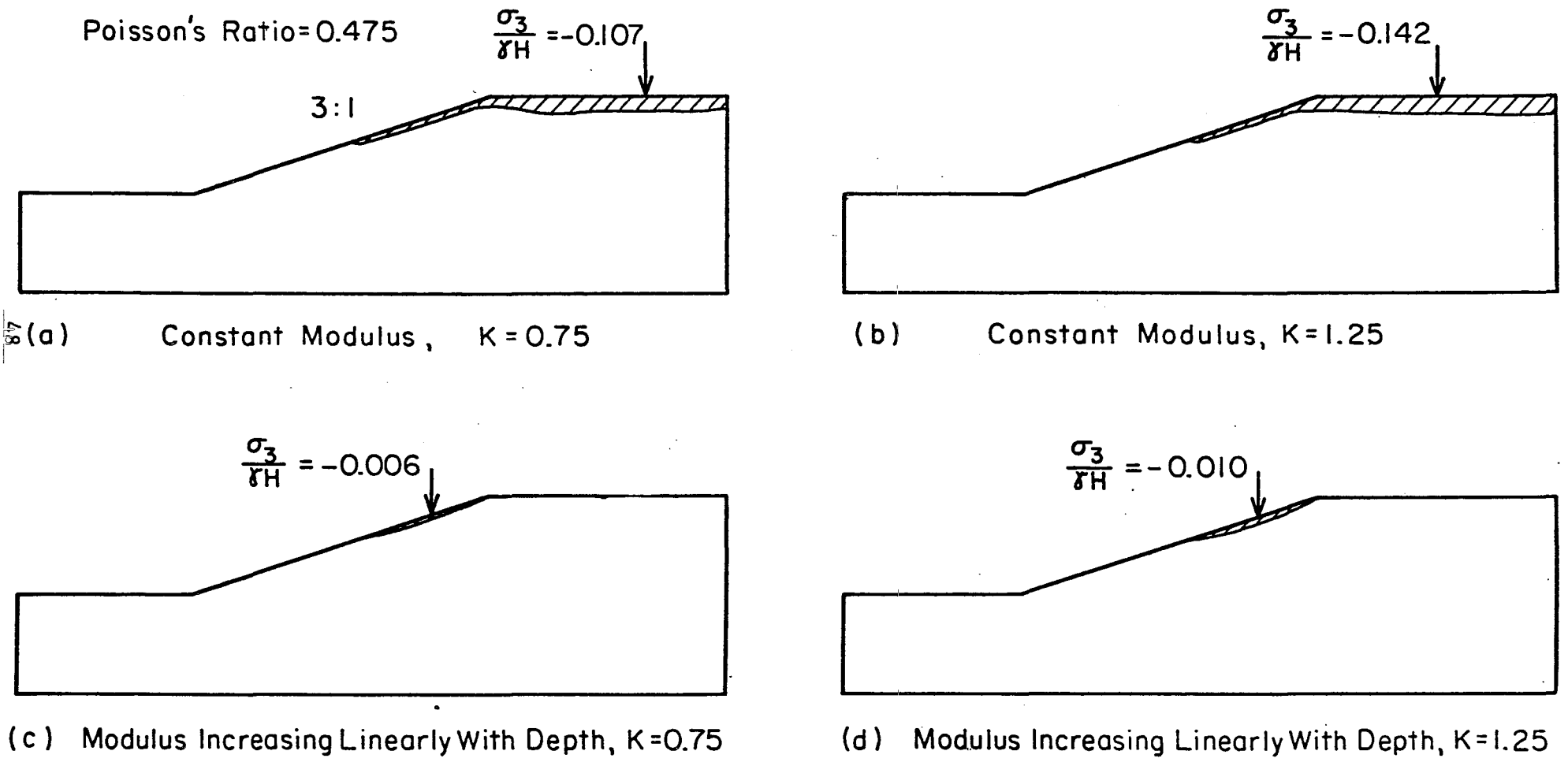

(a) Constant Modulus, K = 0.75

(b) Constant Modulus, K = 1.25

(c) Modulus Increasing Linearly With Depth, K = 0.75

(d) Modulus Increasing Linearly With Depth, K = 1.25

FIG. 10 EFFECTS OF INITIAL STRESSES AND MODULUS VARIATION ON TENSILE STRESS.

cases in which the modulus values were constant throughout the depth than for the cases where the modulus values increased with depth. The size of the tension zone and the magnitude of the tensile stresses are also larger for higher initial horizontal pressures, or values of K. Additional elastic analyses have shown that the magnitude of the tensile stresses also increase with increasing slope steepness.

Because many soils are very weak in tension, it would be expected that tension cracks might develop due to even fairly small tensile stresses. Crack formation would, of course, eliminate the tension at the crack and cause redistribution of stresses at other points within the slope. Therefore it seems appropriate to consider that the tensile zones shown in Fig. 10 indicate locations where tension cracks would be most likely to develop, but the tension values shown could only be developed in materials with appreciable tension strength.

The magnitudes of the effects of the initial horizontal stress values and modulus variation with depth on the results of linear elastic analyses of excavated slopes are summarized in Table 1. It may be noted that the magnitude of the initial stresses has a significant effect on the stress orientations and the values of shear and tensile stress, whereas only the tensile stress values are significantly influenced by modulus variation with depth.

Table 1. - Effects of Initial Stresses and Modulus Variation with Depth on Stress Orientations, Shear Stress Values, and Tensile Stress Values.

Variable	Effect on		
	Principal Stress Orientations	Maximum Shear Stress Values	Maximum Tensile Stress Values
Initial Stress (K)	Major	Major	Major
Modulus Variation (E)	Minor	Minor	Major

Gravity Turn-on Analyses

The analyses described previously were conducted by simulating analytically the excavation of slopes in clay layers with initially level surfaces, using the procedures discussed in the previous chapter. Under certain circumstances comparable stress values may be calculated by simulating the application of gravity to a finite element mesh representing the final slope configuration. Such "gravity turn-on" analyses may often be done quite simply, using standard finite element structural analysis computer programs.

The correspondence between gravity turn-on and construction sequence analyses may be established quite easily if the gravity turn-on analysis is considered to consist of two separate parts. The first part is application of gravity to a finite element mesh with horizontal top and bottom and vertical lateral boundaries. The top boundary is free, the bottom is fixed, and the lateral boundaries are constrained to move in the vertical direction only. Under plane strain conditions the stresses resulting from gravity turn-on will be:

$$\sigma_v = \gamma Z, \tag{5a}$$

and

$$\sigma_h = \frac{\nu}{1 - \nu} \gamma Z \tag{5b}$$

in which σ_v and σ_h are the vertical and horizontal stresses, γ is the soil unit weight, and Z is the depth beneath the surface. Both the strains and displacements in the horizontal direction will be zero. The vertical strains will be

$$\varepsilon_v = \frac{\gamma Z}{E} \left(1 - \frac{2\nu^2}{(1 - \nu)}\right) \tag{6}$$

where ε_v is the strain in the vertical direction, E is Young's modulus, and ν is Poisson's ratio. The displacement in the vertical direction, δ_v, is found by integrating the strains over the thickness of the layer, T:

$$\delta_v = \frac{\gamma}{2E} \left(1 - \frac{2\nu^2}{(1 - \nu)}\right) (T^2 - Z^2) \tag{7}$$

To complete the gravity turn-on analysis following this first step would require use of a procedure which is exactly the same as the

procedure previously described for construction sequence analyses; stresses which are equal in magnitude but opposite in sign from those calculated during the first part of the analysis, would be applied to the surface being excavated and the resulting stresses, strains, and displacements would be calculated using finite element procedures. Superposition of the results of these two steps would give answers exactly the same as a gravity turn-on analysis performed in a single step, since the material is assumed to have linear elastic stress-strain characteristics.

If a construction sequence analysis had been employed instead of a gravity turn-on analysis, the final stress values would be exactly the same provided the initial stress values conformed to those given by the first step of the gravity turn-on analysis. This would be the case provided the coefficient of total earth pressure, K, was equal to $\nu/(1-\nu)$. The strains and displacements calculated by the construction sequence analysis would be the same as those calculated during the second step of the gravity turn-on analysis, because the two analyses would in fact be identical.

Thus the stresses calculated by adding the initial stresses with the changes in stress would be the same as those calculated using gravity turn-on procedures, provided $K = \nu/(1-\nu)$. The vertical strains calculated by the gravity turn-on procedure would exceed those calculated by the construction sequence analyses by the amount shown by equation (6) and the vertical displacements would differ by the amount shown by equation (7). The horizontal displacements and strains would be the same.

To illustrate the relationship between the results obtained by the two methods, the same 2:1 slope has been analyzed by both methods for the case where $K = \frac{\nu}{1-\nu}$. The calculated stress values (in psf) are shown in Fig. 11. To a very high degree of accuracy, the results of the two analyses are the same. The most significant differences in stress values are associated with triangular elements along the cut slope, and may be attributed to differences in the calculations performed for these elements in the two methods of analysis; initial stress values assigned for construction sequence analyses are associated with element centroids, but Wilson (1963) has shown that values of σ_x, σ_y, and τ_{xy} calculated by finite element techniques for triangular elements are each associated with a

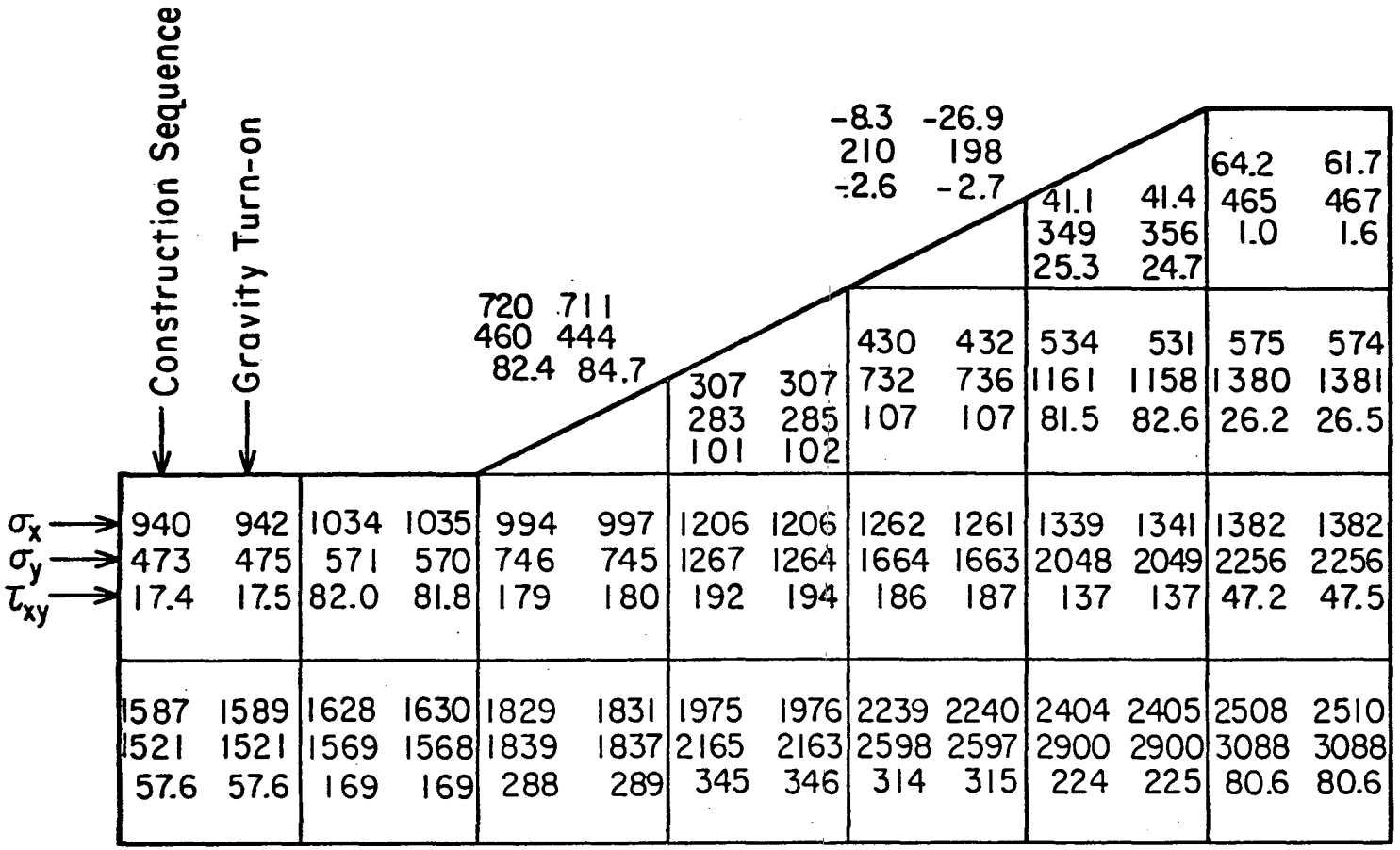

FIG. 11 COMPARISON OF STRESSES CALCULATED USING GRAVITY TURN-ON AND CONSTRUCTION SEQUENCE ANALYSES WITH $K = \nu/(1-\nu)$.

different location within the element. However, because the maximum difference in stress values calculated using the two procedures is only 16 psf compared to average stress values of the order of 1000 psf, it may be concluded that the stress values are equivalent for all practical purposes.

The calculated values of displacement are plotted in Fig. 12. It may be noted that the horizontal displacements calculated by the two methods are the same, but the vertical displacements calculated by the gravity turn-on analysis include an additional downward component.

It should be noted, however, that gravity turn-on analyses suffer from three limitations which limit their usefulness:

1. Because the initial stress coefficient K implicit in gravity turn-on analyses is equal to $\nu/(1 - \nu)$, K values may only range from zero to unity because the value of Poisson's ratio may only range between zero and one-half.

2. The value of Poisson's ratio, ν, appropriate to represent the material behavior may not be consistent with the value of ν appropriate for the initial stress conditions. For example the physical behavior of a saturated normally consolidated clay would approximately be characterized by a value of Poisson's ratio close to 0.5 under undrained conditions, whereas the initial stress conditions might correspond to $K = 0.67$, requiring use of a value of ν equal to 0.4.

3. The strains and displacements calculated by gravity turn-on procedures will include fictitious components of vertical compression and downward displacement.

Provided these limitations are taken into account, gravity turn-on analyses may be useful for many purposes and they can often be performed relatively easily using standard finite element structural analysis computer programs.

Initiation of Failure

The elastic stress distributions described in previous sections may reasonably be expected to be indicative of stress conditions around excavated slopes provided that the calculated shear stress values do not

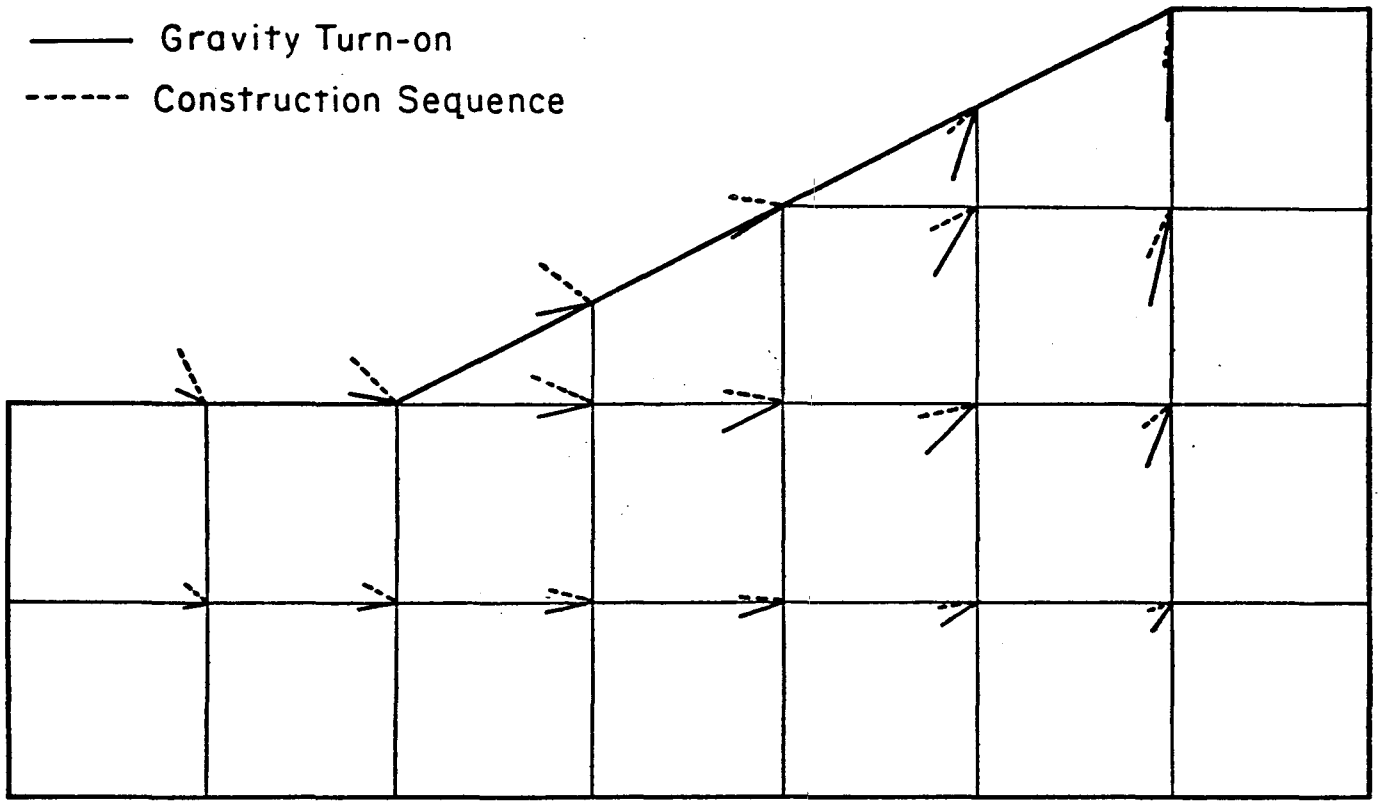

FIG. 12 COMPARISON OF DISPLACEMENTS CALCULATED USING GRAVITY TURN-ON AND CONSTRUCTION SEQUENCE ANALYSES WITH $K=\nu/(1-\nu)$

approach the strength of the clay in any point. They may therefore be useful for considering stress distributions for slopes with sufficiently high factors of safety to prevent even local failure, and they could be used to determine the factor of safety corresponding to the initiation of local failure.

Inspection of the dimensionless shear stress values shown in Fig. 9 indicates that for all of the cases shown the largest values of shear stress occur at the base of the clay layer. Additional finite element analyses have shown that for steeper slopes and higher values of initial horizontal stress, the largest shear stress may occur at the toe of the slope instead of the base of the clay layer. Turnbull and Hvorslev (1967) have also reported results of a photo-elastic study performed by LaRochelle, in which the maximum shear stress occurred at the toe of a 1:1 slope.

Some increase of undrained shear strength with depth is typical of both normally consolidated and overconsolidated clay deposits, with many strength profiles being intermediate between the extreme conditions of constant undrained strength throughout the depth of the layer and strength increasing linearly with depth from zero at the surface of the deposit. The extremes of constant strength and linearly increasing strength with depth may be described very conveniently in terms of values of S_u (for constant strength) or S_u/p (for linear increase with depth). Using the shear stress distributions previously described, values of S_u or S_u/p may be determined which correspond to failure at a single location adjacent to the slopes. For this purpose it seems most appropriate to consider that shear stress values calculated using constant modulus throughout the depth of the layer would apply best to cases where the shear strength is also assumed to be constant, because of the proportionality between undrained shear strength and modulus values. Similarly, it would seem appropriate to consider that shear stress values calculated using modulus increasing linearly with depth would apply best to cases where the shear strength also increases linearly with depth.

For the two cases shown in Fig. 9 where the modulus was constant throughout the depth, the largest shear stress values were: for K = 0.75, $\tau_{max} = 0.40\ \gamma H$. If these shear stress values were equal to the undrained

undrained strength of the clay ($S_u = 0.35\ \gamma H$ or $S_u = 0.4\ \gamma H$) failure would occur at one location at the base of the layer.

For deposits in which the shear strength increases linearly with depth, determination of the values of S_u/p corresponding to initiation of failure requires comparison of shear stress and strength values over the full depth of the layer. Comparisons of this type are shown in Fig. 13. The shear stress variations shown in Fig. 13 were determined using the shear stress contours shown in Fig. 9 for the two cases in which modulus values increased linearly with depth. The shear strength variations shown were selected so that the shear stresses and shear strengths would be equal at the most critical locations. It may be noted that a considerably more rapid increase of shear strength with depth is required for the case with high initial horizontal stresses ($K = 1.25$) than for the case with low initial horizontal stresses ($K = 0.75$). For the case with high initial horizontal stresses, representative of overconsolidated clays, local failure would occur first near the toe of the slope, whereas for the case with low initial horizontal stresses representative of normally consolidated clays, failure would occur first just below and slightly behind the crest of the slope.

To determine values of S_u/p from the strength profiles shown in Fig. 13, it has been assumed that the saturated unit weight of the clay is 100 lb/ft^3 and that the water table before excavation coincided with the ground surface. Under these conditions the initial effective vertical pressure at any depth Z below the surface is $p = 27.6\ Z$ psf where Z is in feet. For the two cases shown in Fig. 13, the values of S_u/p corresponding to development of local failure at one location are: for $K = 0.75$, $S_u/p = 0.62$ and for $K = 1.25$, $S_u/p = 0.89$.

In order to determine the values of factor of safety corresponding to the initiation of failure, these slopes have been analyzed using the "$\phi = 0$" method of analysis. The values of S_u and S_u/p corresponding to a factor of safety of unity are shown in Table 2, together with the values required so that the elastic shear stresses will not exceed the shear strength in any location. The ratio of the strengths or strength ratios determined by these two methods is also shown in Table 2. Because factors of safety computed by the $\phi = 0$ analysis are proportional to shear strength,

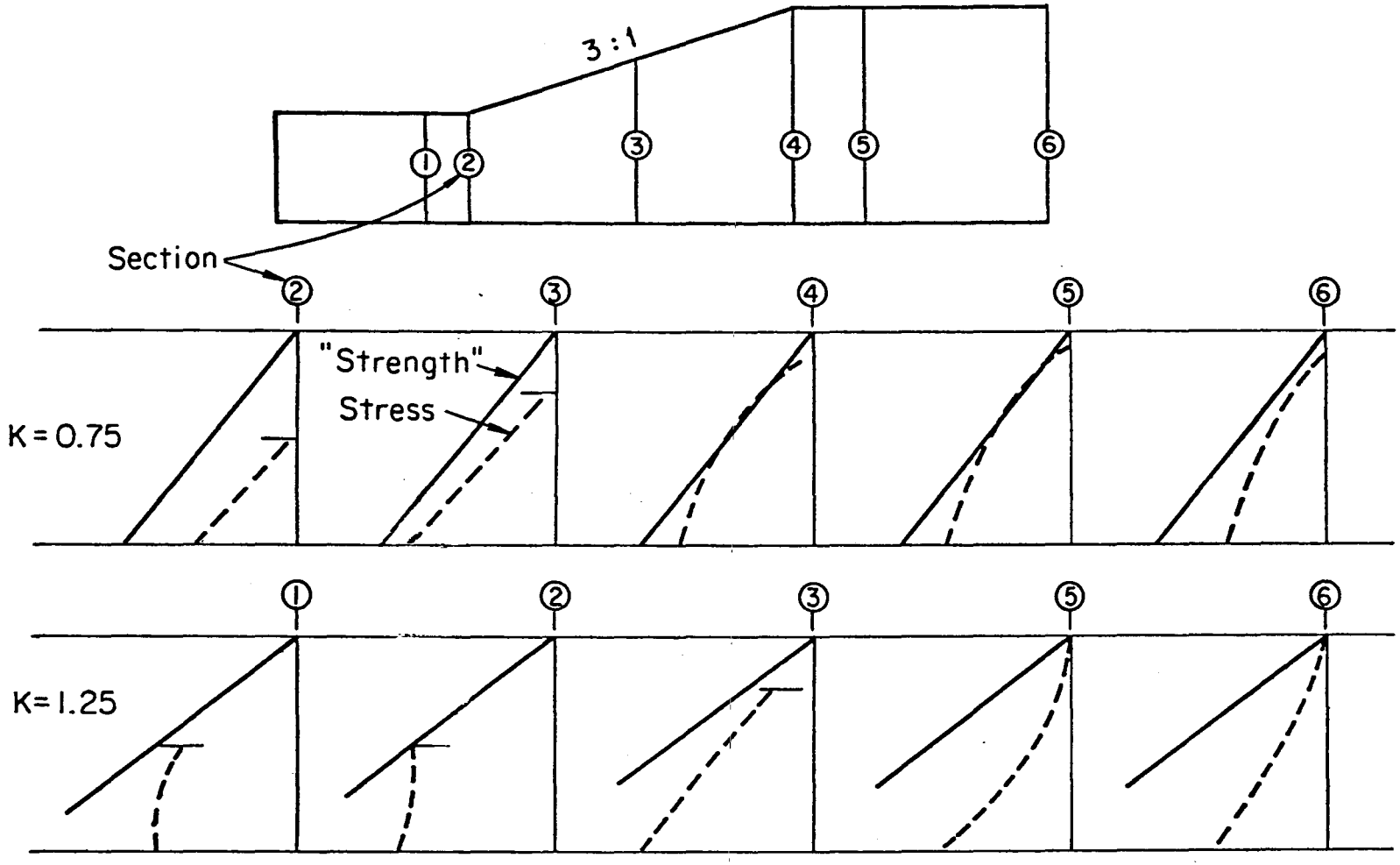

FIG. 13 SHEAR STRENGTH AND SHEAR STRESS VARIATIONS FOR LINEAR ELASTIC SLOPES WITH MODULUS INCREASING LINEARLY WITH DEPTH.

Table 2. Values of S_u and S_u/p Required for 3:1 Slopes.

Modulus or Strength Variation with Depth	Earth Pressure Coefficient K	Value Required So Elastic Shear Stresses Do Not Exceed Shear Strength		Value Required For Plastic Equilibrium, by "$\phi = 0$" Method		Ratio
		S_u	S_u/p	S_u	S_u/p	
Constant Throughout Depth	0.75	$0.35\gamma H$	--	$0.16\gamma H$	--	2.19
	1.25	$0.40\gamma H$	--	$0.16\gamma H$	--	2.50
Increasing Linearly With Depth	0.75	--	0.62	--	0.36	1.72
	1.25	--	0.89	--	0.36	2.47

the values of the ratio shown in Table 2 represent the factors of safety by the $\phi = 0$ method corresponding to development of the first local failure. These values range between 1.72 and 2.5, depending on the strength variation with depth and the initial stress conditions. The higher the initial stresses before construction, the higher the factor of safety corresponding to failure at a single location within the slope. Similar analyses have shown that the factor of safety corresponding to first local failure also depends on the slope inclination and the depth to the rigid layer beneath the clay. For the most critical combination of the controlling factors investigated (vertical slope excavated completely to the rigid base, with a K value of 1.60), the factor of safety corresponding to initiation of failure was found to be greater than 5.

It is interesting to note that the smallest value of the ratio shown in Table 2 corresponds to the case in which modulus and shear strength values increase linearly with depth, for initial stress conditions representative of normally consolidated clays. For these conditions the value of the ratio is only 1.72, indicating that if a 3:1 slope with a factor of safety equal to 1.72 or more was excavated in normally

consolidated clay, not even local failure would develop. For all of the other cases shown, appreciably higher factors of safety would be required to prevent local failure. Thus it seems likely that normally consolidated clay deposits are less subject to local failure, and to possible subsequent development of progressive failure, than overconsolidated clays having higher initial horizontal stresses and more uniform strength profiles.

Use of Elastic Stresses for Stability Analyses

Bennett (1951) suggested an interesting procedure for assessing the stability of slopes using the results of stress analyses: Potential failure surfaces are selected so that at any point the angle between the major principal stress orientation (stress trajectory) and the failure surface is $45 - \frac{\phi}{2}$ degrees. Various trial failure surfaces are selected by choosing different starting points on the ground surface near the toe of the slope and tracing out the corresponding failure surfaces in accord with the stress orientations. The average value of shear stress is calculated for each of the trial failure surfaces, the one requiring the largest value of shear stress for stability being the most critical.

Brown and King (1966) have illustrated the use of this method, employing finite element analyses to determine elastic stress distributions for homogeneous slopes. A value of ϕ equal to zero was used in determining the failure surface locations, so that the failure surfaces investigated were trajectories of maximum shear stress. For a 45 degree slope, and initial stresses corresponding to $K = 1.0$, Brown and King found that the shear strength required for stability on the most critical maximum shear stress trajectory was $0.14\ \gamma H$, slightly less than the required shear strength value which Taylor (1937) found for the most critical circle, $0.15\ \gamma H$.

Bennett's stress trajectory method and the circular arc method both employ repeated trials to determine the most critical failure surface, which is the one requiring the largest average value of shear stress to maintain stability. Therefore, of the two methods, the one which results in the largest value of required shear strength must be considered more correct. On this basis the circular arc method appears to be preferable,

although for the slope mentioned previously the difference in results amounts to only about 7%.

Using the stress orientations determined by the finite element analyses described previously, failure surfaces have been established using $\phi = 0$ and $\phi = 30°$. Those established using $\phi = 0$ are shown in Fig. 14. In each case the lowest trial failure surface shown does not intersect the surface behind the crest of the slope, but instead intersects the bottom boundary. Similarly, all trial failure surfaces beginning further down the slope or further to the left of the toe of the slope also intersect the bottom boundary. Such trial failure surfaces were considered not to be kinematically acceptable, and were not used in determining values of shear strength required for stability.

For the two cases shown in which the modulus was constant throughout the depth, the maximum values of shear strength required for equilibrium were found to be 0.064 γH for $K = 0.75$ and 0.063 γH for $K = 1.25$. Considerably less than required for stability on the most critical circle (0.16 γH). Even smaller values of required strength were determined for the two cases in which the modulus values increased with depth. The same slopes were also analyzed using $\phi = 30°$ to determine failure surfaces compatible with the stress orientations. The values of shear strength required for stability on these surfaces were also considerably smaller than that required for stability on the most critical circular arc: For the two cases in which the modulus was constant throughout the depth, the maximum values of required strength were 0.037 γH for $K = 0.75$ and 0.091 γH for $K = 1.25$. For the cases in which the modulus values increased with depth, the values of shear strength for equilibrium were again smaller.

On the basis of these results it may be concluded that the use of elastic stress distributions for determining failure surfaces and stability coefficients is not a desirable procedure, because the values of shear strength required for equilibrium on the most critical of such failure surfaces are considerably smaller than that required for stability on the most critical circular arc. It is interesting to note that the use of trial circular failure arcs with $\phi = 0$ constitutes a valid application of the upper bound method of plasticity theory. According to the

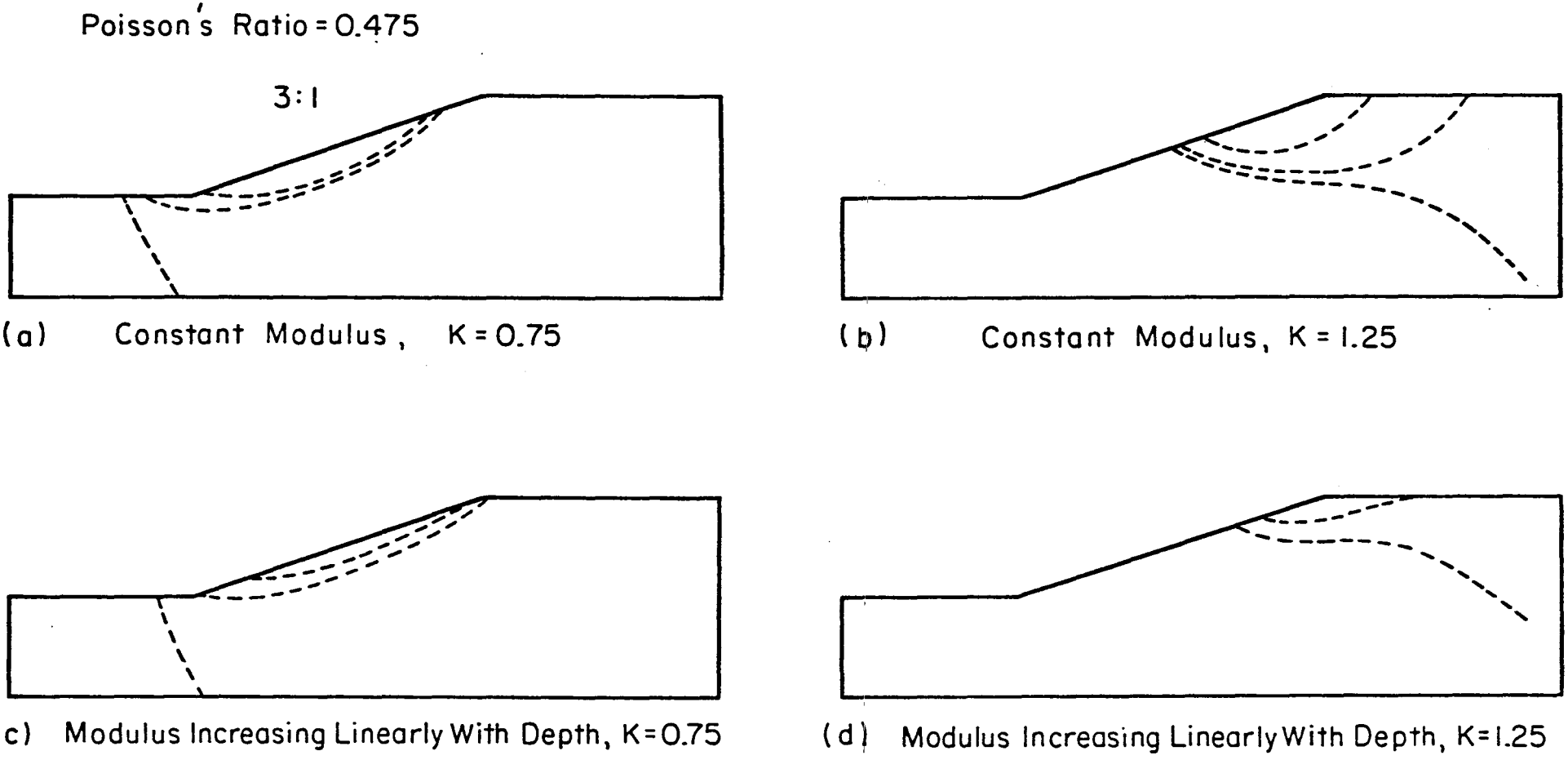

FIG. 14 POSSIBLE FAILURE SURFACES DETERMINED FROM STRESS ORIENTATIONS USING $\phi = 0$.

upper bound theorem, values of shear strength required for stability using upper bound methods will be either unconservative (too low) or correct, and no method indicating lower values of required shear strength than an upper bound method can be correct. Therefore, even though the method suggested by Bennett (1951) satisfies the required relationship between stress orientations and failure surface orientations, it is apparently less accurate than the commonly used circular arc method.

Summary

The assumption of linear elastic stress-strain behavior provides the simplest possible basis for slope analyses. The studies performed indicate:

(1) Values of maximum shear stress and stress orientations around slopes are influenced to a major extent by initial stress conditions (value of K), but are influenced only to a small degree by the manner in which the modulus values vary with depth.

(2) Values of tensile stress and the size of the tension zone near the crest of slopes is influenced significantly by both the initial stress conditions and the modulus variation with depth.

(3) The values of the largest shear and tensile stresses around excavated slopes increase with increasing slope steepness.

(4) Gravity turn-on analyses will result in the same values of stress and horizontal displacement as analyses conducted simulating the excavation of slopes, provided the initial earth pressure coefficient is related to the value of Poisson's ratio by $K = \nu/(1 - \nu)$. The values of vertical displacement calculated using gravity turn-on procedures contain an additional downward component, however.

(5) The factor of safety corresponding to the development of local failure within slopes is influenced to a large extent by the initial stress conditions, and to a lesser extent by the variation of modulus and shear strength with depth.

(6) Linear elastic stress distributions and stress orientations cannot be used for reliable assessment of slope stability.

CHAPTER 3

ANALYSES OF SLOPES USING BILINEAR STRESS-STRAIN BEHAVIOR

The analyses described in this chapter were conducted to investigate the growth of failure zones around slopes during excavation. In order to simulate reduced resistance to deformation subsequent to failure, the analyses were conducted in a series of steps representing successive stages of excavation and the modulus value for any zone where local failure occurred was reduced for subsequent steps in the analyses. Thus any particular element was assigned one of two possible modulus values depending on the stress conditions: a relatively large value prior to failure, and a relatively small value after failure. The stress-strain curve for any particular element was thus bilinear, consisting of two straight line portions corresponding to the two values of modulus.

Bilinear Stress-Strain Behavior

The relationship between the modulus values used in these analyses and the undrained stress-strain and strength characteristics of a typical normally consolidated clay is illustrated in Fig. 15. For a normally consolidated clay deposit with the ground water table some distance beneath the surface, the undrained strength would be expected to increase with depth in the manner shown in Fig. 15(a). Hypothetical undrained stress-strain curves for specimens from two different depths, and bilinear representations of these curves are shown in Fig. 15(b). If the values of strain corresponding to the breaks in the bilinear curves were the same, then both curves could be represented by a single normalized stress-strain relationship as shown in Fig. 15(c), in which the ordinate is the compressive stress divided by the undrained compressive strength, q_u. The slope of the initial portion of this normalized curve is equal to the ratio of the modulus to the undrained compressive strength, E/q_u, as shown in Fig. 15. Therefore, if the breaks in the two bilinear curves occur at the same value of strain, the modulus value for the initial portion of either curve will be equal to the same constant times the undrained strength.

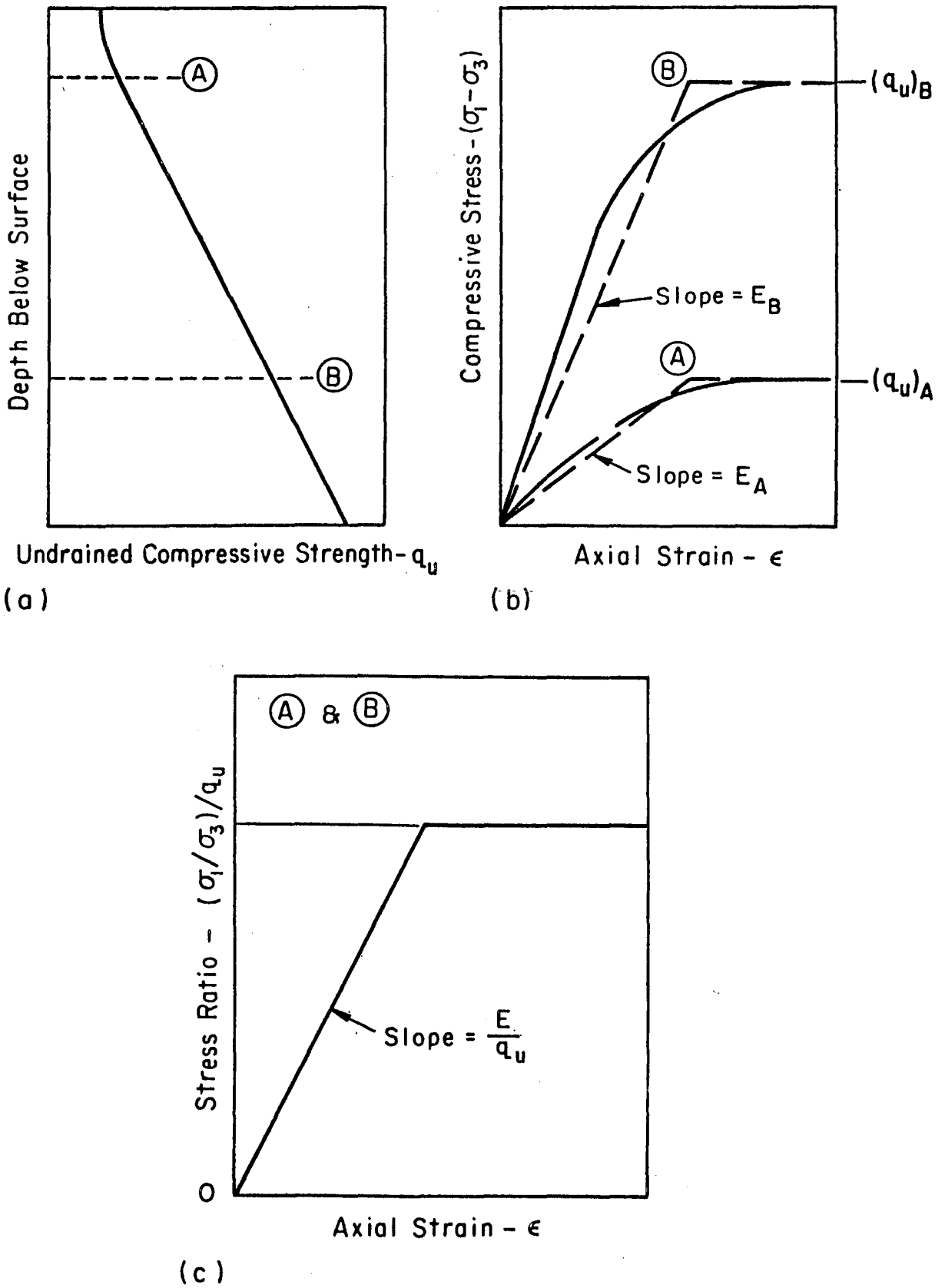

FIG. 15 BILINEAR STRESS-STRAIN RELATIONSHIPS

In the bilinear slope analyses conducted during the course of this investigation, it has been assumed that the modulus values representing the initial portions of the stress-strain curves are proportional to the undrained strength. Thus the curve representing the variation of modulus with depth is in each case similar to the strength-depth profile. The initial modulus values used in the analyses were typically 100 times the undrained shear strength. The modulus values used in the analyses influence the magnitudes of the strains and displacements which occur both before and after failure, but have no appreciable effect on the values of stress calculated. Subsequent to failure, very small modulus values, typically 10 lb/ft^2, were assigned.

Stress-Strain Curves and Failure Criteria

Although the initial values of strain and displacement at each point were taken to be zero, the initial stress conditions considered were those representative of a clay deposit with a horizontal surface, in which both the vertical and horizontal stress values increase linearly with depth. As in the case of the linear analyses described in the previous chapter, the initial vertical stress at any depth was equal to γZ, and the initial horizontal stress was $K\gamma Z$.

Under these conditions the position of the stress-strain curve and the value of strain corresponding to the break in the stress-strain curve for any location around the slope depend on the orientations of the changes in stress. Two possible orientations of change in stress, and the resulting stress-strain curves, are shown in Fig. 16. The initial stress conditions correspond to the major principal stress acting vertically, as shown in Fig. 16(a). The changes in stress at this point might conceivably be oriented in any direction; changes in which the major principal changes in stress are vertical and horizontal are shown in Fig. 16(a), and the corresponding stress-strain curves are shown in Fig. 16(b). The stress difference $(\sigma_a - \sigma_\ell)$ represents the stress difference in the a-direction, which is the orientation of the major principal change in stress and the ℓ-direction, which is the orientation of the minor principal change in stress.

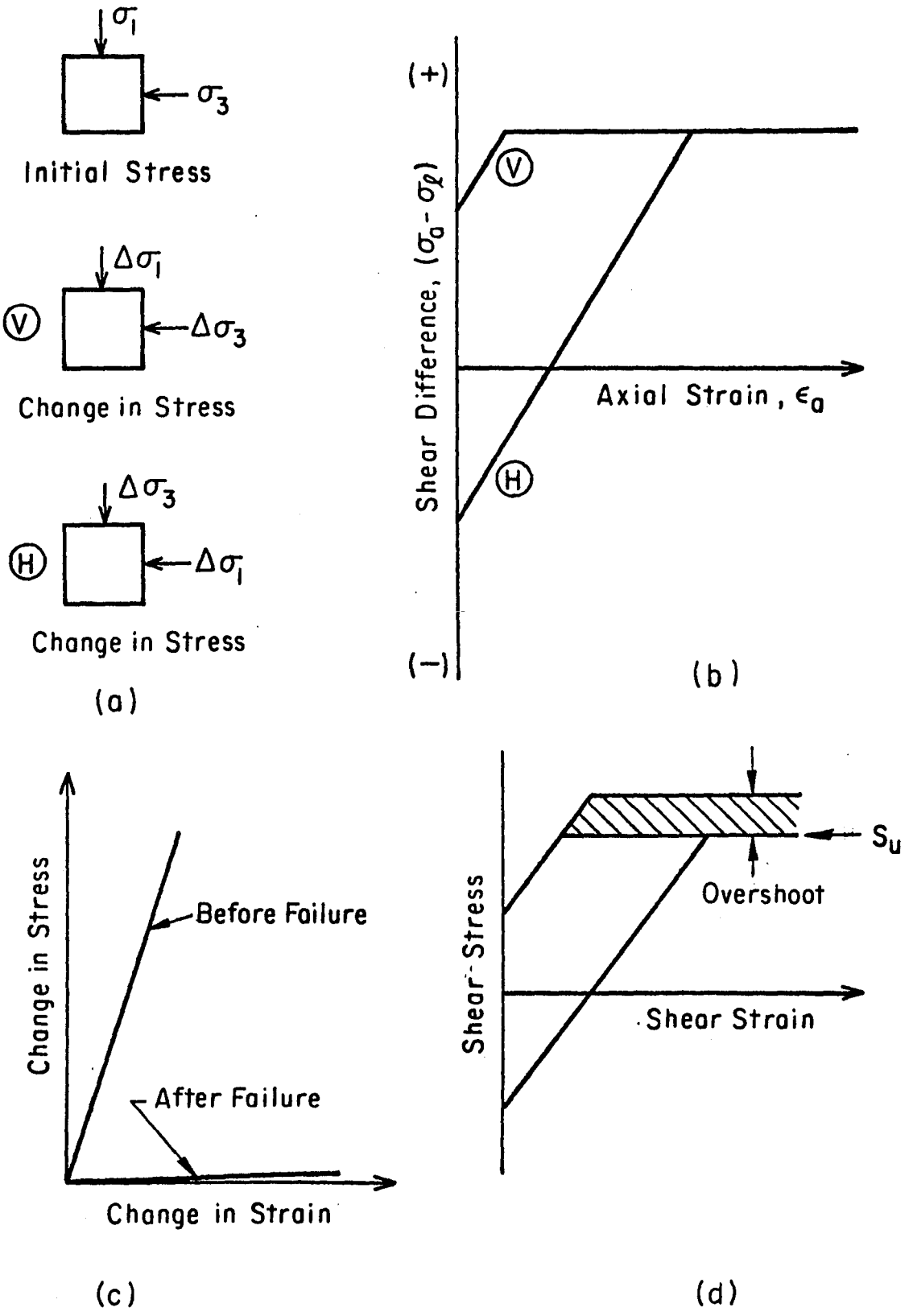

FIG. 16 STRESS-STRAIN CURVES AND STRENGTH CRITERION

For the curve labelled V in Fig. 16(b), the stress difference is increased monotonically to failure when the major principal change in stress is oriented vertically. However, when the major principal change in stress is horizontal, the initial value of stress difference is negative, and its value increases through zero to a value sufficiently large to cause failure as shown by the curve labelled H in Fig. 16(b). Because the slopes of the initial portions of both stress-strain curves are the same, the values of strain corresponding to the breaks in the curves are different, being larger for curve H than for curve V. This variation in the value of strain at failure is representative of the behavior of San Francisco Bay Mud determined using vertical and horizontal plane strain tests; Duncan and Seed (1966) found that the strain at failure under stress changes of the type labelled V in Fig. 16 were about 3.6% and the strain at failure under stress changes of the type labelled H in Fig. 16 were about 10.2%.

For stress change orientations intermediate between those shown in Fig. 16, the stress orientations change with the addition of each stress increment. Because principal stress values may not be added directly unless their directions coincide, stress-strain curves for arbitrary stress-change orientations cannot be represented in the manner shown in Fig. 16(b). No matter what the orientation of the principal stress changes, however, the relationship between change in stress and change in strain is represented by a straight line as shown in Fig. 16(c). Before failure the relationship between stress changes and strain changes was represented by a relatively large modulus value (the steeper curve in Fig. 16(c)) whereas after failure a relatively small modulus value was employed (the flatter curve). Following each step in the simulated excavation of the slope, the stress conditions in each element in the remaining configuration were evaluated and compared to the failure criterion. If the maximum shear stress in any element was found to be greater than or equal to the assigned undrained strength value for that element, the smaller modulus value was used in evaluating the stiffness of that element for the next step.

Using this procedure it was sometimes found that during a single step the maximum shear stress had changed from a value less than the undrained

strength to a value appreciably in excess of the undrained strength. Although reduction of the modulus to a small value for subsequent steps was effective in preventing further increase in shear stress, once the shear stress in any element exceeded the undrained strength, it remained at that value throughout subsequent steps of the analysis. As illustrated in Fig. 16(d), therefore, there was inevitably a degree of "overshoot" involved in application of the failure criterion in the manner adopted. Although this overshoot might be reduced or eliminated by using very small steps or iterative procedures for each step, it amounted to only about 10% on the average in the analyses performed, and it was not considered warranted to use more complex and time-consuming procedures to reduce it to a smaller value.

Shear Strength Profiles

For use in the bilinear analyses conducted in this investigation, three different strength profiles were selected which are representative of the variations of undrained shear strength with depth in normally consolidated and overconsolidated clays. These strength profiles are shown in Fig. 17. For many normally consolidated clays the shear strength increases approximately linearly with depth beneath the water table; two such strength variations are represented in Fig. 17, one for $S_u/p = 0.25$ and one for $S_u/p = 0.30$. Both of these strength profiles correspond to a saturated unit weight of 125 lb/ft^3. The strength profile representing an overconsolidated clay is characterized by relatively high strength values near the surface, where the effect of overconsolidation would be the greatest, and values gradually approaching those for the normally consolidated clay near the base of the 100 ft. thick clay layer. The step-wise strength variations actually used in the finite element analyses are shown in Fig. 17 by dotted lines. In addition to the profiles shown in Fig. 17, some analyses were performed using strength values increasing linearly from the surface, or constant throughout the depth of the clay layer.

Computer Program for Bilinear Slope Analyses

The procedures described for bilinear analyses have been incorporated in a finite element computer program; the operation of this program (which

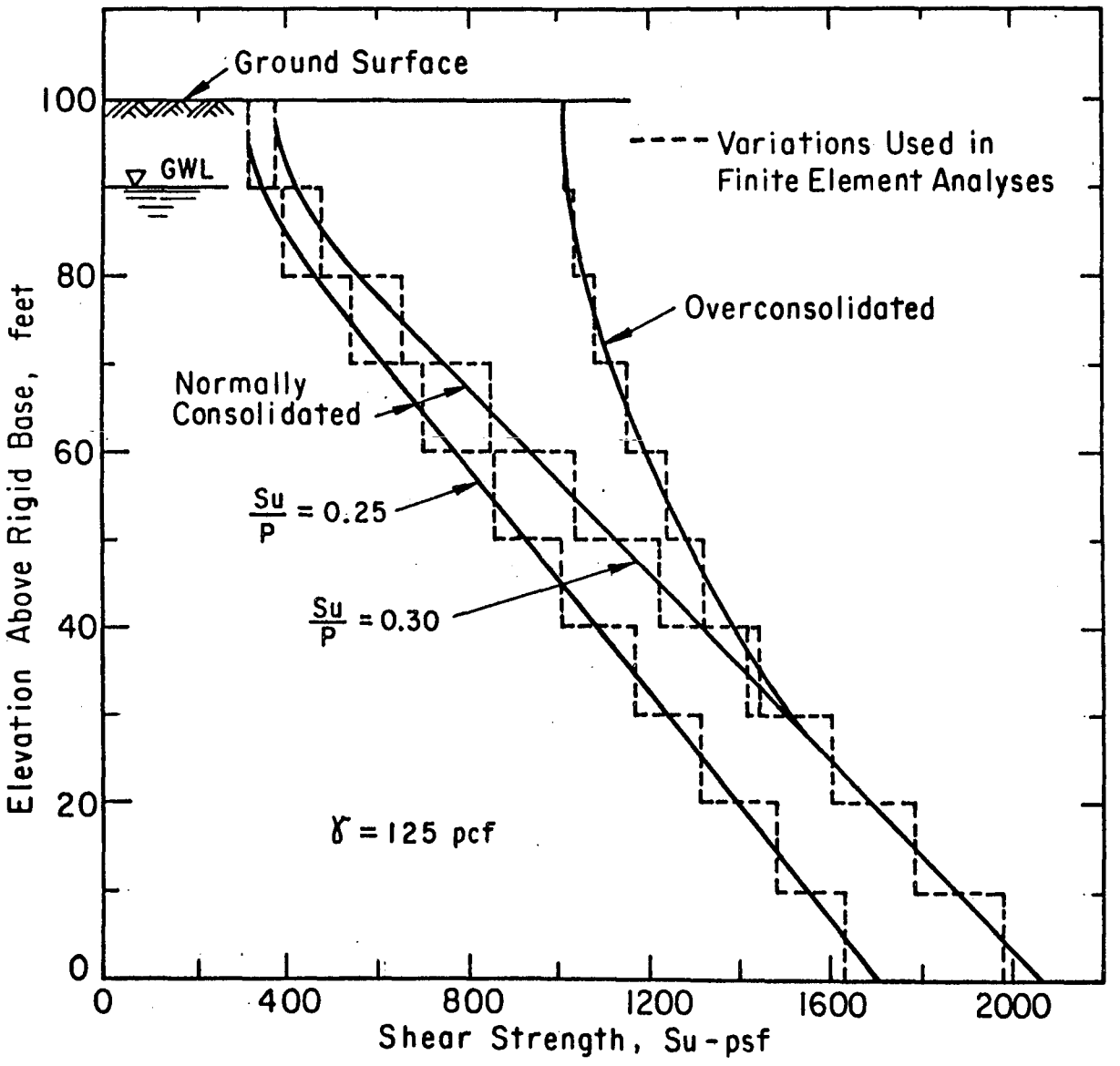

FIG. 17 STRENGTH VARIATION WITH DEPTH FOR BILINEAR SLOPE ANALYSES.

is included in Appendix C) is illustrated by the simplified flow diagram shown in Fig. 18. Data describing the positions of boundaries between layers and rows of elements, the unit weights, initial stress conditions, and the elastic and strength properties of the clay serve to define the problem. From these basic input data, the computer program calculates element numbers, nodal point coordinates and initial stress values for each element.

Using the initial stress values, the computer program then calculates the nodal point forces required to simulate excavation of the first layer of material. The modulus values of elements in the excavated zone are reduced to a very small value (typically 0.01 psf) and the modulus values of all other elements are set equal to the initial value prescribed for material at that depth. Using the assigned elastic properties, stiffness values are calculated for each element in the system, and the individual stiffness values are added into the structural stiffness matrix, which is appropriately modified for the specified force and displacement boundary conditions. The simultaneous equations (2 for each nodal point) represented by the stiffness matrix coefficients are then solved for the unknown displacements, which are printed by the computer. Subsequently, the changes in strain and stress are evaluated for each element, added to the initial values, and the resulting values are printed.

The excavation of additional layers is simulated in the same way, beginning with evaluation of the necessary nodal point forces to simulate removal of the next layer of elements.

Example of Bilinear Analysis

To illustrate the operation of this computer program, an analysis has been performed using a system containing 32 elements and 42 nodal points, as shown in Fig. 19. Each row of elements in this configuration was assigned a different material number, 1 for the top row through 4 for the bottom; the material properties associated with these material numbers are shown in Table 3. Material 5 is the number assigned to elements after failure, and material 6 is the number assigned to elements which are being or have been removed.

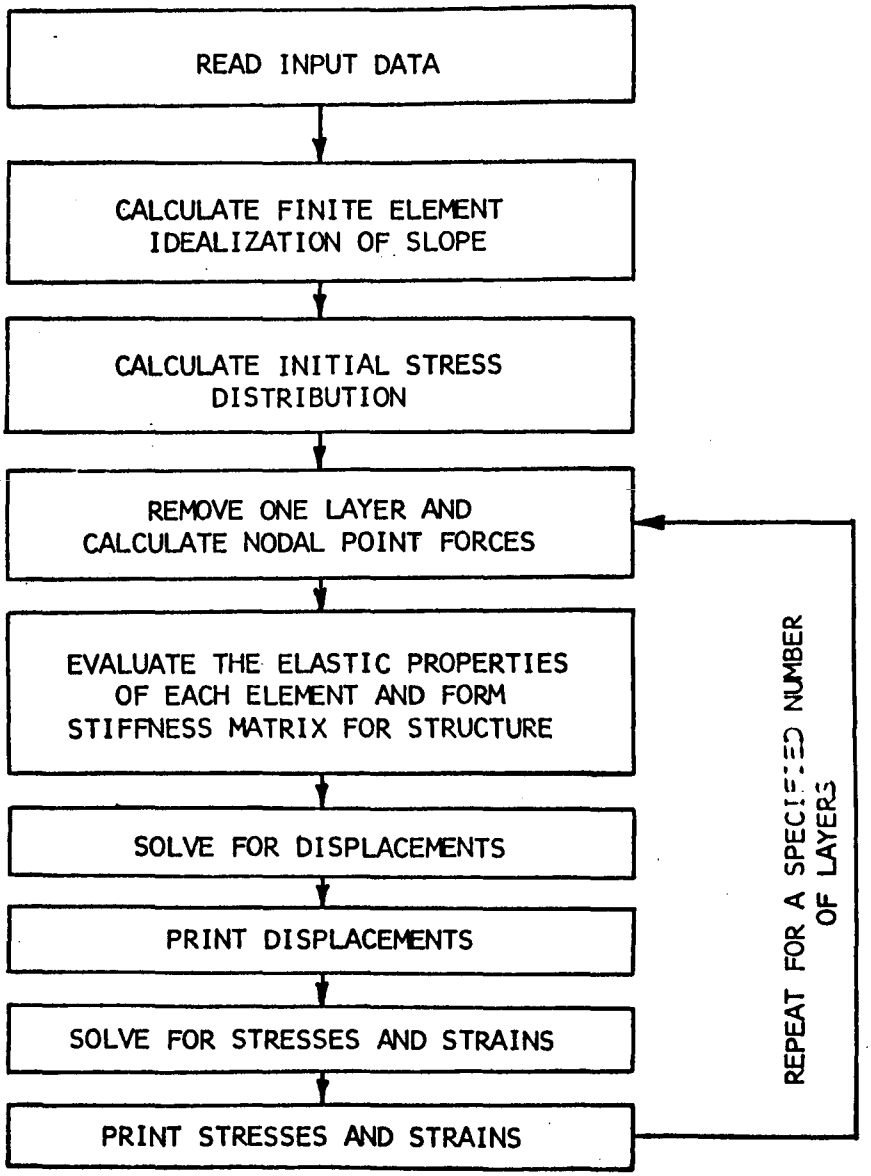

FIG. 18 SIMPLIFIED FLOW DIAGRAM FOR BILINEAR ELASTIC ANALYSES.

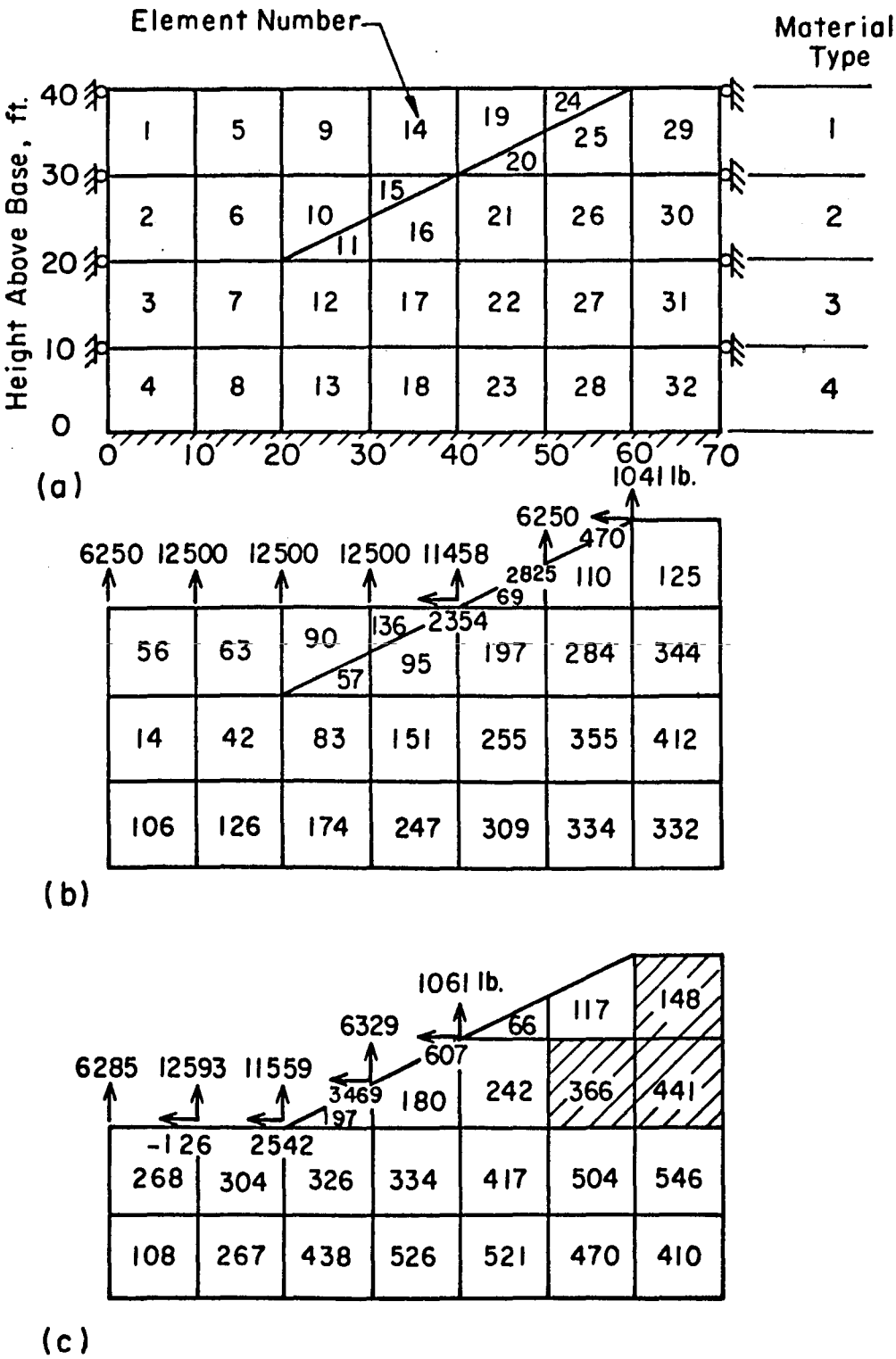

FIG. 19 EXAMPLE BILINEAR ANALYSIS.

Table 3. Material Numbers and Properties for Example Bilinear Analysis

Material	Weight pcf	Elastic Modulus psf	Poisson's Ratio	Undrained Strength psf	Coefficient of Earth Pressure
1	125	13000.	.475	130	.90
2	125	36000.	.475	360	.90
3	125	61000.	.475	610	.90
4	125	85000.	.475	850	.90
5	125	10.	.475	-	-
6	0	.01	.475	-	-

The equivalent nodal point forces on the boundary were calculated from the stresses in the elements adjoining the boundary and the reverse of these forces are shown in Fig. 19(b) for the removal of the first layer. The elements above the cut surface are changed from material type 1 to material type 6 simulating their removal. Elements below the cut surface have material types corresponding to their elevations. The configuration shown in Fig. 19(b) is then solved to determine nodal point displacements, and element strains and stresses. The values of stress after the first step were calculated by adding the stress changes from the construction step to the original stresses for the horizontal deposit. Maximum shear stress values at the end of the first construction step are shown in each element in Fig. 19(b). It may be seen that the maximum shear stress nowhere exceeds the strength and therefore no elements failed in the first cut step.

A second construction step was undertaken using as an initial condition the stresses at the end of the first step. The nodal point forces shown in Fig. 19(c) were calculated, and the second layer was "removed" (material type changed). The configuration shown in Fig. 19(c) was solved for displacements, strains and stresses. Again the stresses due to this step were added to those existing prior to the step (Fig. 19(b) and the maximum shear stresses calculated. The resulting values of

maximum shear stress are shown in the individual elements in Fig. 19(c). It may be seen that the values in elements 26, 29 and 30, shown shaded, exceed the specified shear strength values.

Thus, at the end of the second step, failure has occurred in three elements beneath the crest of the slope. Using the configuration shown in Fig. 19, it is not possible to continue the analysis further, because the element configuration beneath the base of the excavation is not suitable for further extension of the cut surface. If it were desired to investigate the continued development of the failed region as the excavation was made deeper, it would be necessary to use a new configuration to represent a deeper excavation.

Similar procedures, but using many more layers and elements were used for all the studies described in this section of the report.

The Effect of the Initial Stresses and Strength Variation with Depth

In order to differentiate between the effects of the initial stresses and the modulus variation it is convenient to consider each independently of the other. The resulting initial stresses and strength variation in any one analysis may not be consistent (i.e., a normally consolidated strength profile may not be consistent with an initial stress condition with K = 1.25), but, by examining the full range of combinations of variables it is possible to evaluate separately the effects of the initial stresses and strength profile on the slope behavior.

The effect of the initial stress conditions is illustrated by the analyses shown in Fig. 20. The normally consolidated strength profile shown in Fig. 17, with $S_u/p = 0.3$, was used in both of the analyses shown in Fig. 20, but initial stress conditions corresponding to K = 1.25 were used for the case shown on the left, while smaller initial stresses corresponding to K = 0.75 were used in the analysis illustrated on the right.

The upper configurations in Fig. 20 represent an early stage in the excavation process, when the 1.5:1 slope had been excavated to a depth of 10 ft in the 100 ft thick layer. Even at this early stage, a small region beneath the bottom of the excavation has failed for the case where the initial horizontal stresses are high. The other slope however, in

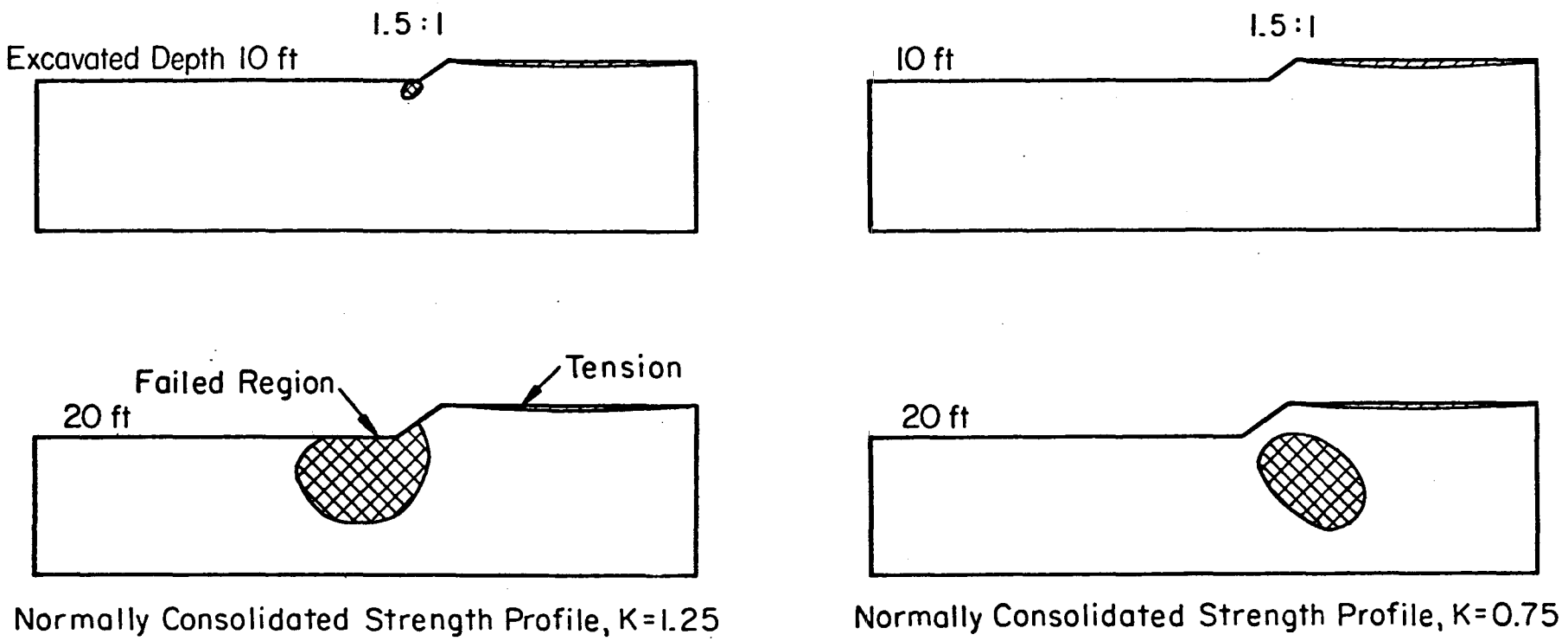

FIG. 20 EFFECT OF INITIAL STRESSES ON THE DEVELOPMENT OF FAILED REGIONS (Su/P = 0.30)

which the initial stresses are small, has not suffered any local failure at this stage. It may be noted that a small zone of tension has developed in both cases behind the crest, the maximum tensile stress value being somewhat larger for the case with higher initial stresses. Up to this point in the analyses, i.e. during the removal of the first layer, the analyses correspond to the linear elastic analyses described in the previous chapter, and the same results could have been determined using the results of those analyses, which also showed higher shear stress and tensile stress values for a deposit with larger initial horizontal stresses. Even the location of the first local failure could have been determined from the linear analyses. For the following step of the bilinear analyses, however, the modulus values within the small failure zone were reduced before the second layer was removed. The conditions after removal of the second layer, when the slopes were 20 ft. high, are shown by the lower configurations in Fig. 20. It may be noted that in both cases there is a failure zone of considerable size beneath the slopes at this stage. The magnitudes of the tensile stresses are also somewhat higher than they were following the first stage. For the case in which the initial stresses were larger, the failure zone is also larger and extends to the surface at the bottom of the excavation, whereas for smaller initial stresses the failure zone is entirely beneath the surface and extends behind the crest of the slope.

Although analysis of the slope on the right could be continued, it is not possible to do so for the slope on the left, because the failure zone after the second stage intersects the base of the excavation. Nodal point forces to simulate further excavation may be calculated as before, but application of these forces to nodal points in the failed zone, which now has a very low modulus value, will result in theoretical displacements of an extremely large order of magnitude, perhaps tens or hundreds of feet. Displacements of this order are obviously not realistic, and it is therefore not meaningful to continue the analysis beyond the stage shown. In a real slope containing a failure zone like the one shown, it would probably be observed that continued excavation would result in gradual bulging of soil in the base of the excavation, the phenomena which Terzaghi and Peck have described as "lost ground" (p. 520). Loss of

ground would probably result in relaxation of stress around the base until the shear stress values became compatible with the strength values, at which time the bulging would stop. Using the analytical procedures adapted for this investigation, however, it is not possible to simulate this redistribution of stresses, and the analyses must be terminated once the failure zone encompasses nodal points to which forces must be applied during the next stage.

While it is unfortunate that the analyses cannot be continued to a stage where overall failure of the slope is imininant or has occurred, it is interesting to observe that heaving near the toe of slopes has been observed in excavations in overconsolidated clays containing high initial horizontal stresses. For example, Bjerrum (1967) has reported that the operation of a clay pit near Sandnes, Norway was particularly convenient for the owners because the pit, which was excavated in summers, was always found to have filled itself with clay squeezing up from the bottom during the winter. During the time the pit was operated a large landslide developed on the adjacent hill, with the lower end of the sliding surface intersecting the bottom of the clay pit. In excavations in overconsolidated clays, bulging near the toe of the slope may precede the full development of a sliding surface, and catastrophic failure of the slope.

To determine the influence of the variation of strength with depth, two analyses have been performed, the results of which are shown in Fig. 21. In the case illustrated on the left, the strength of the clay is constant throughout the depth of the layer, and for the case on the right the strength increases linearly with depth, from zero at the surface. Both cases were analyzed using the same initial stress conditions, corresponding to $K = 0.90$.

After the first stage of excavation, when the 3:1 slopes are 10 ft high, a zone of tension has developed behind the crest of the slope in the layer with constant strength, and a sizable failure zone has formed around the slope in the layer with strength increasing with depth. Although this zone intersects the surface of the excavation, it does not wholly encompass any nodal points to which forces must be applied during the next stage, so the analysis can be continued.

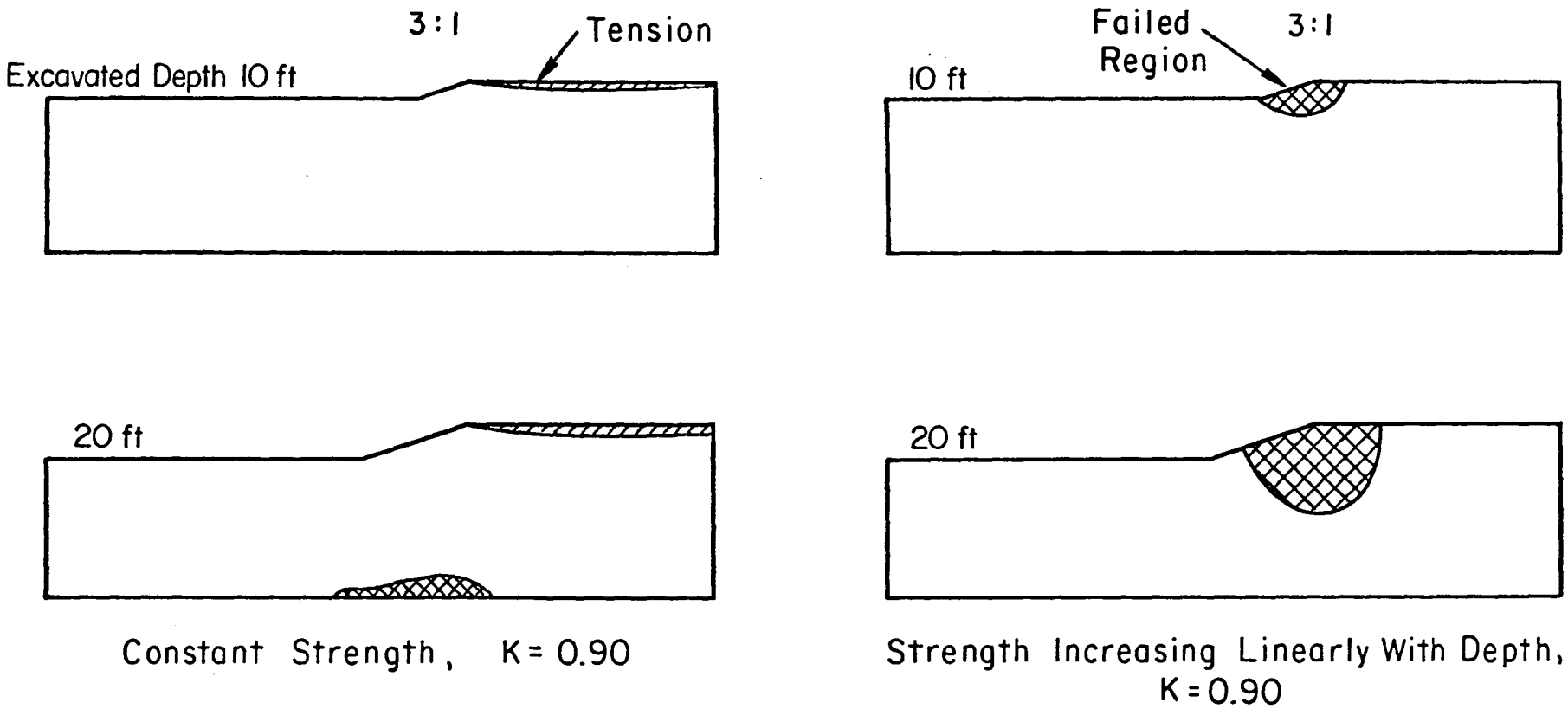

FIG. 21 EFFECT OF STRENGTH VARIATION WITH DEPTH ON THE DEVELOPMENT OF FAILED REGIONS.

At the next stage, when the slopes are 20 ft high, the size of the tension zone has increased, and failure has developed at the bottom of the layer with constant strength. The size of the failure zone around the slope in the layer with strength increasing with depth has increased approximately in proportion with the increase in slope height.

These analyses indicate that the principal effects of strength (and modulus) variation with depth are concerned with the development of tensile stresses and the location where shear failure occurs. The results shown in Fig. 21 are in qualitative agreement with the results of equilibrium methods of stability analysis for the two strength profiles considered: Taylor (1937) found that, when the shear strength is constant throughout the depth of the layer, the critical circle for flat slopes always extends to the base of the layer, which is in agreement with the fact that failure occurs first at the base of the layer according to the bilinear analysis. Kenney (1963), on the other hand, found that the factor of safety of a slope was independent of the slope height when the shear strength increases linearly with depth from zero at the surface; the bilinear analysis shows that the size of the failure zone increases approximately in proportion to the slope height, and remains about the same shape. Kenney also found that toe circles and slope circles are most critical when strength increase with depth, which is consistent with the formation of a shallow zone of failure in the bilinear analyses. It seems likely therefore that the analytical procedure adopted is capable of providing a means of studying the development of zones of failure around slopes.

Failure Zones Around Slopes in Normally Consolidated and Overconsolidated Clays

While the analyses described in the previous section indicate very clearly the various effects of initial stress conditions and strength variation with depth, the cases analyzed are not necessarily representative of the behavior of slopes in either normally consolidated or overconsolidated clay layers. For example, although it is clear from the previous analyses that higher values of initial horizontal stress, characteristic of overconsolidated clays, will result in higher values of shear stress, it is also apparent that overconsolidated clays are stronger than normally

consolidated clays; thus the effect of higher shear stresses may be offset by higher shear strength. To study the effects of initial stress and strength variations with depth in realistic combinations, several slope analyses have been performed using initial stress conditions and strength profiles characteristic of normally consolidated and overconsolidated clays.

The strength profiles used in these analyses were the two normally consolidated profiles shown in Fig. 17 for $S_u/p = 0.25$ and $S_u/p = 0.30$, and the overconsolidated profile shown in the same figure. In all cases initial stress conditions corresponding to $K = 0.75$ were used with the normally consolidated strength profiles, and $K = 1.25$ was used with the overconsolidated strength profile.

Four stages during the excavation of 3:1 slopes in overconsolidated and normally consolidated ($S_u/p = 0.30$) clay layers are illustrated in Fig. 22. During excavation of the first 10 ft layer, small tension zones develop behind the crest of both slopes, but no shear failure occurs. During excavation of the second 10 ft layer, a small failure zone develops beneath the crest of the slope in overconsolidated clay, but the slope in overconsolidated clay remains completely stable. Upon excavation of the next layer, the failure zone in the normally consolidated layer increases in size, and a fairly large failure zone extending from the base of the excavation to the bottom of the layer develops in the overconsolidated layer. Because this zone encompasses only a very small area on the excavated surface at this stage, however, it was possible to simulate the excavation of an additional 10 ft of clay, as shown in the bottom of Fig. 22; it may be noted that the failure zones in both layers have reached a considerable size by the time the excavations are 40 ft deep. Both failure zones intersect the base of the layer at this stage, but they extend upward in different directions. The one in the overconsolidated clay extends upward to the bottom of the excavation and the lower portion of the slope, but the failure zone in the normally consolidated layer extends up toward the surface behind the crest of the slope, but does not intersect the surface.

In neither of the cases shown in Fig. 22 does the failure surface intersect the surface of the slope in such a way as to suggest development of a curved surface of sliding. Because the failure zone encompasses

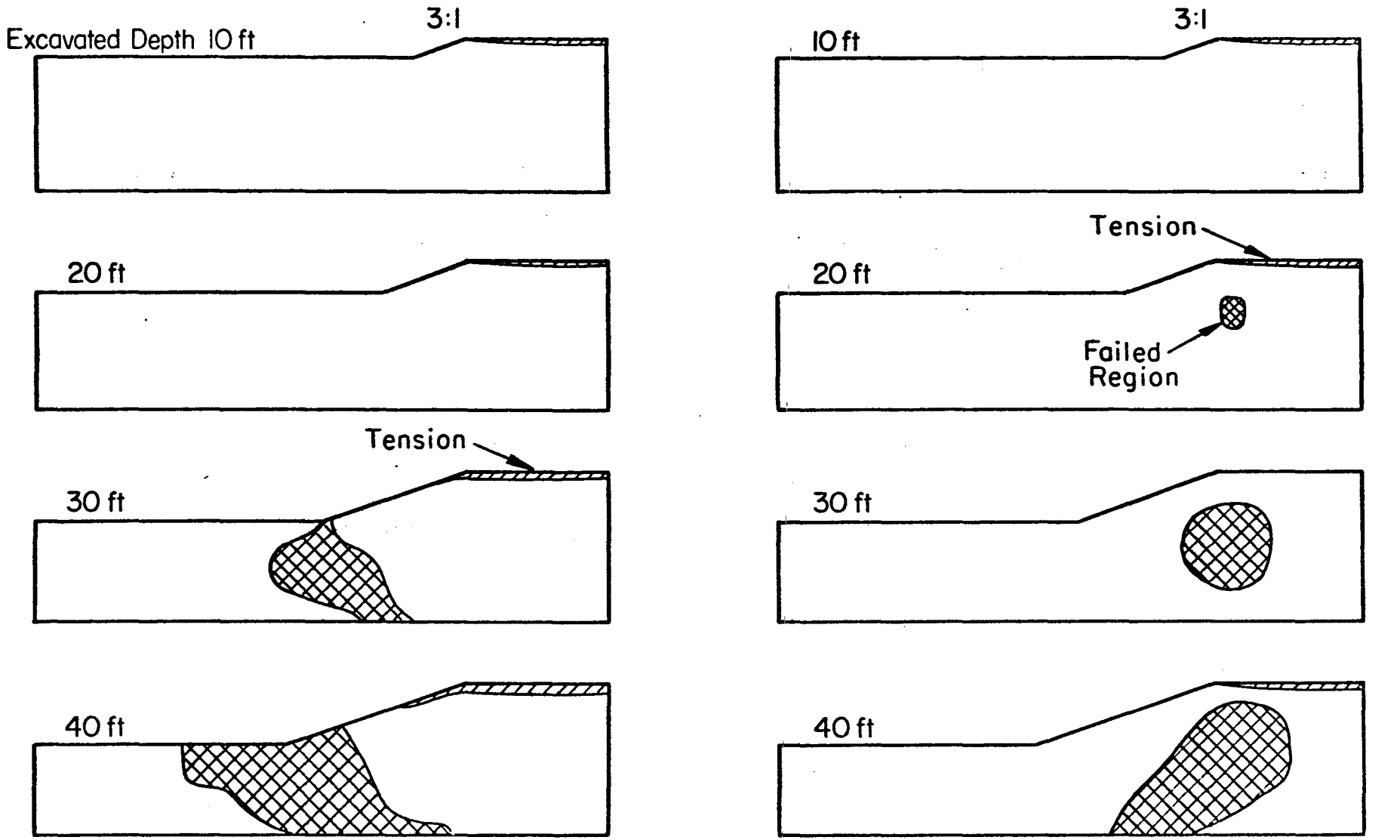

FIG. 22 DEVELOPMENT OF FAILURE ZONES AROUND A 3:1 SLOPE IN OVERCONSOLIDATED AND NORMALLY CONSOLIDATED CLAY LAYERS.

a considerable area in the bottom of the slope in overconsolidated clay, however, it was necessary to terminate the analysis at the stage shown. As mentioned previously, practical difficulties might be experienced in extending a real excavation beyond this stage, because of loss of ground.

In determining zones of failure, only shear failure has been considered. It may be noted, however, that tension zones of considerable size have developed behind both slopes by the time the slopes are 40 ft high. Tension failure in these zones would result in formation of cracks which would also influence the overall stability of the slopes.

Comparisons of steeper slopes in normally consolidated and overconsolidated clay layers are shown in Fig. 23. The development of failure zones around these 1.5:1 slopes is qualitatively very similar to the 3:1 slopes discussed previously, but at each stage the extent of the failure zones and the tension zones are larger than in the case of the flatter slopes. As before, the analysis of the slope in overconsolidated clay could not be continued beyond the stage shown because the failure zone encompasses a large area along the lower portion of the slope and in the bottom of the excavation.

In order to study the influence of the value of S_u/p on the extent of the failure zone around slopes in normally consolidated clays, analyses were made of 3:1 slopes excavated in clay layers with the two normally consolidated strength profiles shown in Fig. 17. The results of these analyses are shown in Fig. 24, for the 6 stages involved in excavation to a depth of 60 ft. The series of steps on the left represent the progressive development of failure in a clay layer with $S_u/p = 0.30$, and those on the right show the development of failure in a clay layer with $S_u/p = 0.25$. At each stage in the excavation process the failure zones are larger for the lower strength values, as would be expected. In both cases failure occurs first below and behind the crest of the slope, then extends down to the bottom of the clay layer and out under the toe of the slope as excavation proceeds. In the case of the weaker clay layer, the failure zone also extends up to the surface behind the crest of the slope. The last stage shown for the case in which S_u/p was equal to 0.25 represents a condition strongly resembling the development of a curved sliding surface.

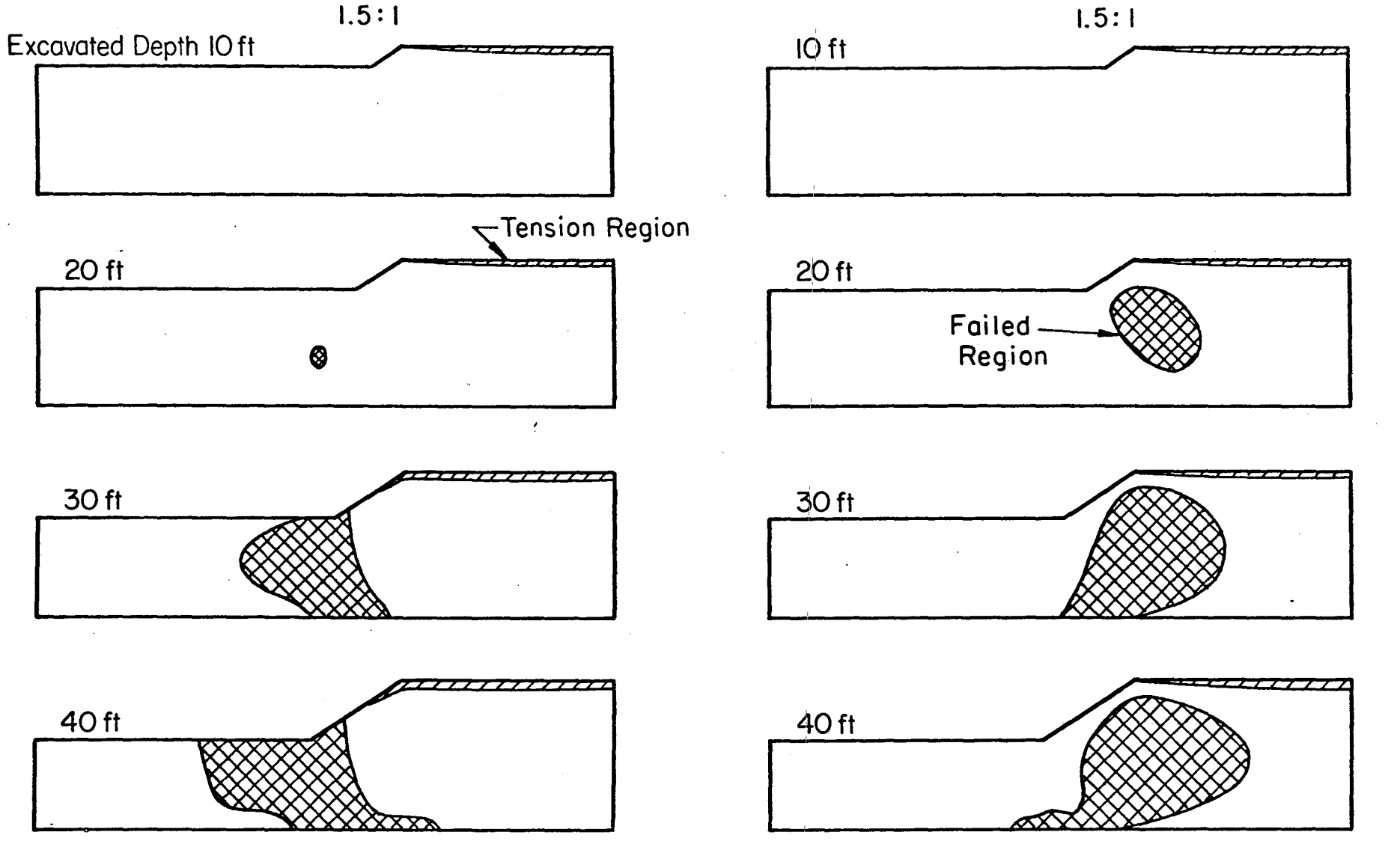

FIG. 23 DEVELOPMENT OF FAILURE ZONES AROUND A 1.5:1 SLOPE IN OVERCONSOLIDATED AND NORMALLY CONSOLIDATED CLAY LAYERS.

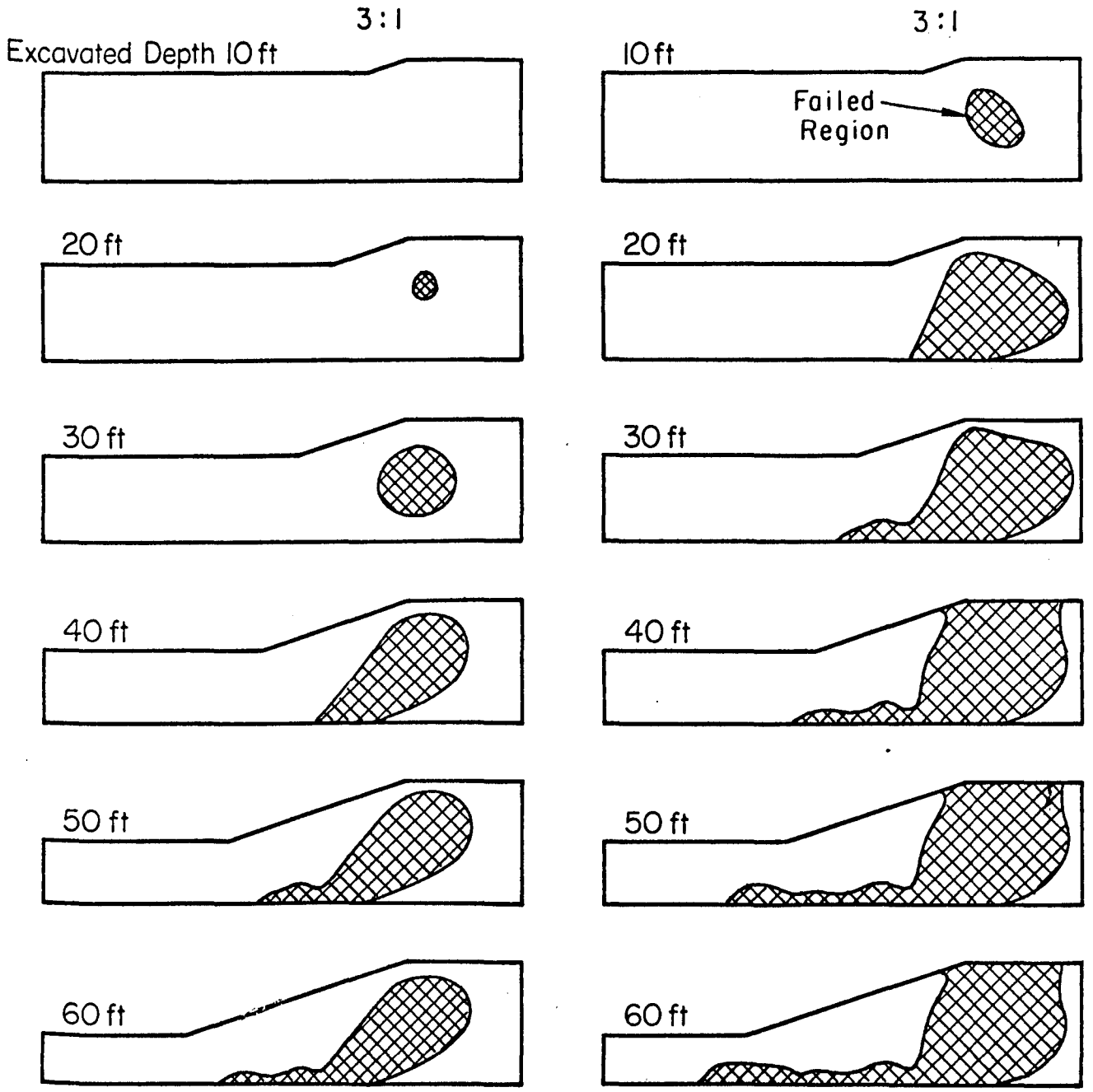

FIG. 24 DEVELOPMENT OF FAILURE ZONES AROUND 3:1 SLOPES IN TWO NORMALLY CONSOLIDATED CLAY LAYERS WITH Su/P=0.30 AND Su/P = 0.25

The Effect of Compressibility on Slope Behavior

The values of bulk modulus, K, and Young's modulus, E, for isotropic elastic materials are related to each other by the value of Poisson's ratio, as shown by equation 8 below:

$$K = \frac{E}{3(1 - 2\nu)} \tag{8}$$

Thus if the value of Young's modulus is reduced following failure while the value of Poisson's ratio remains unchanged, the value of bulk modulus is reduced in the same proportion as the value of Young's modulus. It has been noted that the use of this procedure often reduces the bulk modulus value sufficiently that appreciable volume changes occur in the failure zone during subsequent steps of the analyses.

This type of behavior does not appear to be consistent with the expected behavior of saturated clays: It seems logical to assume that the bulk compressibility of clay under undrained conditions depends primarily on its degree of saturation and not upon the values of shear stress or shear strain to which the clay has been subjected. Therefore it seems likely that the bulk compressibility of the clay should be the same after failure as before.

In order to simulate this aspect of clay behavior in slope analyses it is necessary to use values of bulk modulus in the failure zone which are several orders of magnitude larger than the values of Young's modulus, and the corresponding values of Poisson's ratio for the failure zones are very nearly equal to one-half. Conventional plane strain finite element computer programs cannot be used with values of Poisson's ratio larger than about 0.49, but special formulations have been developed (Herman and Toms, 1964) which may be used with even completely incompressible materials, corresponding to Poisson's ratio equal to one-half. These programs are considerably more expensive to use than conventional finite element programs, requiring about 70% more time for solution of a given problem. In spite of the additional expense, some of the slope analyses described previously were performed using constant values of bulk modulus, or using values of Poisson's ratio equal to one-half, in order to determine if the change in bulk compressibility after failure had any significant influence on the results.

In the analyses performed using a constant value of bulk modulus, the value selected was one-tenth of the bulk modulus of water (5×10^6 psf), which would be appropriate to simulate the bulk compressibility of clay having a degree of saturation between 99% and 100%. The values of Poisson's ratio required to achieve this constant value of bulk modulus varied between 0.498 and 0.49999.

A comparison of two analyses of a 3:1 slope in a clay layer with constant shear strength throughout the depth of the layer is shown in Fig. 25. In the analysis illustrated on the left, the value of Poisson's ratio was constant throughout, so that the bulk modulus in the failure zone was reduced in the same proportion as Young's modulus after failure. The analysis illustrated on the right was conducted using a constant value of bulk modulus (5×10^6 psf) both before and after failure. It may be noted that the behavior of the two slopes is essentially the same, except that failure occurs at the toe of the slope at an earlier stage in the analysis performed using a constant value of poisson's ratio. This difference is relatively minor when compared to the extent of the regions already failed, and in the final stage shown in Fig. 25, there is almost no difference between the failure zones as determined by the two analyses.

A similar comparison is shown in Fig. 26 for 1.5:1 slopes excavated in normally consolidated clay layers with $S_u/p = 0.30$. As opposed to the comparison shown in Fig. 25, in which the failure zone was somewhat more extensive for the analysis performed using a constant value of Poisson's ratio, the failure region in this case is somewhat larger for the case in which the bulk modulus was constant, especially following the third and fourth stages of excavation. After the last stage shown, when the slopes are 70 ft high, there is little difference between the results of the two analyses except that the one conducted using a constant value of Poisson's ratio is continuous from the base of the excavation to the surface behind the crest of the slope, whereas in the analysis performed using a constant value of bulk modulus, the failure zone emerges on the surface of the slope near the top and the bottom. Additional results for the final stage of these same two analyses are shown in Fig. 27. It may again be noted that although there are some differences between the shear strain, principal stress orientations and deformed shapes for the two cases, the

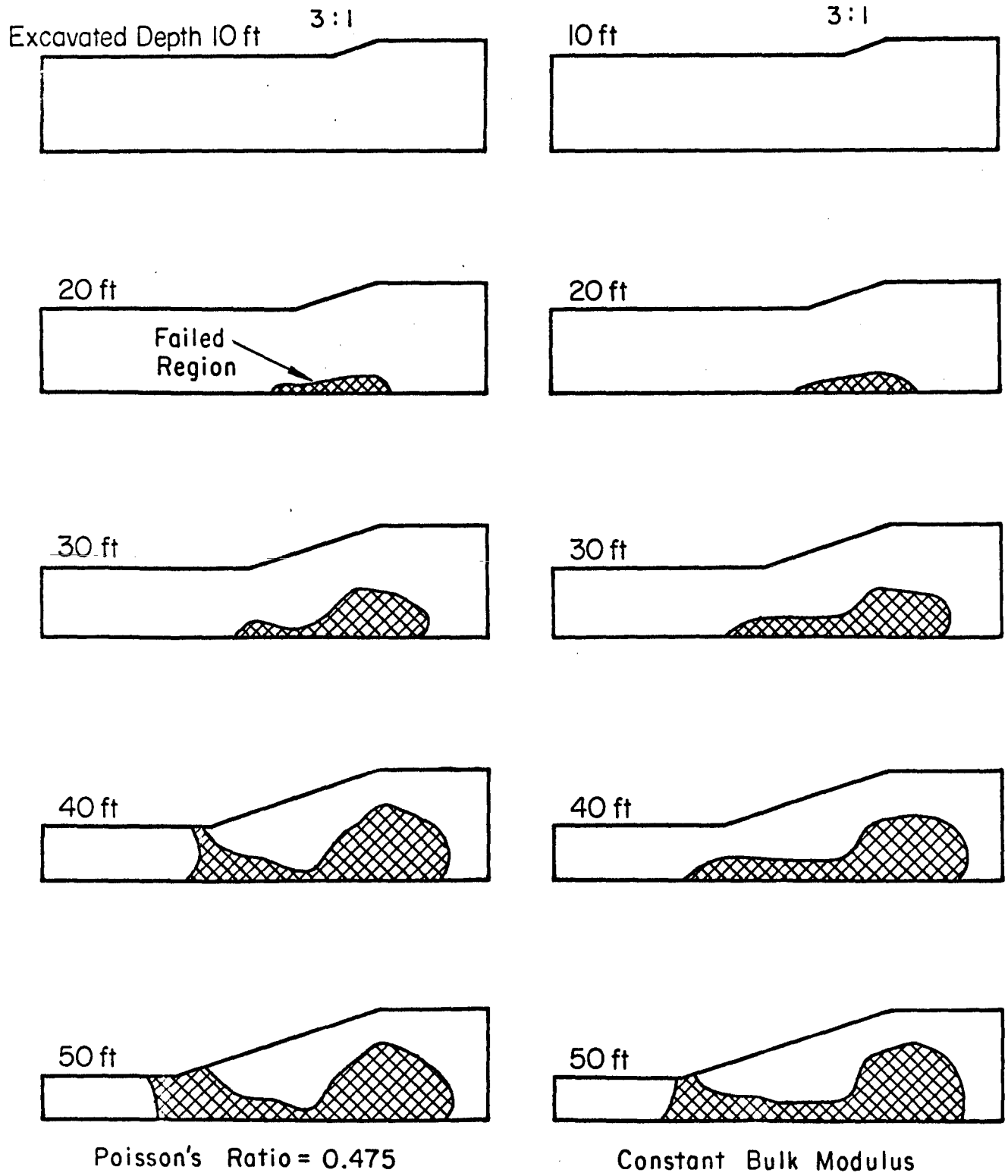

FIG. 25 EFFECT OF BULK COMPRESSIBILITY ON DEVELOPMENT OF FAILURE ZONES AROUND A 3:1 SLOPE IN CLAY WITH CONSTANT SHEAR STRENGTH.

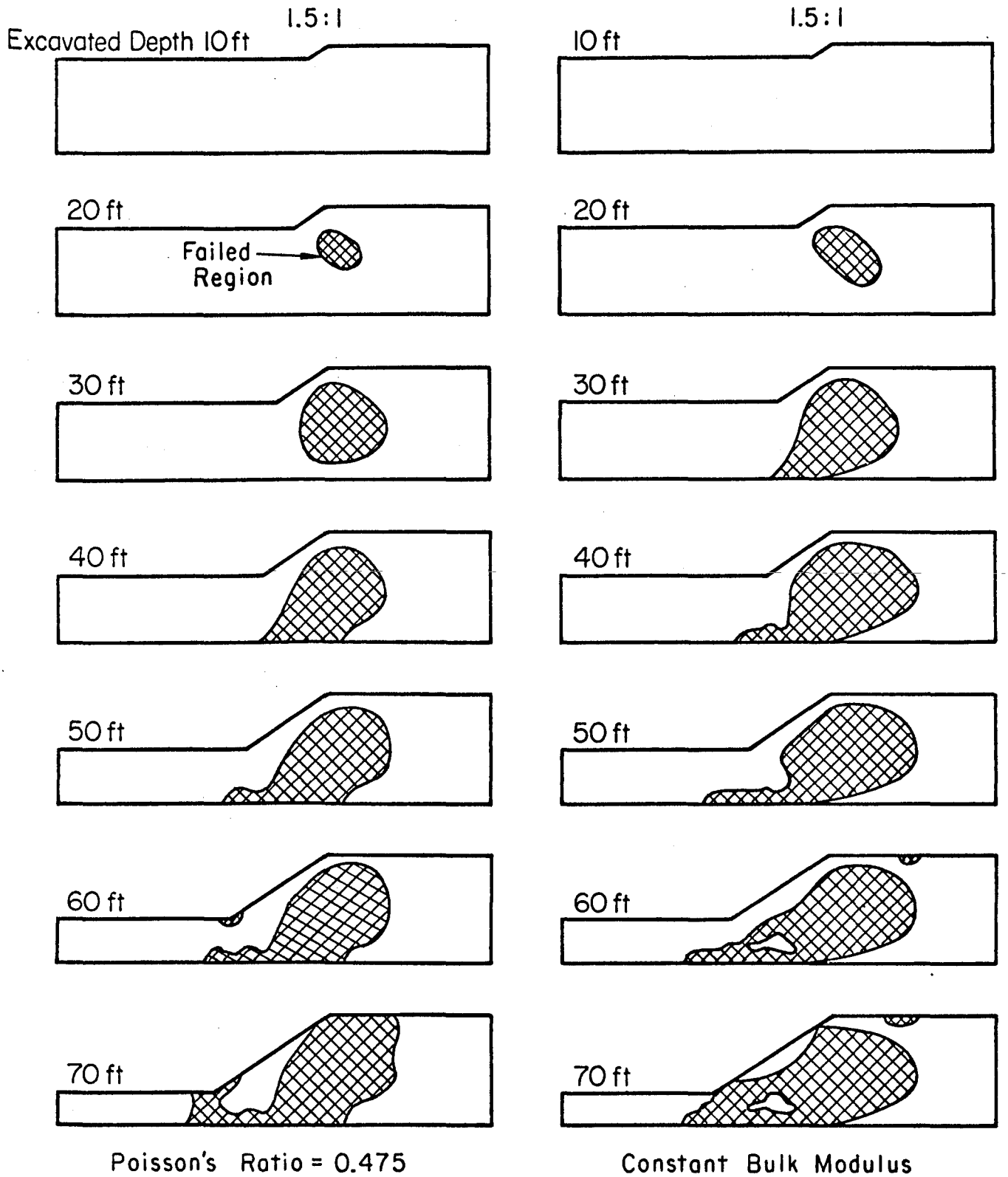

FIG. 26 EFFECT OF BULK COMPRESSIBILITY ON DEVELOPMENT OF FAILURE ZONES AROUND A 1.5:1 SLOPE IN NORMALLY CONSOLIDATED CLAY WITH Su/P = 0.30

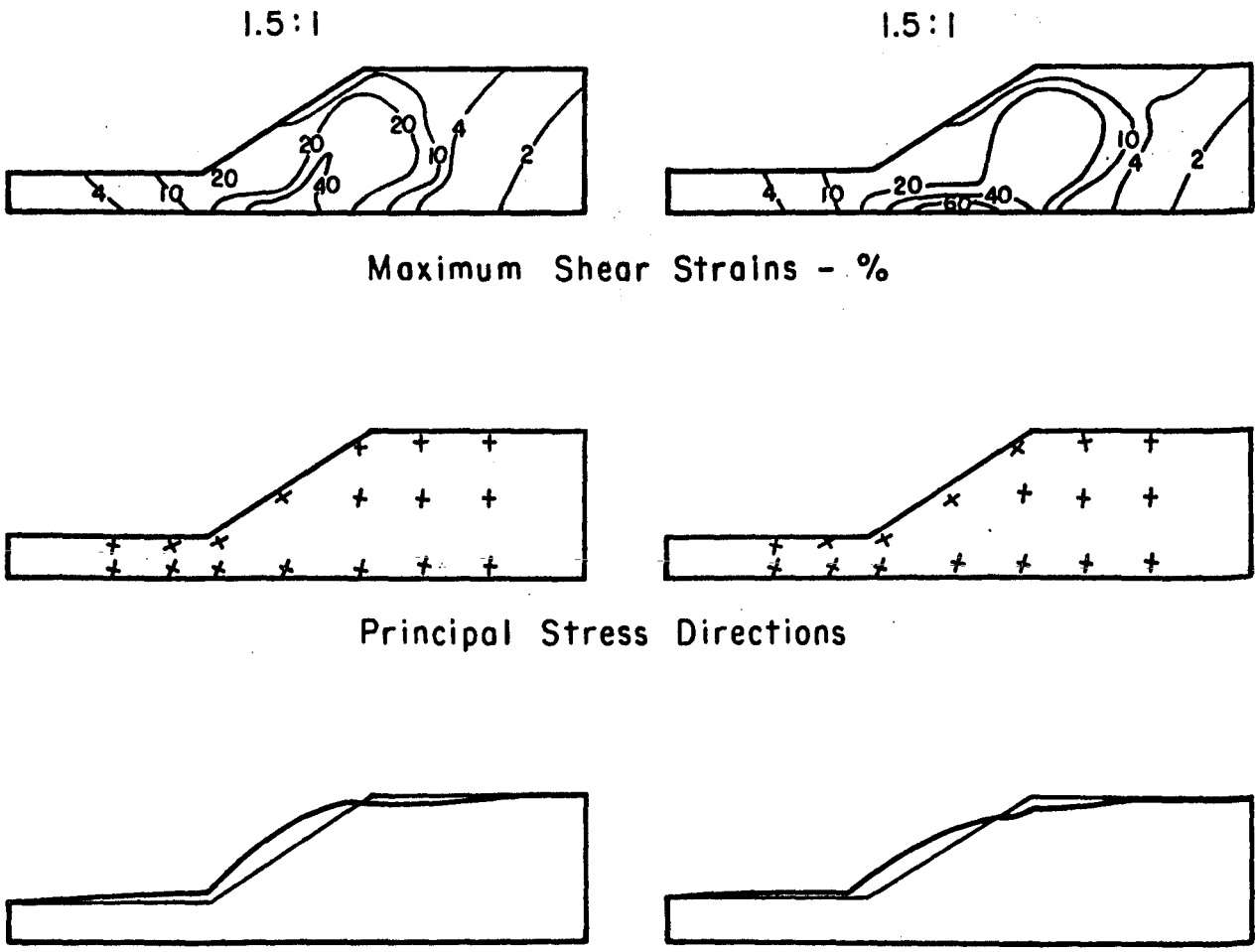

FIG. 27 EFFECT OF BULK COMPRESSIBILITY ON MAXIMUM SHEAR STRAINS, PRINCIPAL STRESS ORIENTATIONS AND DEFORMATIONS AROUND A 1.5:1 SLOPE IN NORMALLY CONSOLIDATED CLAY WITH $S_u/P = 0.30$

behavior as analyzed using either method is essentially the same.

It may be noted that the strain contours in Fig. 27 indicate values of shear strain as large as 60% in the failure zone near the base of the clay layer. Although strains of this magnitude are not consistent with the small strain theory used in the analyses, these extremely large strains occurred only in the failed regions where changes in shear stress are very small; therefore it would be expected that the resultant errors in calculated changes in stress in the unfailed regions would also be small. Furthermore, the geometry of each element was generally changed after each step in accordance with the displacements calculated on the previous step, thereby accounting for nonlinearity due to changes in configuration as suggested by Clough (1965). Using this approach it is the incremental strain values which should be compared to the acceptable values consistent with small strain theory; the maximum incremental values are only about 10%, considerably smaller than the cumulative values shown in Fig. 27. The use of small strain theory in soil mechanics analyses has been discussed by Clough and Woodward (1967) who suggest that the resulting errors are not significant for strain values less than 5% or 10%. Thus while some degree of error must undoubtedly arise from the use of small strain theory in these slope analysis problems, it is believed that the error is not very important, because the largest strains occur in the failed regions where stresses remain almost constant after failure.

In order to further study the influence of bulk compressibility, the behavior of 1.5:1 slopes excavated in a layer of overconsolidated clay were analyzed using values of Poisson's ratio equal to 0.475 and 0.500, the latter value corresponding to an infinite value of bulk modulus and completely incompressible material. The results of these analyses are shown in Fig. 28. The failure zones, shown in the upper part of the figure are similar for both analyses; no failure occurred after excavation of the first layer, but a sizable failure zone developed beneath the toe of the slope following excavation of the second step. The zones determined in the two analyses are similar in shape but slightly larger for the analysis in which Poisson's ratio was equal to 0.475, as was the case for the comparison illustrated in Fig. 26. The values of

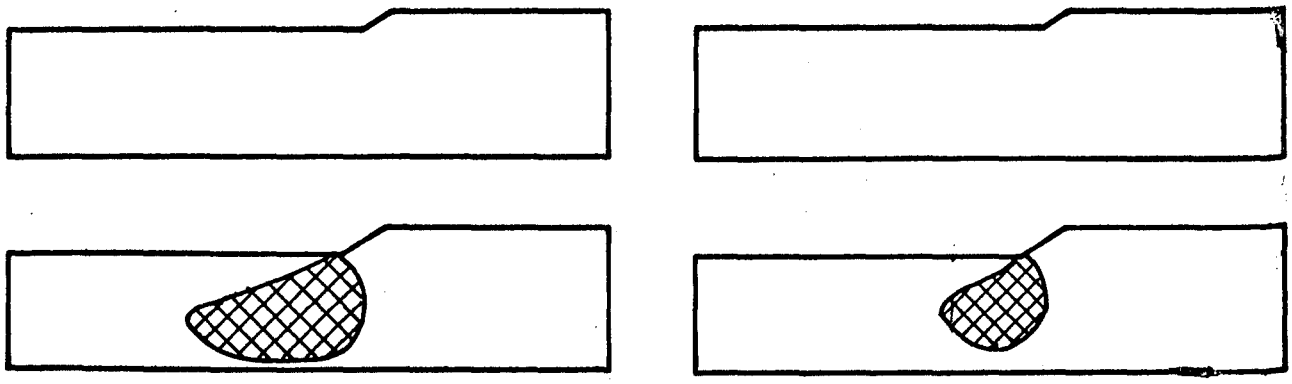

Failure Zones

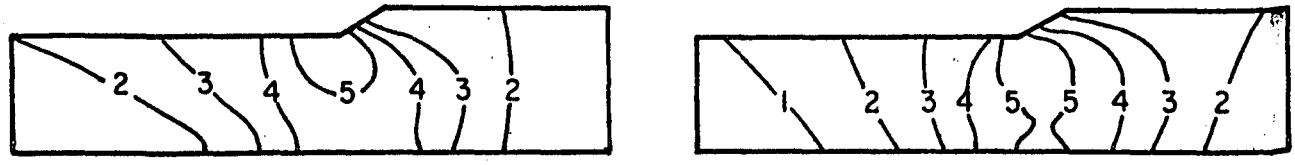

Maximum Shear Strains, %

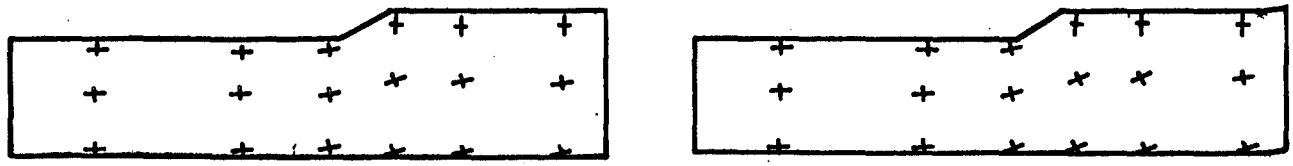

Principal Stress Directions

Poisson's Ratio = 0.475, K = 1.25
Overconsolidated Strength Profile

Poisson's Ratio = 0.500, K = 1.25
Overconsolidated Strength Profile

FIG. 28 EFFECT OF BULK COMPRESSIBILITY ON FAILURE ZONES, MAXIMUM SHEAR STRAINS AND STRESS ORIENTATIONS AROUND 1.5:1 SLOPES IN OVERCONSOLIDATED CLAY.

maximum shear strain and the stress orientations, which are also shown in Fig. 28, are virtually the same for both analyses.

On the basis of these analyses it was concluded that the differences between the results of analyses conducted using a value of Poisson's ratio equal to 0.475, and the results of analyses performed with constant value of bulk modulus or incompressible material were not significant. Certainly the overall behavior is not changed, and it appears that in some cases the failure zones are larger for $\nu = 0.475$ (the 4th and 5th steps in Fig. 25) while in other cases they are larger for constant bulk modulus (the 3rd, 4th, and 5th steps in Fig. 26). Thus there seems to be little reason to believe that it is necessary to use more complex and expensive computer programs formulated for incompressible materials.

Slope Stability

Although the bilinear analyses illustrate in a graphic manner the development and growth of failure zones around slopes, it is difficult to assess the degree of stability of the slopes against catastrophic overall failure on the basis of these results. In order to obtain a quantitative measure of the stability of the slopes, they have also been analyzed using the "$\phi = 0$" equilibrium method with circular arc trial failure surfaces.

The last two steps in the analysis of one of the slopes described previously are shown in Fig. 29; the stages shown represent the extent of the failure zone when the slope was 40 ft high and 50 ft high. The slope inclination was 3:1 and the assigned value of shear strength was constant throughout the depth of the deposit. The bilinear analysis was performed using a constant value of bulk modulus, $K = 5 \times 10^6$ psf. Because the shear strength is constant throughout the depth and the slope is fairly flat, the critical circular arc intersects the hard layer at the bottom of the clay. The critical circles for both conditions are shown on the figure. The values of factor of safety shown on the figure were calculated using the mobilized values of shear strength in the failure zone, which were higher than the assigned shear strength value because of overshoot. Comparisons of the mobilized and assigned values of shear strength are shown in the lower part of Fig. 29 for the last stage of the

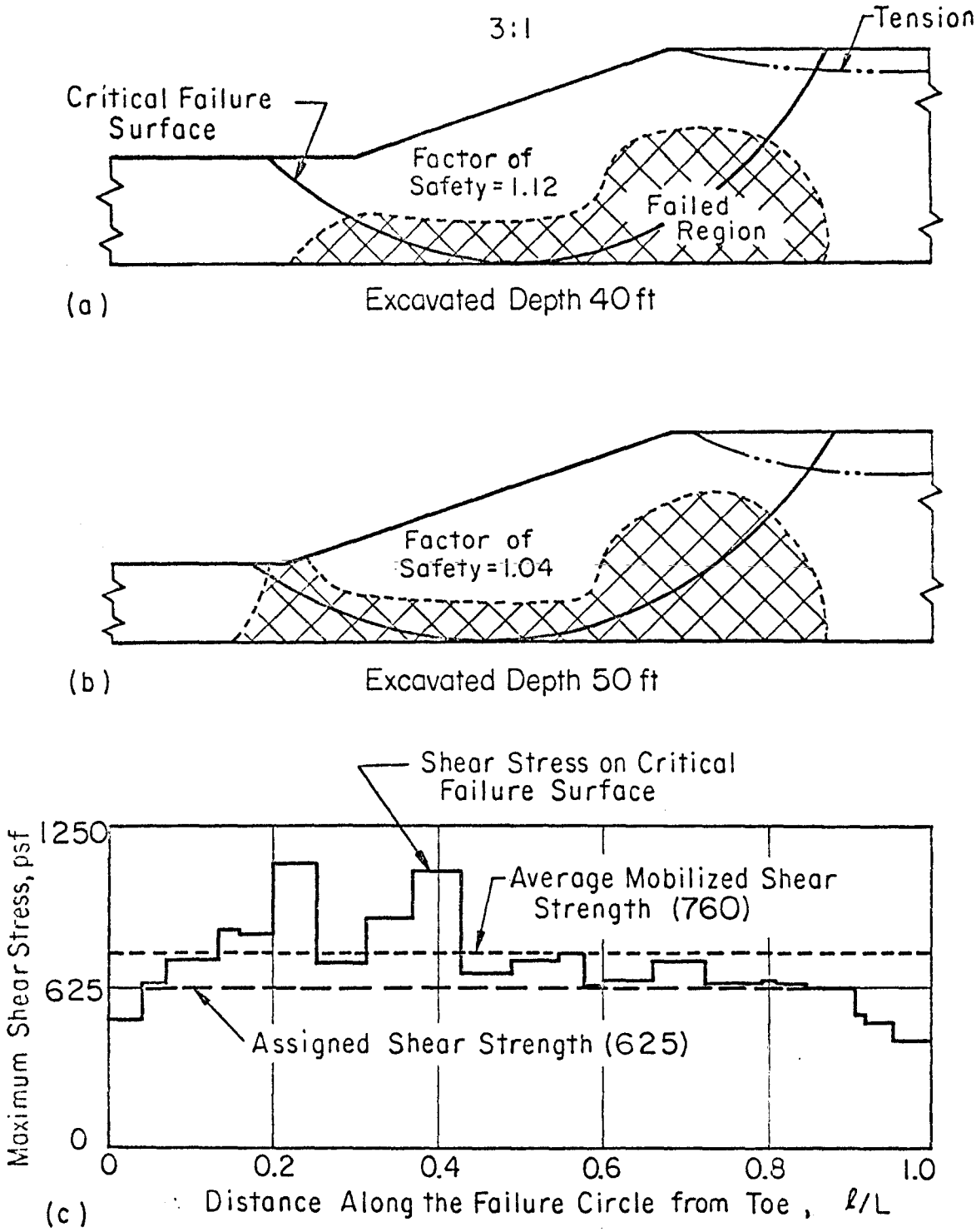

FIG. 29 CORRELATION BETWEEN FAILURE ZONES AND FACTOR OF SAFETY FOR A 3:1 SLOPE IN A CLAY LAYER WITH CONSTANT SHEAR STRENGTH.

analysis. It may be noted that the mobilized shear strength exceeds the assigned value by a considerable amount beneath the lower part of the slope, and the average value of mobilized strength is 760 psf compared to the assigned value, 625 psf. Thus the average amount of overshoot amounts to more than 20%. This particular analysis was performed using 8 layers, which are too few to prevent a large amount of overshoot. In subsequent analyses, performed using 10 layers, the amount of overshoot was much less.

The values of factor of safety shown in the figure, 1.12 for the next-to-last stage in the analysis, and 1.04 for the last stage, indicate that the slope is close to catastrophic failure for both stages even though the failure zone does not encompass the entire length of the critical arc. This might be expected, however, because even outside the failure zone the mobilized shear stress values were very nearly equal to the shear strength.

The final two stages in the excavation of a 1.5:1 slope in a normally consolidated clay layer with $S_u/p = 0.30$ are shown in Fig. 30. The bilinear analysis was conducted using a constant value of bulk modulus, $K = 5 \times 10^6$ psf. The slope configuration consisted of 10 layers each 10 ft thick, and at the stages shown in Fig. 30 the slope was 60 ft high and 70 ft high. For both cases the critical circular arc passes through the toe of the slope, and lies for the most part within the failure zone.

The factors of safety shown in the figure were calculated using the mobilized shear stress values which, as in the case illustrated in Fig. 29, are somewhat in excess of the assigned shear strength values. It is apparent, however, that the amount of overshoot is considerably less in this case, amounting to only about 5% or 10% on the average. For the next-to-last stage, shown at the top of Fig. 30, the calculated value of factor of safety is only 1.01, even though the failure zone beneath the slope has not yet intersected the surface. In the last stage the failure zone has intersected the surface at both the top and the bottom of the slope, and the factor of safety against failure on the most critical circular arc is less than one.

A similar analysis for a 3:1 slope excavated in an overconsolidated clay layer is shown in Fig. 31. At the stages illustrated this slope was

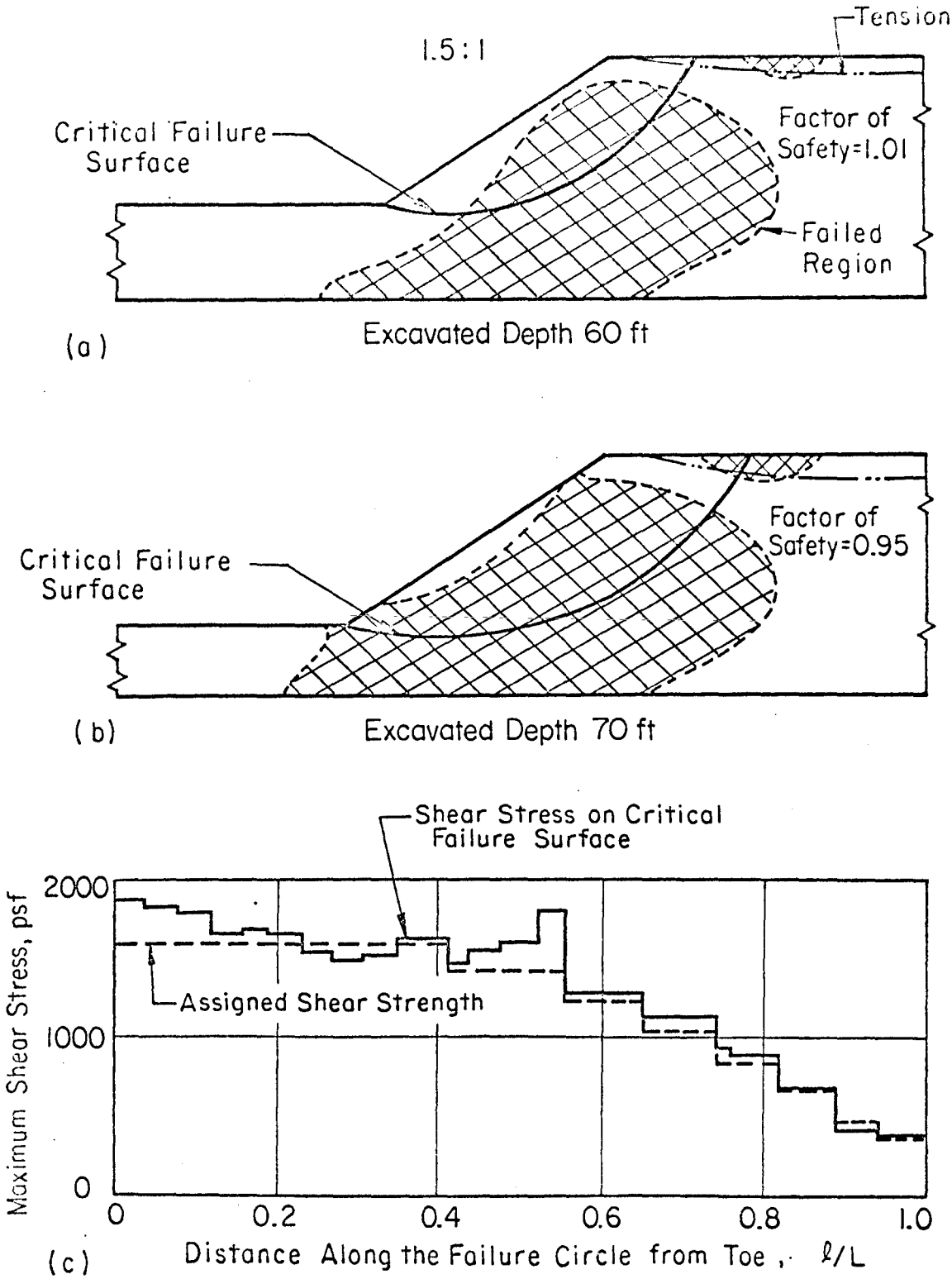

FIG. 30 CORRELATION BETWEEN FAILURE ZONES AND FACTOR OF SAFETY FOR A 1.5:1 SLOPE IN A NORMALLY CONSOLIDATED CLAY LAYER WITH $S_u/P \doteq 0.30$

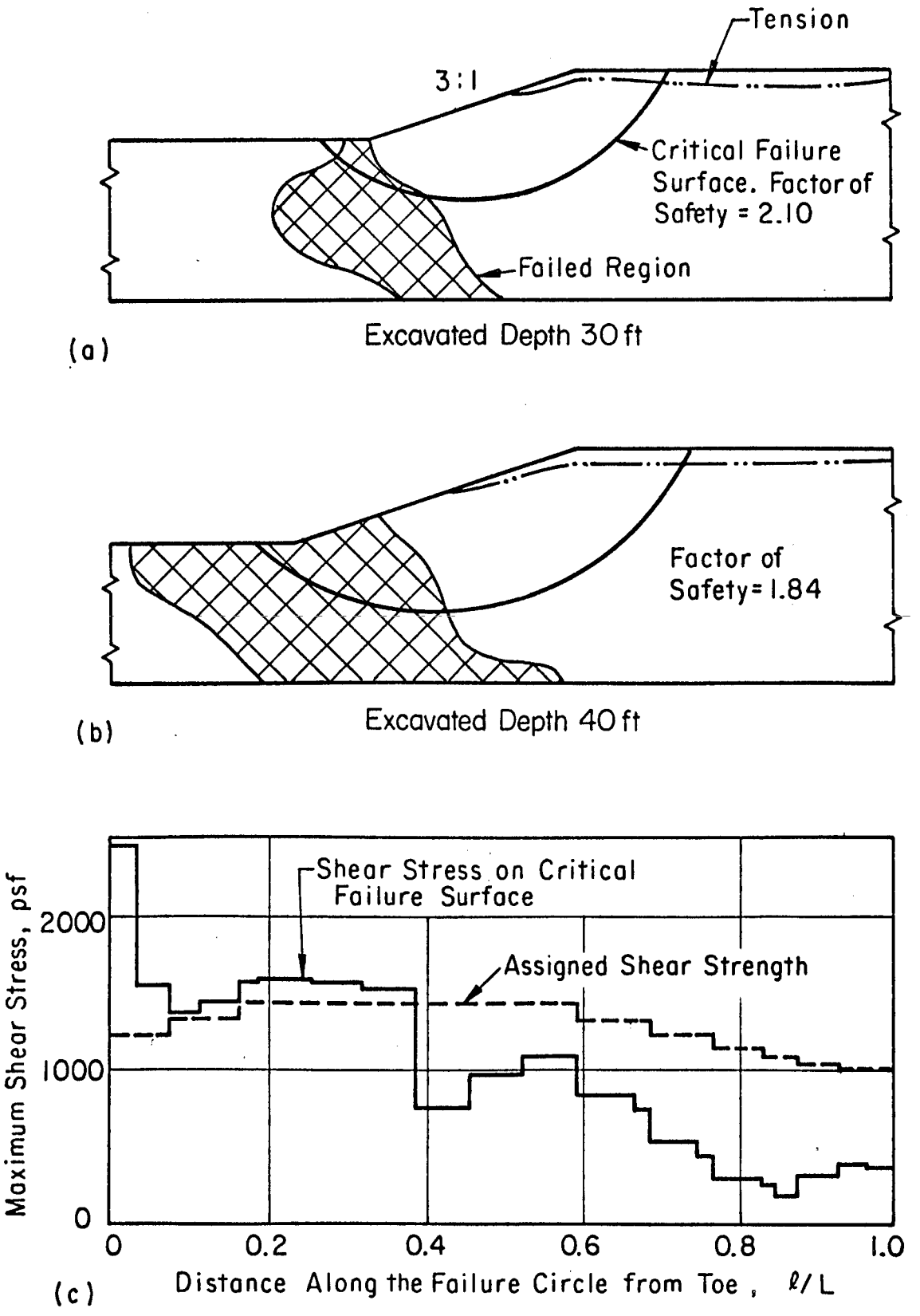

FIG. 31 CORRELATION BETWEEN FAILURE ZONES AND FACTOR OF SAFETY FOR A 3:1 SLOPE EXCAVATED IN AN OVERCONSOLIDATED CLAY LAYER.

30 ft high and 40 ft high. In both stages the critical failure arc passes mainly through intact clay, and the factors of safety are quite high: 2.10 for the next-to-last stage and 1.84 for the last stage. Thus as is suggested by the limited extent of the failure zones, the slope at both stages has a fairly high degree of safety according to the $\phi = 0$ analysis.

In contrast to the results for slopes in normally consolidated clay layers, the position of the critical circular arc and the failure zone are not in good agreement. The failure zone extends down from the bottom of the excavation and along the base of the clay layer, whereas the critical circle is fairly shallow and does not intersect the bottom of the clay layer. There is some evidence to indicate that the failure zones determined using bilinear analyses may be in better agreement with observed failures than are the critical failure surfaces determined from $\phi = 0$ stability analyses: Bjerrum (1967) observed that failure surfaces in overconsolidated clays typically dip down from the base of the excavation, then extend horizontally back toward the crest of the slope and then rise steeply to the surface. One such failure surfaced, observed in the hill adjacent to the Seattle Freeway excavation, is illustrated in Fig. 32. Apparently no hard layer was noted at the elevation of the horizontal portion of the failure surface, but the bedding may have controlled the orientation in this section. It is interesting that one of the symptoms of trouble in the Seattle Freeway excavation was bulging near the toe of the slope; as shown in Fig. 32, the slide triggered by the excavation ultimately involved a large portion of the hillside.

Summary

Bilinear analyses appear to provide a simple, useful means of studying the development of failure zones around excavated slopes. The studies performed indicate:

(1) In slopes in layers having high initial horizontal stresses, the failure zone develops first beneath the toe, subsequently progressing back beneath the slope. When the initial stresses are low, however, the failure zone develops first beneath the slope crest, subsequently progressing downward and toward the slope.

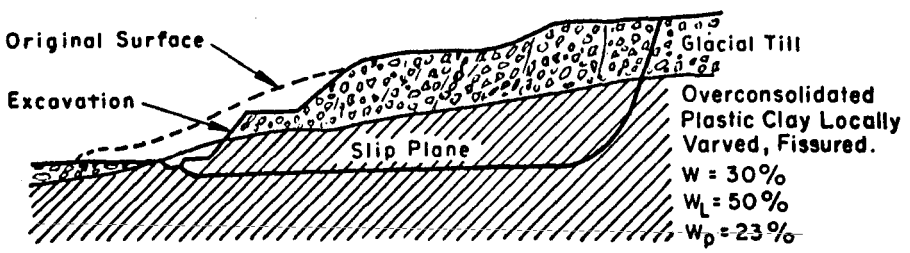

FIG. 32 SLOPE FAILURE OBSERVED IN OVERCONSOLIDATED CLAY, EXCAVATION FOR SEATTLE FREEWAY-AFTER BJERRUM (1967).

(2) For uniform strength throughout the depth of the layer, failure occurs first at the bottom of the layer beneath the slope and extends upward toward the bottom of the excavation and the crest of the slope in subsequent stages. For strength increasing linearly with depth, from zero at the surface, a pie-shaped failure zone develops around the slope crest; as excavation continues the failure zone grows in proportion with the size of the slope while remaining about the same shape.

(3) The failure zones around slopes in layers simulating initial stress conditions and strength profiles representative of normally consolidated soils begin beneath the slope and extend upward toward the slope crest, and downward toward the toe of the slope and the base of the layer as excavation continues. The final shapes of failure zones strongly suggests the possibility of failure on a curved surface of sliding. For the final stages, when the failure zones encompassed the major portions of the regions beneath the slope, factors of safety calculated by the "$\phi = 0$" method ranged from 0.95 to 1.15.

(4) For slopes in layers representing overconsolidated clays, the failure zones begin beneath the base of the excavation, extending upward toward the bottom of the excavation and downward toward the base of the layer as excavation progresses. The analyses could not be continued beyond the stage where the failure zone encompassed several nodal points to which forces would be applied during the next step. Although these failure zones do not suggest the development of a curved surface of sliding, accounts of experiences with failures in overconsolidated clays indicate that these analytical results may correspond to the bulging or loss of ground observed in actual slope failures. For the stages at which the bilinear analyses were terminated, the factors of safety calculated by the "$\phi = 0$" method were found to range from 1.84 to 2.10.

(5) Whether analyses are performed using a value of Poisson's ratio equal to 0.475, or using a constant value of bulk modulus

representative of saturated clay under undrained conditions, or using a value of Poisson's ratio equal to one-half does not appear to have any major effect on the results.

CHAPTER 4

UNDRAINED STRESS-STRAIN BEHAVIOR OF SATURATED CLAY

Introduction

The full potential of computers for providing accurate and useful solutions to soil mechanics problems involving stress and deformation under load can only be realized when methods have been established for characterizing the stress-strain characteristics of soils.

The assumption of linear elastic stress-strain behavior, often made for purposes of simplifying analyses, is not compatible with the nonlinear behavior of many soils. As a result it is very difficult, or perhaps impossible in some cases, to select a single value of modulus representative of the behavior of a large mass of soil. Ladd (1964) has shown that selection of a single modulus value to represent soil behavior involves consideration of many factors including consolidation pressure, stress level or strain, and stress orientation, and is perhaps highly subjective. He showed that modulus values determined using isotropically consolidated-undrained triaxial tests were 2 to 4 times higher than values back-calculated from prototype analyses. In other cases, modulus values determined from unconsolidated-undrained tests have been found to be much smaller than values inferred from prototype performance, very probably as a result of disturbance effects.

With the advent of the finite element method of analysis and the availability of large capacity, high speed digital computers, it is possible to analyze problems involving nonlinear stress-strain behavior, but it is first necessary to investigate and formulate the nonlinear behavior of the materials involved. Two approaches to this problem may be conceived: the first is to develop relationships of a basic nature which embody the fundamental relationships between stress and strain (constitutive laws). For soils this is a formidable task. While it is highly desirable to develop constitutive laws for soils, their development is likely to require a considerable number of years. The second approach consists in the development of empirical relationships expressing the stress-strain behavior under specified conditions, such as the stress-strain characteristics of normally

consolidated clay under undrained conditions. This technique, which is simpler, appears to offer the best method for immediate applications. An important aspect of this task is to develop means of checking and verifying the empirical relationships developed.

The study described in this chapter was conducted to determine the nonlinear stress-strain characteristics of a normally consolidated clay under undrained conditions. San Francisco Bay Mud was used for this study because undisturbed samples of high quality were easily obtainable, and because a considerable amount of valuable data were available from previous studies.

Properties of San Francisco Bay Mud

San Francisco Bay Mud is a soft, silty marine clay containing silt lenses and small amounts of shells and roots. All of the samples used in this investigation were taken from the University of California field test site at Hamilton Air Force Base in Marin County, California. The properties of the Bay Mud at this site are summarized in Fig. 33.

The results of a number of plane strain tests conducted on Bay Mud during previous investigations are summarized in Table 4. In each of these tests the specimens were consolidated without lateral strain, simulating additional consolidation to higher values of pressure than existed in the ground where the specimens were obtained. Referring to the in-situ conditions, the major principal stress during consolidation acted in the vertical direction in all cases. The undrained shear tests were conducted using two techniques: In the first, the stress acting in the vertical direction was increased until the specimen failed. This was termed a vertical plane strain (VPS) test. In the second, the stress acting in the horizontal direction was increased until the specimen failed. This was termed a horizontal plane strain (HPS) test. It may be noted that the values of the pore pressure coefficient $\bar{A}_f$, the values of strain at failure, and the values of $(\sigma_a - \sigma_\ell)_f/\sigma'_{ac}$ are quite different for the two types of test. $[(\sigma_a - \sigma_\ell)_f/\sigma'_{ac}$ is the stress difference at failure divided by the major principal stress during consolidation, or twice the value of $S_u/p.]$

Differences in the results of the two types of test have been shown by Duncan and Seed (1966) to be due to anisotropy and stress reorientation,

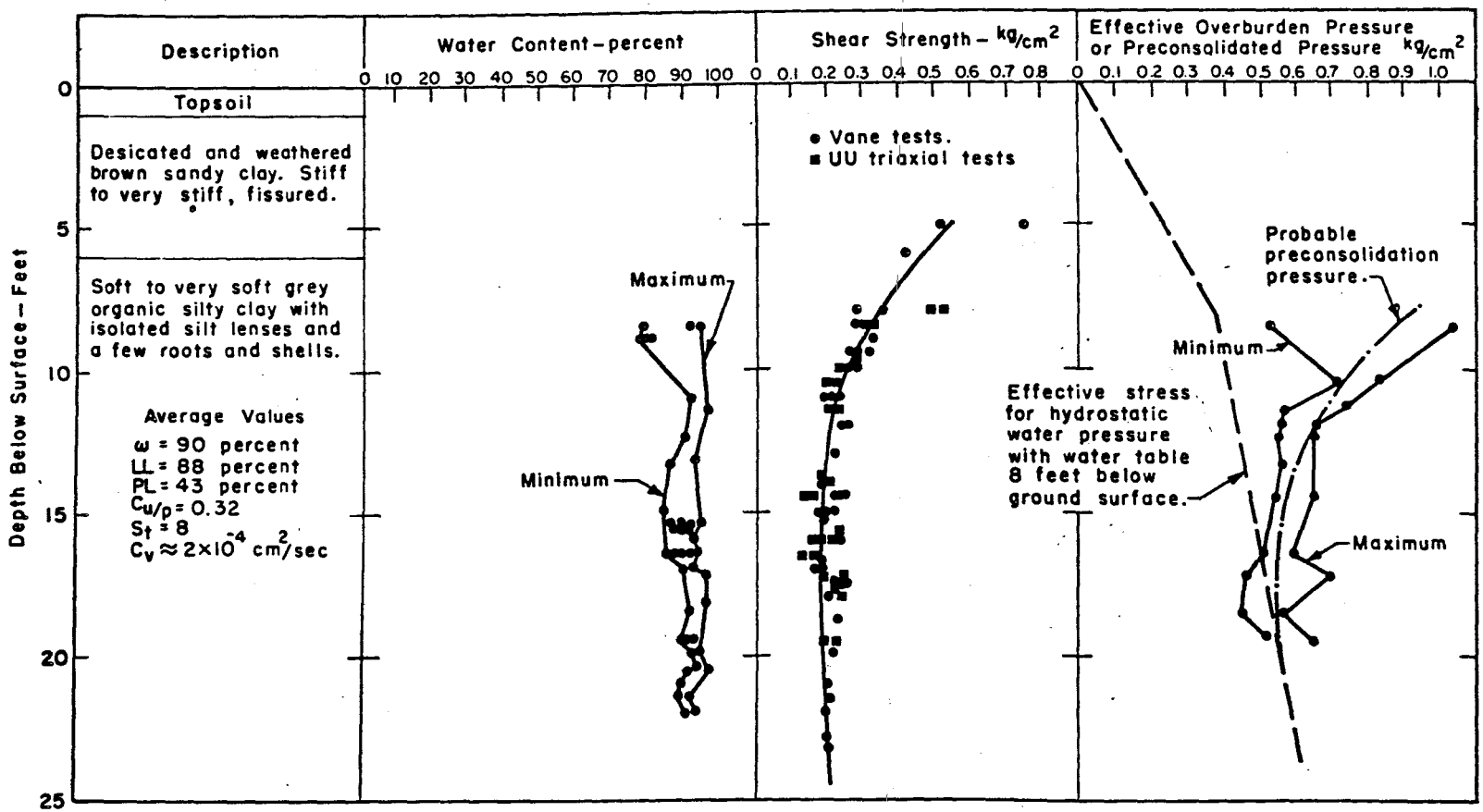

FIG. 33. SUMMARY OF THE PROPERTIES OF SAN FRANCISCO BAY MUD (SAMPLES FROM HAMILTON AIR FORCE BASE, MARIN COUNTY).

Table 4. Summary of Plane Strain Test Results on Undisturbed Specimens of Bay Mud.

Test	σ_{ac}'	$\sigma_{\ell c}'$	t_f	$\sigma_1'_f$	$\sigma_3'_f$	K_o	$\bar{A}_f$	ε_{af}	$\left(\frac{\sigma_a-\sigma_\ell}{\sigma_{ac}'}\right)_f$
VPS- 3	3.67	1.81	5.25	3.61	0.91	.49	1.07	3.10	.732
VPS- 4	0.64	0.35	5.75	0.66	0.15	.55	0.91	4.00	.784
VPS- 5	1.39	0.70	6.00	1.34	0.31	.50	1.15	3.20	.737
VPS- 6	2.14	1.07	7.00	2.07	0.65	.50	1.14	4.20	.735
VPS- 8	2.90	1.44	6.75	2.77	0.65	.50	1.18	3.80	.727
VPS- 9	3.72	1.77	4.50	3.66	0.90	.48	1.07	3.50	.740
VPS- 10	0.63	0.35	4.25	0.62	0.16	.56	0.95	3.80	.721
VPS- 11	1.37	0.69	4.25	1.38	0.31	.50	0.98	3.90	.778
VPS-L-1	1.38	0.71	4.00	1.37	0.34	.51	1.03	3.80	.742
VPS-L-2	1.41	0.73	4.00	1.35	0.33	.52	1.20	4.0	.718
VPS-L-3	0.62	0.34	4.00	0.63	0.17	.55	1.06	4.0	.732
VPS-L-4	0.63	0.35	4.00	0.62	0.17	.55	1.09	4.0	.706
AVERAGE							1.08	3.9	.74
HPS- 4	0.69	1.61	4.50	1.12	0.31	.43	0.75	11.1	.518
HPS- 5	1.20	3.15	4.50	2.28	0.63	.38	0.70	9.6	.584
HPS- 6	0.34	0.81	5.00	0.61	0.20	.42	0.69	9.0	.531
HPS- 7	0.99	2.40	5.25	1.72	0.44	.41	0.72	10.0	.569
HPS- 9	1.47	3.98	5.25	3.04	0.81	.37	0.67	10.6	.625
HPS- 11	1.66	4.00	4.50	3.04	0.80	.42	0.68	10.6	.585
HPS- 12	1.52	3.18	5.25	2.43	0.66	.48	0.65	9.8	.530
HPS- 13	0.56	1.51	4.25	1.13	0.31	.37	0.68	11.5	.615
HPS- 15	0.30	0.79	4.00	0.51	0.13	.38	0.77	9.0	.540
HPS-L-1	0.28	0.79	4.00	0.48	0.12	.36	0.77	10.0	.527
HPS-L-2	0.33	0.82	4.25	0.50	0.16	.40	0.79	11.0	.502
HPS-L-3	0.65	1.51	4.25	1.12	0.36	.43	0.67	10.6	.520
HPS-L-4	0.52	1.55	4.25	1.12	0.31	.34	0.68	10.3	.610
Average							0.71	10.4	.56

and signify that the behavior of Bay Mud under undrained conditions, and its undrained strength, depend on the orientation of the stress changes causing failure. The stress-strain curves, as well as the strengths, differ markedly for these two types of test. The stress-strain curves for all of the tests shown in Table 4 have been corrected for the effects of piston friction, end plate friction, filter paper drains and rubber membranes. The curves were then normalized by dividing the stress ordinates by the value of the consolidation pressure, $p = \sigma'_{ac}$. Normalized stress-strain curves for vertical plane strain tests are shown in Fig. 34, and those for horizontal plane strain tests are shown in Fig. 35. The stress difference in each case is $(\sigma_a - \sigma_\ell)$, the difference between the axial and lateral stress values. σ_a acts in the vertical direction for the VPS tests, and in the horizontal direction for HPS tests.

These test results show that the stress-strain characteristics of San Francisco Bay Mud depend to a considerable extent on the orientation of the stress changes causing deformation. It might be expected, therefore, that many normally consolidated clays will be characterized by similar anisotropic stress-strain relationships, because there is no reason to believe that Bay Mud possesses an unusually high degree of anisotropy. In attempting to develop empirical stress-strain relationships for Bay Mud, it was considered imperative to take into account the influences of stress orientation and anisotropy.

Modulus Values. For purposes of analysis, it is convenient to represent the normalized stress-strain curves shown in Figs. 34 and 35 by curves representing the variations of normalized modulus values with strain, as shown in Fig. 36. These curves represent variations of the instantaneous tangent modulus, E_i, with the value of maximum shear strain, γ_{max}. Because the stress-strain curves shown in Figs. 35 and 36 correspond to plane strain conditions, the instantaneous modulus values, E_i, are equal to $(1 - \nu^2)$, or 0.75 times the instantaneous slope of the stress-strain curves. Maximum shear strain has been found to be a convenient strain parameter because it affords a measure of the total amount of shear distortion, independent of the stress or strain directions.

Because no test results were available for orientations intermediate between horizontal and vertical compression, it was necessary to hypothesize

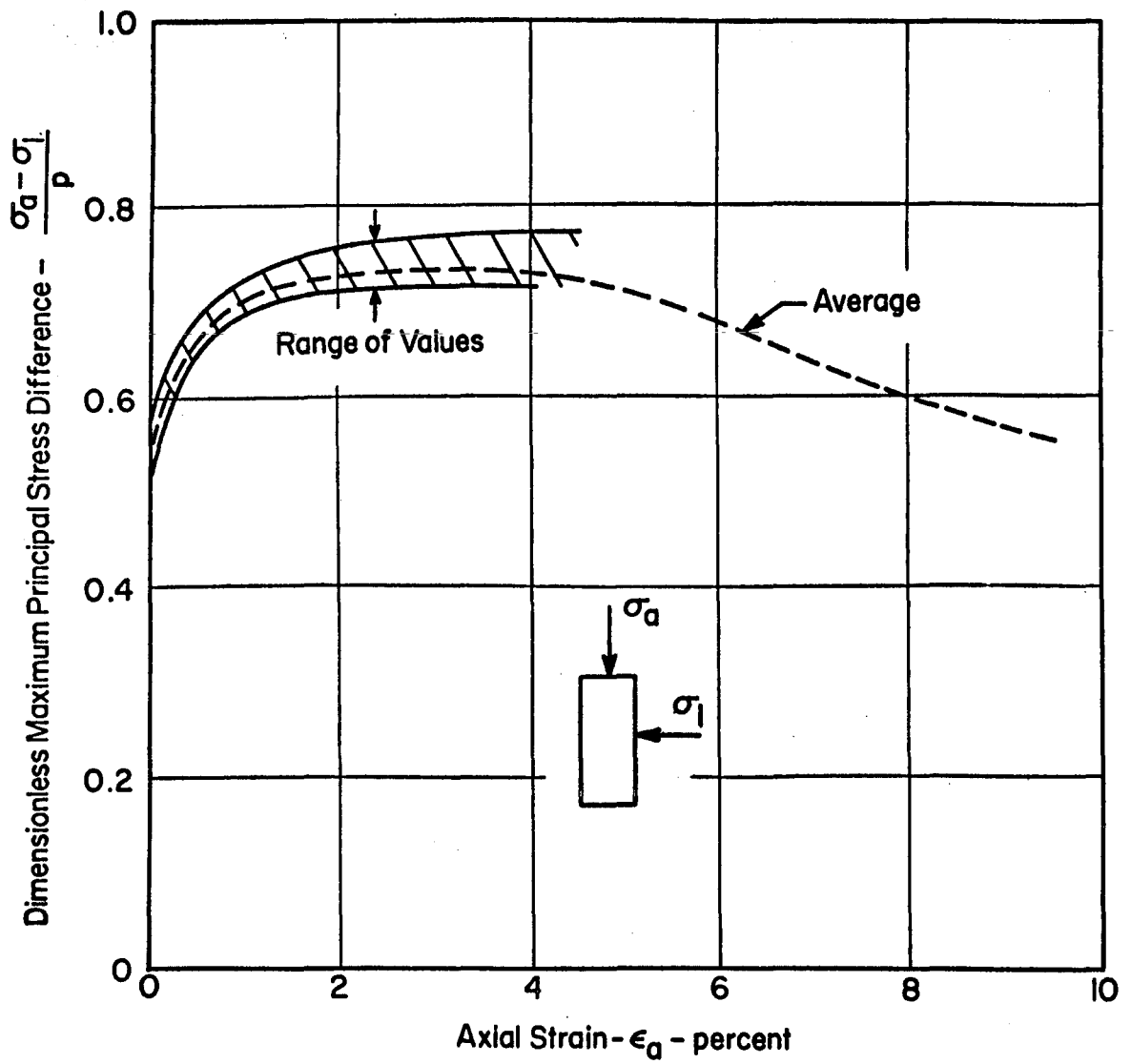

FIG. 34. STRESS-STRAIN BEHAVIOR OF SAN FRANCISCO BAY MUD IN VERTICAL PLANE STRAIN.

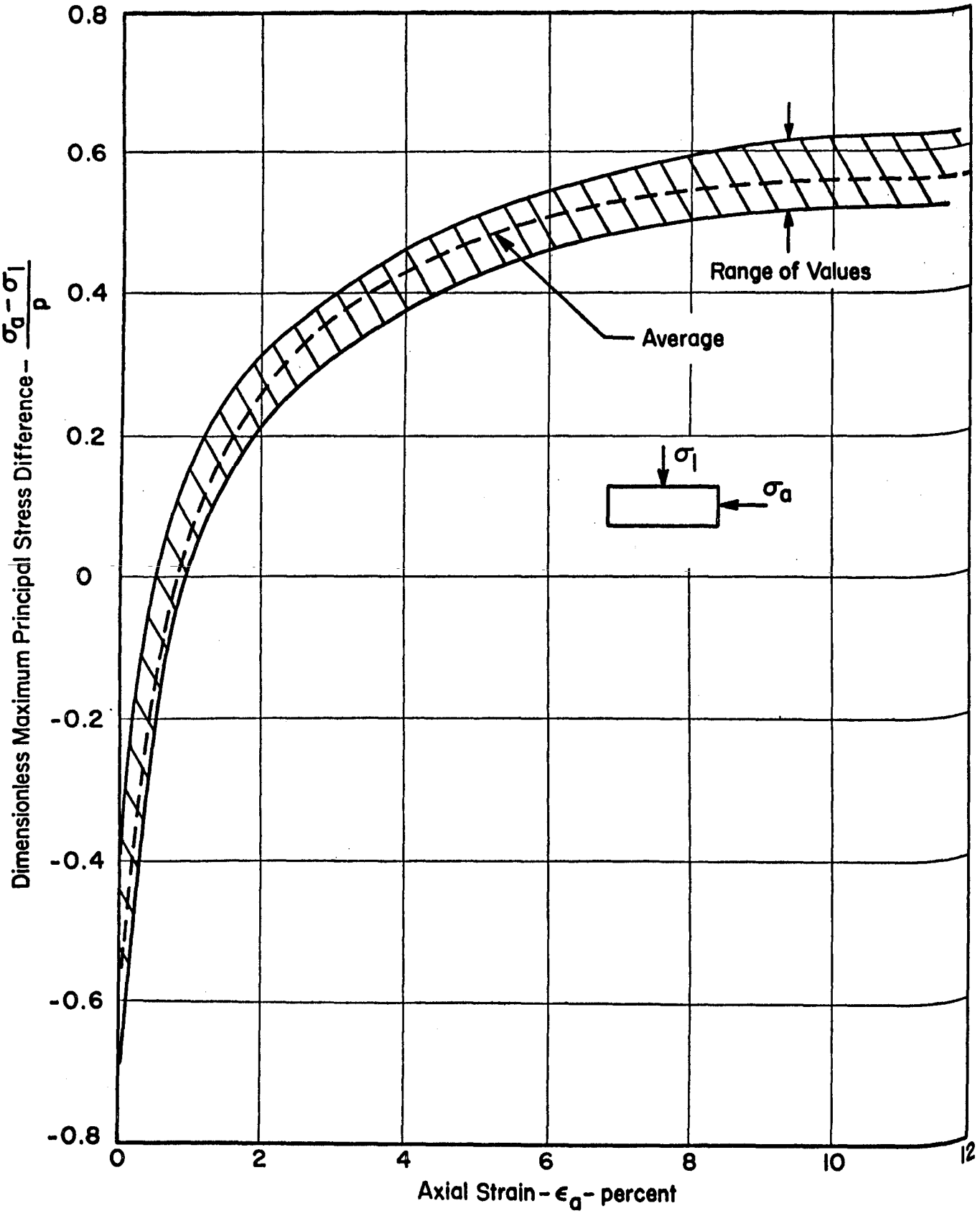

FIG. 35. STRESS-STRAIN BEHAVIOR OF SAN FRANCISCO BAY MUD IN HORIZONTAL PLANE STRAIN.

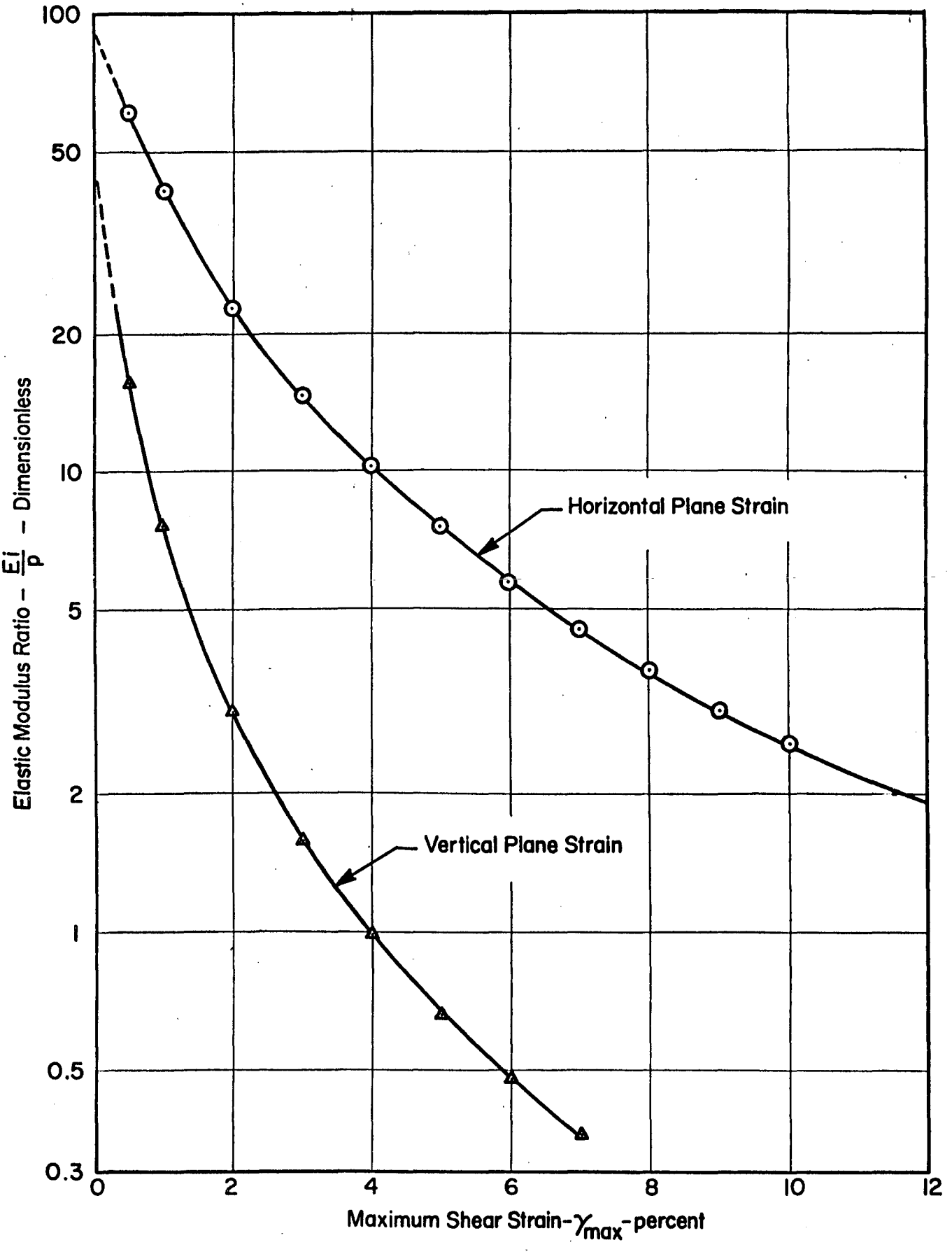

FIG. 36. MODULUS-STRAIN VARIATION FOR SAN FRANCISCO BAY MUD

how the value of E_i might vary with stress orientation at any value of maximum shear strain. Because the values of E_i for horizontal and vertical compression logically represent the extremes, values of E_i for other stress orientations would be expected to be intermediate between those shown in Fig. 36. Furthermore, because the variations must be symmetrical about the horizontal and vertical orientations, it seems logical to believe that the variation would be represented by a smooth curve of the type shown in Fig. 37. The simplest means for representing a curve of this shape is by the equation:

$$E_{\beta_i} = E_H - (E_H - E_V) \sin^2\beta_i \qquad (9)$$

in which β_i is the angle between horizontal and the instantaneous direction of compression, E_{β_i} is the instantaneous modulus value in the β_i-direction, and E_H and E_V are the modulus values for horizontal and vertical compression, respectively.

Using the curves shown in Fig. 36, together with equation 9, it is possible to determine instantaneous modulus values for any value of shear strain in the range of values shown, and for any direction of compression. The values of modulus are proportional to the consolidation pressure p. It should be noted that these relationships would only be expected to apply to conditions corresponding to the test conditions on which they are based, i.e. undrained plane strain deformation of Bay Mud normally consolidated without lateral strain. However, these conditions are satisfied by short-term slope problems involving cuts or fills of large longitudinal extent, and the relationships postulated may be useful for analyses of these and similar types of problems.

Pore Pressure Coefficients. In addition to the amounts of strain or deformation, it is desirable for many types of problems to develop techniques for predicting changes in pore pressure induced by changes in total stress under undrained conditions. One convenient means for making such predictions involves use of the pore pressure coefficients $\bar{A}$ and B suggested by Skempton (1954). According to the definition of these coefficients, the change in pore pressure induced by changes in total stress may be expressed as

$$\Delta u = B \cdot \Delta\sigma_3 + \bar{A} \cdot (\Delta\sigma_1 - \Delta\sigma_3) \qquad (10)$$

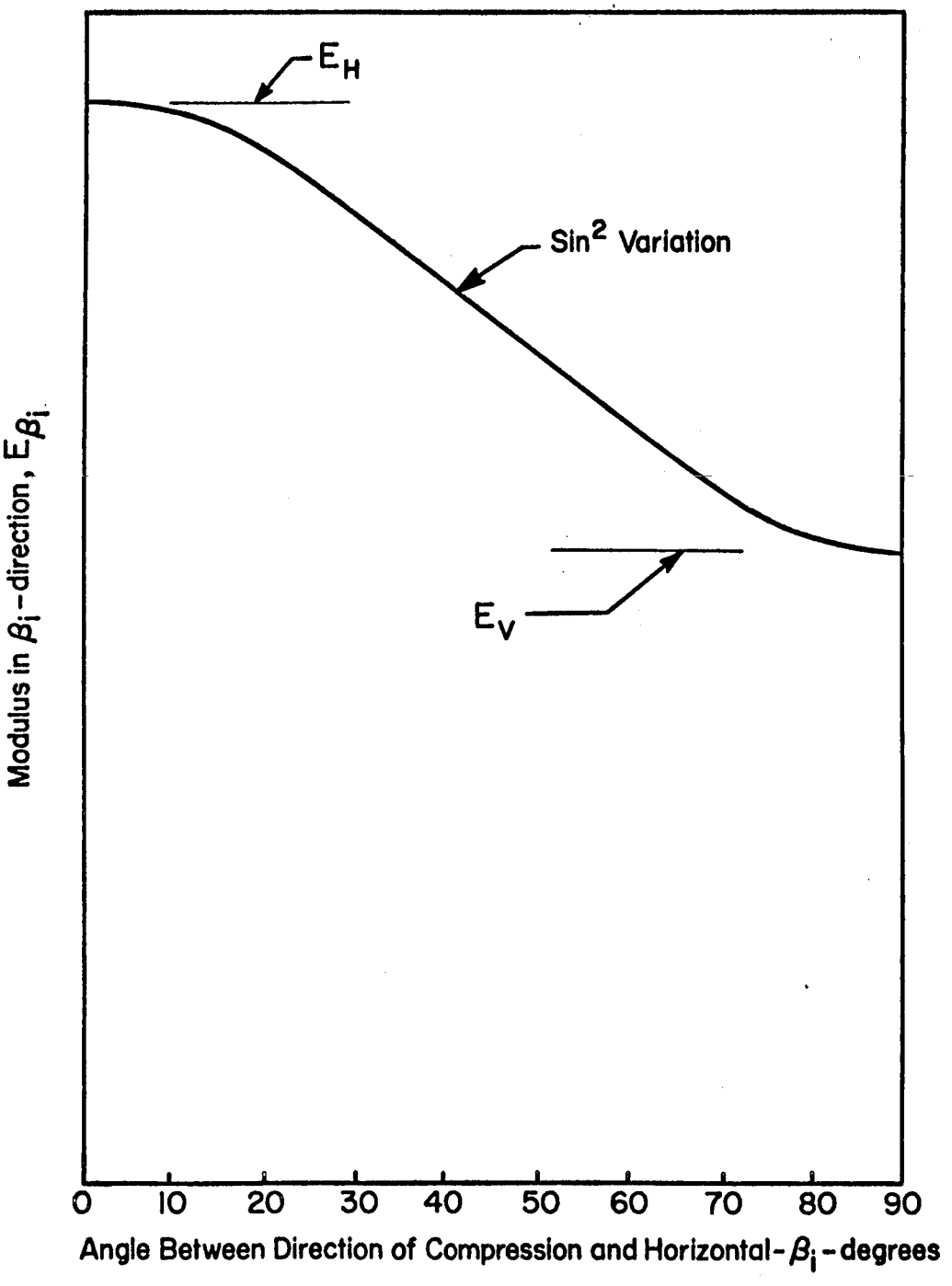

FIG. 37. VARIATION OF MODULUS WITH DIRECTION OF COMPRESSION.

in which Δu is the change in pore-water pressure, $\Delta\sigma_1$ and $\Delta\sigma_3$ are the major and minor principal changes in stress, and $\bar{A}$ and B are pore pressure coefficients determined by measuring pore-water pressures under undrained test conditions. It is worthy of note that equation 10 may be applied with equal validity to triaxial and plane strain test conditions, provided the values of $\bar{A}$ have been measured under appropriate test conditions. The value of the coefficient B depends primarily on the degree of saturation of the soil, and for soft saturated clays, B is equal to unity for all practical purposes.

The value of the pore pressure coefficient $\bar{A}$ has been found to depend on the direction of compression as indicated by the plane strain test results summarized in Table 4. The average values of $\bar{A}$ at failure ($\bar{A}_f$) were found to be 0.71 for horizontal compression and 1.08 for vertical compression. Values for intermediate orientations of the major principal stress at failure (β_f) may be derived from the variation of undrained strength with stress orientation at failure. Duncan (1967) has shown that the value of $\bar{A}_f$ corresponding to any value of β_f is given by the expression

$$\bar{A} = \frac{1}{2} + \frac{\frac{c'}{p\tan\phi'} + \frac{1}{2}(1+K_o) - \frac{S_u}{p\sin\phi'}}{2\left[\left(\frac{S_u}{p}\right)^2 - \frac{S_u}{p}(1-K_o)\cos 2\left(\frac{\pi}{2}-\beta_f\right) + \left(\frac{1-K_o}{2}\right)^2\right]^{1/2}} \qquad (11)$$

in which c' and ϕ' are the effective stress shear strength parameters, S_u is the undrained strength, p is the major principal stress during consolidation, K_o is the coefficient of earth pressure at rest, and β_f is the angle between horizontal and the major principal stress at failure. Using the variation of undrained strength with β_f determined from unconsolidated-undrained triaxial tests, it was found that the value of $\bar{A}_f$ varies with β_f as shown by the solid curve in Fig. 38.

For the purpose of calculating changes in pore water pressure prior to failure, it is more convenient to relate the value of $\bar{A}$ to the direction in which changes in stress are applied, β_i. Except for horizontal and vertical compression ($\beta_f = 0$ and $\beta_f = 90°$) the values of β_i are different from the values of β_f. For any given value of β_f, however, the corresponding

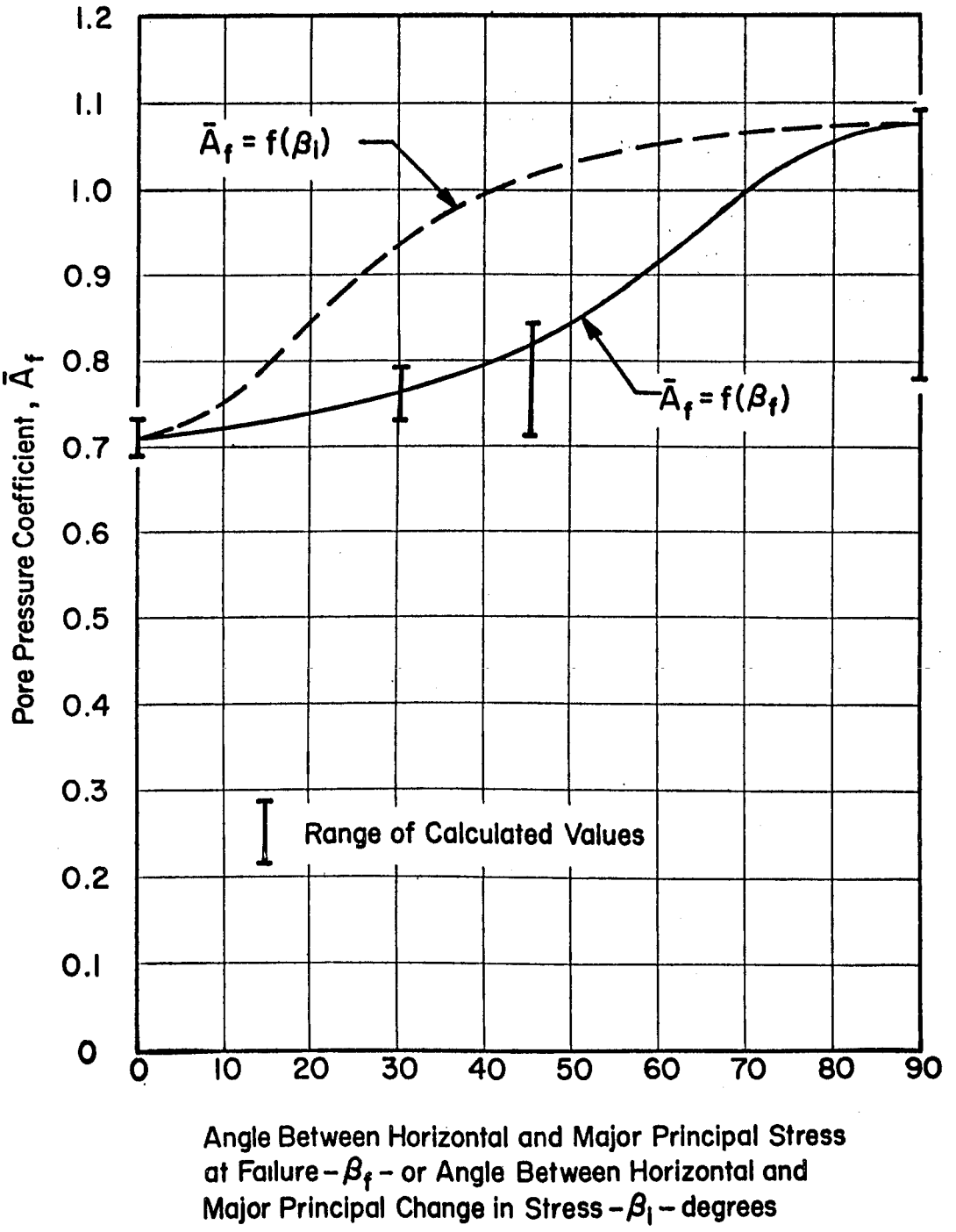

FIG. 38. VARIATION OF THE VALUE OF $\bar{A}_f$ WITH DIRECTION OF COMPRESSION FOR SAN FRANCISCO BAY MUD.

value of β_i may be found by repeated trials, provided failure is caused by a single stress increment. For example, in order to cause failure with the major principal stress oriented 70° from horizontal, beginning from at-rest pressure conditions with the major principal stress vertical, the major principal change in stress must be oriented 38° from the horizontal. Thus $\beta_f = 70°$ corresponds to $\beta_i = 38°$, and the value of $\bar{A}_f$ corresponding to $\beta_f = 70°$ would also correspond to $\beta_i = 38°$. Using this technique, the relationship between $\bar{A}_f$ and β_i was determined which is shown by the dotted line in Fig. 38.

In using the relationship shown in Fig. 38 to calculate pore water pressure changes prior to failure, it is assumed that the value of $\bar{A}$ does not vary with stress level or strain. Duncan and Seed (1966) found that the value of $\bar{A}$ was nearly independent of stress level and strain throughout horizontal plane strain tests. Although the value of $\bar{A}$ was found to increase with increasing strain in vertical plane strain test conditions and has also been found to do so in triaxial tests, this may occur only because of incomplete equalization of nonuniform pore water pressures during the early stages of these tests. Bishop, et. al (1960) found that the more slowly undrained tests were conducted, and the higher the degree of equalization in the early part of the test, the less the value of $\bar{A}$ varied with strain. Therefore it seems reasonable to assume that values of $\bar{A}_f$ may be used to calculate changes in pore water pressure prior to failure as well as at failure.

The nonlinear stress-strain relationship illustrated by Figs. 36 and 37, and the variation of $\bar{A}_f$ with β_i shown in Fig. 38 could be used in conjunction with the finite element method to calculate stresses, strain, displacements and pore water pressures for slopes in San Francisco Bay Mud and for similar problems involving undrained loading conditions. However, before performing analyses of this type it was considered highly desirable to check the validity of the relationships developed. For this purpose a series of simple shear tests were conducted on San Francisco Bay Mud. The measured results of these tests were then compared to the values predicted using the stress-strain and pore pressure relationships discussed previously. The results of this study are described in subsequent sections of this chapter.

Simple Shear Tests

Two types of simple shear test devices have been developed in recent years, both of which afford considerable improvement over direct shear apparatus with respect to uniformity of stresses and strains within the test specimens. One of these devices, developed at the Swedish Geotechnical Institute and also manufactured by the Norwegian Geotechnical Institute, employs a short cylindrical specimen enclosed in a rubber membrane. The membrane is reinforced by an embedded wire spiral to restrict lateral expansion, and the top and bottom of the specimen are in contact with parallel rigid metal discs through which horizontal and vertical loads or displacements may be applied to the specimen, as shown in Fig. 39.

Another device, developed at Cambridge University, employs a rectangular parallelpiped specimen, also enclosed in a rubber membrane. The specimen and membrane are both enclosed within a rigid box having elaborate bearings and hinges such that the top may move vertically or horizontally, but always remains parallel to the base. As the top translates, the rigid sides of the box rotate as shown in Fig. 39 so that the sides of the specimen remain straight. The device has been described in some detail by Peacock and Seed (1967).

Although both of these devices were available for use, only the Cambridge University device was used for this study. During previous tests on Bay Mud using the SGI-NGI device, some of the specimens were observed to deform nonuniformly, as shown in Fig. 39. Furthermore, because the steel sides of the Cambridge University device are more rigid than the reinforced membrane used with the SGI-NGI device, it is better suited for pore pressure measurements. The principal drawback of the Cambridge apparatus is that friction between the membrane and the box sides tends to resist relative movement. Grease was used to lubricate these sliding surfaces, and corrections were made for the remaining friction forces; these corrections are described in Appendix B.

Test Procedures. The simple shear tests were conducted using undisturbed specimens of San Francisco Bay Mud from Hamilton Air Force Base. Before testing, the specimens were consolidated one-dimensionally under higher pressures than those in-situ at the depths from which the specimens were obtained. Because the vertical travel of the cap in the

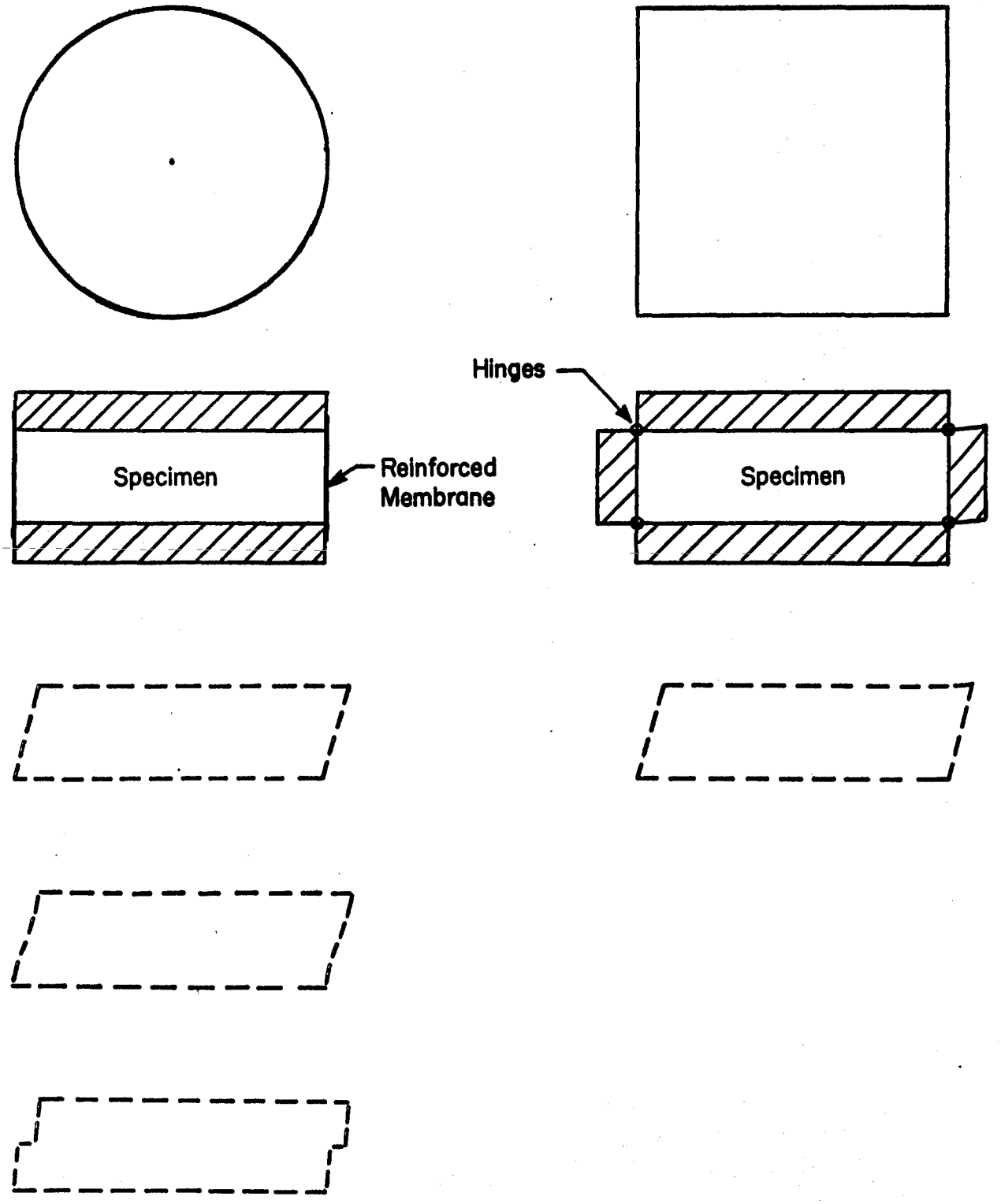

Swedish Geotechnical Institute and
Norwegian Geotechnical Institute

Cambridge University

FIG. 39 TWO TYPES OF SIMPLE SHEAR APPARATUS

simple shear device is restricted, the specimens were consolidated initially in a large consolidometer, then trimmed to the required dimensions (6 cm square by 2 cm high), and installed in the simple shear device. They were then consolidated a small additional amount in the device, to insure that they were properly seated and normally consolidated under the desired test pressure. Consolidation within the shear box was one-dimensional, and it was necessary to infer the lateral pressure values from previous tests which showed that K_o for Bay Mud is approximately 0.45. Specimens were allowed to consolidate for 48 hours at the final pressure to insure that they reached equilibrium, and a back pressure of 1.5 to 2.0 kg/cm^2 was used to insure that the specimens were fully saturated.

After consolidation the specimens were tested undrained, by applying shear stress at a rate sufficient to cause failure within 1-1/4 to 3-3/4 hours; for these test durations the estimated degree of equalization of nonuniform pore water pressures ranged from 92% to 98%. Variations of shear stress and pore water pressure with shear strain for the first test are shown in Fig. 40. Shear stress values are shown for both the top and midheight, the two values differing by about 8% at large values of strain. This difference in shear stress values is indicative of some degree of nonuniformity in the stress distribution within the specimen, and the measured amount of difference is in good agreement with values calculated using linear elastic stress analyses presented by Roscoe (1953). The results of this analysis are shown in Fig. 41.

The stresses shown in Fig. 41 are those induced by applied shear loads only; the stresses at any stage are represented by the sum of the initial stresses, due to vertical loading, and those induced by shear loading. It may be noted that shear loading induces changes in normal stress $\Delta\sigma_x$ and $\Delta\sigma_y$ as well as shear stresses τ_{xy}. For horizontal equilibrium, the resultant of the shear stresses at any elevation must equal the resultant of the shear stresses at the top plus the resultant of the changes in normal stress $\Delta\sigma_x$ between the top and that elevation. Thus the shear stress values increase from the top and bottom toward the middle, reaching their maximum values at midheight. These stress nonuniformities result from the fact that although simple shear deformation is enforced by the boundary displacements, complementary shear stresses are not applied

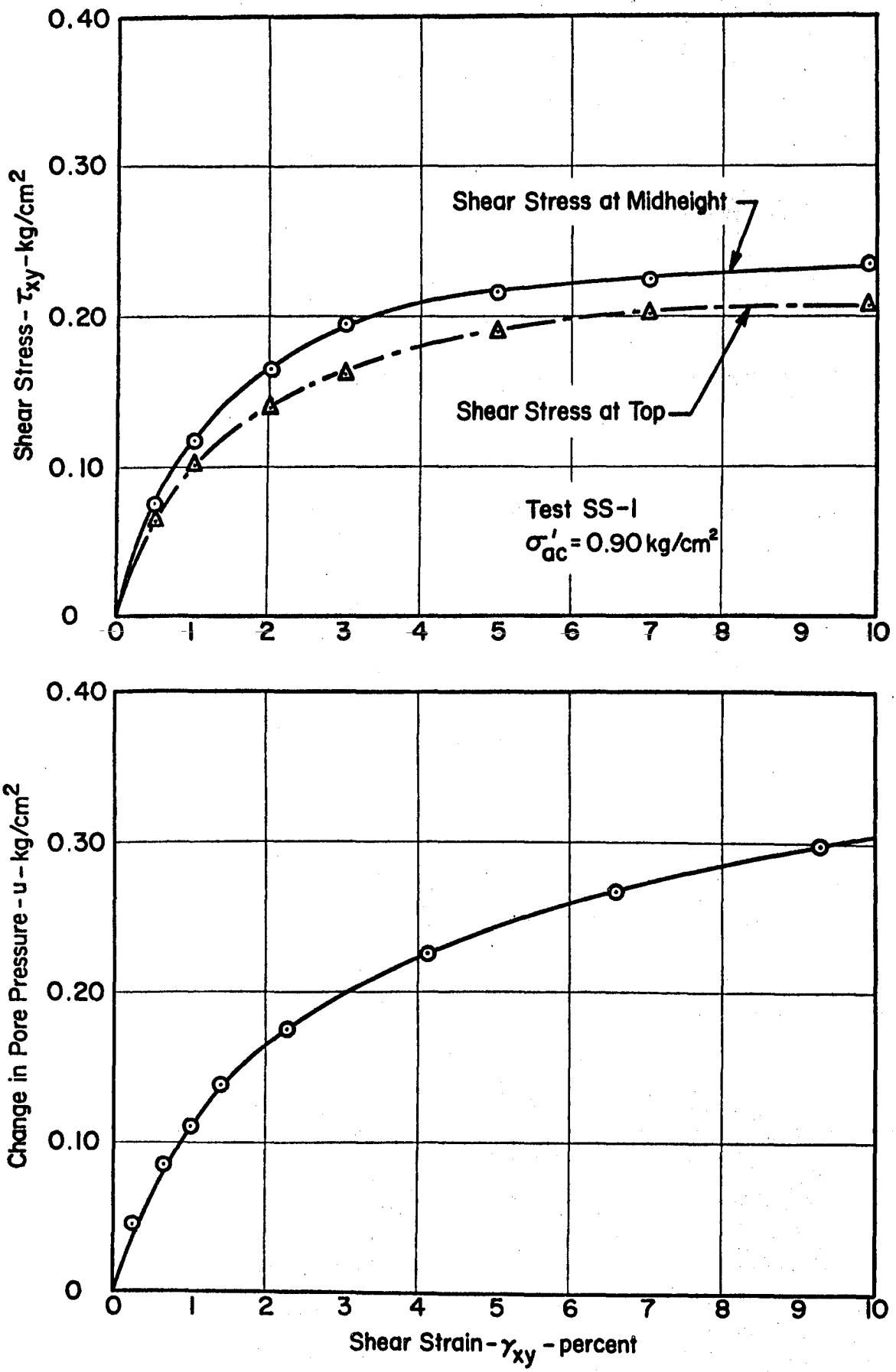

FIG. 40. VARIATIONS OF SHEAR STRESS AND POREWATER PRESSURE WITH SHEAR STRAIN IN SIMPLE SHEAR TESTS ON SAN FRANCISCO BAY MUD.

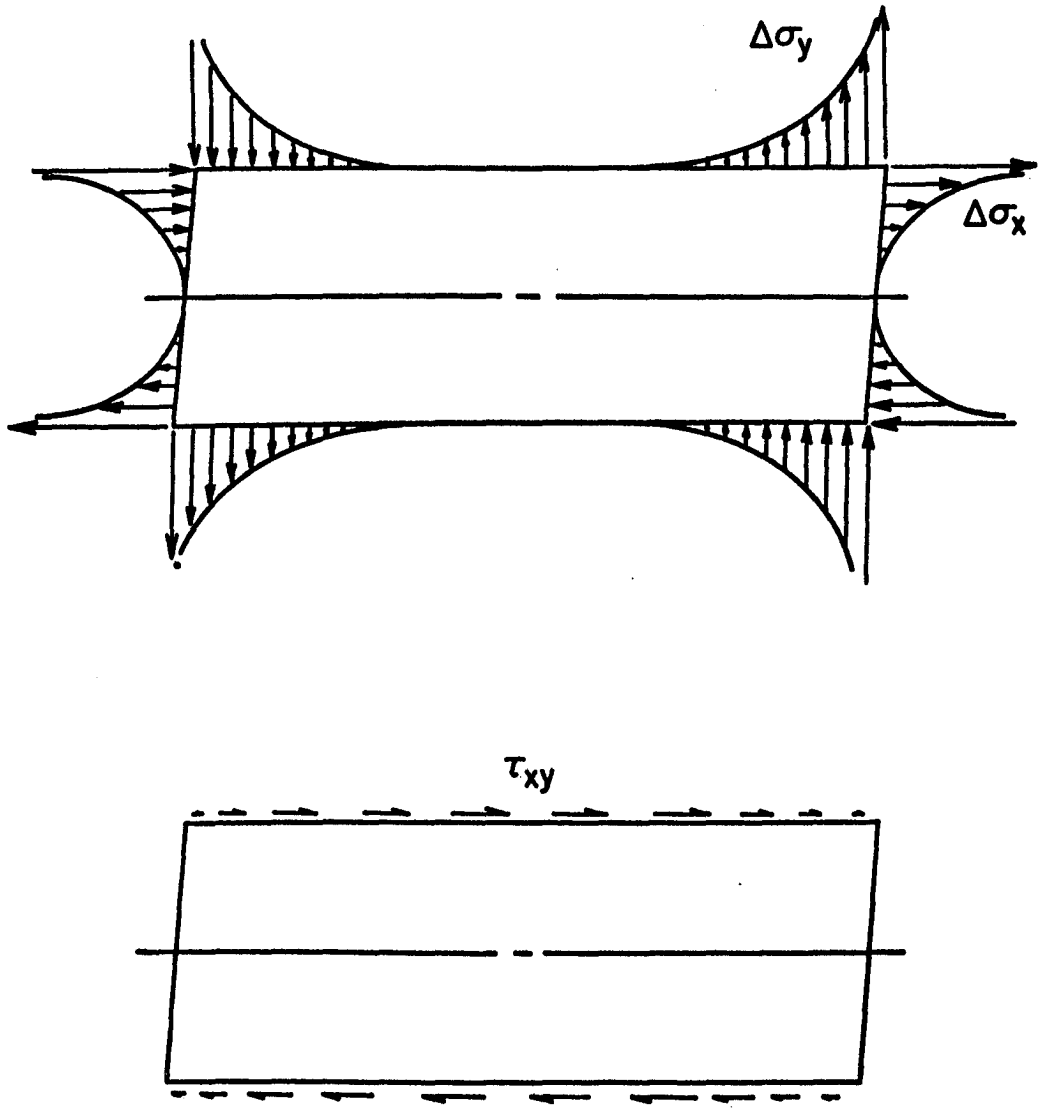

FIG. 41. NORMAL AND SHEAR STRESSES INDUCED BY SHEAR LOADING. AFTER ROSCOE (1953).

to the ends of the specimen. Using these stress distributions, the difference between the average values of shear stress at the top and at midheight were calculated to be about 6%, compared to the measured difference of 8%. Nonlinear finite element analyses indicate that the value may range from 4% to 8% theoretically, with the largest difference corresponding to the early stages of the tests.

The values of shear stress at the top of the specimen were measured using an electronic load cell, whereas those measured at midheight were calculated by applying the required friction corrections to the applied shear loads. The close agreement between the calculated and measured differences in shear stress values was considered to indicate that both methods of measurement were sufficiently accurate.

Two additional shear tests were performed on San Francisco Bay Mud at higher consolidation pressures (σ'_{ac} = 1.04 kg/cm^2 and 1.34 kg/cm^2) using the same loading procedures. The results of all three tests have been corrected for friction effects and are shown together in Fig. 42. The stress-strain and pore pressure curves have been normalized by dividing the stress ordinates by σ'_{ac} = p, the major principal stress during consolidation. The normalized results of all the tests exhibit a degree of scatter comparable to the plane strain test results discussed previously.

Comparison of Predicted and Measured Results. Using the empirical stress-strain relationships developed for San Francisco Bay Mud, finite element analyses were performed for the simple shear test conditions employed in the testing program, in order to evaluate the usefulness of the empirical relationship.

The finite element configuration used in these analyses is shown in Fig. 43. The nodal points on the bottom of the specimen were fixed, and the row of nodal points at the top of the specimen were given a uniform horizontal displacement, simulating full adhesion between the soil and the top and bottom plates. The nodal points at the ends were given horizontal displacements in proportion to their height above the base, and were free to move in the vertical direction. The analysis was accomplished in a series of increments; 10 displacement increments were used from 0% to 5%, and 5 more increments from 5% to 10% strain. A new value of modulus was calculated for each element after each increment, based on the average

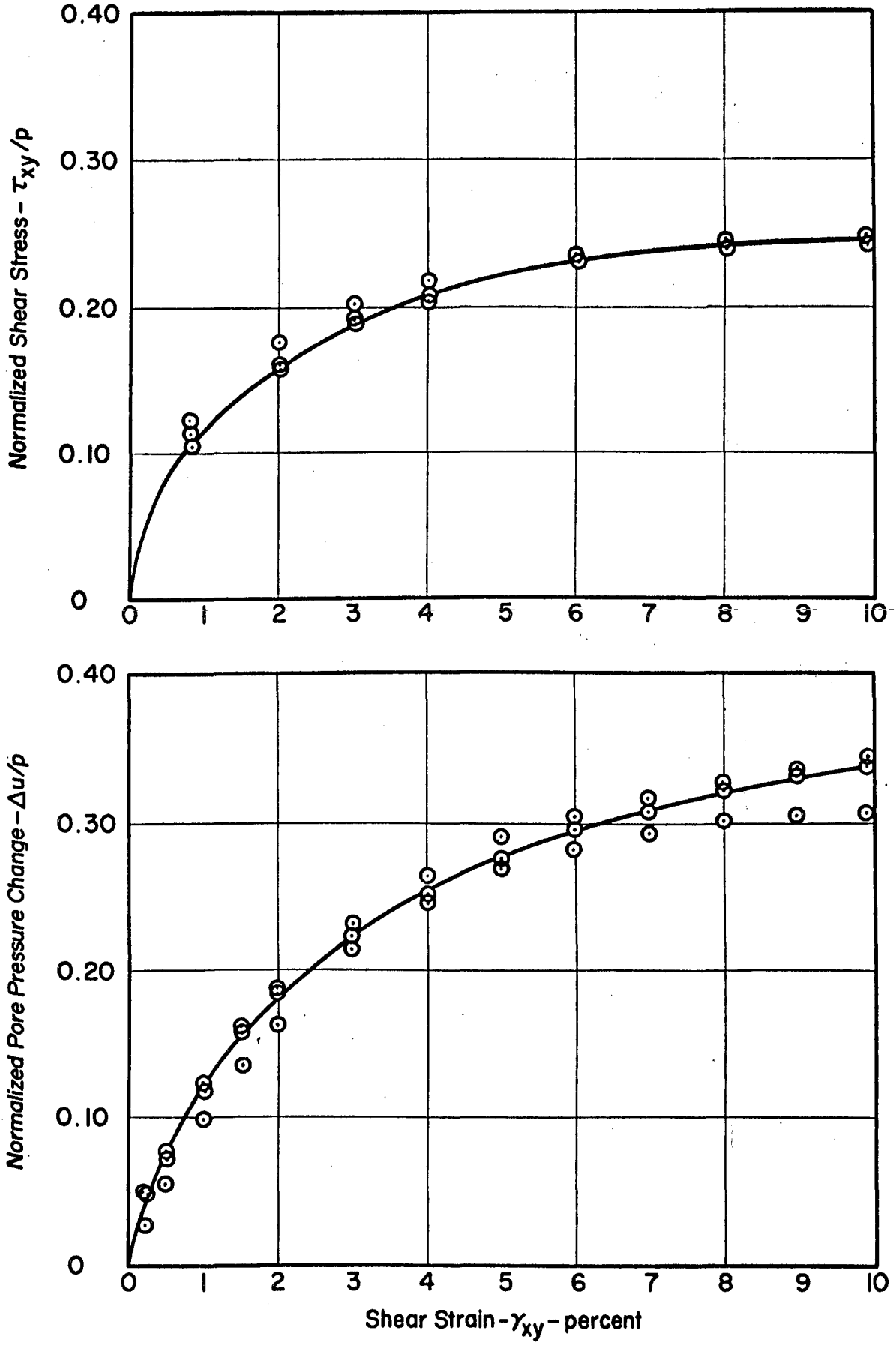

FIG. 42 NORMALIZED SHEAR STRESS - SHEAR STRAIN AND PORE PRESSURE - SHEAR STRAIN CURVES FOR SIMPLE SHEAR TESTS ON SAN FRANCISCO BAY MUD.

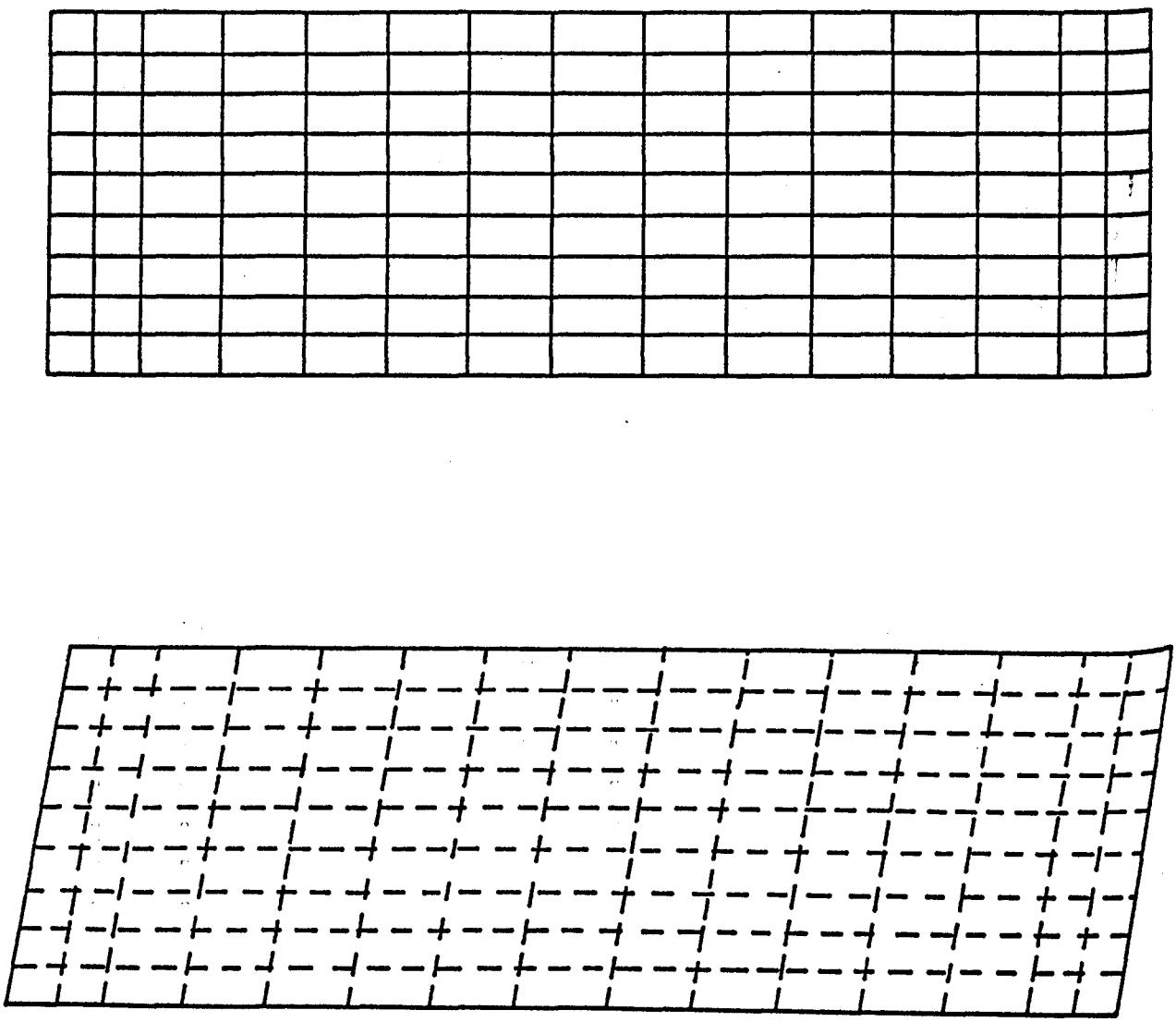

FIG. 43 FINITE ELEMENT IDEALIZATION OF THE SIMPLE SHEAR SPECIMEN, SHOWING INITIAL AND DEFORMED SHAPE.

value of strain anticipated for the subsequent increment. Using this procedure, no iteration was necessary even though the analysis was non-linear, because the strain values could be anticipated with a high degree of accuracy.

Displacements were calculated for each nodal point, and strains and stresses for each element, after each displacement increment. The incremental values were added to the previous values each time. Using the variation of $\bar{A}$ shown in Fig. 38, changes in pore water pressure were also calculated for each element following each step. The values of strain, stress, and pore water pressure varied throughout the specimen, as would be expected on the basis of the linear elastic analysis performed by Roscoe (1953). To develop interpretations consistent with the experimental results, an average value of shear stress at midheight was calculated using the individual element stresses, and average values of shear strain were calculated from the boundary displacements. Average values of change in pore water pressure were calculated assuming no volume change, and taking into account the fact that the slopes of the primary consolidation and rebound curves are not the same.

The predicted and measured results are compared in Fig. 44. At all values of strain the predicted values of shear stress and pore water pressure are approximately 20% to 30% higher than the measured values, although the measured and predicted curves have similar shapes. It therefore appears that the instantaneous modulus values used in the analysis were too large, by about 25% on the average. It seems likely that the modulus values corresponding to horizontal and vertical compression are accurate, because these were determined directly from the plane strain test data. For intermediate directions of compression, however, it was necessary to hypothesize the relative modulus values, as shown by the $\sin^2$ variation in Fig. 37. Because the stress increment orientations in the simple shear conditions have an average orientation close to 45° from horizontal, it appears that a more correct variation of modulus with stress increment orientation would lie below the $\sin^2$ variation over the central portion of the curve. The basic shape of the curve should logically remain the same, however, with horizontal asymptotes at the ends.

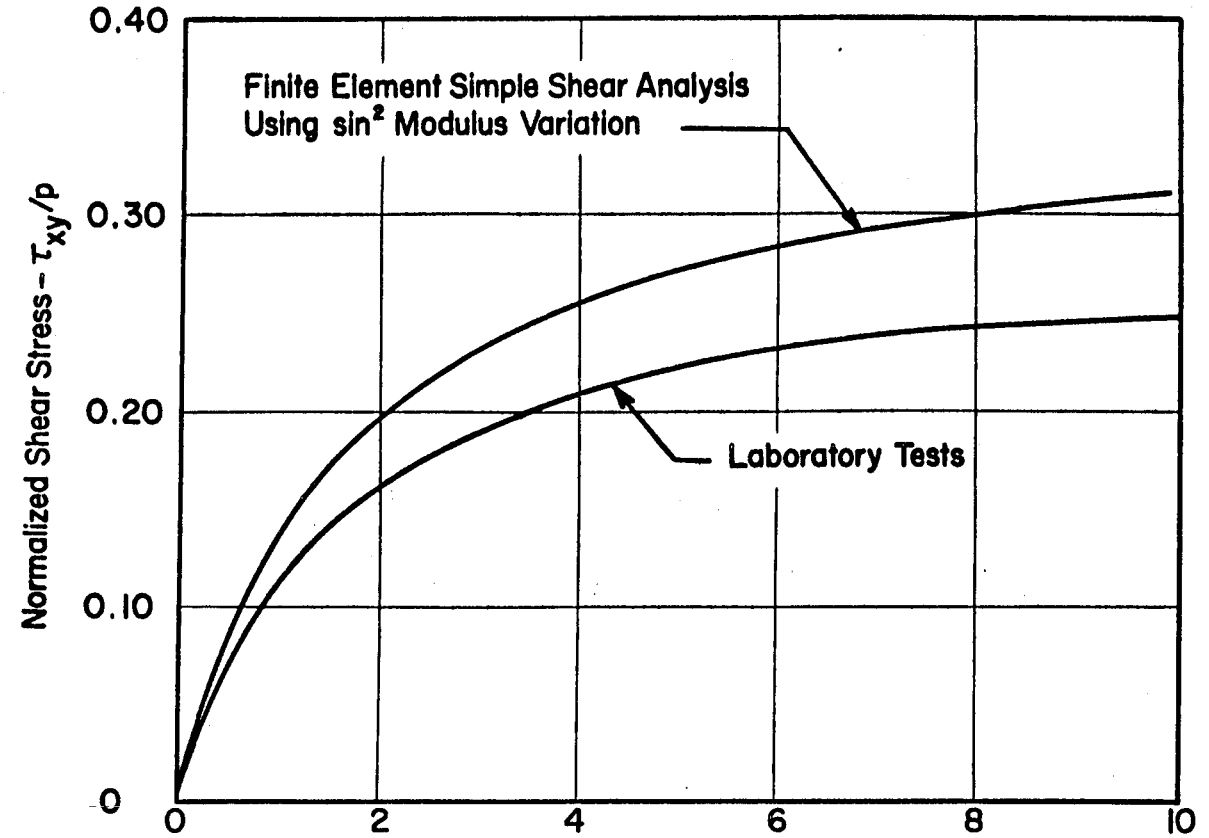

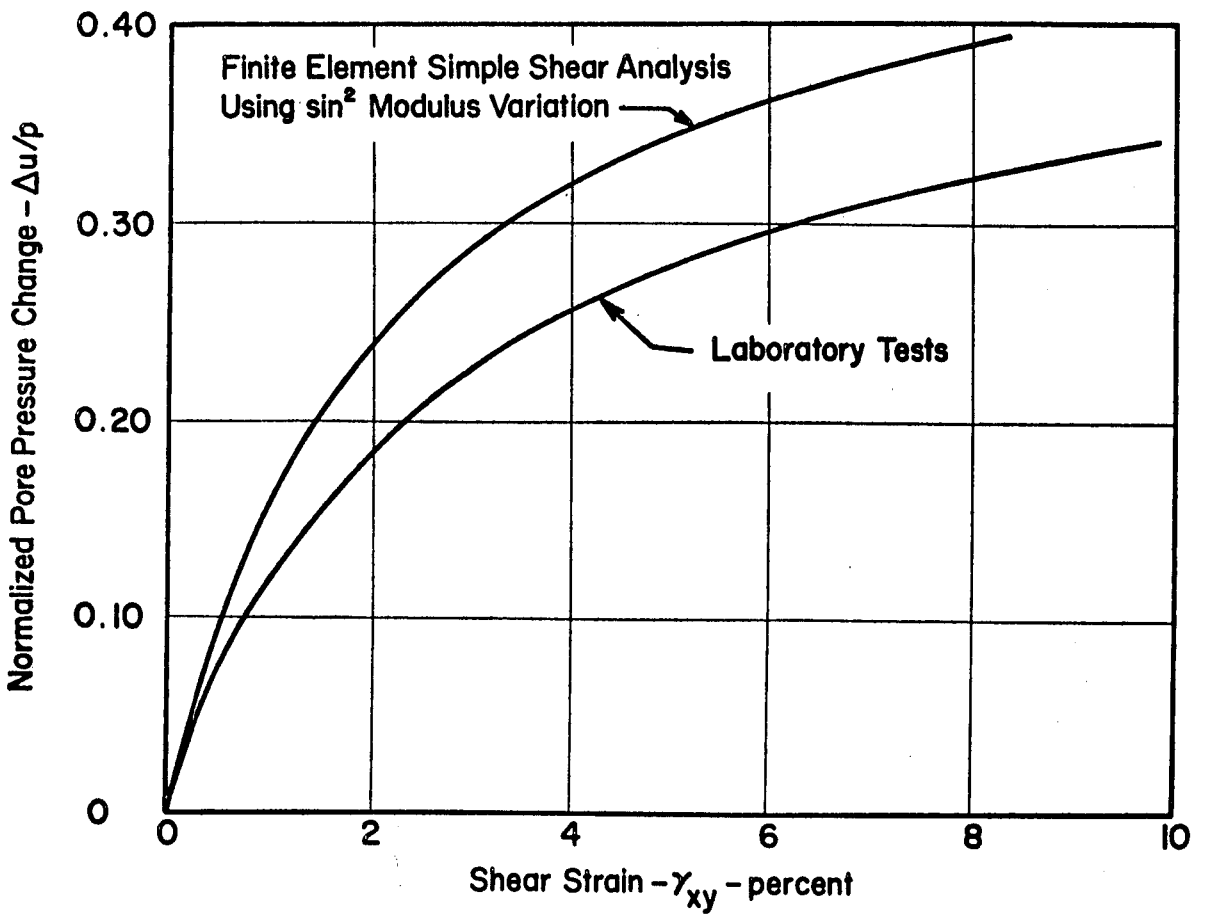

FIG. 44. COMPARISON OF EXPERIMENTAL AND ANALYTICAL SIMPLE SHEAR TEST RESULTS.

A modified modulus variation satisfying these criteria is shown in Fig. 45, together with the $\sin^2$ variation used in the previous analysis. The modified modulus variation may be expressed by the equation

$$E_{\beta_i} = E_H - (E_H - E_V)(\sin^2\beta_i + 0.2 \sin 2\beta_i) \qquad (12)$$

in which β_i is the orientation of the major principal stress increment, E_{β_i} is the modulus in the β_i direction, and E_H and E_V are the modulus values in the horizontal and vertical directions, respectively.

An additional finite element analysis of the simple shear test conditions was performed using this modified modulus variation and the same analytical procedure described previously. The results of this analysis are compared to the experimental results in Fig. 46. It may be noted that the predicted values of shear stress and pore pressure are less than the measured values at values of shear strain larger than 4%; at 10% strain the predicted values are about 10% less than the measured values. Thus, by reducing the modulus values for stress orientations other than horizontal and vertical, fairly good agreement has been achieved between the predicted and measured simple shear test results. While it seems almost certain that even better agreement could be achieved between the predicted and measured stress-strain curves, it was not considered necessary to achieve closer agreement to establish the usefulness of the stress-strain characteristics as formulated for these analyses.

Although the shape of the predicted and measured stress-strain curves in Fig. 46 are very similar, the predicted pore pressure-strain curve crosses the measured one, because the predicted values of pore pressure are somewhat too high at low values of strain. As explained previously, it has been assumed that the nonuniform pore-water pressures were completely equalized at all stages of the test in computing the predicted values. Thus the predicted values correspond to tests of longer duration than those actually performed, which lasted between 1-3/4 and 3-1/4 hours. Since the measured values of pore-water pressure were found to increase slightly with increasing test duration, it seems likely that the variation of pore pressure with strain measured in a test of long duration would be more similar in shape to the predicted curve in Fig. 46.

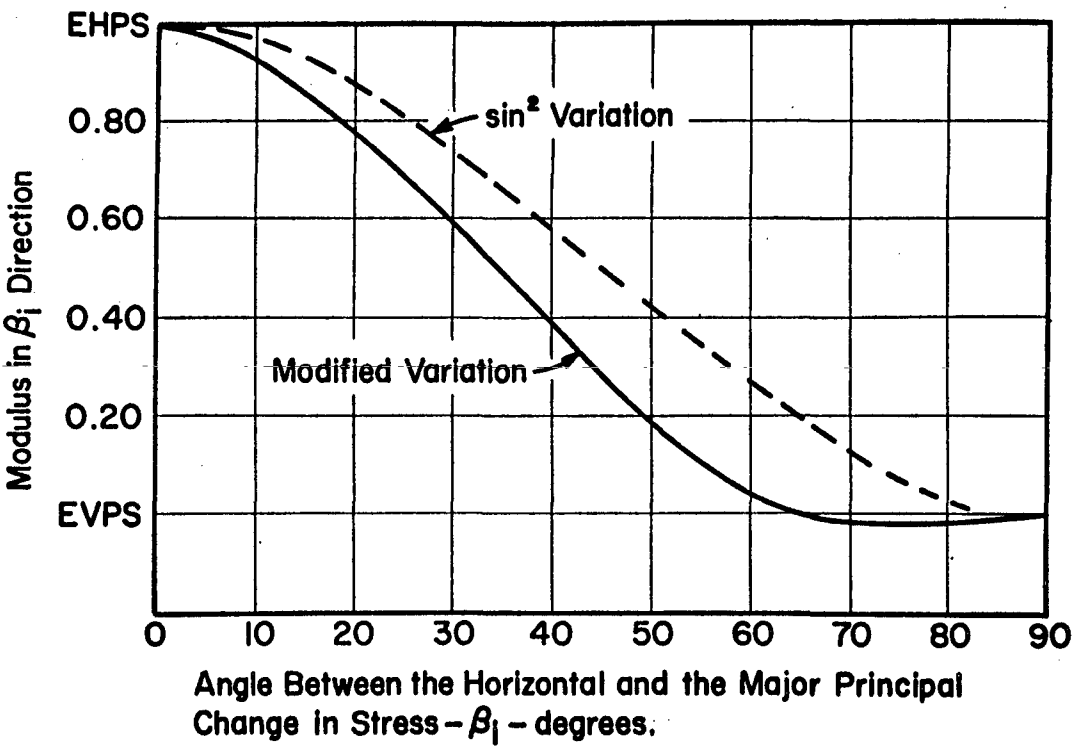

FIG. 45 MODIFIED MODULUS VARIATION FOR SAN FRANCISCO BAY MUD.

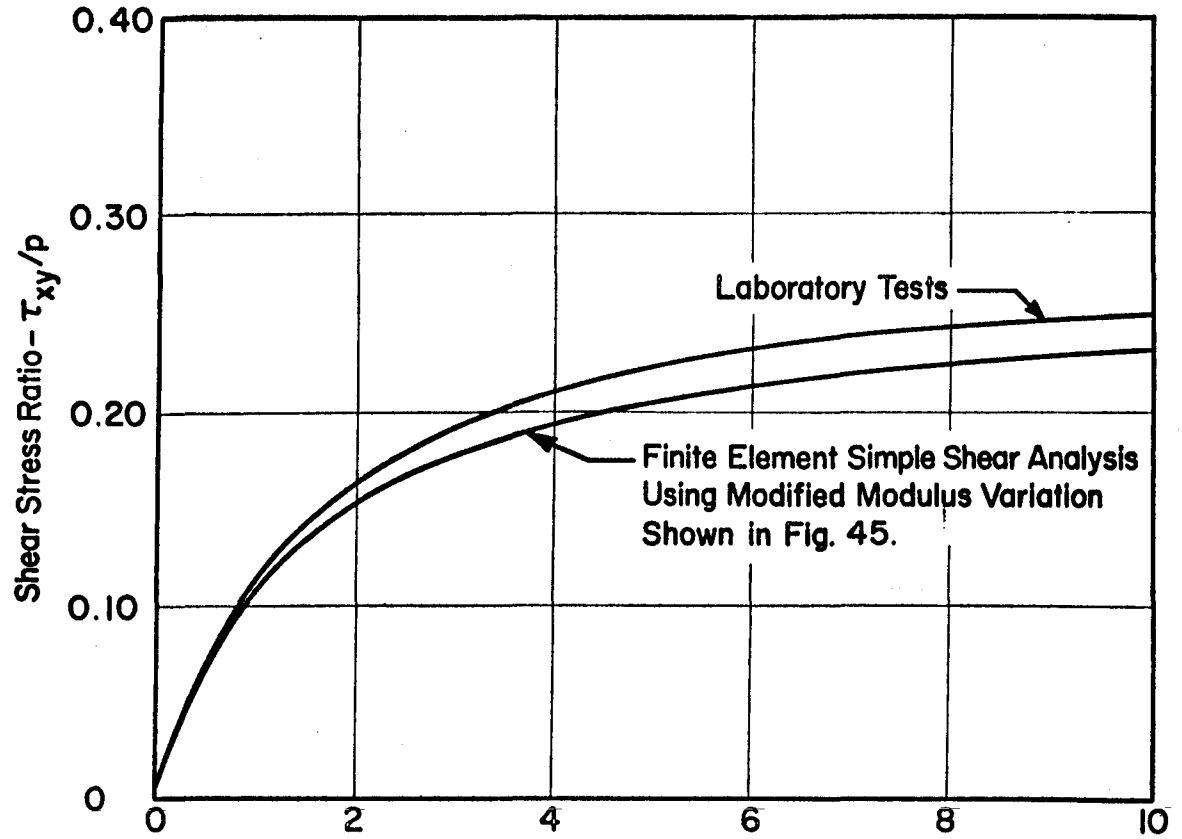

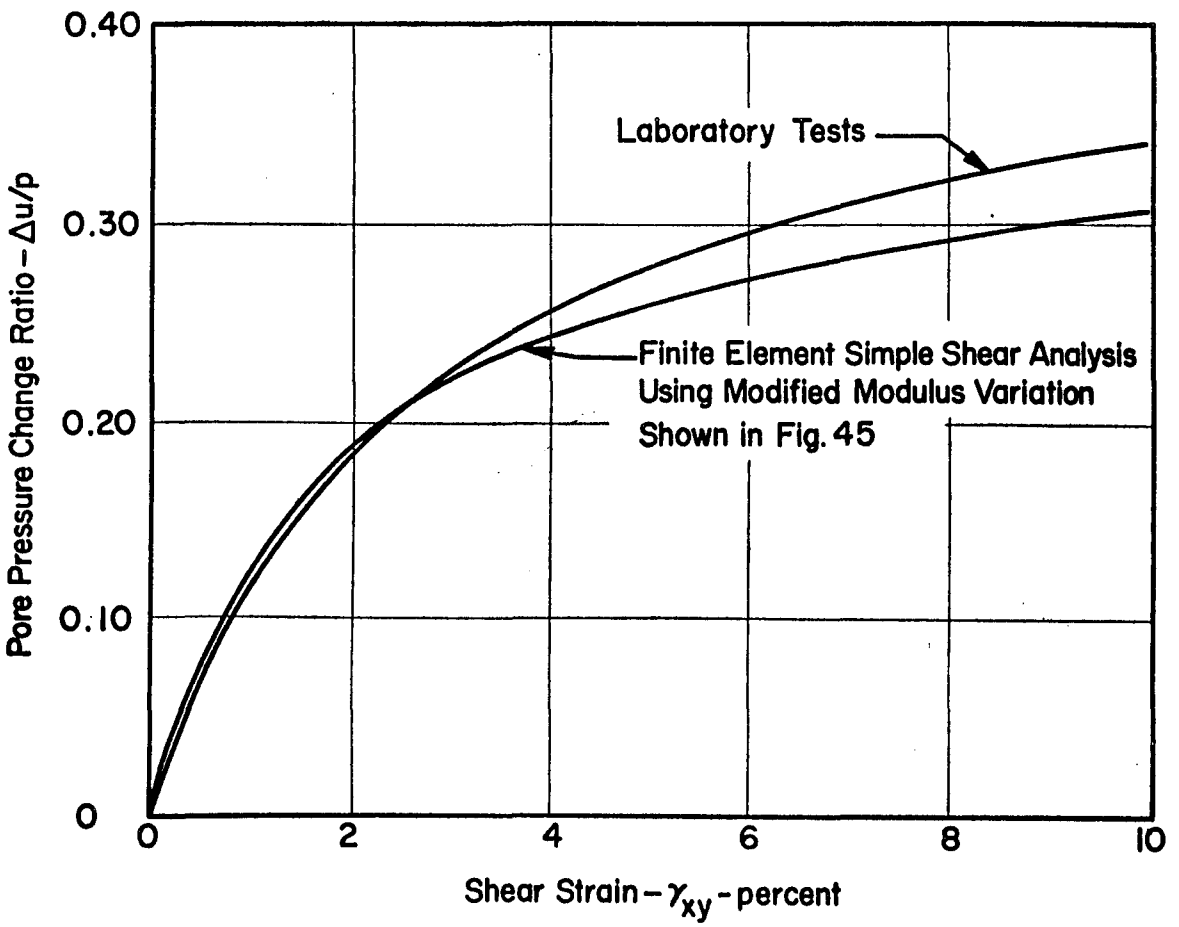

FIG. 46 COMPARISON OF EXPERIMENTAL AND ANALYTICAL SIMPLE SHEAR TEST RESULTS.

Progressive Failure in Simple Shear

During the course of these analyses it became evident that a specimen of clay may fail progressively under simple shear test conditions. Using the finite element method, stresses were calculated for each element in the configuration at each value of imposed strain. It was thus possible to determine where failure occurred initially and how the size of the failure zones increased with increasing amounts of distortion. Six stages of the analysis, corresponding to values of shear strain from 5% to 10%, are shown in Fig. 47; the cross-hatched areas indicate zones in which the maximum shear stress has become equal to the shear strength of the clay. Failure begins, near the ends of the specimen, at 6% shear strain. The size of these failure zones gradually increases and the zones merge at 8% strain, the size of the failure zone subsequently increasing still more until only a small stable region remains around the edge of the specimen at 10% strain.

It is thus evident that the stress conditions are sufficiently nonuniform to result in early failure in some regions in the specimen. Although the peak of the stress-strain curve has not been reached even at 10% shear strain, initial failure occurs at 5% strain. For a soft clay like San Francisco Bay Mud, with little or no reduction in shear resistance beyond the peak, the occurence of local failure at an early stage of the test is not likely to be significant. For a soil with considerably reduced shear resistance beyond the peak, however, early failure of a portion of the specimen might influence the test results to a considerable degree. Determination of the likelihood of progressive failure in simple shear for other soils, however, would require additional analyses using appropriate stress-strain behavior.

Simplified Simple Shear Analysis

The nonuniform stress conditions which develop within simple shear test specimens makes full interpretation of the test results quite complex, requiring use of detailed stress analyses. For some purposes, however, it is feasible to approximate the nonuniform simple shear conditions by uniform pure shear. The linear stress analysis performed by Roscoe (1953) and the nonlinear finite element analyses performed during this study all

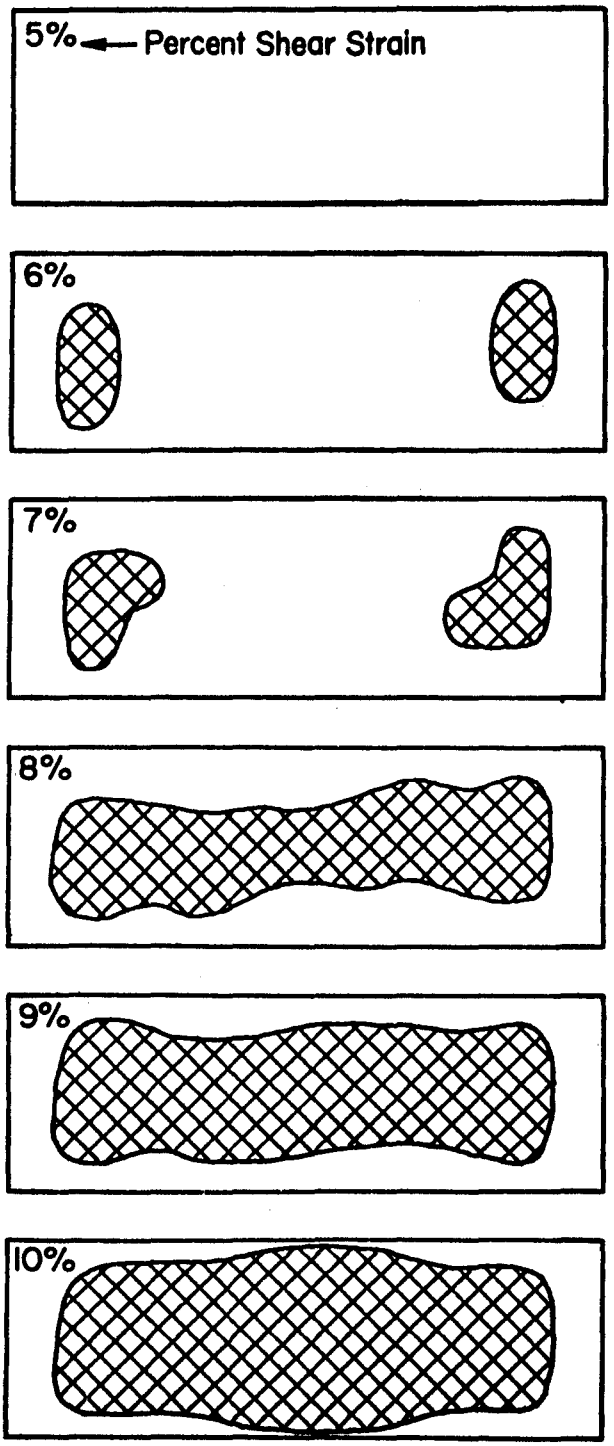

FIG. 47. DEVELOPMENT OF FAILURE ZONES IN SIMPLE SHEAR.

show that the stress nonuniformities in simple shear are most severe near the ends of the specimen. As illustrated in Fig. 48, simple shear differs from pure shear by the absence of complementary shear stresses at the ends of the specimen. The magnitudes of the shear stresses on planes parallel to the ends increase toward the center, however, and the stresses in the interior of a simple shear specimen correspond closely to pure shear conditions.

Pure shear is a convenient approximation for the stress changes in simple shear because the stresses are uniform and also because the changes in stress are extremely simple, as shown in Fig. 48. Pure shear may be represented by equal and opposite changes in shear stress or by equal and opposite changes in normal stress on perpendicular planes. The stress state resulting from an increment of pure shear is shown by the Mohr diagram in Fig. 48. The initial stress conditions are represented by $\sigma_{xo} = \sigma_3$ and $\sigma_{yo} = \sigma_1$, as would be appropriate for a normally consolidated clay specimen prior to shear. Application of changes in shear stress $\pm\Delta\tau_{xy}$ to the x and y planes, or changes in normal stress $\Delta\sigma_1$ and $\Delta\sigma_3$ to their bisectors results in the same state of stress, as shown in Fig. 48.

If it is considered that simple shear may be represented by pure shear, it is possible to predict the stress-strain curve for simple shear tests very easily using the stress-strain relationships developed. In pure shear the direction of compression is at 45° from the horizontal ($\beta_i = 45°$), and modulus values for this incremental stress orientation may be determined by evaluating equation 12 for $\beta_i = 45°$. The resulting expression is

$$E_{45°} = 0.3\ E_H + 0.7\ E_V \qquad (13)$$

in which E_H, E_V, and $E_{45°}$ are instantaneous modulus values for horizontal, vertical, and 45° compression at the same values of strain. To compute the stress-strain curve for pure shear, the instantaneous moduli E_H and E_V at increments of 1% shear strain, beginning with 0.5%, have been evaluated using Fig. 36. These values, and the corresponding values of $E_{45°}$, are listed in Table 5. To calculate corresponding stress changes, the relationships between increments of stress and strain are considered: For pure shear stress increments with the maximum shear stresses applied to the

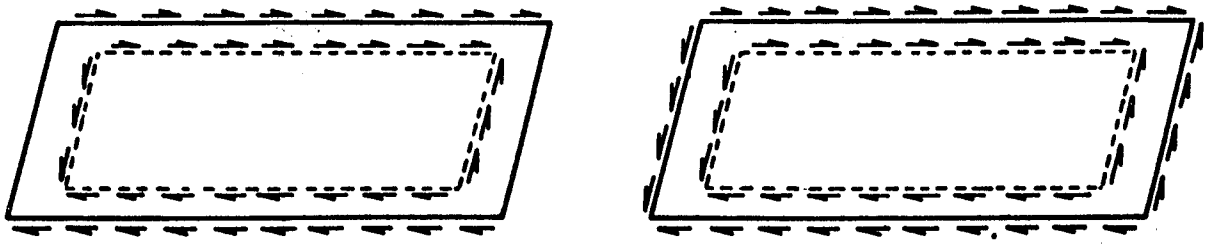

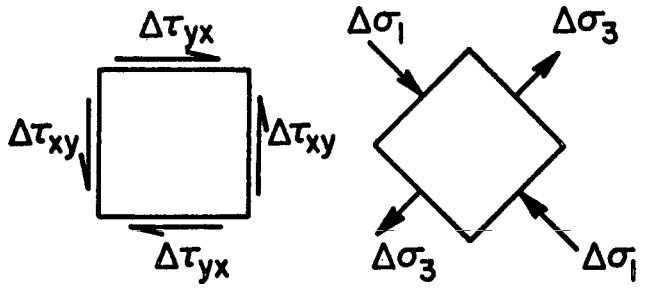

Pure Shear

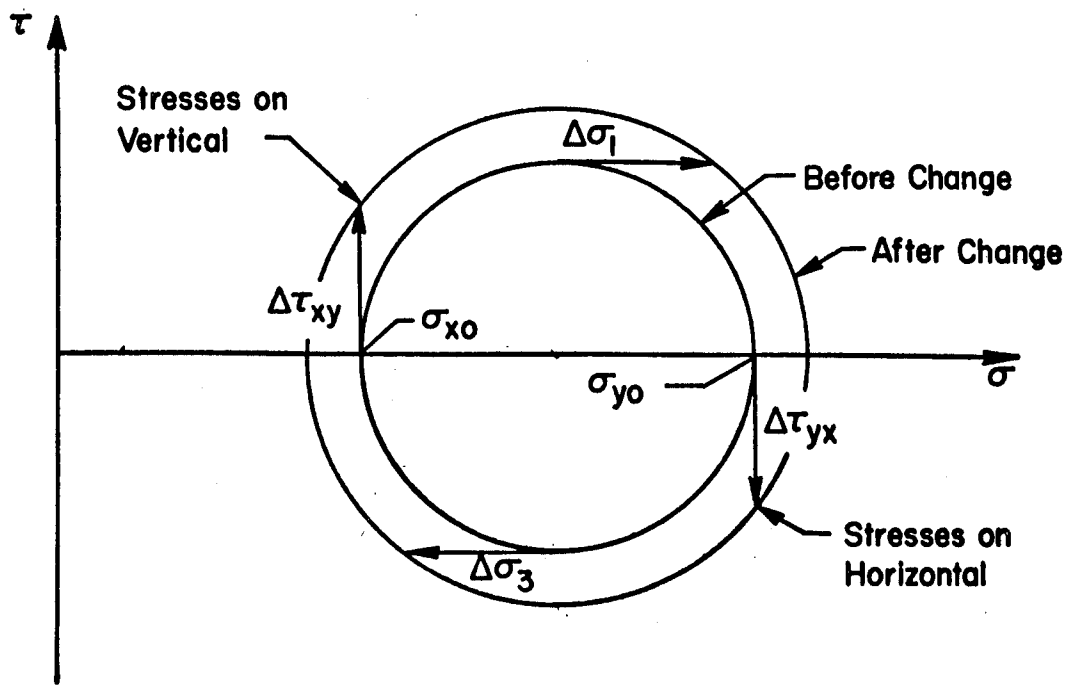

FIG. 48 SIMPLE SHEAR AND PURE SHEAR.

Table 5. Pure Shear Analysis

Shear Strain Increment $\Delta\gamma$ %	Average Values for Increment				Stress Increments			Pore Pressure $\frac{u}{p}$	Shear Stress $\frac{\tau_{xy}}{p}$	Shear Strain γ %
	γ %	$\frac{E_H}{p}$	$\frac{E_V}{p}$	$\frac{E_{45°}}{p}$	$\frac{(\Delta\sigma_1-\Delta\sigma_3)}{p}$	$\frac{\Delta u}{p}$	$\frac{\Delta t_{xy}}{p}$			
1.0	0.5	61	16	29.5	0.197	0.100	0.099			
								0.100	0.099	1.0
1.0	1.5	31	4.6	12.5	0.084	0.043	0.042			
								0.143	0.141	2.0
1.0	2.5	18	2.2	6.94	0.046	0.023	0.023			
								0.166	0.164	3.0
1.0	3.5	12	1.2	4.44	0.030	0.015	0.015			
								0.181	0.179	4.0
1.0	4.5	8.7	0.8	3.17	0.021	0.011	0.011			
								0.192	0.190	5.0
1.0	5.5	6.6	0.6	2.40	0.016	0.008	0.008			
								0.200	0.198	6.0
1.0	6.5	5.1	0.4	1.81	0.012	0.006	0.006			
								0.206	0.204	7.0
1.0	7.5	4.1	0.3	1.44	0.010	0.005	0.005			
								0.211	0.209	8.0
1.0	8.5	3.3	0.2	1.13	0.008	0.004	0.004			
								0.215	0.213	9.0
1.0	9.5	2.7	0.2	0.95	0.006	0.003	0.003			
								0.218	0.216	10.0

x and y planes, the various stress changes are related as shown in Fig. 48, i.e.

$$\Delta\tau_{xy} = \Delta\sigma_1 = -\Delta\sigma_3 \tag{14a}$$

and

$$\Delta\sigma_2 = 0 \tag{14b}$$

in which $\Delta\tau_{xy}$ is the shear stress increment, and $\Delta\sigma_1$, $\Delta\sigma_2$, and $\Delta\sigma_3$ are the major, intermediate and minor principal stress increments. These stress increments may be expressed in terms of the corresponding strain increments and the instantaneous modulus values as follows

$$\Delta\tau_{xy} = (G_i)_{xy} \cdot \Delta\gamma_{xy} \tag{15}$$

in which G_i is the instantaneous shear modulus value and $\Delta\gamma_{xy}$ is the shear strain increment. The shear modulus may be expressed in terms of Young's modulus as

$$G = \frac{E}{2(1+\nu)} \tag{16}$$

and for $\nu = 0.5$, appropriate for saturated clay under undrained conditions,

$$G = \frac{E}{3} \tag{17}$$

Substituting this expression for G into equation (15), the shear stress increment may be expressed in terms of the instantaneous value of Young's modulus:

$$\Delta\tau_{xy} = \frac{(E_i)_{45}}{3} \cdot \Delta\gamma_{xy} \tag{18}$$

and the incremental stress difference may be expressed as

$$(\Delta\sigma_1 - \Delta\sigma_3) = 2\Delta\tau_{xy} = \frac{2}{3}(E_i)_{45} \cdot \Delta\gamma_{xy} \tag{19}$$

Equations (18) and (19) have been used to calculate the stress increments in Table 5.

From these increments of total stress, increments of pore-water pressure may be calculated using the pore pressure coefficients $\bar{A}$ and B proposed by Skempton (1953):

$$\Delta u = B \cdot \Delta\sigma_3 + \bar{A}(\Delta\sigma_1 - \Delta\sigma_3) \tag{20}$$

For pure shear conditions, the direction of compression is 45° from the horizontal (β_i = 45°). The value of $\bar{A}$ for this stress increment orientation is 1.01 for San Francisco Bay Mud, as shown in Fig. 38, and the value of B is equal to 1.00 because the clay is saturated. These values of $\bar{A}$ and B have been used to evaluate the pore pressure increments in Table 5.

Variations of shear stress and pore pressure with strain were calculated, as shown in Table 5, by summing the incremental values, and the resulting variations are shown in Fig. 49. The values of shear stress calculated using the simplified pure shear analysis are somewhat smaller than the measured values, as in the case of the finite element analysis shown in Fig. 46, which was also performed using the modified modulus variation. At 10% shear strain, the shear stress values calculated by pure shear analysis are 13% lower than the measured values, whereas those calculated by the finite element analysis were about 10% smaller. Thus the shear stress-strain curve determined by the pure shear analysis is in very good agreement with the one determined by finite element analysis. As mentioned previously, the analytical and experimental variations could be brought into closer agreement if a slightly different modulus variation than the one expressed by equation (12) was used in the analysis.

The difference between the calculated and measured values of pore-water pressure are much larger, as shown in Fig. 49. Values of $\frac{u}{p}$ calculated by pure shear analysis are 35% lower than the measured values at 10% shear strain. Values calculated by finite element analysis, shown in Fig. 46, are only about 10% lower than the measured values.

On the basis of these results it appears to be feasible to represent simple shear conditions by idealized pure shear stress increments for the purpose of determining stress-strain behavior. Application of the same procedures to determine changes in pore pressure, however, results in large differences between calculated and measured values. It seems likely that the reason for this discrepancy lies in the fact that changes in pore-water pressure in simple shear are influenced to a considerable degree by nonuniformities in stresses: As initially nonuniform pore pressures equalize, the equilibrium value is higher than the average because of the difference between the slopes of the consolidation and rebound curves.

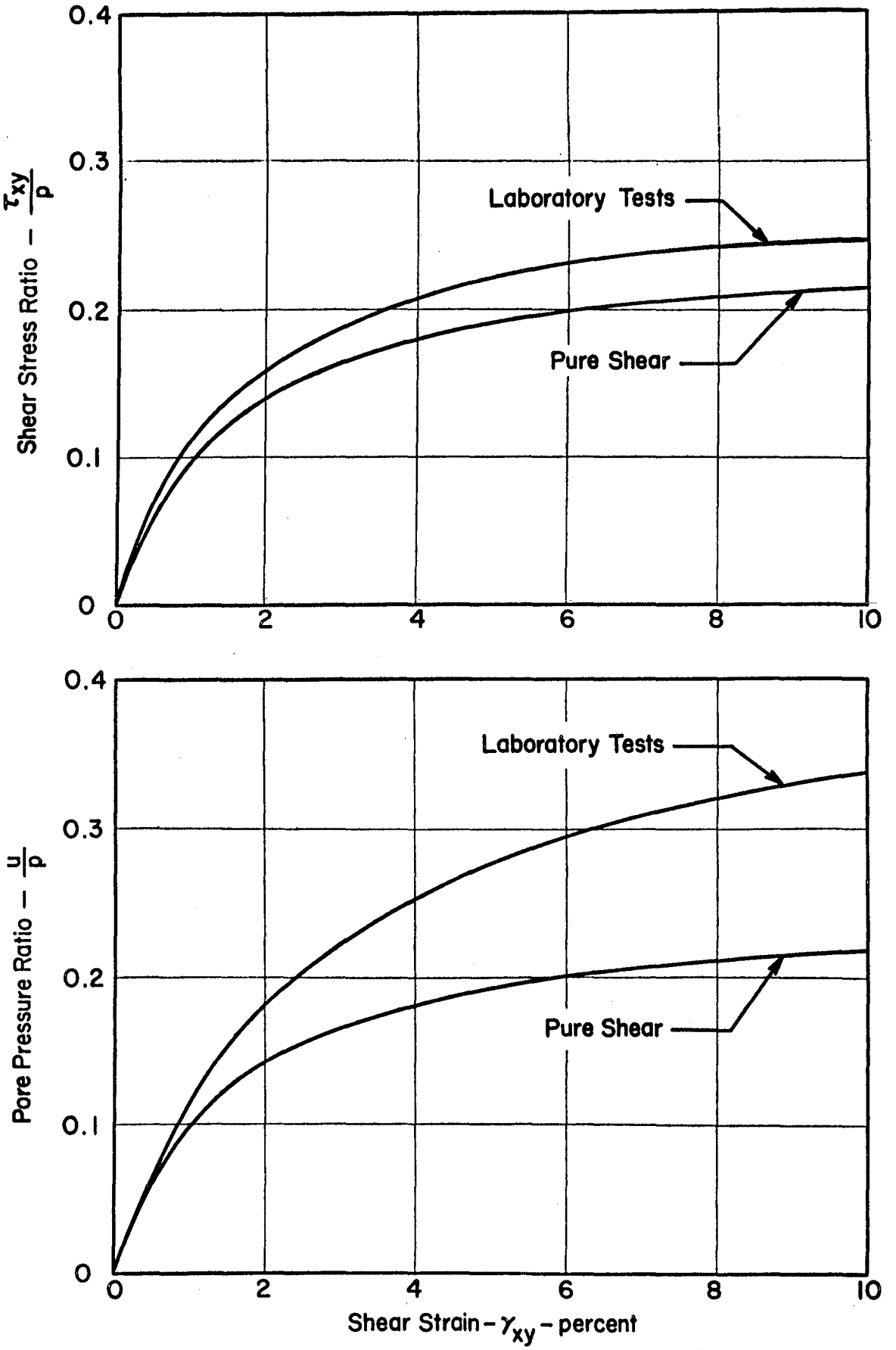

FIG. 49. COMPARISON OF LABORATORY SIMPLE SHEAR TEST RESULTS WITH PURE SHEAR ANALYSES.

Stress and pore pressure nonuniformities are taken into account in finite element analyses, but they are ignored in pure shear analyses.

Summary

An empirical nonlinear stress-strain relationship has been developed for San Francisco Bay Mud under undrained conditions which appears to provide a convenient and accurate basis for nonlinear analyses of stress and deformation. The relationship evolved encompasses the reduction in instantaneous tangent modulus with increasing degrees of distortion (shown in Fig. 36) and the influence of stress orientation or anisotropy (shown in Fig. 45). The values of modulus are proportional to the consolidation pressure, p.

Finite element analyses of simple shear test conditions have demonstrated the utility of the hypothesized stress-strain relationship, and comparison of the predicted and measured simple shear results has made it possible to refine the proposed relationship. These simple shear analyses have shown that progressive failure is likely in simple shear because of nonuniform stress conditions, and that these stress nonuniformities may effect the measured values of pore-water pressure to an appreciable degree. The actual, nonuniform simple shear stress conditions may be adequately represented by uniform pure shear stress conditions for purposes of considering stress-strain behavior, but not for considering the development of pore-water pressures due to the applied shear stresses.

CHAPTER 5

ANALYSIS OF A SLOPE USING NONLINEAR STRESS-STRAIN BEHAVIOR

If finite element analyses of excavated slopes are conducted using a series of steps representing successive stages in the excavation, the modulus value of each of the elements representing the slope may be changed after each step of the analysis in accordance with the current values of stress and strain. It is possible, therefore, to simulate nonlinear stress-strain behavior with a series of linear increments. This procedure has been employed in analyzing the behavior of a 50-ft. high slope excavated in San Francisco Bay Mud, to determine the practicability of the procedure and to examine the influence of gradually changing modulus values.

Stress-Strain and Strength Characteristics

The empirical stress-strain relationships developed in the previous chapter were employed in the analysis; the variation of modulus values with shear strain is shown in Fig. 36, and the variation with direction of compression is shown by the modified variation in Fig. 45. These are the same relationships employed in the analyses of simple shear conditions shown in Fig. 46.

The variation of undrained strength with depth used in the analysis is representative of conditions at the University of California field test site at Hamilton Air Force Base. As shown in Fig. 50, the ground water table is 10 ft. below ground surface, and a desiccated crust overlies the normally consolidated clay beneath. The higher strength values shown correspond to vertical compression, and the lower values correspond to horizontal compression (Duncan and Seed, 1966). The variation of undrained strength with direction of compression between these extremes is shown in Fig. 51. This variation was determined using undrained plane strain and simple shear tests on normally consolidated specimens. The initial values of horizontal stress used were three-quarters as large as the overburden pressure (K = 0.75).

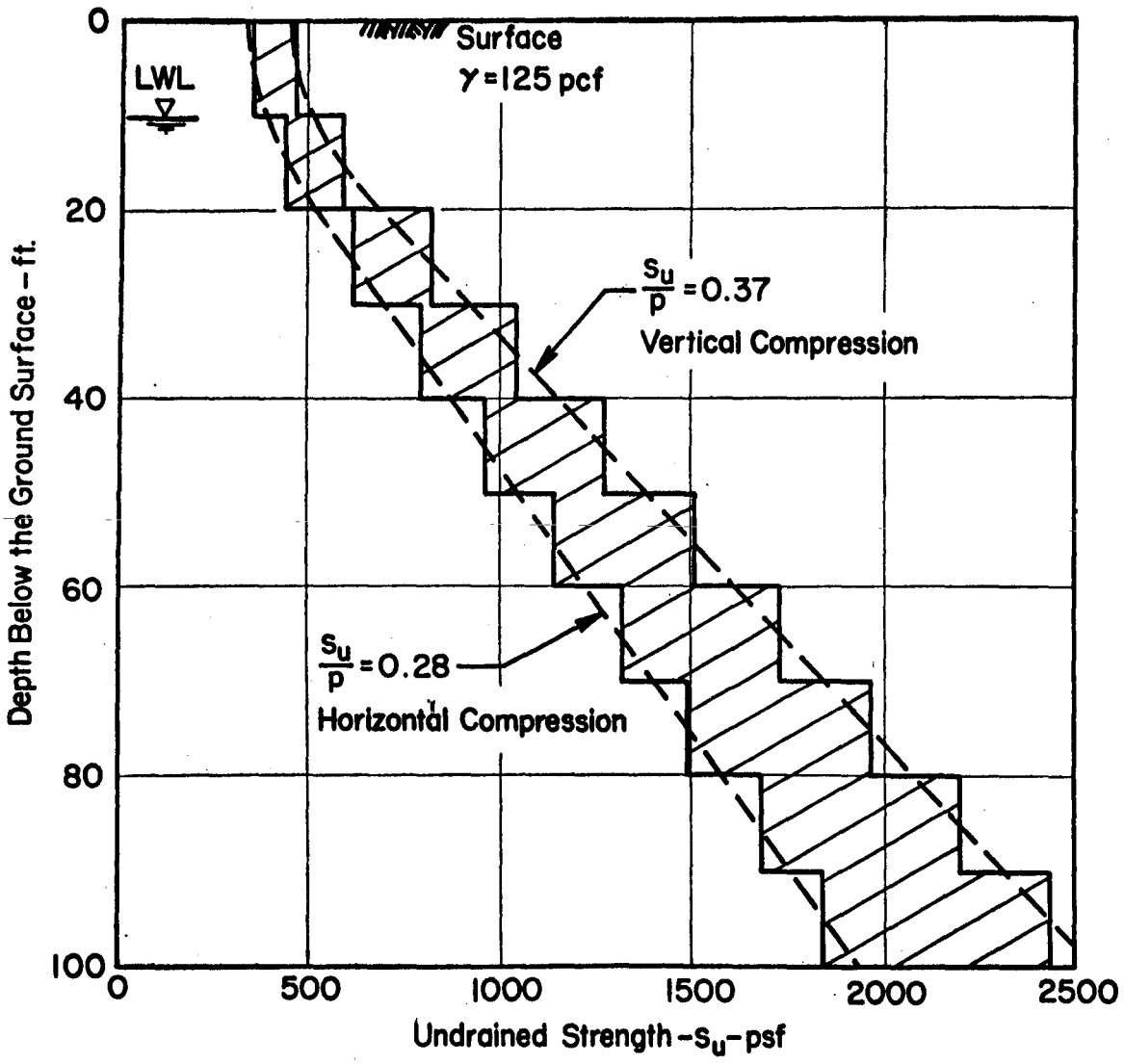

FIG. 50 VARIATION OF THE UNDRAINED STRENGTH WITH DEPTH BELOW THE GROUND SURFACE.

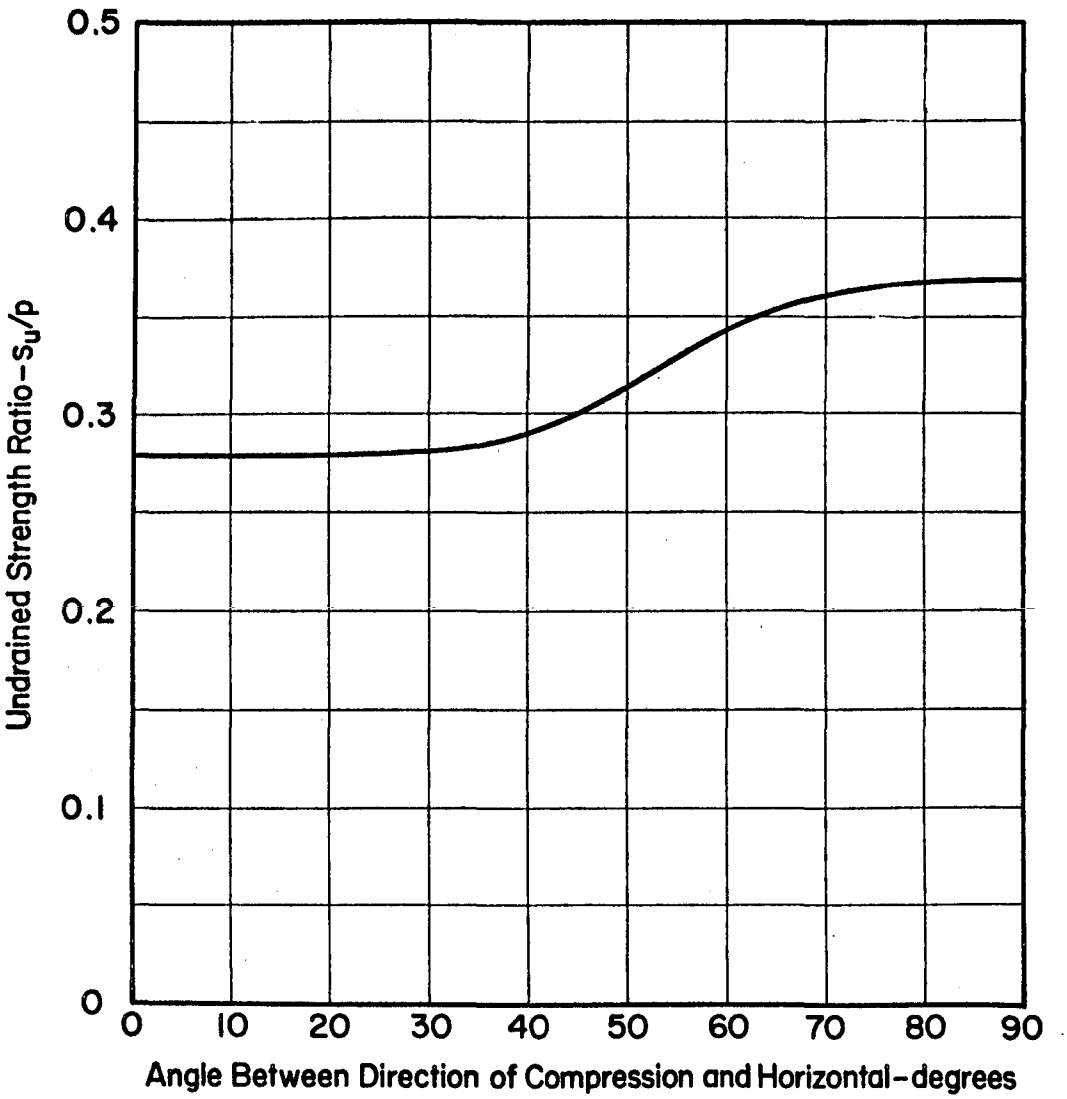

FIG.5I. VARIATION OF UNDRAINED STRENGTH WITH DIRECTION OF COMPRESSION FOR SAN FRANCISCO BAY MUD.

Analytical Procedure

The method of analysis employed was similar to the bilinear slope analyses described previously, except that the modulus for each element was reevaluated after each step in the analysis. A simplified flow diagram for the computer program employed is shown in Fig. 52. It may be noted that each time a layer is removed, the resulting displacements and stresses are calculated more than once. The first time the modulus values are evaluated using the strains at the end of the previous step. The second and subsequent times, the modulus values are evaluated using average values of strain during removal of the layer. This repeated solution insures close correspondence between the desired nonlinear stress-strain characteristics and the linear segments employed in the analysis. In the analysis described in this chapter, the displacements and stresses were calculated only twice, because preliminary analyses indicated that this resulted in satisfactory simulation of the desired nonlinear behavior.

The analysis was performed by simulating removal of 5 layers, each 10 ft. thick, the final height of the 3:1 slope being 50 ft. The finite element configuration employed represented a clay layer 100 ft. thick (50 ft below the toe of the slope) and contained 330 elements and 368 nodal points. The analysis required 15 minutes of IBM 7090-7094 computer time.

Slope Behavior

The stress conditions after excavation of the slope to its full 50 ft depth are illustrated in Fig. 53 by contours showing percentage of shear strength mobilized. It may be noted that no region has failed, the most critical conditions corresponding to about 80% strength mobilized. The most highly stressed regions are near the toe of the slope and along the contact between the bottom of the clay and the region layer beneath. This behavior is somewhat different from that established using bilinear analyses with similar strength profiles and initial stress conditions. In those cases it was found that failure occurred first in a zone beneath the crest of the slope. The difference in behavior probably results from the fact that the strength values employed in the present nonlinear analysis vary with direction of compression, and would thus be smaller

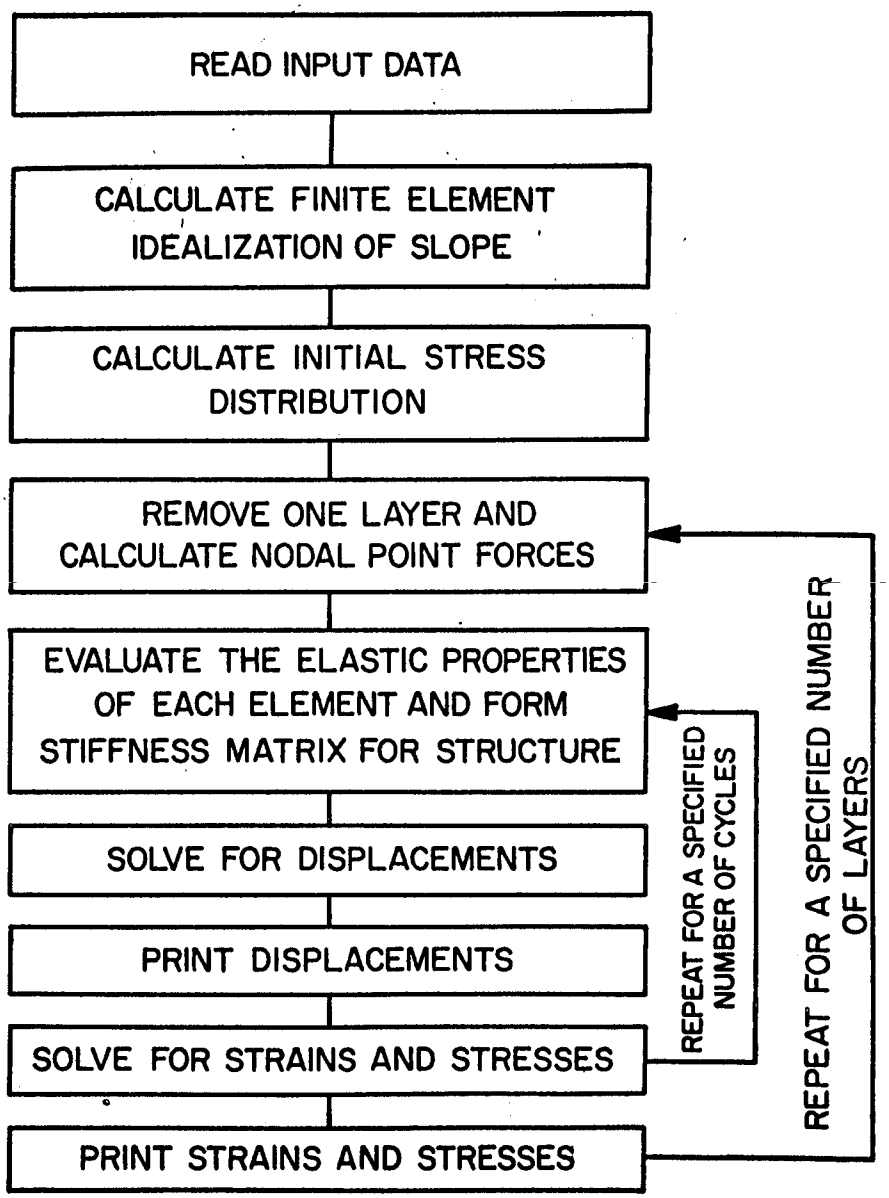

FIG.52. SIMPLIFIED FLOW DIAGRAM FOR MULTILINEAR SLOPE ANALYSES.

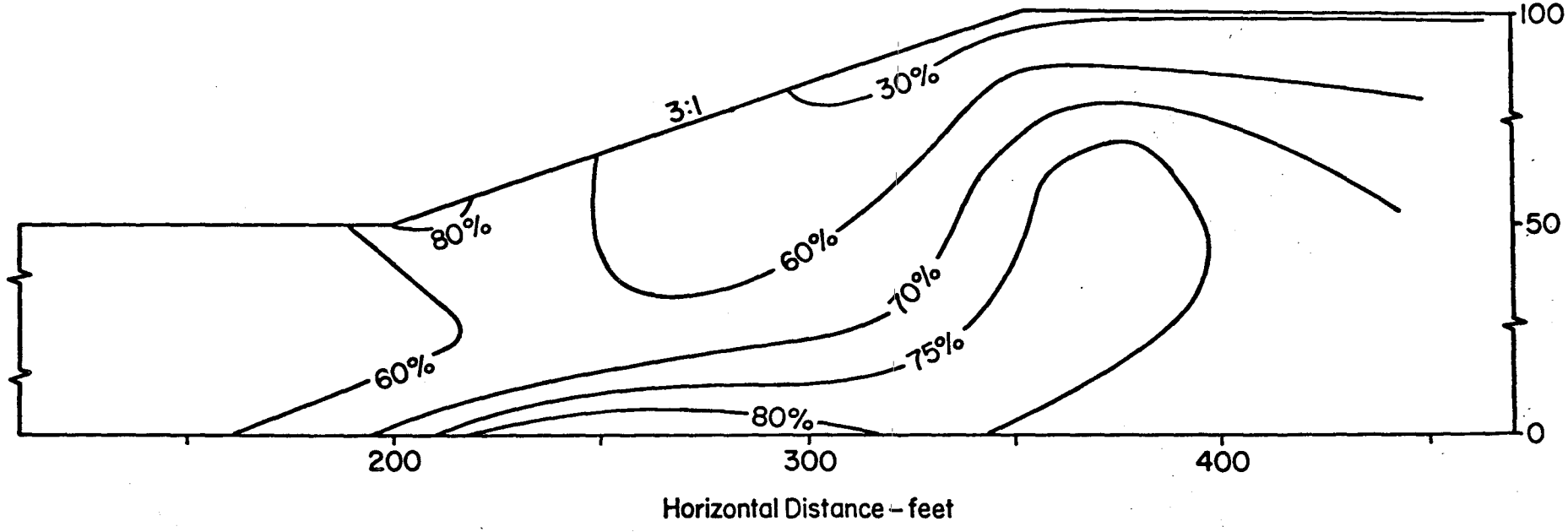

FIG. 53. PERCENT OF SHEAR STRENGTH MOBILIZED IN THE MULTILINEAR ANALYSIS.

for the regions near the toe of the slope and along the base, where the direction of compression is close to horizontal.

Whereas the linear analyses indicated that local failure would begin by the time the overall factor of safety had been reduced to about 1.7, the nonlinear analysis indicates that no local failure has developed even though the overall factor of safety is only 1.52. Thus the use of gradually changing modulus values, as opposed to abruptly changing values, tends to prevent the development of stress concentrations and early local failure. Since modulus values are lowest in the zones most highly stressed, they are subjected to less severe stress changes during subsequent stages of excavation.

The values of tensile stress calculated were very small. The values of stress at the centroids of the upper row of elements were all compressive, but, by extrapolating these stress values to the surface of the layer, it was determined that tensile stresses on the order of 0.035 γH would exist at the surface. These values are smaller than indicated by the previous linear and bilinear analyses, probably because the modulus values corresponding to horizontal extension (or vertical compression) are relatively low.

The major principal stress orientations and the deformed shape of the slope are shown in Fig. 54. The stress orientations beneath the bottom of the excavation are nearly horizontal, whereas those determined using linear analyses with similar modulus variation with depth and initial stress conditions were more steeply inclined, as shown in Fig. 8. The difference in behavior may result from the fact that the stress-strain relationship employed in the nonlinear analysis is anisotropic; at any stress level the modulus values are higher for horizontal compression than for any other direction of compression. Therefore, beneath the base of the excavation, where the direction of compression is horizontal, the soil is relatively stiff, and additional horizontal stresses are transmitted to the stiffer region.

The deformed shape of the slope shown in Fig. 54 is similar to those determined using linear and bilinear analyses. It is interesting to note that the deformations are quite appreciable, amounting to about 0.6 ft slumping near the crest, and .5 ft bulging near the toe of the slope, even though the factor of safety is about 1.5.

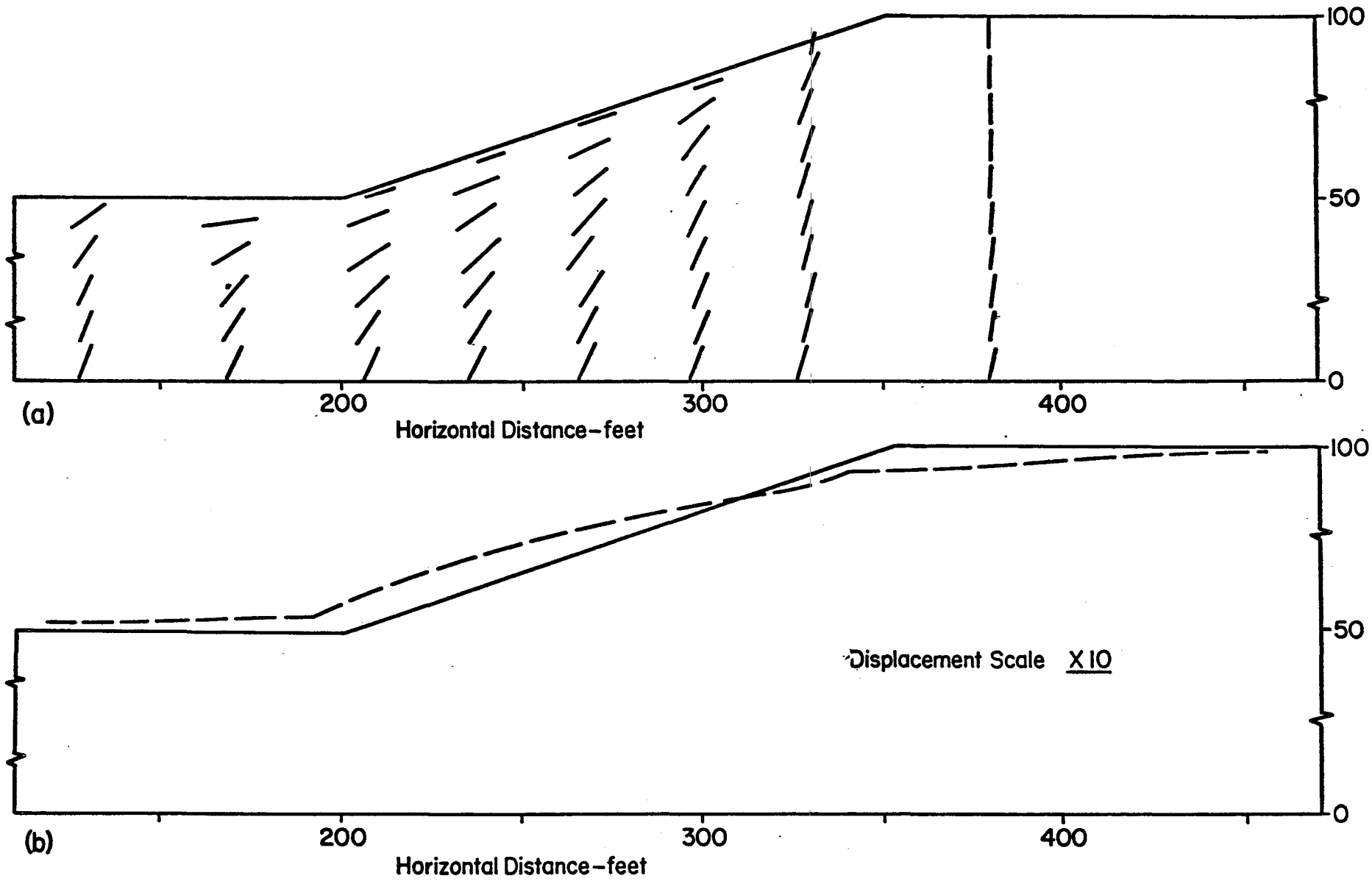

FIG.54. (a) MAJOR PRINCIPAL STRESS DIRECTIONS , (b) DEFORMED SHAPE OF SLOPE.

Summary

On the basis of this analysis it appears that gradual reduction of modulus values with increasing strain reduces the tendency for local overstress to a very significant degree. Thus both linear and bilinear analyses probably overestimate the extent of local failure for stable slopes. Variations of modulus values and strength values with direction of compression also influence the stress distribution and the position of the zones where the percentage of strength mobilized is highest.

CHAPTER 6

PORE PRESSURES AT THE END OF CONSTRUCTION OF EXCAVATED SLOPES AND EMBANKMENTS

The analyses described in previous chapters of this report simulated short-term, undrained loading conditions for saturated clays, and were therfore performed using stress-strain relationships formulated in terms of total stresses. It is possible, however, to predict pore-water pressures for the end-of-construction period using the results of these analyses. This procedure may provide a useful alternative to total stress analyses for the period immediately following construction. If pore pressure values are predicted for this period, stability analyses may be performed using effective stress methods. Comparison of the predicted pore pressures with values measured during construction could then provide a very convenient technique for evaluating the adequacy of the design continually during construction.

Pore Pressure Coefficients

For purposes of expressing pore pressure changes in terms of changes in total stress, the pore pressure coefficients proposed by Skempton (1954) are very convenient. According to the equation proposed by Skempton, the relationship is expressed as

$$\Delta u = B\Delta\sigma_3 + \bar{A}(\Delta\sigma_1 - \Delta\sigma_3) \qquad (23)$$

in which Δu is the change in pore pressure, $\Delta\sigma_1$ and $\Delta\sigma_3$ are the major and minor changes in total stress, and $\bar{A}$ and B are pore pressure coefficients. The coefficient B reflects the contribution to the change in pore pressure caused by equal all-around changes in total stress, and for soft saturated clays is equal to 1.0. The coefficient $\bar{A}$ reflects the influence of the change in stress difference. The value of $\bar{A}$ for a particular clay depends on the degree of overconsolidation and on the direction in which the clay is compressed, among other factors. Values of $\bar{A}_f$ ($\bar{A}$ at failure) are shown in Table 6 for normally consolidated San Francisco Bay Mud under conditions of horizontal and vertical compression. Between these extremes

the value of $\overline{A}_f$ varies with the direction of compression as shown in Fig. 55. (This is the same variation discussed in Chapter 4 of this report and illustrated in Fig. 38). Also shown in Table 6 is the value of $\overline{A}_f$ determined for Bay Mud using isotropically consolidated-undrained (IC-U) triaxial tests, in which the specimens are consolidated under equal all-around pressure and then tested undrained. It may be noted that the value of $\overline{A}_f$ for IC-U triaxial tests ($\overline{A}_f$ = 1.05) is only

Table 6. Values of $\overline{A}_f$ for Normally Consolidated San Francisco Bay Mud.

Type of Undrained Test	Value of $\overline{A}_f$
Horizontal Plane Strain	0.71
Vertical Plane Strain	1.08
IC-U Triaxial (vertical)	1.05

slightly higher than the average for the stress orientations shown in Fig. 55. This value may therefore represent a reasonable value for use with all directions of compression.

Changes in Pore Pressure and Pore Pressure Ratios

The initial pore-water pressure distribution in a saturated, normally consolidated clay layer with the water table at the ground surface is shown in Fig. 56; the pore-water pressure increases linearly with depth from zero at the surface to 6240 psf at the base of the layer 100 ft below the surface. To calculate changes in pore-water pressure during excavation of a slope, equation 23 was employed, using values of $\Delta\sigma_1$ and $\Delta\sigma_3$ calculated by the finite element method. The values of change in pore pressure shown by the contours in Fig. 56 were calculated assuming that the clay is linearly elastic and that $\overline{A}$ is equal to 1.05 for any direction of compression. The values of pore-water pressure for each element in the configuration representing the slope were calculated by the computer at the same time the changes in total stress were calculated. Since the

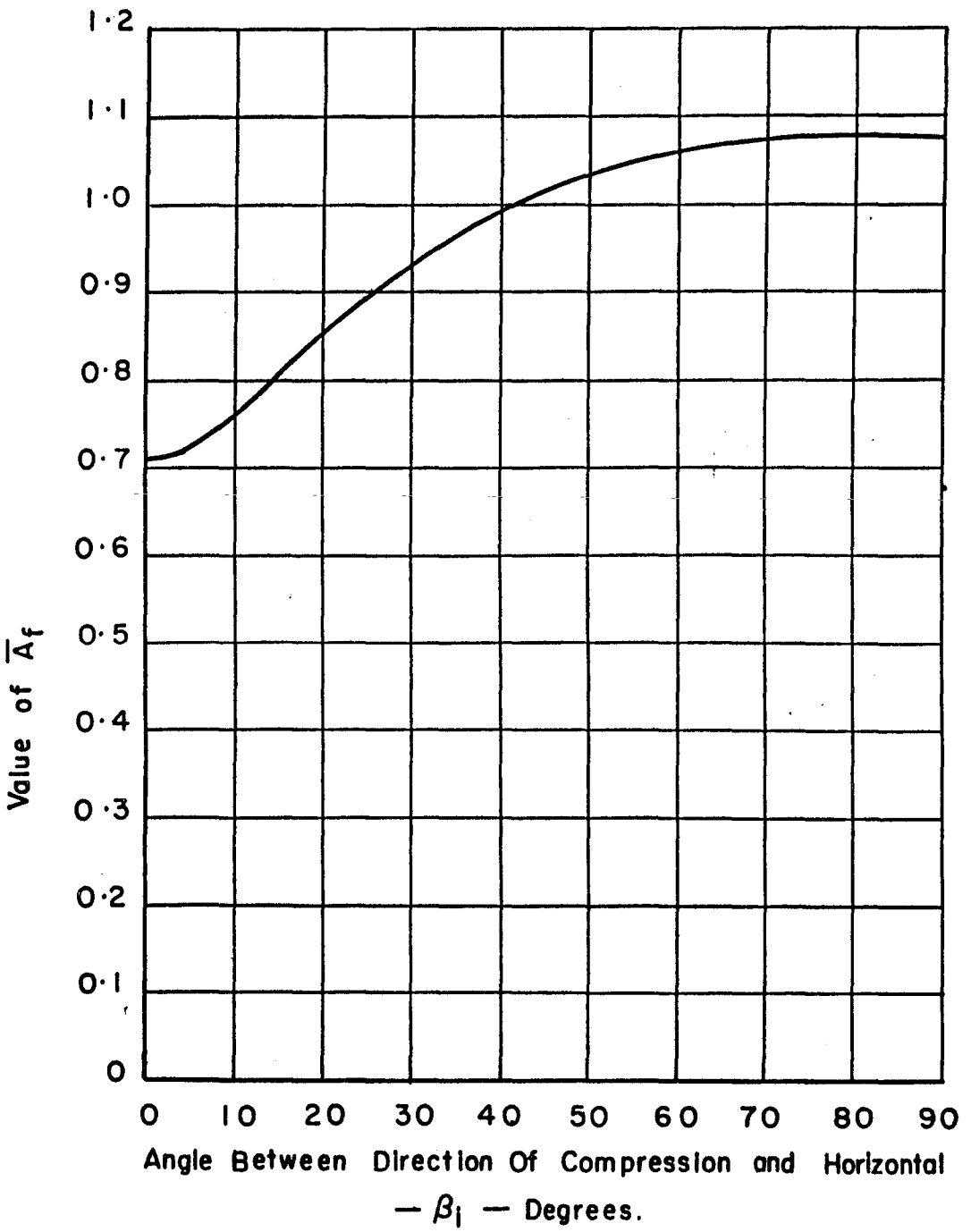

FIG. 55. VARIATION OF VALUES OF $\bar{A}_f$ WITH DIRECTION OF COMPRESSION FOR SAN FRANCISCO BAY MUD.

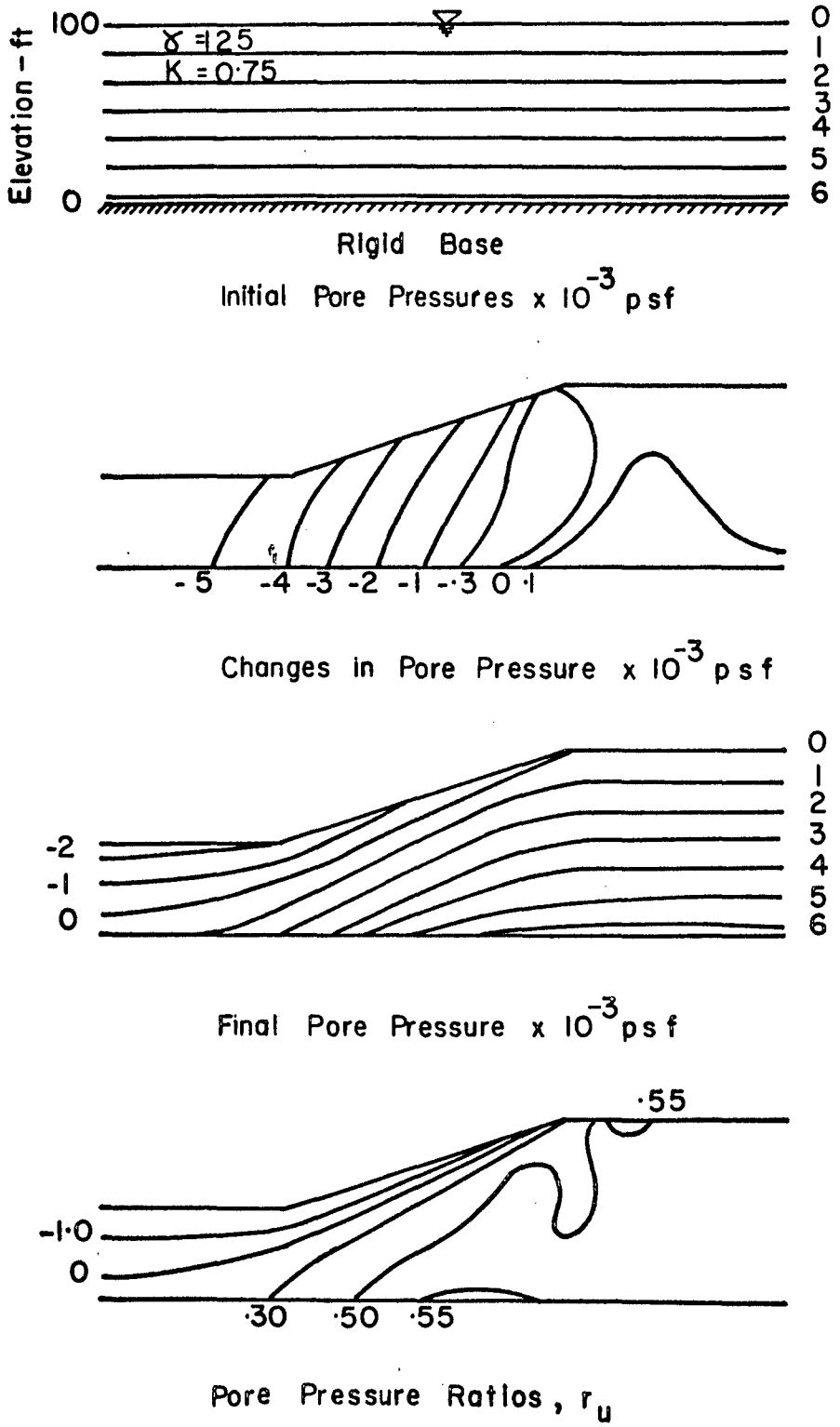

FIG. 56. PORE PRESSURES AND PORE PRESSURE RATIOS.

changes in stress during excavation are predominantly negative, the changes in pore-water pressure are also mostly negative. The largest changes occur near the toe of the slope where the amount of unloading is greatest, and only very small changes occur behind the crest of the slope.

Addition of the initial values with the changes in pore pressure results in the final values shown in Fig. 56. Immediately below the base of the excavation and the surface of the slope the pore pressures are negative, whereas at greater depths the values are positive. At the extreme right, behind the crest of the slope, the pore pressures have not changed appreciably during excavation.

The same final pore pressures are represented in a different manner in the lower part of Fig. 56. The value of pore pressure at each point has been divided by the overburden pressure. The resulting ratio, $u/\gamma h$, has been given the symbol r_u for pore pressure ratio by Bishop and Morgenstern (1960). It represents the portion of total overburden pressure carried by water, and has been found to be a very convenient means of expressing water pressure conditions for purposes of stability analyses. For the clay layer shown at the top of Fig. 56, the initial water pressures correspond to a constant value of r_u throughout the layer; for $\gamma = 125$ lb/ft^3, the value of r_u representative of the initial conditions is 62.4/125.0, or 0.50. Comparing this value to the contours of r_u shown in the lower part of Fig. 56, it may be seen that the value of r_u is reduced during excavation in the region of the slope.

Effect of Bulk Compressibility

The influence of bulk compressibility on stresses, strains and displacements around excavated slopes has been studied and found to have no great effects. However, since the principal effect of a change in bulk compressibility would logically be to alter the value of mean normal stress, it was considered that changes in bulk compressibility might influence the calculated values of pore-water pressure significantly, and a study was made to investigate this possibility.

The same slope has been analyzed using two different assumptions concerning bulk compressibility. The first assumption was that Poisson's

ratio was 0.475; thus the bulk modulus of the clay, $K = \frac{E}{3(1-2\nu)}$, was, in each element, equal to 6.67 times Young's modulus. When the value of Young's modulus for an element is reduced to a small value after failure, the value of the bulk modulus is also reduced by the same factor. A better representation of the behavior of saturated clays is represented by the second assumption made, that the bulk modulus remains constant ($K = 10^6$ psf) regardless of the amount of shear stress or strain to which the clay is subjected.

Both analyses were performed using bilinear stress-strain characteristics with the same strength profile corresponding to $S_u/p = 0.3$. The initial stresses were represented by a value of K equal to 0.75, and the values of $\overline{A}$ used in the analyses varied with direction of compression as shown in Fig. 55. The results of the two analyses are illustrated in Fig. 57 by contours showing the calculated values of r_u. The values are virtually identical for both cases, indicating that the influence of bulk modulus value is not large for this slope. On this basis it was decided to perform subsequent analyses using a constant value of Poisson's ratio (0.475), permitting the use of more rapid computer programs.

Pore Pressures Around Excavated Slopes

Several analyses have been made to investigate the effects of modulus variation with depth, stress-strain behavior, and values of $\overline{A}$ on the calculated pore pressures around excavated slopes. In this study two variations of modulus with depth were considered; modulus constant throughout the depth and modulus increasing with depth. Three types of stress-strain behavior were considered; linear, bilinear, and anisotropic nonlinear. Two possible pore pressure coefficient values were considered; the constant value determined using IC-U triaxial tests on San Francisco Bay Mud, and the values of $\overline{A}$ determined using horizontal and vertical plane strain tests, which vary with direction of compression. Of the 12 possible combinations among these parameters, 6 meaningful combinations, which are shown in Table 7, were selected for study. The results of these analyses are discussed in the following sections.

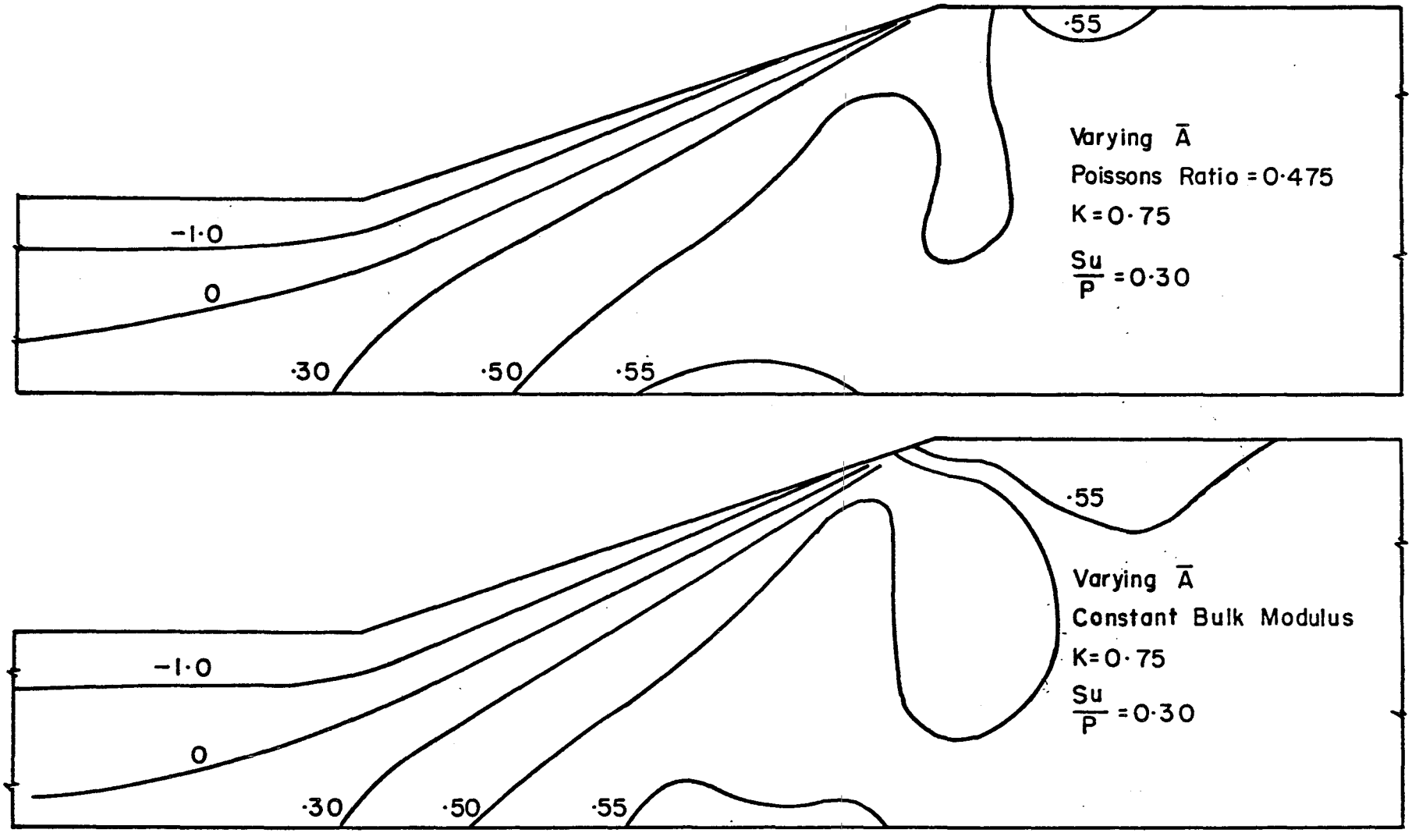

FIG. 57. EFFECT OF BULK COMPRESSIBILITY ON PORE PRESSURES AROUND EXCAVATED SLOPES IN NORMALLY CONSOLIDATED CLAY.

Table 7. Analyses of Pore Pressures Around Excavated Slopes

Analysis	Variation of $\bar{A}$ with Direction of Compression	Stress-Strain Relationship	Variation of Modulus with Depth	Results Shown in Fig. No.
1	Constant	Linear	Constant	58 (top)
2	Constant	Linear	Increasing	58 (bottom)
3	Varying	Linear	Increasing	59 (top)
4	Varying	Bilinear	Increasing	59 (bottom) and 60 (top)
5	Varying	Anisotropic Nonlinear	Increasing	60 (bottom) and 61 (bottom)
6	Constant	Anisotropic Nonlinear	Increasing	61 (top)

Modulus Variation with Depth. The results of two analyses, performed using linear elastic stress-strain behavior and the same value of $\bar{A}$ for all directions of compression, are shown in Fig. 58. The values of r_u shown in the upper part of the figure were calculated using a constant value of Young's modulus throughout the thickness of the layer, and those shown in the lower part were calculated using modulus values increasing linearly with depth. The values calculated by the two methods are nearly the same; the value of r_u for any point in the upper diagram is at most only a few percent different from that for the same point in the lower diagram, indicating that the influence of modulus variation with depth is small.

Local Failure. The effect of failure on the subsequent development of pore pressures is illustrated by Fig. 59. The values of r_u shown in the upper part were calculated using linear elastic stress-strain characteristics, with modulus increasing linearly with depth. The values shown in the lower part were calculated using bilinear stress-strain characteristics, and a normally consolidated strength profile corresponding to $S_u/p = 0.30$ as shown in Fig. 17. As in all of these analyses, the unit weights used were 125 lb/ft^3. Both the linear and the bilinear

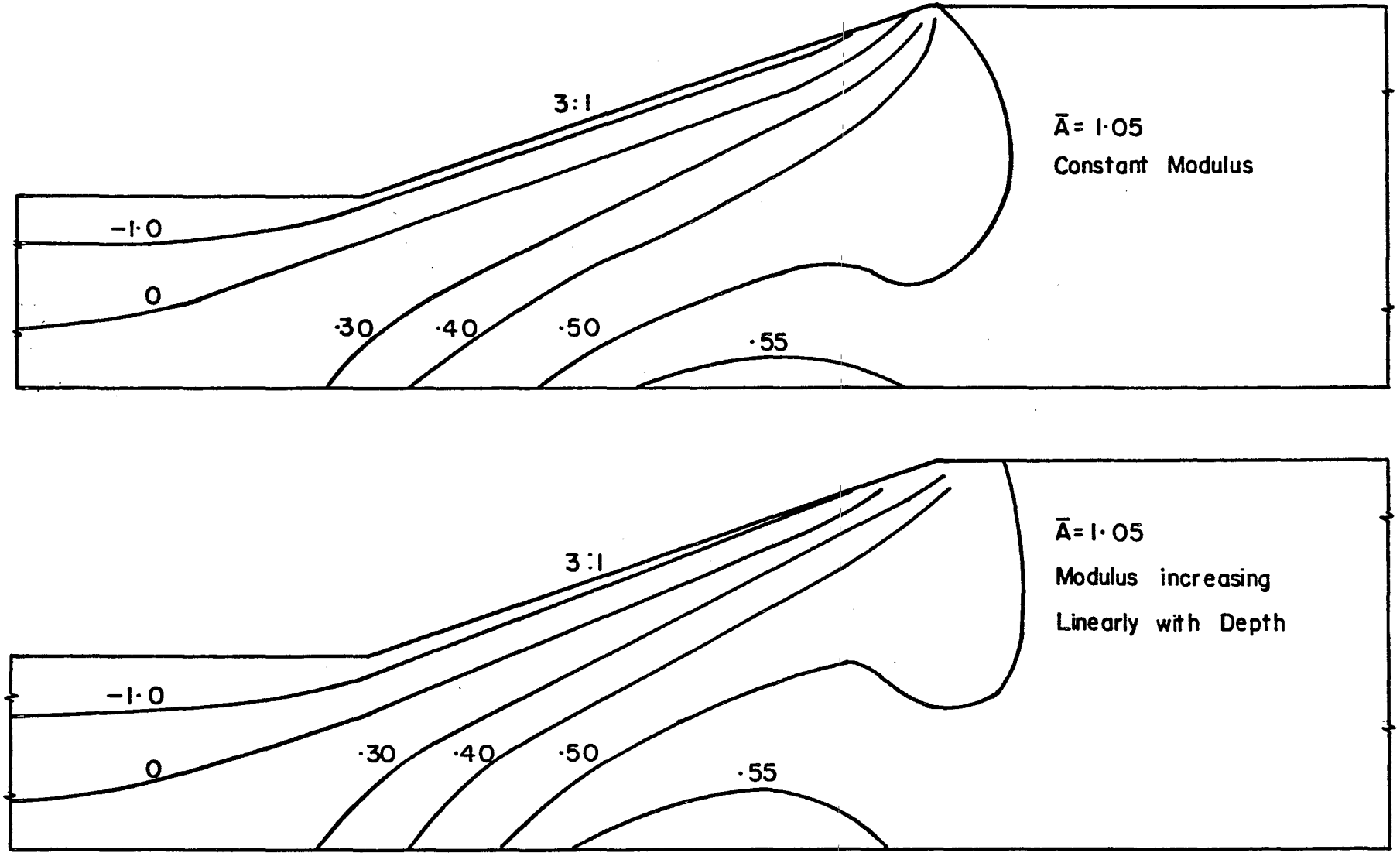

FIG. 58. PORE PRESSURE RATIOS CALCULATED FOR EXCAVATED SLOPES USING LINEAR ELASTIC ANALYSIS.

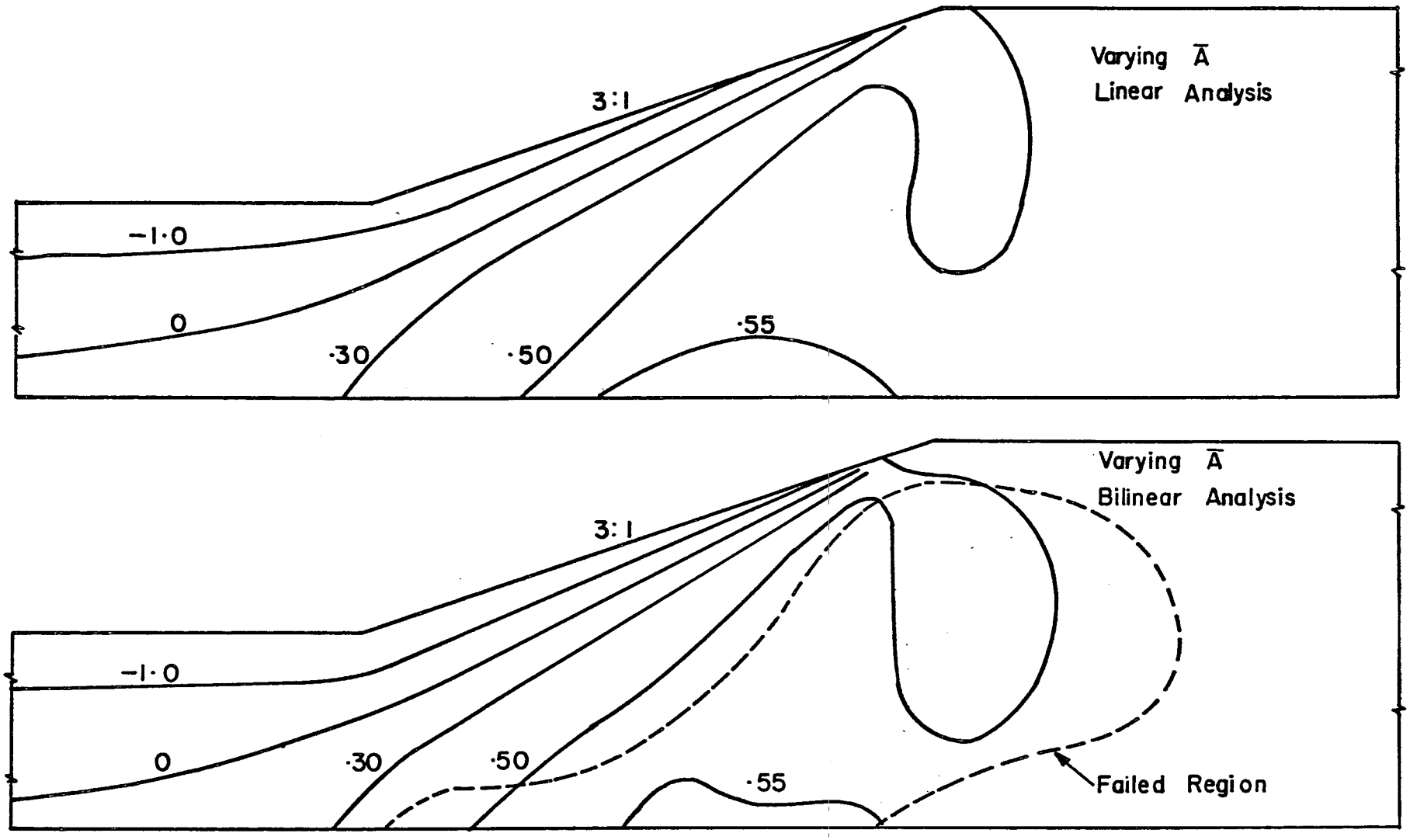

FIG.59. PORE PRESSURE RATIOS CALCULATED FOR EXCAVATED SLOPES USING LINEAR AND BILINEAR ANALYSIS

analyses were performed using values of $\bar{A}$ varying with incremental stress orientation, or direction of compression, as shown in Fig. 55. Even though a sizable failure zone developed in the slope analyzed using bilinear behavior, the calculated values of r_u are for practical purposes the same as those determined on the basis of linear behavior.

Anisotropic Stress-Strain Behavior. Perhaps the most realistic representations of the stress-strain and pore pressure characteristics of San Francisco Bay Mud are represented by the nonlinear, anisotropic relationships discussed in Chapter 4. Variations of instantaneous modulus values with increasing strain are illustrated in Fig. 36, and the influence of stress orientation on modulus values is shown in Fig. 45. These relationships have been employed in an analysis of the post-excavation pore pressures around a 3:1 slope shown in Fig. 60. The overall factor of safety of the slope at its final height of 50 ft was found to be about 1.5, and at this stage no failure zones had developed anywhere around the slope; the largest percentage of strength mobilized was about 80% at the base of the clay layer and near the toe of the slope, based on the strength profiles shown in Fig. 50. Also shown in Fig. 60 are values of r_u calculated using a similar strength profile and bilinear stress-strain behavior. The variation of $\bar{A}$ with direction of compression shown in Fig. 55 was used in both analyses. The values of pore pressure ratio calculated using multilinear stress-strain behavior are significantly higher than those calculated using bilinear behavior, especially in the region below the lower half of the slope and beneath the bottom of the excavation. The difference apparently results from the difference in instantaneous modulus values for this region in the two analyses. The modulus values for horizontal compression used in the bilinear analysis are relatively large, resulting in larger pore pressures in regions subjected to horizontal compression.

Anisotropy with Respect to $\bar{A}$. Values of r_u have also been calculated using anisotropic, multilinear behavior by employing a constant value of $\bar{A}$, independent of stress increment orientation. The value of $\bar{A}$ used in these calculations ($\bar{A}$ = 1.05) was measured in IC-U triaxial tests on San Francisco Bay Mud. The calculated values of r_u are shown in Fig. 61

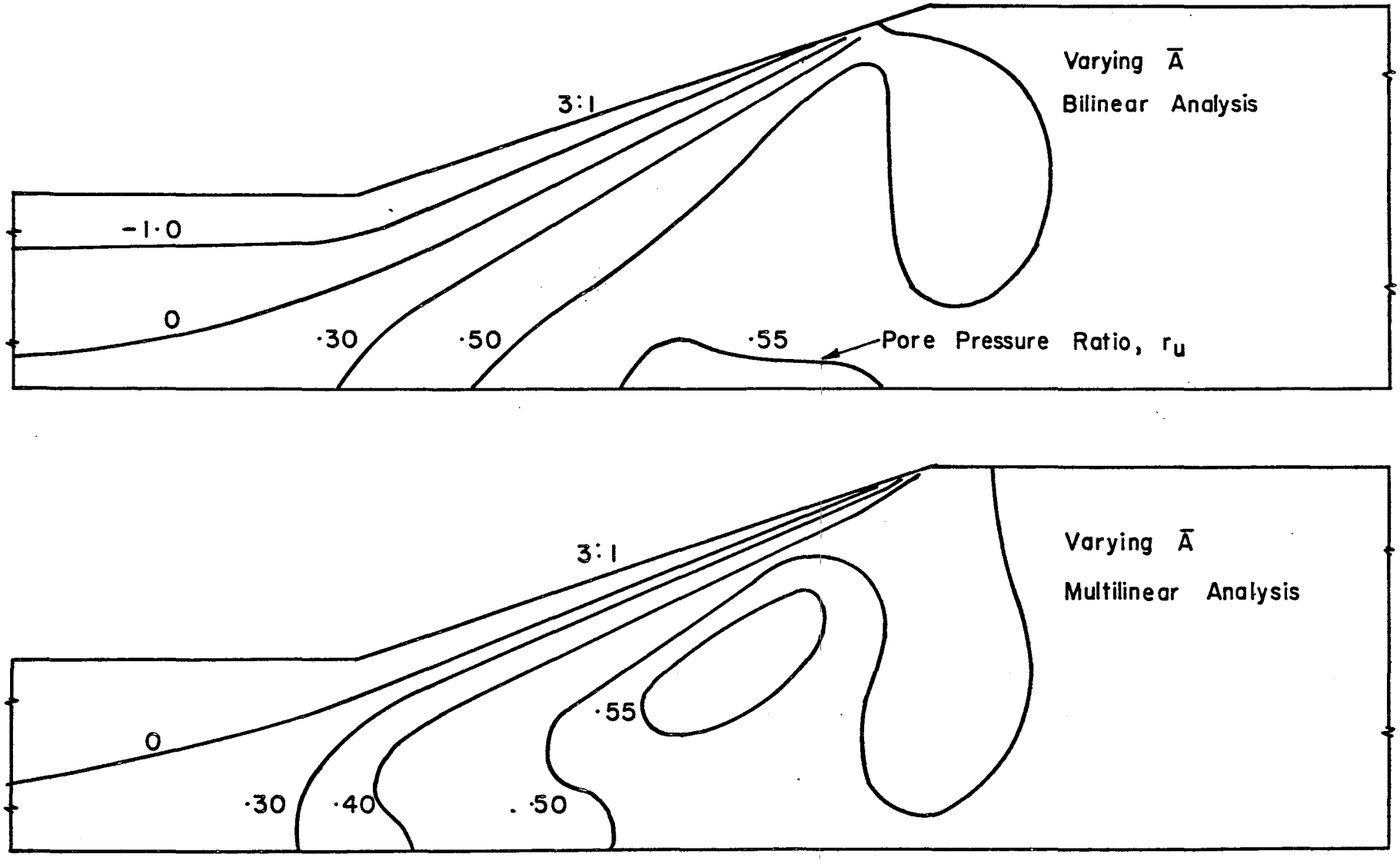

FIG. 60. PORE PRESSURE RATIOS FOR EXCAVATED SLOPES CALCULATED USING BILINEAR AND MULTILINEAR ANALYSIS.

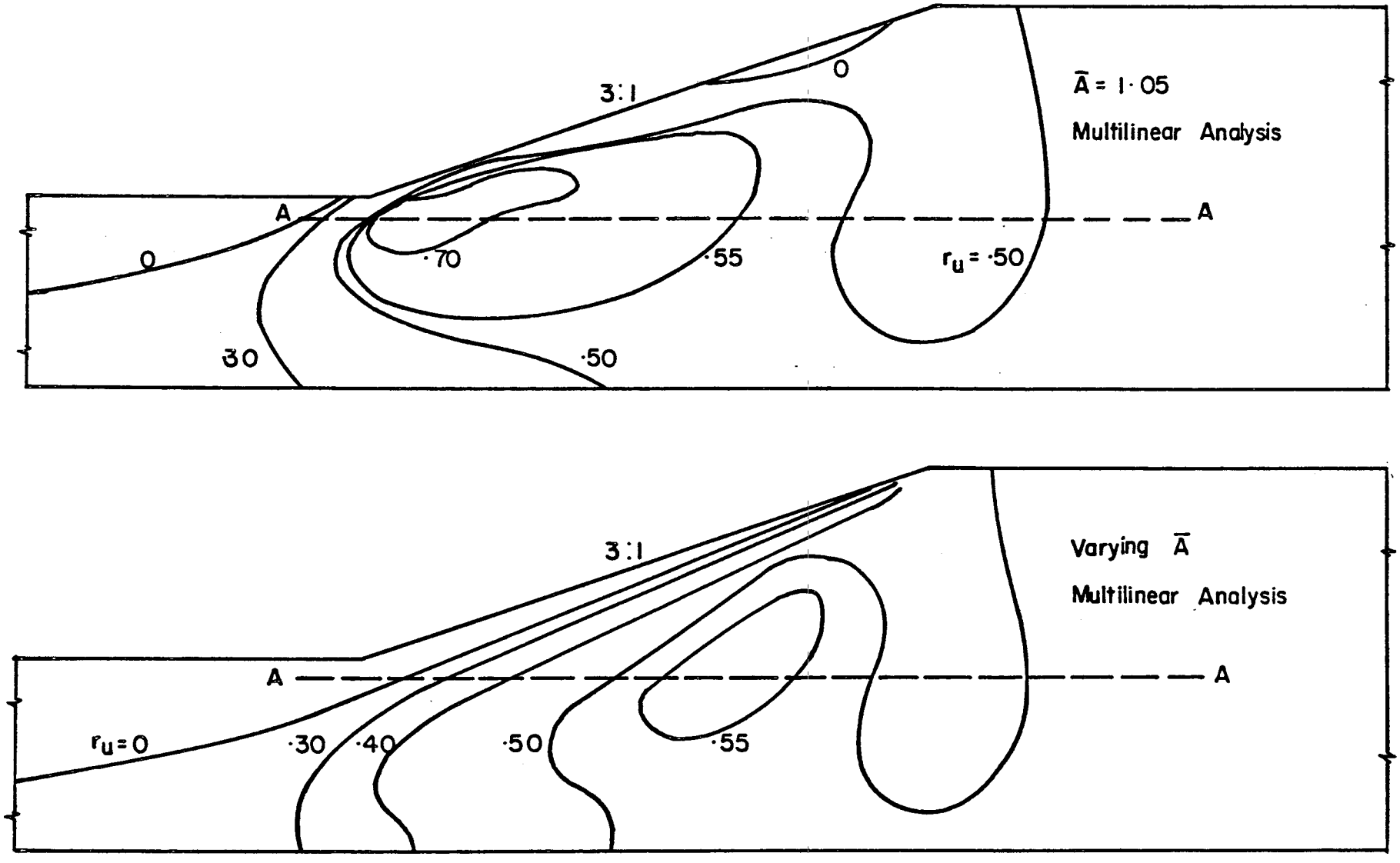

FIG. 61. PORE PRESSURE RATIOS FOR EXCAVATED SLOPES CALCULATED USING CONSTANT $\bar{A}$ AND USING $\bar{A}$ VARYING WITH STRESS ORIENTATION.

together with those determined using values of $\bar{A}$ varying with the direction of compression, as is appropriate for Bay Mud. It may be noted that the values of r_u calculated using $\bar{A} = 1.05$ for all regions of the slope are much higher, especially in the region beneath the lower part of the slope. This difference arises from the fact that the stress increments for this region are nearly horizontal, and the appropriate values of $\bar{A}$ for this stress orientation are about 0.7 as shown in Fig. 55, much less than the value 1.05 determined from IC-U triaxial tests.

The differences between the values of r_u shown in Figs. 60 and 61 are further illustrated in Fig. 62, where values of r_u for a horizontal plane beneath the toe of the slope are plotted. While all three methods result in the same values of r_u for the region beneath the upper part of the slope, there are very large differences for the region beneath the toe. Taking the values calculated using the multilinear analysis and varying values of $\bar{A}$ as being most correct, it may be concluded that the use of bilinear, isotropic stress-strain behavior results in pore pressures which are too low, and the use of a constant value of $\bar{A}$ determined from IC-U triaxial tests results in pore pressures which are too high.

Analyses performed using isotropic stress-strain behavior (Fig. 50, Fig. 59, upper part of Fig. 60) all result in approximately the same pore pressure distributions. Analyses performed using anisotropic stress-strain behavior, however, result in higher pore pressures near the base of the slope (Fig. 61). Thus it seems reasonable to infer that analysis performed using isotropic stress-strain behavior result in values of r_u which are too low near the lower part of the slope, no matter which values of $\bar{A}$ are used in the analyses. Thus it appears that the variation of modulus values with direction of compression (anisotropy with respect to stress-strain behavior) is quite important in determining the pore pressures after construction.

Pore Pressures in Soft Clay Foundations Beneath Embankments

The methods of analysis developed for excavated slopes may also be used to determine pore pressures in embankment foundations. These are perhaps of greater practical significance because the period immediately following construction of an embankment on a soft clay layer may be the

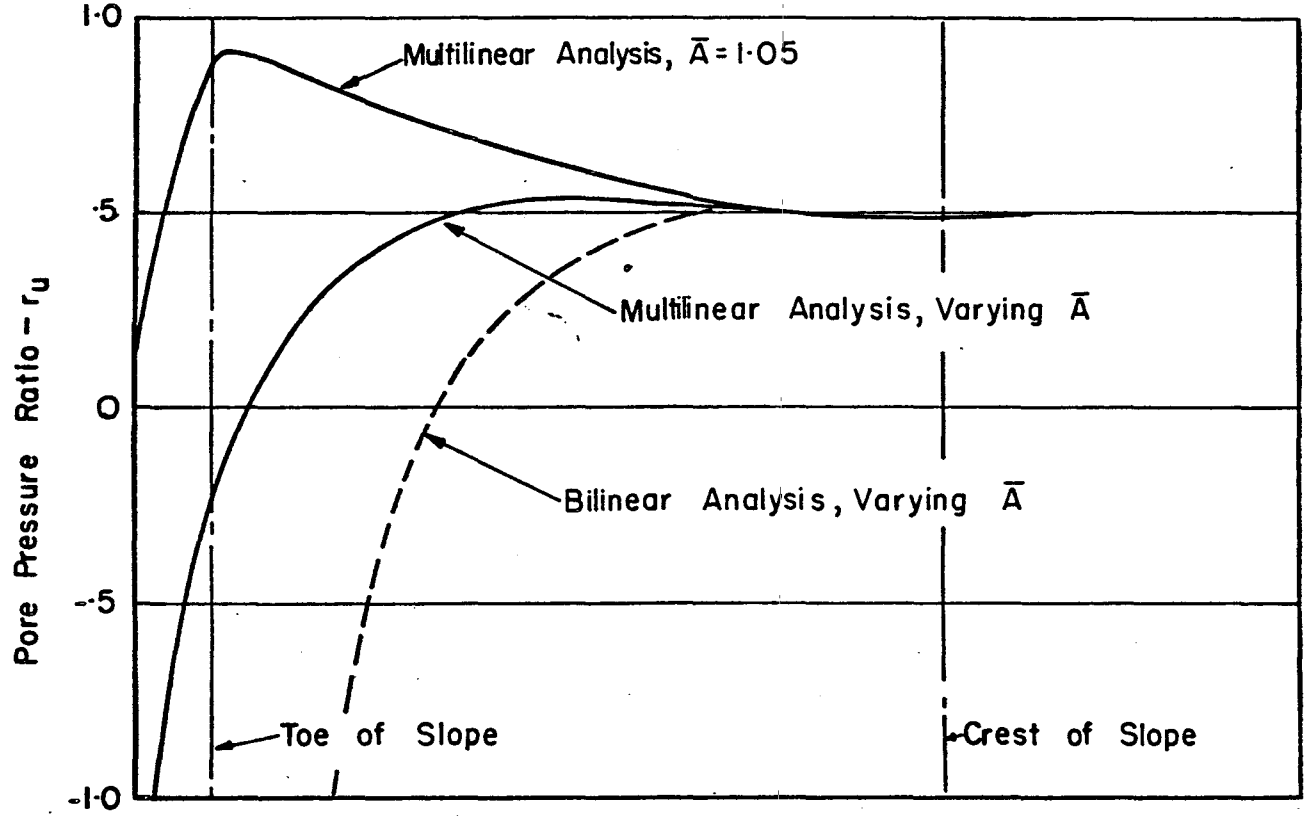

FIG. 62 . PORE PRESSURE RATIOS ON A HORIZONTAL PLANE.

most critical period in its entire life, whereas the critical period in the life of an excavated slope often occurs some time after construction, when the pore pressures have reached equilibrium with the ground water conditions in the region of the slope.

To illustrate the utility of the methods of analysis for predicting pore pressures in soft clay foundations, several analyses have been performed using different procedures. The embankment considered in each case was the same: A symmetrical 25 ft high embankment with 3:1 side slopes constructed on a 35 ft thick clay layer. Construction of the embankment was simulated by application of 5 lifts each 5 ft thick. The unit weight of both the embankment and the foundation was 125 lb/ft^3, and the stress-strain characteristics of the embankment soil were in each case assumed to be linearly elastic, with Young's modulus equal to 10^5 psf, and Poisson's ratio equal to 0.475. The initial pore pressures in the foundation layer were in equilibrium with the ground water level at the surface, so that the value of r_u representative of the initial conditions was 0.50 at all points in the layer. The initial stress conditions in the foundation layer were represented by a value of the total stress earth pressure coefficient, K, equal to 0.75 (horizontal stress 75% as large as the overburden pressure).

Analyses have been made to determine the effects of the properties of the foundation clay layer on the calculated pore pressures beneath embankments. The combinations of values of $\bar{A}$, stress-strain behavior, and modulus variation with depth selected for study are shown in Table 8, and the results of the analyses are described in the following sections.

Anisotropy with Respect to $\bar{A}$. For the purpose of examining the influence of the values of $\bar{A}$ on the final pore pressures, two analyses were performed using constant values of modulus (E = 60,000 psf) for the foundation layers. The results of these analyses are shown in Fig. 63. The values of r_u calculated using the value of $\bar{A}$ determined from IC-U triaxial test results ($\bar{A}$ = 1.05) are somewhat higher than those calculated using values of $\bar{A}$ varying with stress increment direction as shown in Fig. 55. The largest difference in calculated values of r_u is in the region beneath the toe of the embankment and just beyond. The largest value of r_u calculated using varying values of $\bar{A}$ is 2.0, whereas the largest value

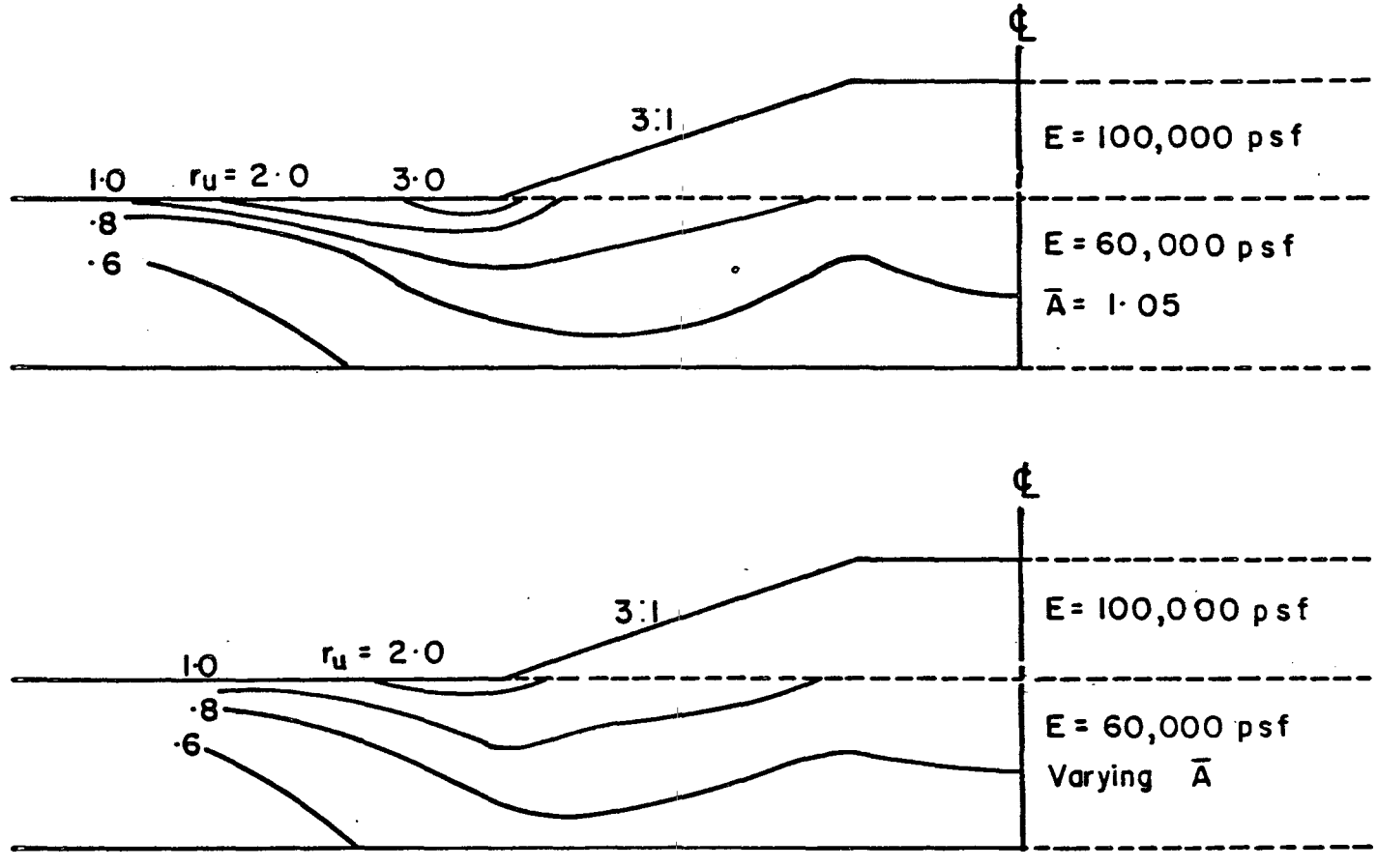

FIG. 63. EFFECT OF THE VALUE OF $\bar{A}$ ON PORE PRESSURES IN EMBANKMENT FOUNDATIONS

Table 8. Analyses of Pore Pressures in Embankment Foundations.

Analysis	Variation of $\bar{A}$ with Direction of Compression	Stress-Strain Relationship	Variation of Modulus with Depth	Results Shown in Fig. No.
1	Constant	Linear	Constant	63 (top)
2	Varying	Linear	Constant	63 (bottom) and 64 (top)
3	Varying	Linear	Increasing	64 (bottom)
4	Varying	Bilinear	Increasing	65 (top)
5	Varying	Anisotropic Nonlinear	Increasing	65 (bottom)

calculated using $\bar{A}$ = 1.05 is 3.0, some 50% higher. It may be noted however, that these large values of r_u correspond to shallow depths, only 3 ft below the surface, where the overburden pressure is small (375 psf). Thus the difference in pore pressures at this location amounts to 375 psf; compared to pore pressure values of about 3300 psf near the base of the layer this difference may not be extremely significant.

Another aspect of the values shown in Fig. 63 deserves consideration; in the regions near the toe of the slope where r_u exceeds 1.0, the corresponding values of effective vertical stress are negative (tensile). At any depth the total overburden pressure p is equal to γh, and the porewater pressure u is equal to $r_u(\gamma h)$. Therefore the effective vertical stress, $p' = p - u$, is equal to $(1 - r_u)\gamma h$ and is negative for values of r_u exceeding unity. For soils like soft clays which have little or no tensile strength, it is physically impossible to develop significant negative effective stresses, and calculated values of $(1 - r_u)$ less than zero may thus indicate only a tendency for development of large pore pressures which cannot be realized physically. If values of r_u greater than 1.0 are ignored, it may be noted that the remainder of the pore pressure ratios calculated using the two methods illustrated in Fig. 63 are in very good agreement.

Modulus Variation with Depth. Analyses were also performed to study the influence of variation of modulus of the clay foundation layer with depth. In both analyses, which are illustrated in Fig. 64, values of $\overline{A}$ varying with stress orientation were used to calculate values of r_u. One of the analyses, shown in the upper part of Fig. 64 was conducted using a constant value of modulus throughout the depth of the layer, whereas the analysis depicted in the lower part of Fig. 64 was performed using values of modulus increasing linearly with depth, the ratio of Young's modulus to initial effective overburden pressure (E/p) being equal to 100 at all depths. Thus the value of modulus at the bottom of the layer was about 300,000 psf. The values of r_u shown in Fig. 64 are very nearly the same for both methods of analysis, indicating that varying modulus values with depth has a very small effect on the pore pressures in the foundation.

Stress-Strain Behavior and Local Failure. To examine the effects of stress-strain behavior and local failure on the foundation pore pressures, two analyses have been performed using the bilinear and multilinear stress-strain relationships previously described. In both analyses, shown in Fig. 65, failure zones developed near the surface of the layer. The failure zone was restricted to the area beneath the center of the embankment in the bilinear analysis, whereas failure occurred only in a small region near the toe of the slope in the more realistic multilinear analysis. The pore pressure ratio values are somewhat higher in the failed regions, i.e., the values of r_u are higher beneath the center of the embankment for the bilinear analysis and beneath the toe of slope for the multilinear analysis.

It is interesting to note that for the embankment studied, the values of r_u calculated using the simplest and most complex methods of analysis are practically identical: The values calculated using linear elastic stress-strain behavior with constant modulus and constant value of $\overline{A}$, shown in the upper part of Fig. 63, are very nearly the same as those calculated using multilinear stress-strain behavior and values of $\overline{A}$ varying with stress increment orientation which are shown in the lower part of Fig. 65. The similarity results from the fact that using a constant value of $\overline{A} = 1.05$ for all stress orientations tends to overestimate pore pressures

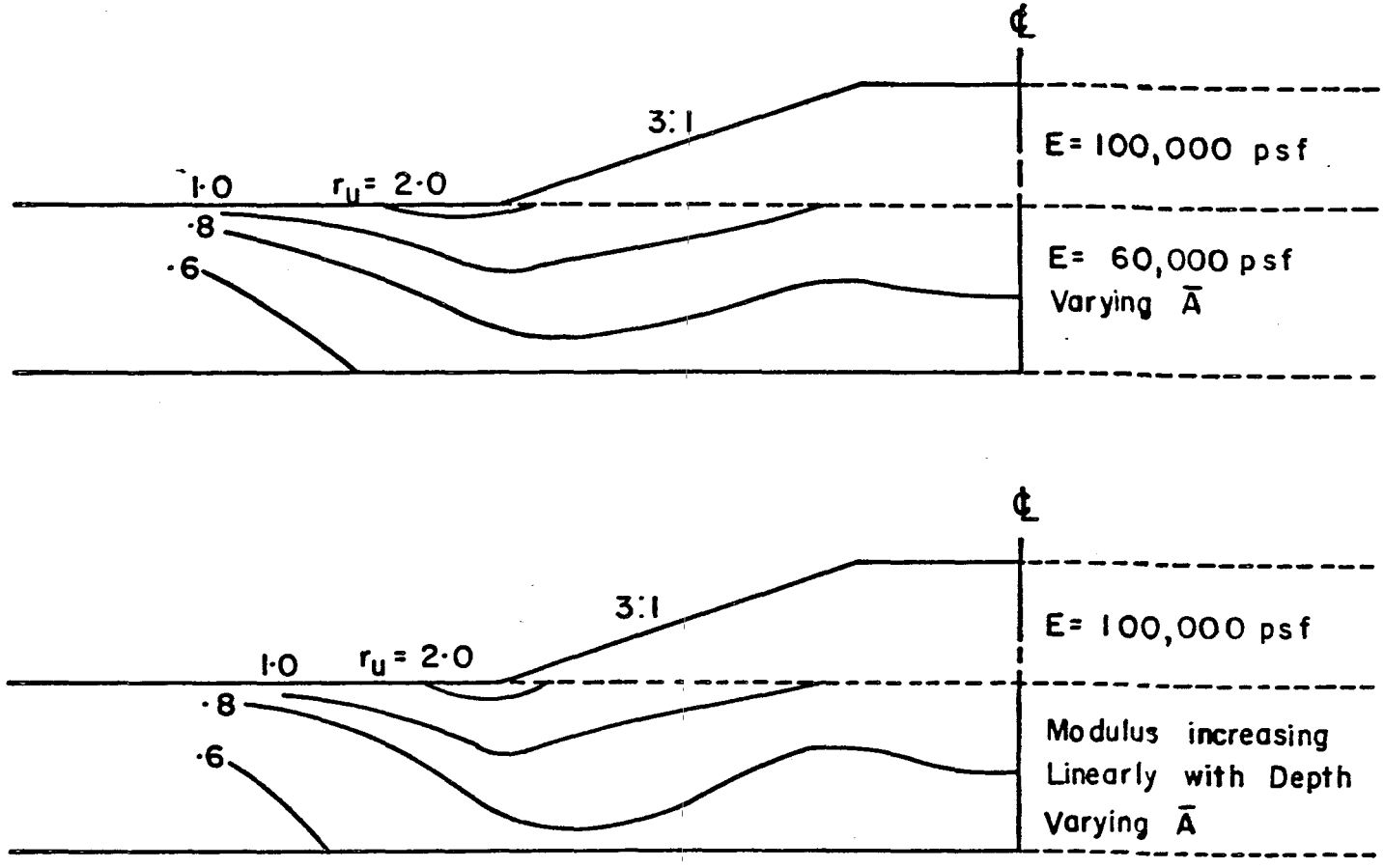

FIG. 64. EFFECT OF MODULUS VARIATION WITH DEPTH ON PORE PRESSURES IN EMBANKMENT FOUNDATIONS.

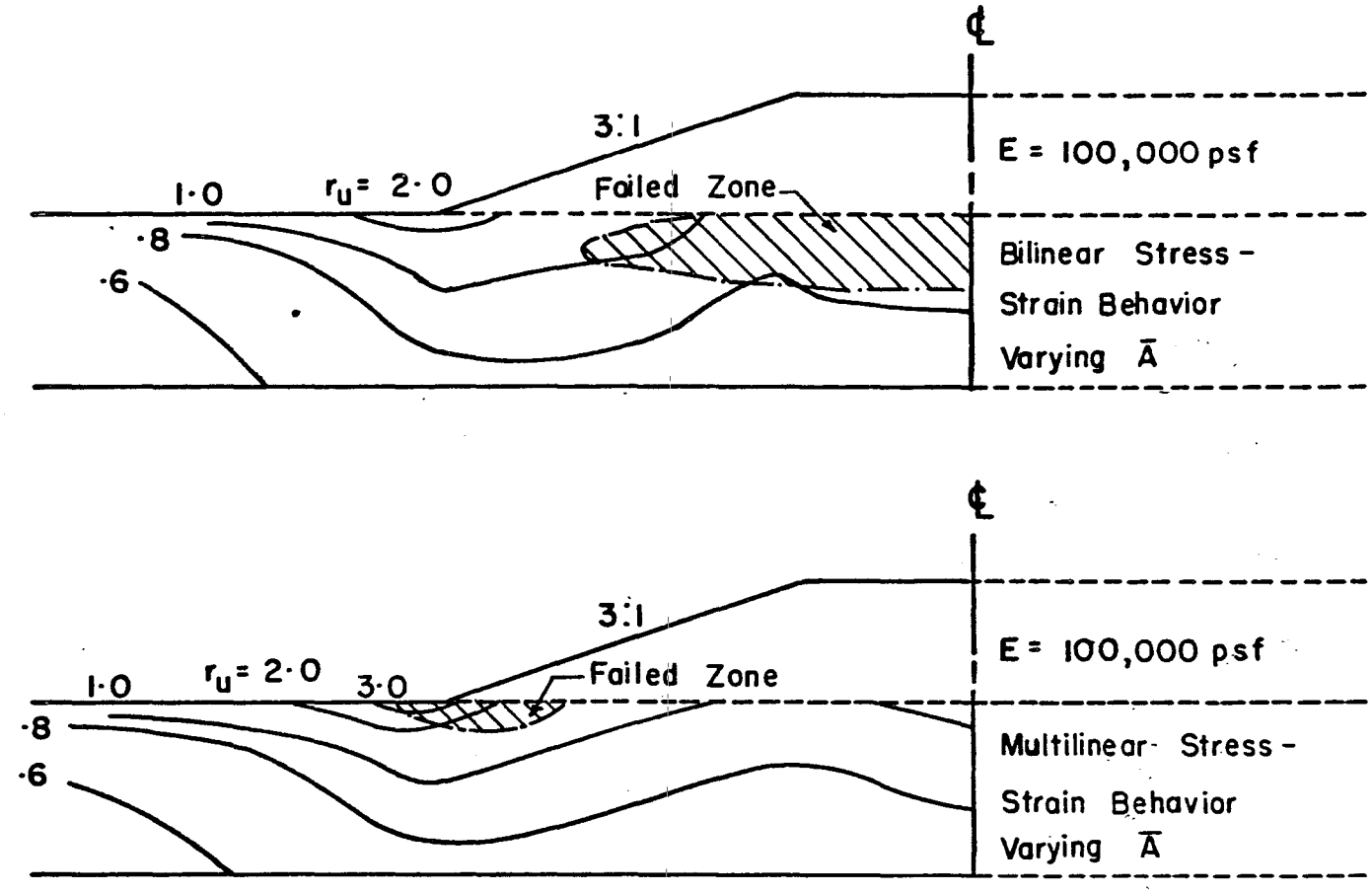

FIG. 65. EFFECT OF STRESS-STRAIN BEHAVIOR ON PORE PRESSURES IN EMBANKMENT FOUNDATIONS.

near the toe, whereas using isotropic stress-strain behavior tends to underestimate pore pressures in the same region. For the conditions analyzed the two factors offset each other almost perfectly.

Summary

The analyses described in this chapter show that finite element analyses may be readily employed for predicting pore-water pressures at the end of construction of excavated slopes and embankments, a procedure which would be very useful if measured values of pore pressure are used to assess the stability of slopes during construction. In order to determine the accuracy of the analytical methods developed, it is highly desirable to compare calculated values of pore pressure with values measured in actual slopes and embankment foundations during construction. Such comparisons would be very helpful for determining the effectiveness and practicality of the procedures.

CHAPTER 7

CONCLUSION

The study described in the preceding pages was conducted to investigate (1) the stress, strain and pore-water pressure distribution and the possibility of progressive failure in excavated slopes in clay; and (2) the stress, strain and pore-water pressure distribution in soft clay foundations for embankments.

The accuracy of such a study necessarily depends in large measure on (1) the development of suitable analytical procedures for evaluating the behavior of slopes and embankments composed of materials with known properties and characteristics and (2) the validity of the procedures used to evaluate and represent in the analyses the properties of the clay soils.

The studies have shown that the finite element method of analysis provides a suitable technique for investigating the stability and performance of excavated slopes and embankments, taking into account (1) variations in the stress-strain characteristics of soils, (2) variations in initial stress conditions in the soil, (3) variations in strength in the soil deposit and (4) the construction procedure. Criteria have been established for the lateral extent of finite element configurations to represent slopes in layers of large lateral extent and procedures have been developed for simulating analytically the excavation of slopes in horizontal layers.

Analyses have been performed using two types of finite element computer programs, the commonly available type which cannot be used with values of Poisson's ratio much higher than about 0.49, and a program specially formulated for use with incompressible materials. Using the latter program it was possible to use high values of bulk modulus appropriate for saturated clays under undrained loading conditions, but the program requires approximately twice as much computer time as commonly available finite element computer programs. Analyses performed showed that the use of values of Poisson's ratio higher than 0.475 does not lead to greatly different results, and thus use of the specially formulated computer program is not necessary.

Previous investigations have shown that most soft clays have curvilinear stress-strain relationships and exhibit a considerable degree of anisotropy with respect to strength, stress-strain and pore pressure characteristics. During the course of the studies, procedures were developed for representing mathematically the anisotropy and curvilinear stress-strain characteristics of soft clays and their validity demonstrated by using them to predict the results of simple shear tests on San Francisco Bay Mud. A stress-strain relationship was developed for Bay Mud from the results of horizontal and vertical plane strain tests; the resulting relationship was non-linear, anisotropic and stress-dependent but even so it was sufficiently simple to be incorporated in finite-element analyses. The good agreement between the predicted and observed results of simple shear tests on Bay Mud was considered indicative of the suitability of the material property representation for making reasonably accurate evaluations of the behavior of soil deposits.

For analysis purposes, the complex characteristics of soft-clays described above are often simplified to facilitate the analytical procedures. Thus, in order of increasing complexity and accuracy, the stress-strain properties of soils may be represented, for analyses purposes, in the following ways:

(1) linear, isotropic stress-strain characteristics

(2) bi-linear, isotropic, stress-strain and strength characteristics

(3) multi-linear, isotropic, stress-strain and strength characteristics

(4) multi-linear, anisotropic stress-strain and strength characteristics

Similarly the pore pressure characteristics may be represented by

(1) a uniform, isotropic, pore pressure coefficient $\overline{A}$

or (2) anisotropic variations in the pore pressure coefficient $\overline{A}$.

Clearly different combinations of the above material property representations are possible, providing results with differing degrees of accuracy. In general it would be anticipated that the least accurate results would be obtained by analyses based on the assumption of a linear isotropic stress-strain relationship and a uniform isotropic pore pressure coefficient for a clay soil; similarly the most accurate solutions would be anticipated

from analyses incorporating multi-linear, anisotropic stress-strain relationships and anisotropic variations in the pore-pressure coefficient. However it should also be recognized that the introduction of compensating errors can in some cases lead to reasonably accurate results despite the use of grossly simplified material property representations.

Analyses based on the use of isotropic linear elastic stress-strain characteristics have been found to be useful for evaluating some aspects of the performance of stable slopes, and might logically serve as a basis for initial investigations of many practical slope behavior studies. In the present investigation they were used to examine the significance of the initial stress conditions and variations in soil modulus values with depth on the stress distribution within an excavated slope. It was found that values of the maximum shear stress and the principal stress orientations in the vicinity of slopes are influenced to a major extent by the initial stress conditions (represented by the coefficient of earth pressure at rest, Ko) but only slightly affected by the variation of modulus values with depth in the deposit; furthermore the factor of safety corresponding to the development of local failure within excavated slopes was found to vary appreciably with changes in the initial stress conditions, a result which may have practical applications in slopes composed of extremely brittle materials. However, in general, it was concluded that analyses based on the use of linear elastic characteristics, would not provide a basis for reliable assessments of slope stability.

Analyses of excavated slopes in which the clay soil is considered to have isotropic bi-linear stress-strain characteristics, and in which consideration of the strength of the soil may therefore be incorporated, have proved to be useful for determining where local failure begins and how the failure zones grow as excavation progresses. Analyses of this type for slopes cut in layers having initial stress conditions and strength profiles representative of normally consolidated clay deposits indicate that failure begins beneath the slope and extends upward towards the slope crest and downwards toward the toe of the slope and the base of the layer as excavation continues. The final shapes of the failure zones are compatible with the development of a curved surface of sliding and in the final stages, when the failure zones encompassed the major portions

of the region beneath the slope (see Fig. 66), factors of safety calculated by the $\phi = 0$ or S_u-method of analysis ranged from 0.95 to 1.15.

On the other hand, for slopes in layers with initial stresses and strength profiles representative of overconsolidated clays, failure was found to develop initially beneath the base of the excavation, extending upward toward the bottom of the excavation and downwards toward the base of the layer as excavation progressed. When the factor of safety, based on a $\phi = 0$ analysis, was still about 2 a large failure zone had developed around the bottom of the excavation, as shown in Fig. 66. This type of behavior is similar to the phenomenon described by Terzaghi and Peck (1948) as "loss of ground" wherein the soil in the base of the excavation bulges continually as excavation progresses. This bulging may often be the first sign of distress foreshadowing catastrophic failure of slopes in overconsolidated clay.

Finally, analyses of the stress distribution within an excavated slope in soft clay taking into account the multi-linear anisotropic stress-strain and strength characteristics of the soil showed that linear and bilinear analyses tend to overestimate the extent of local failure in stable slopes. Furthermore the stress distribution determined by this more refined analysis also showed significant differences from that determined by the use of bi-linear material characteristics. A comparison of the stress distributions determined by these two approaches is shown in Fig. 67.

The various analytical procedures incorporating different representations of the clay stress-strain characteristics were also used, in conjunction with different representations of the variation of pore pressure coefficient within the slope, to evaluate the pore-water pressure distribution, within excavated slopes in clay. Fig. 68 shows a comparison of the results determined by analyses based on the following material characteristics:

(1) linear elastic stress-strain characteristics and constant value of $\overline{A}$

(2) linear elastic stress-strain characteristics and anisotropic values of $\overline{A}$

(3) bi-linear stress-strain characteristics and anisotropic values of $\overline{A}$

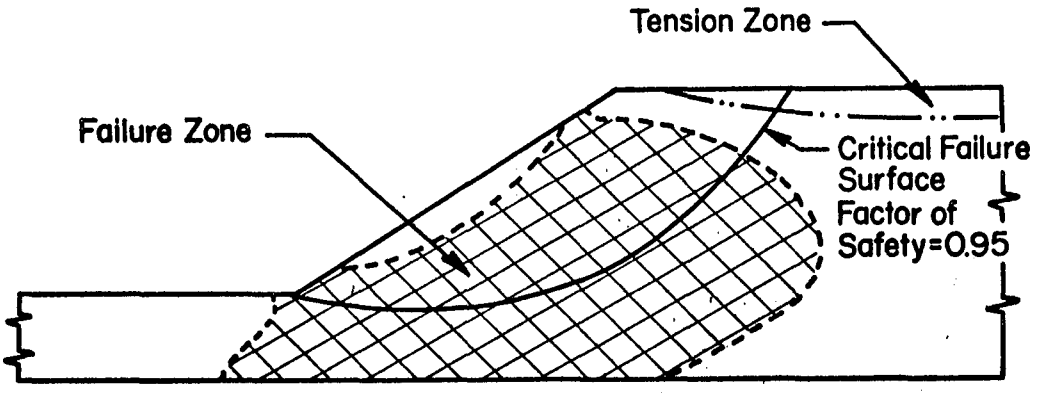

Normally Consolidated

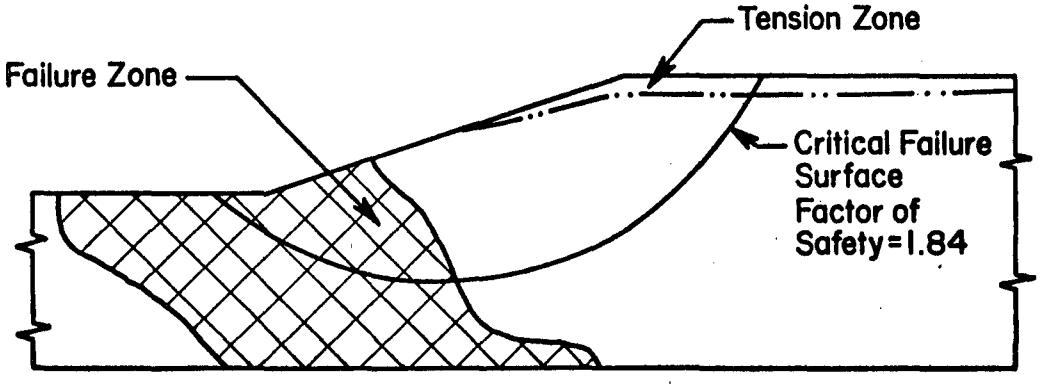

Overconsolidated

FIG. 66. CORRELATION BETWEEN FAILURE ZONES AND FACTORS OF SAFETY FOR EXCAVATED SLOPES.

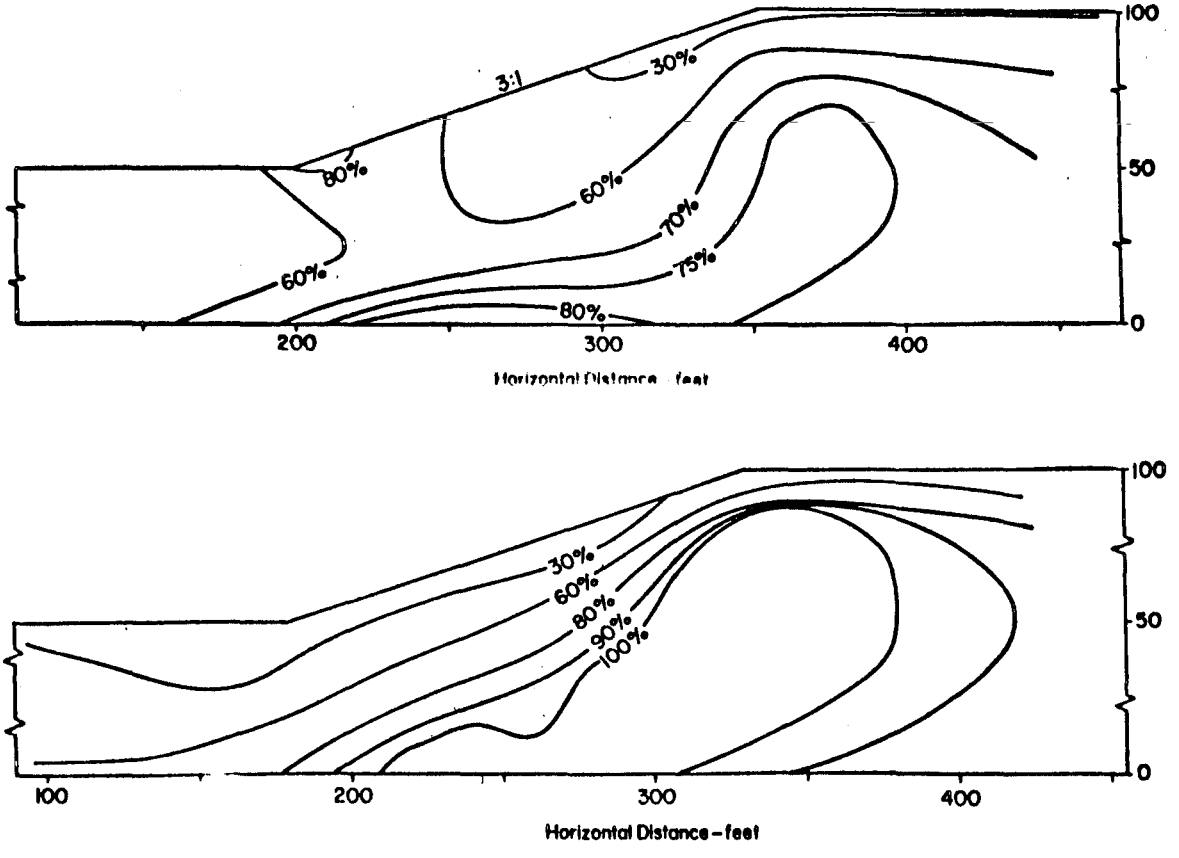

FIG. 67. COMPARISON OF STRESS CONDITIONS AROUND AN EXCAVATED SLOPE AS DETERMINED BY ISOTROPIC BILINEAR AND ANISOTROPIC MULTILINEAR ANALYSES.

Linear Elastic Stress-Strain Characteristics And Constant Value of $\bar{A}$

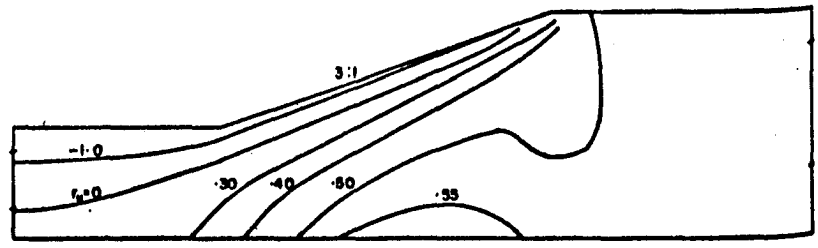

Linear Elastic Stress-Strain Characteristics And Anisotropic Values of $\bar{A}$

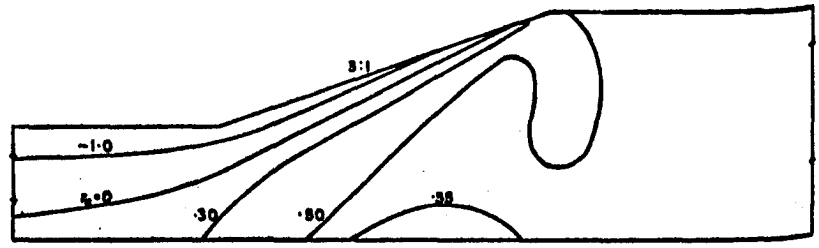

Bilinear Stress-Strain Characteristics And Anisotropic Values of $\bar{A}$

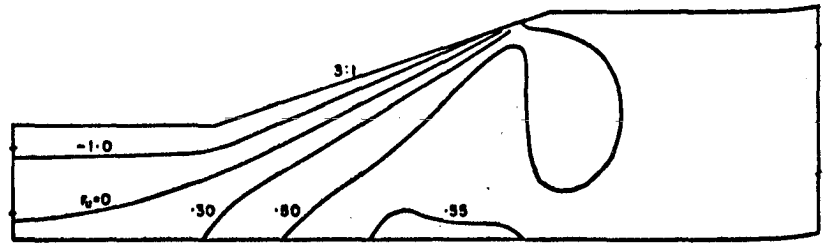

Multilinear Stress-Strain Characteristics And Constant Value of $\bar{A}$

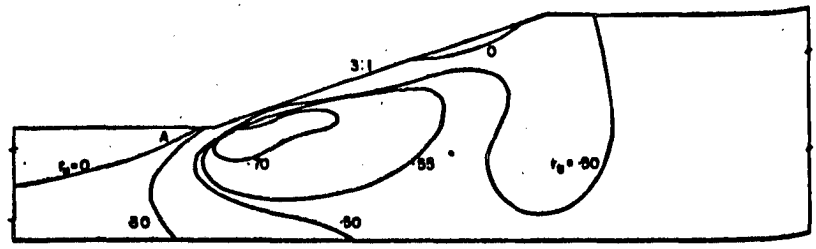

Multilinear Stress-Strain Characteristics And Anisotropic Values of $\bar{A}$

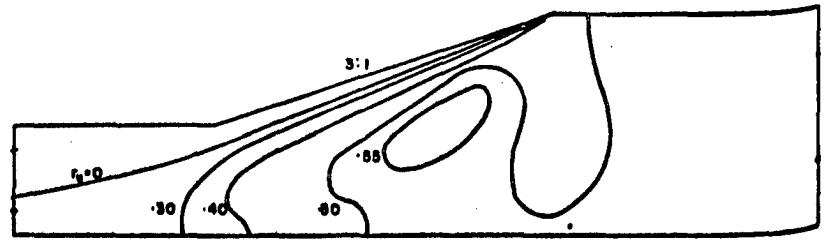

FIG. 68. COMPARISONS OF PORE PRESSURES AROUND EXCAVATED SLOPES AS DETERMINED BY VARIOUS METHODS OF ANALYSIS.

(4) multilinear stress-strain characteristics and constant value of $\overline{A}$

(5) multilinear stress-strain characteristics and anisotropic values of $\overline{A}$

The differences in the computed pore pressure distributions are readily apparent. If the analysis incorporating multi-linear stress strain characteristics and anisotropic values of $\overline{A}$ is considered the most realistic representation of conditions in an actual slope, then it would appear that an analysis incorporating linear stress-strain properties and a constant value of $\overline{A}$ under-estimates the pore-water pressures in the lower part of the slope; an analysis based on linear stress-strain relationships but including anisotropic values of $\overline{A}$ gives improved results but the computed values pore pressure are still too low in the lower part of the slope; an analysis based on bi-linear stress-strain characteristics and anisotropic values of $\overline{A}$ is still further improved; and an analysis based on multi-linear stress strain characteristics and a constant value of $\overline{A}$ over-estimates the pore pressures in the lower part of the slope.

The potential variations in pore-water pressure distributions disclosed by these different analyses illustrates the need for the use of the best possible representation of material characteristics in order to evaluate the pore-water pressure conditions in actual slopes and the possible errors resulting from grossly simplified procedures.

Fig. 69 shows a similar comparison of the pore pressure distributions computed by the various analyses in a soft clay foundation for an embankment. In this case the pore pressure distribution does not vary appreciably whether the analysis is based on the use of linear, bilinear or multilinear stress-strain characteristics, constant or varying values of the pore pressure coefficient $\overline{A}$, or constant or varying values of material characteristics with depth. Thus in this case an entirely satisfactory evaluation of the pore-water pressure conditions could be obtained using the simplest method of analyses--that is, an analysis based on linear elastic material characteristics and a constant value of $\overline{A}$--even though the actual properties are considerably more complex.

It is hoped that these results will help to further the understanding of the behavior of excavated slopes in clays and of soft clay foundations

Linear Elastic Stress-Strain Characteristics, Constant Value of Modulus And Constant Value of $\bar{A}$.

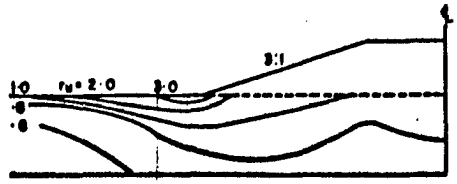

Linear Elastic Stress-Strain Characterics, Constant Value of Modulus And Anisotropic Values of $\bar{A}$.

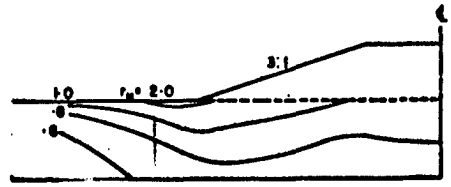

Linear Elastic Stress Strain Characteristics, Modulus Increasing Linearly With Depth And Anisotropic Values of $\bar{A}$.

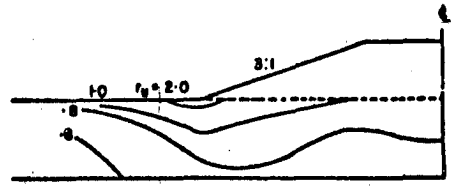

Bilinear Stress-Strain Characteristics, Modulus Increasing Linearly With Depth And Anisotropic Values of $\bar{A}$.

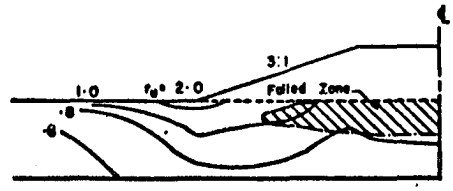

Multilinear Stress-Strain Characteristics, Modulus Increasing Linearly With Depth And Anisotropic Values of $\bar{A}$.

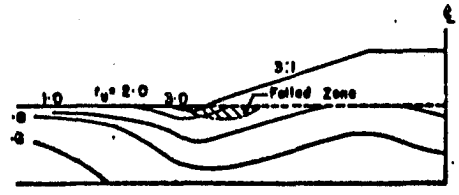

FIG. 69. COMPARISONS OF PORE PRESSURES IN EMBANKMENT FOUNDATIONS AS DETERMINED BY VARIOUS METHODS OF ANALYSIS.

for embankments; furthermore, that the analytical procedures presented will serve as a basis for improved evaluations of the performance of cut slopes and embankments involving insensitive saturated clays.

REFERENCES

Bennett, P. T. (1951), "Notes on Embankment Design," Proceedings of the Fourth Congress on Large Dams, Vol. 1, pp. 223-238.

Bishop, A. W. (1952), "The Stability of Earth Dams," Thesis presented to the University of London, at London, England, in 1952, in partial fulfillment of the requirements for the degree of Doctor of Philosophy.

Bishop, A. W. (1955), "The Use of the Slip Circle in the Stability Analysis of Slopes," Geotechnique, Vol. 5, No. 1, pp. 7-17.

Bishop, A. W., Blight, G. E. and Donald, I. B. (1960), Closure of "Factors Controlling the Strength of Partly Saturated Soils," Proceedings, ASCE Conference on Shear Strength of Cohesive Soils, 1960, pp. 503-532.

Bishop, A. W. and Morgenstern, N. R. (1960), "Stability Coefficients for Earth Slopes," Geotechnique, Vol. 10, No. 4, pp. 129-150.

Bjerrum, L. (1955), "Stability of Natural Slopes in Quick Clay," Geotechnique, Vol. 5, No. 1, pp. 101-119.

Bjerrum, L. (1967), "Progressive Failure in Slopes of Overconsolidated Plastic Clay and Clay Shales," Journal of the Soil Mechanics and Foundations Division, Vol. 93, No. SM5, pp. 1-50.

Bjerrum, L. and Eide, O. (1956), "Stability of Strutted Excavation in Clay," Geotechnique, Vol. 6, No. 1, March, 1956, pp. 32-47.

Brooker, E. W. and Ireland, H. O. (1965), "Earth Pressures at Rest Related to Stress History," Canadian Geotechnical Journal, Vol. 2, No. 1, pp. 1-15.

Brown, C. B. and King, I. P. (1966), "Automatic Embankment Analysis: Equilibrium and Instability Conditions," Geotechnique, Vol. 16, No. 3, pp. 209-219.

Chang, T. Y., Ko, H. Y., Scott, R. F. and Westman, R. A. (1967), "An Integrated Approach to the Stress Analysis of Granular Materials," Report of the Soil Mechanics Laboratory, California Institute of Technology, Pasadena, California.

Clough, R. W. and Woodward, R. J., III (1967), "Analysis of Embankment Stresses and Deformations," Journal of the Soil Mechanics and Foundations Division, ASCE, Vol. 93, No. SM4, pp. 529-549.

Clough, R. W. and Rashid, Y. (1965), "Finite Element Analysis of Axi-Symmetric Solids," Journal of the Engineering Mechanics Division, ASCE, Vol. 91, No. SM1, pp. 71-85.

Clough, R. W. (1965), "The Finite Element Method in Structural Mechanics," Stress Analysis Ed. Zienkiewicz, O. D., J. Wiley (1965).

Collin, A. (1846), Landslides in Clay, University of Toronto Press, 1956.

Duncan, J. M. (1965), "The Effect of Anisotropy and Reorientation of Principal Stresses on the Shear Strength of Saturated Clay," Thesis presented to the University of California, at Berkeley, California, in 1965, in partial fulfillment of the requirements for the degree of Doctor of Philosophy.

Duncan, J. M. (1967), "Undrained Strength and Pore-Water Pressures in Anisotropic Clays," Proceedings of the 5th Australia-New Zealand Conference on Soil Mechanics and Foundation Engineering, August, 1967.

Duncan, J. M. and Seed, H. B. (1966a), "Anisotropy and Stress Reorientation in Clays, Journal of the Soil Mechanics and Foundations Division, Vol. 92, No. SM5, pp. 21-50.

Duncan, J. M. and Seed, H. B. (1966b), "Strength Variation Along Failure Surfaces in Clay," Journal of the Soil Mechanics and Foundations Division, ASCE, Vol. 92, No. SM6, pp. 81-104.

Duncan, J. M. and Seed, H. B. (1967), "Corrections for Strength Test Data," Journal of the Soil Mechanics and Foundations Division, Vol. 93, No. SM5, pp. 121-137.

Duncan, J. M., Monismith, C. L. and Wilson, E. L. (1967), "Finite Element Analyses of Pavements," to be published in the Proceedings of the Highway Research Board, 1968.

Duncan, J. M. and Dunlop, P. (1968), "The Significance of Cap and Base Restraint," Journal of the Soil Mechanics and Foundations Division, ASCE, Vol. 94, No. SM1, January 1968.

Goodman, L. E. and Brown, C. B. (1963), "Dead Load Stresses and the Instability of Slopes," Journal of the Soil Mechanics and Foundations Division, ASCE, Vol. 89, No. SM3, pp. 103-134.

Herrmann, L. R. and Toms, R. M. (1964), "A Reformulation of the Elastic Field Equation, in Terms of Displacements, Valid for All Admissible Values of Poisson's Ratio," Journal of Applied Mechanics, ASME, Vol. 31, No. 1, pp. 140-141.

Idriss, I. M. (1966), "The Response of Earth Banks During Earthquakes," Thesis presented to the University of California, at Berkeley, California, in 1966, in partial fulfillment of the requirements for the degree of Doctor of Philosophy.

Ireland, H. O., (1954), "Stability Analysis of the Congress Street Open Cut in Chicago," Geotechnique, Vol. 4, No. 4, pp. 163-168.

Kenney, T. C. (1963), "Stability of Cuts in Soft Soils," Journal of the Soil Mechanics and Foundations Division, ASCE, Vol. 89, No. SM5, pp. 17-37.

King, I. P. (1965), "Finite Element Analysis of Two Dimensional Time Dependent Stress Problems," Report No. 65-1, Institute of Engineering Research, University of California, Berkeley.

Kjellman, W., (1951), "Testing the Shear Strength of Clay in Sweden," Geotechnique, Vol. 2, No. 3, pp. 225-235.

Ko, H. Y. and Scott, R. F. (1967), "Deformation of Sand in Hydrostatic Compression," Journal of the Soil Mechanics and Foundations Division, Vol. 93, No. SM3, pp. 137-156.

Ladd, C. C. (1964), "Stress-Strain Modulus of Clay in Undrained Shear," Journal of the Soil Mechanics and Foundations Division, Vol. 90, No. SM5, pp. 103-132.

LaRochelle, P. (1960), "The Short-Term Stability of Slopes in London Clay," Thesis presented to the University of London, at London, England, in 1960, in partial fulfillment of the requirements for the degree of Doctor of Philosophy.

Middlebrooks, T. A. (1936), "Foundation Investigation of the Fort Peck Dam Closure," Proceedings, 1st International Conference on Soil Mechanics and Foundation Engineering, Vol. 1, pp. 135-145.

Peacock, W. H. and Seed, H. B. (1967), "Liquefaction of Saturated Sand Under Cyclic Loading Simple Shear Conditions," Report No. TE-67-1, Office of Research Services, University of California, Berkeley, California, 1967.

Roscoe, K. H. (1953), "An Apparatus for the Application of Simple Shear to Soil Samples," Proceedings of the 3rd International Conference on Soil Mechanics and Foundation Engineering, Vol. 1, pp. 186-191.

Roscoe, K. H. and Poorooshasb, H. B. (1963), "A Theoretical and Experimental Study of Strains in Triaxial Compression Tests on Normally Consoli-Dated Clays," Geotechnique, Vol. 13, No. 1, pp. 12-38.

Rowe, P. W. (1962), "The Stress-Dilatancy Relation for Static Equilibrium of an Assembly of Particles in Contact," Proceedings of the Royal Society, 269, pp. 500-527.

Seed, H. B. and Idriss, I. M. (1967), "Analysis of Soil Liquefaction: Niigata Earthquake," Journal of the Soil Mechanics and Foundations Division, ASCE, Vol. 93, No. SM3, pp. 83-108.

Seed, H. B. and Wilson, S. D. (1967), "The Turnagain Heights Landslide, Anchorage, Alaska," Journal of the Soil Mechanics and Foundations Division, Vol. 93, No. SM4, pp. 325-354.

Sevaldson, R. A., (1956), "The Slide in Lodalen, October 6, 1954," Geotechnique, Vol. 6, No. 4, Dec. 1956, pp. 167-182.

Skempton, A. W. (1945), "A Slip in the West Bank of Eau Brink Cut," Journal of the Inst. of Civil Engineers, No. 7, pp. 267-287.

Skempton, A. W. (1954), "The Pore Pressure Coefficients A and B," Geotechnique, Vol. 4, No. 4, pp. 143-147.

Tan, T. K. (1957), Discussion, Proceedings, Fourth International Conference on Soil Mechanics and Foundation Engineering, Vol. 3, pp. 87-89.

Taylor, D. W. (1937), "Stability of Earth Slopes," Journal of the Boston Society of Civil Engineers, Vol. 24, No. 3, pp. 197-246.

Terzaghi, K. and Peck, R. B. (1948), Soil Mechanics in Engineering Practice, Wiley, New York.

Turnbull, W. J. and Hvorslev, M. J. (1967), "Special Problems in Slope Stability," Journal of the Soil Mechanics and Foundations Division, ASCE, Vol. 93, No. SM4, pp. 499-528.

Wilson, E. L. (1963), "Finite Analysis of Two Dimensional Structures," Report No. 63-2, Structures and Materials Research, Department of Civil Engineering, University of California, Berkeley, June 1963.

Zienkiewicz, O. C., Mayer, P., and Cheung, Y. U. (1966), "Solution of Anisotropic Seepage by Finite Elements," Journal of the Engineering Mechanics Division, ASCE, Vol. 92, No. EM1, pp. 111-120.

APPENDIX A

REQUIREMENTS FOR BOUNDARY CONDITIONS, ELEMENT SIZES AND ELEMENT SHAPES

The amount of computer time required to solve a finite element problem depends upon the number of nodal points (and elements) used to represent a structure. For efficient operation, these should be kept to the minimum necessary for accurate representation of the system being studied. The number of elements required is dependent upon the size, shape and distribution of the elements, which in turn depend on the problem being analyzed.

Studies to establish criteria for elements and the location of arbitrary boundaries may be made for a class of problems, such as the static analyses of slope behavior, once a general scheme for the configurations and the type of element is chosen. In the analyses of slopes described in preceding sections, the basic finite element used was a quadrilateral composed of four constant strain triangles. The arrangement of elements within the slope configuration is shown in Fig. 70. It may be noted that rectangles are used throughout with the exception of the region immediately adjacent to the sloping face, where triangles and trapezoids are employed alternately. This scheme of elements was considered to be well-suited to the simulation of slope excavation by the "removal" of elements outside the slope and it was also convenient for automatic mesh generation within the computer. Whenever possible however, quadrilateral elements should be employed rather than triangular elements since it has been shown by Wilson (1963) that the stresses obtained for a triangular element do not represent the stresses acting at any one point in the element.

It was assumed that the soil deposit was underlain by a much more rigid stratum, which was simulated in the finite element analysis by constraining the bottom row of nodal points in the configuration from moving vertically or horizontally. The nodal points on the artificial lateral boundaries were allowed to move freely in the vertical direction but were constrained in the horizontal direction.

If the excavation being analyzed was bounded left and right by vertical planes of symmetry or rigid boundaries, these could be simulated

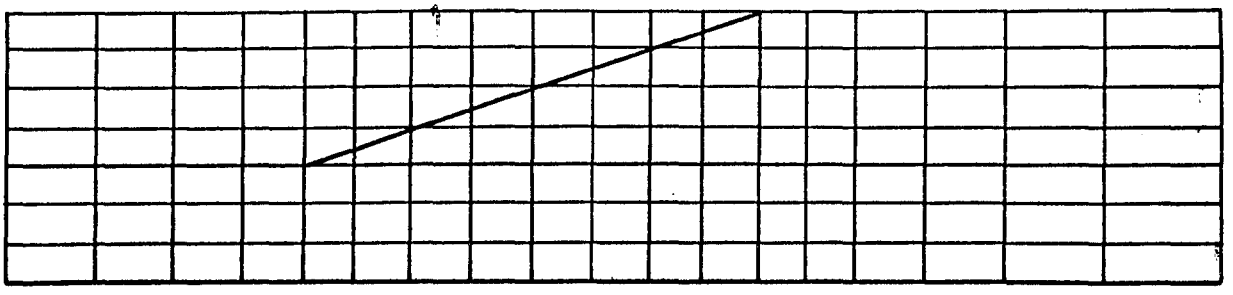

(a)

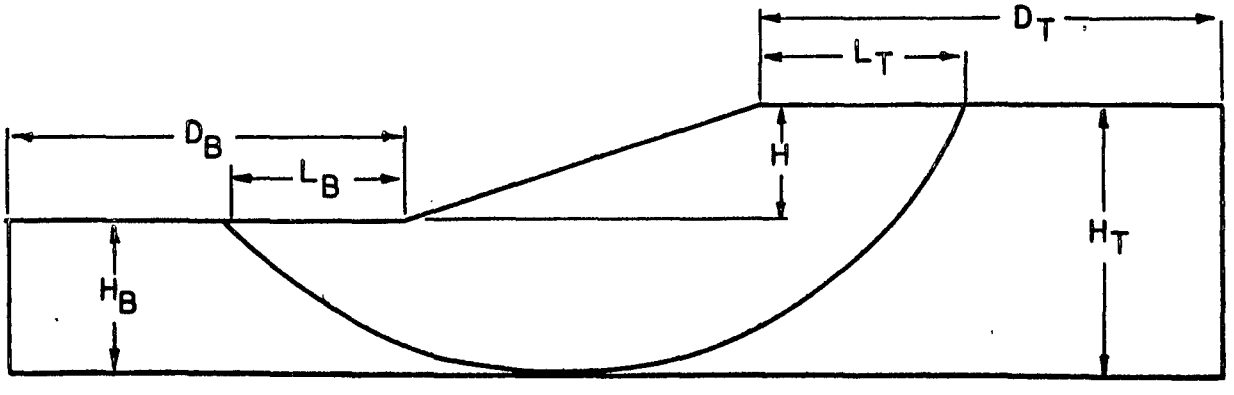

(b)

FIG. 70. (a) FINITE ELEMENT IDEALIZATION OF A SLOPE, (b) CROSS-SECTION OF SLOPE SHOWING LENGTH FACTORS.

in the analysis without approximation. In these analyses, however, it was desired to simulate a slope in a soil layer of very large lateral extent; therefore studies were undertaken to determine positions of the lateral boundaries which would accurately simulate a layer of infinite lateral extent.

Lateral Boundaries

The first step in determining the influence of the artificial lateral boundaries was to define a "region of interest", within which it was desired to calculate accurate displacements, strains and stresses. The accuracy of values calculated for points outside the region of interest was considered unimportant.

The purpose of the analyses was to study the behavior of slopes as they approach a condition of instability and therefore the region of interest was established to contain the unstable portion of the slope. To determine the size of the region of interest, a study was made of the position of failure surfaces within slopes as determined by slope stability analyses and by field observations.

The lateral extent of the failure surface within a slope may be defined in terms of two lengths L_B and L_T as shown in Fig. 70. It is convenient to consider dimensionless ratios L_B/H_B and L_T/H_T and values of L_B/H_B and L_T/H_T have been calculated from data presented by Taylor (1937), based on analyses of slopes in soil with constant strength; these values are shown in Fig. 71. It may be noted that the values of the ratios L_B/H_B and L_T/H_T increase with increasing slope angle to 50°; beyond this angle the values decrease. For a 45° slope L_B/H_B approaches a value of 2 and L_T/H_T approaches a value of 1.5. Thus for slopes flatter than 45° in soils with constant shear strength these analyses indicate that the zone within which failure occurs may extend beyond the toe of a distance equal to twice the depth to rock, and beyond the top for a distance equal to 1-1/2 times the depth to rock.

Values of L_T/H_T calculated from data presented by Kenney (1963), for slopes in soils with strength increasing linearly with depth, are shown in Fig. 72. In this case the values of the ratio L_T/H_T are generally smaller than for the case when the shear strength is constant with depth,

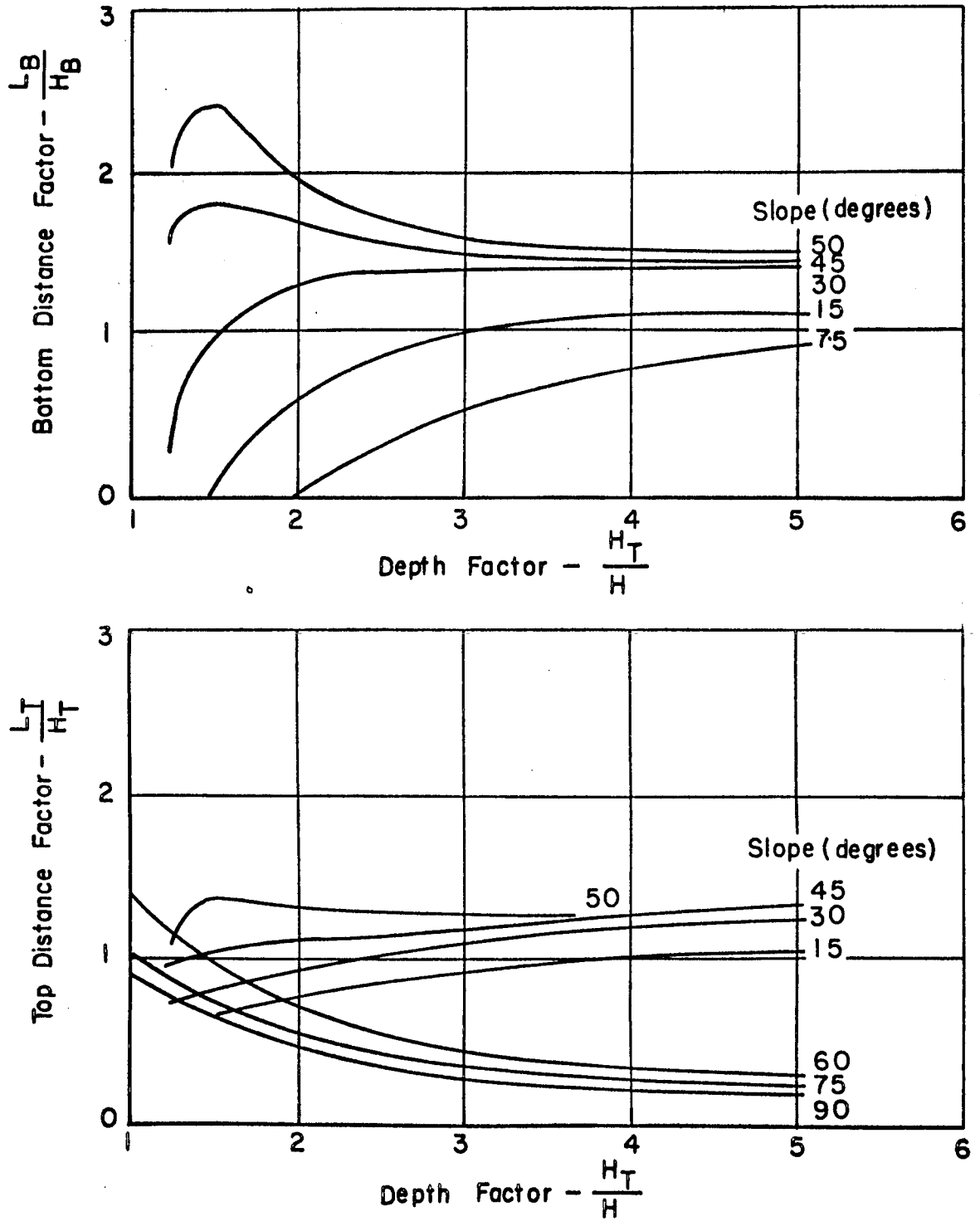

FIG. 71. THE LATERAL EXTENT OF FAILURE SURFACES IN SOIL WITH CONSTANT STRENGTH

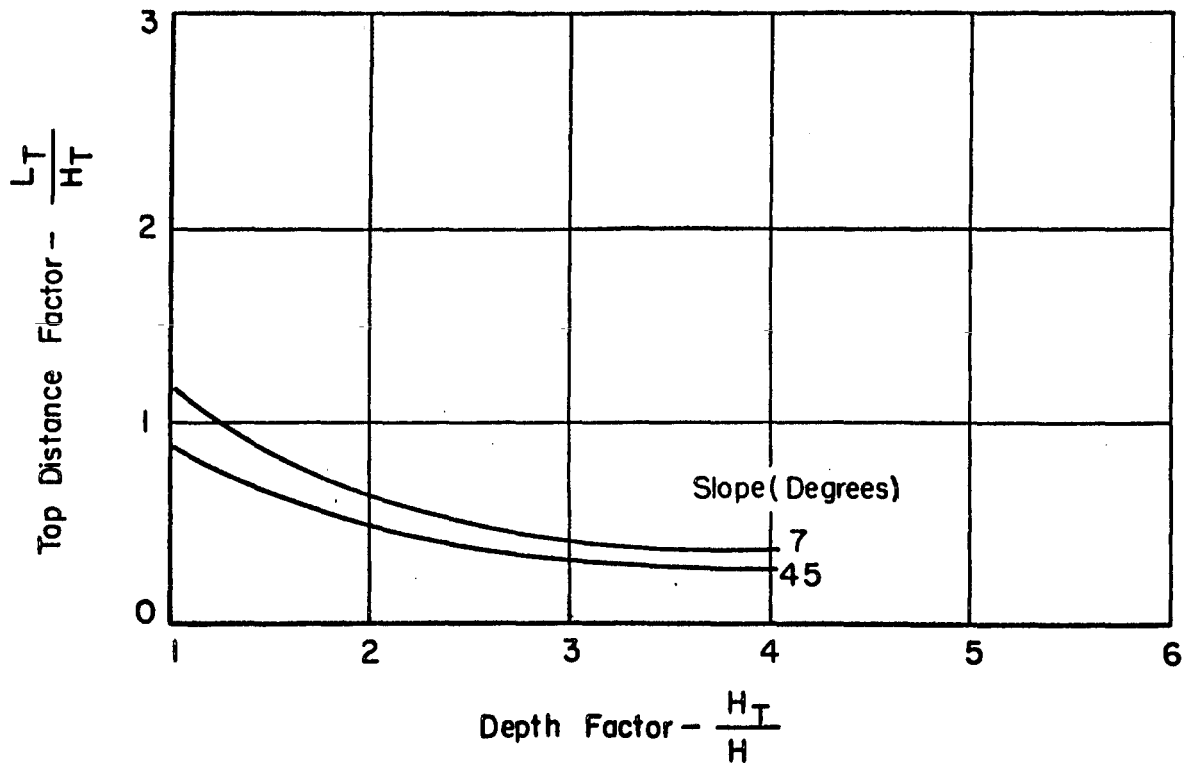

FIG. 72. THE LATERAL EXTENT OF FAILURE SURFACES IN MATERIALS WITH STRENGTH INCREASING LINEARLY WITH DEPTH.

and the values decrease with increasing slope angle and depth factor H_T/H. In all the cases analyzed by Kenney a failure surface passing through or above the toe was found to be most critical and the value of L_B/H_B was therefore zero for all cases. Thus the zone within which failure may occur is smaller for a soil with shear strength increasing linearly with depth than for a soil with a constant shear strength, extending above the top of the slope a maximum distance equal to about 1.2 times the depth to rock and terminating at the toe of the slope.

About twenty total stress slope stability analyses were undertaken in conjunction with the finite element analyses in the preceding sections. In these analyses the undrained shear strength of the soil was used to represent a short-term stability problem and the variations of shear strength with depth used in these analyses are shown in Fig. 73. In all cases the value of L_B was nearly zero, and the value of the ratio L_T/H_T was found to be 0.70 or less for depth factors H_T/H of 1.4 or more, indicating positions of the failure surface intermediate between those determined from Taylor and Kenney. This is consistent with the fact that the undrained shear strength variation is intermediate between those used by Taylor and Kenney.

The position of sliding surfaces observed within several failed cuts are summarized in Table 9. It may be noted that the observed values of L_B/H_B are somewhat greater than those calculated for the same slopes and the observed values of L_T/H_T are somewhat smaller, indicating that the actual failure surface is likely to develop at a shallower depth within the slope than indicated by total stress stability analyses (Skempton, 1945).

It is desirable to define the region of interest so that it will contain the failure surface as determined by analyses or field observations. From the preceding it appears that this criterion will be satisfied in most cases if the region of interest extends for a distance from the toe equal to the depth to rock ($L_B = H_B$) and from the top for a distance equal to the distance to rock ($L_T = H_T$). These criteria were adopted for establishing the size of the region of interest and the necessary boundary locations. Only in cases where the shear strength is constant or the ratio of H_T/H is near unity will L_B and L_T need to be larger.

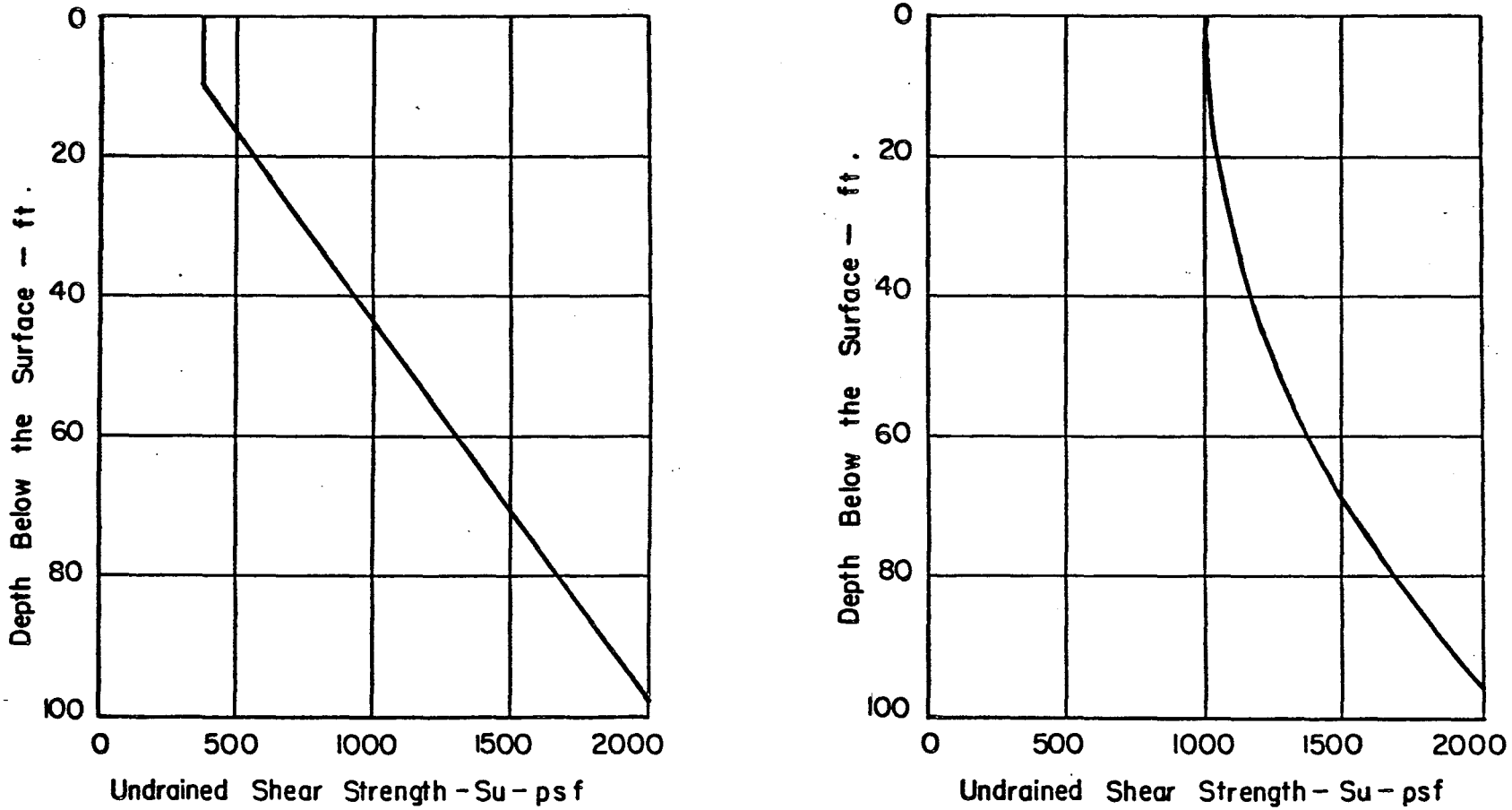

FIG. 73. UNDRAINED SHEAR STRENGTH VARIATIONS USED IN TOTAL STRESS SLOPE STABILITY CALCULATIONS.

Table 9. Observed Failures in Cut Slopes.

Failure	Slope Angle i	Slope Height H	Depth Ratio H_T/H	Calculated $\phi = 0$		Observed		Comments
				L_B/H_B	L_T/H_T	L_B/H_B	L_T/H_T	
Sevaldson, 1956	27°	58'	~1.3	0.0	0.50	1.0	0.25	Long term failure in slightly overconsolidated clay.
Skempton, 1945	25°	27'	1.5	0.0	0.63	0.60	0.10	Long term failure in layered silts and clays.
Ireland, 1954	35°	47'	1.2	0.35	0.64	2.10	0.05	Short term failure in gritty blue clay LL = 33, PL = 18.
Collin, 1846	30°	59'	≥1.0			0.00	.23	Clay shale, short term failure.
Collin, 1846	18°	28'	≥1.0			0.00	0.00	Clay, short term failure.

In choosing finite element configurations for slope analyses in which the construction procedure was simulated, the extent of the region of interest below the toe was always chosen on the basis of the depth to rock (H_B) at any stage in the construction.

No attempt has been made to establish criteria for special slope failures such as regressive failures in quick clays (Bjerrum, 1955), regressive failures caused by liquefaction of sand seams or lenses (Seed and Wilson, 1967) or cases involving overconsolidated clays (Bjerrum, 1967), in which cases the failure surface may extend a very large distance back from the crest of the slope.

Boundary Positions

If the lateral extent of the original horizontal deposit is very large, it may be inefficient to extend the finite element idealization to the physical extent of the deposit. To determine acceptable boundary positions, analyses were made using successively larger distances to the boundaries (D_T) until it was determined that further increases would have a negligible effect on the values of stress, strain and displacement calculated at the boundary of the region of interest. In these studies linear material properties were used in all cases as each step of an analysis employing nonlinear material properties is assumed linear.

Values of horizontal normal stress σ_x, calculated at the up-slope boundary of the region of interest are shown in the lower part of Fig. 74 for various positions of the right boundary of the finite element mesh as shown in the upper part of Fig. 74. In this analysis the up-slope boundary of the region of interest was set at $L_T = H_T$ behind the crest of the slope. It may be noted that as the right mesh boundary is moved from position 1($D_T = 1.1\ H_T$) to position 2($D_T = 2.0\ H_T$) the values of σ_x near the surface decrease by a small amount. Further shift of this mesh boundary produces negligible change in σ_x.

Values of σ_y calculated at the up-slope boundary of the region of interest are shown in the upper part of Fig. 75 and exhibit no influence of the mesh boundary location; the value of σ_y being equal to the weight of material above the point at which the sr ess is calculated. Values of τ_{xy} are plotted in the lower part of Fig. 75 and indicate appreciable

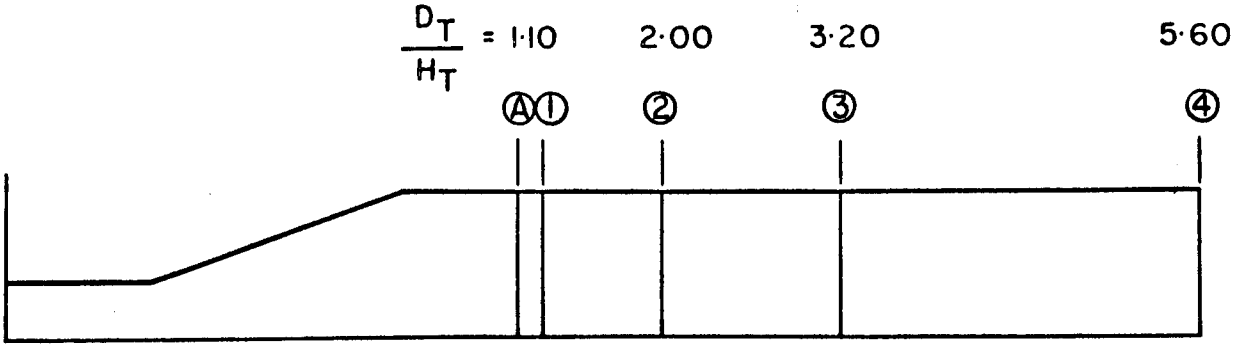

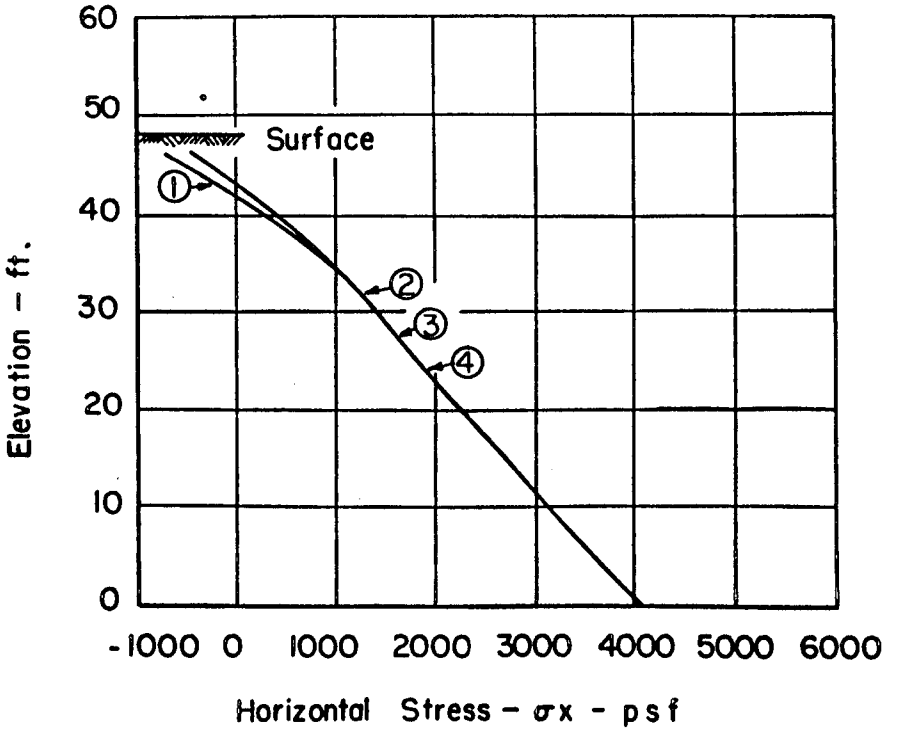

FIG .74 . INFLUENCE OF LATERAL BOUNDARY LOCATION ON HORIZONTAL STRESS .

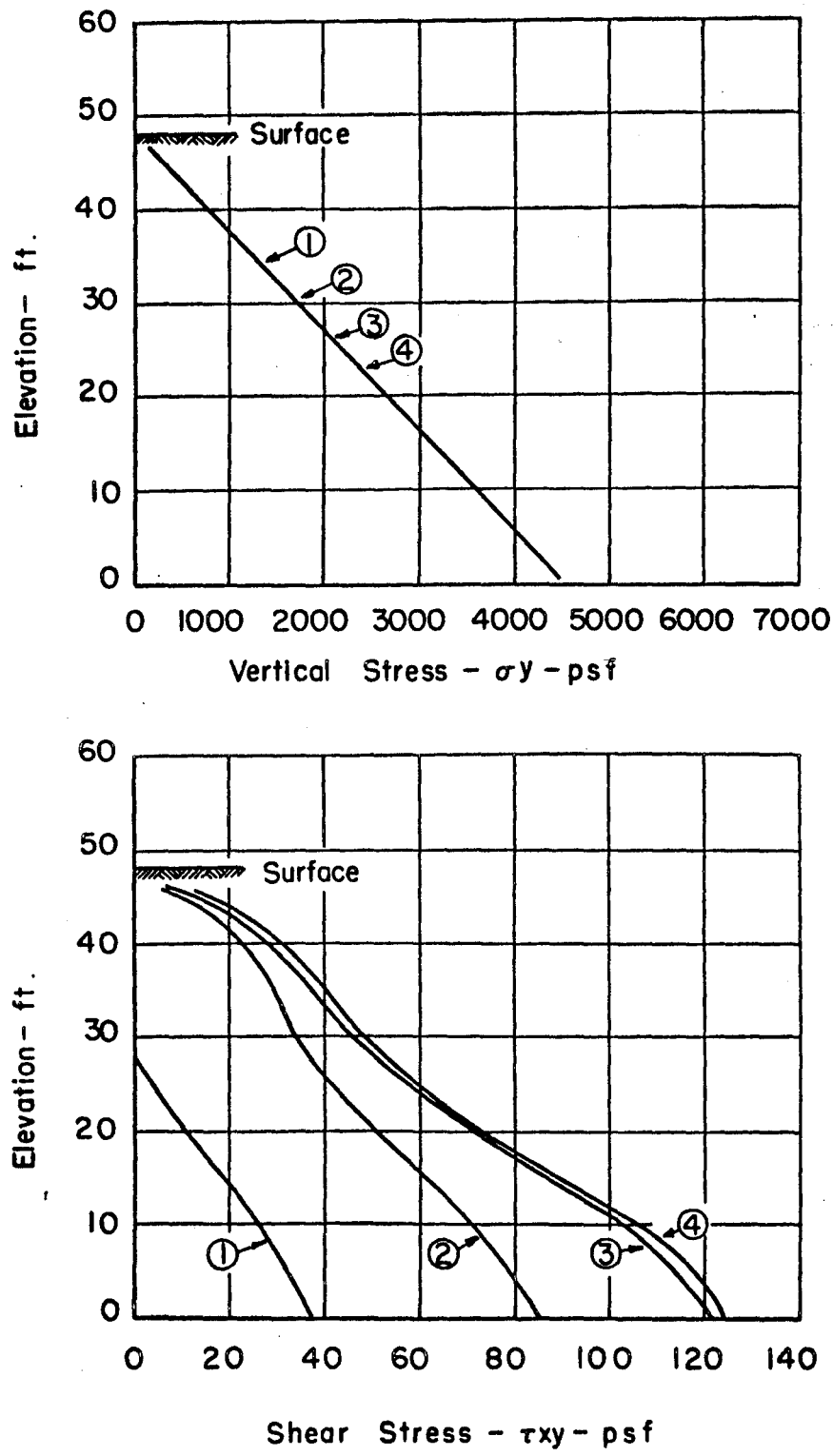

FIG. 75. INFLUENCE OF LATERAL BOUNDARY LOCATION ON VERTICAL STRESS AND SHEAR STRESS.

increase in shear stress with increasing distance to the mesh boundary except from position 3(D_T = 3.2 H_T) to position 4(D_T = 5.6 H_T) where only a small change in shear stress occurs.

Horizontal and vertical displacements for nodal points at the up-slope boundary of the region of interest are shown in Fig. 76 for various positions of the right boundary of the finite element mesh. The horizontal displacements increase appreciably with increasing distance to the mesh boundary for positions 1, 2 and 3; the change from position 3 to 4 is considered negligible. The vertical displacements are affected to a lesser degree by the mesh boundary location and no further change in displacement results for boundary locations beyond position 2. The modulus variation used for the slope analyzed in Figs. 74, 75, and 76 is plotted in the upper part of Fig. 77. This variation was chosen to represent that expected in the upper portion of San Francisco Bay Mud.

On the basis of the analytical results shown in Figs. 74, 75 and 76 it was established that the maximum value of horizontal shear stress at the boundary of the region of interest would represent a good criterion of the effect the location of the mesh boundary. The maximum value of shear stress at the up-slope and down-slope boundaries of the region of interest for various positions of the mesh boundaries are shown in the lower part of Fig. 77. It may be noted that stresses on the up-slope boundary are unaffected by locating the mesh boundary beyond $D_T = 3H_T$; stresses on the down-slope boundary are unaffected if $D_B = 4H_T$ or greater.

Other analyses were also conducted with various values of slope angle, depth factor, regions of interest and elastic modulus variation as indicated in Table 10. For these conditions it was determined that the distance required to eliminate the mesh boundary effects from the region of interest was $2H_T$ from the up-slope boundary and $3H_B$ from the down-slope boundary; the total distances to the mesh boundaries may thus be calculated from:

$$D_B/H_B = L_B/H_B + 3$$

$$D_T/H_T = L_T/H_T + 2$$

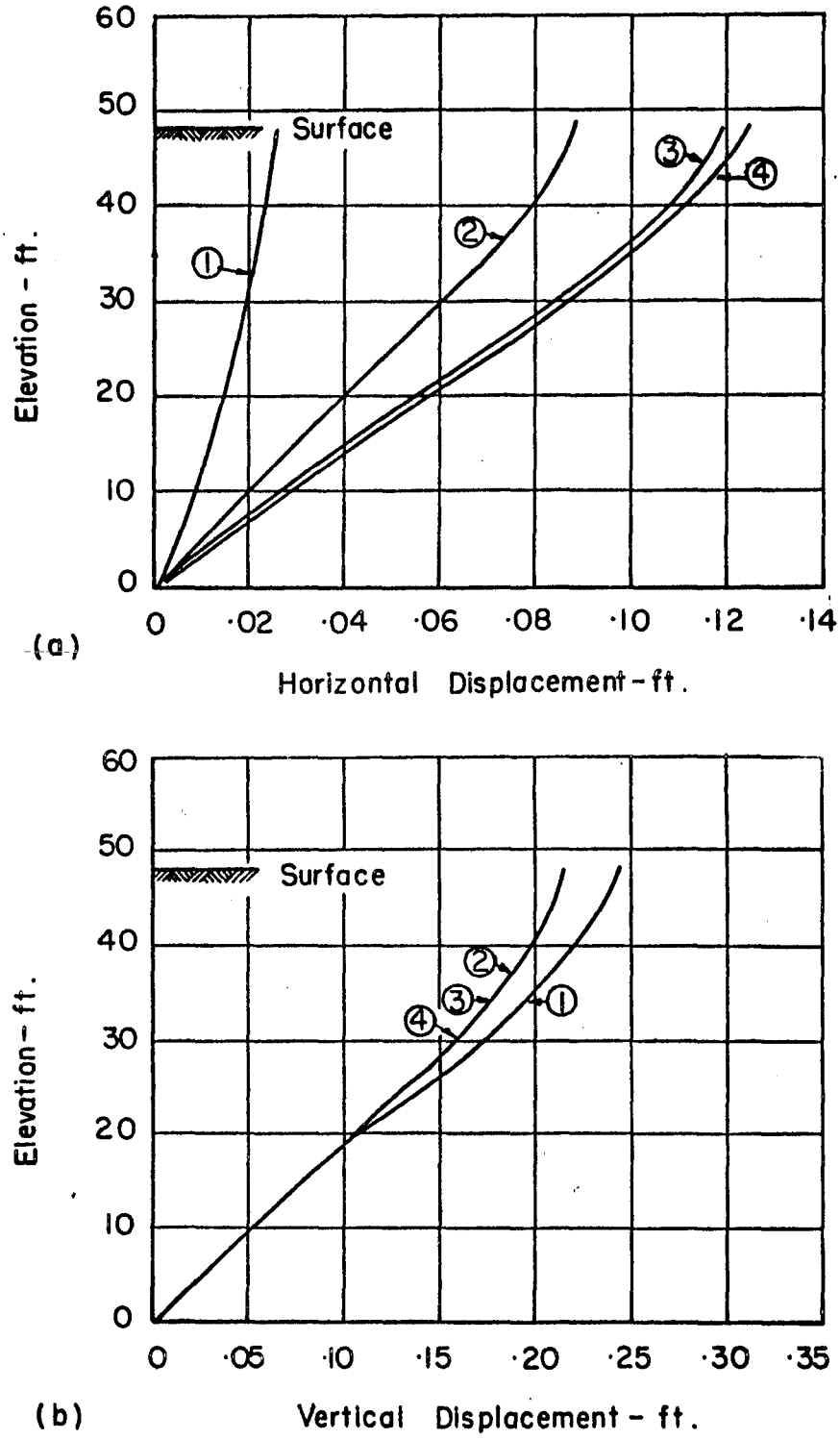

FIG. 76. INFLUENCE OF LATERAL BOUNDARY LOCATION ON HORIZONTAL AND VERTICAL DISPLACEMENTS.

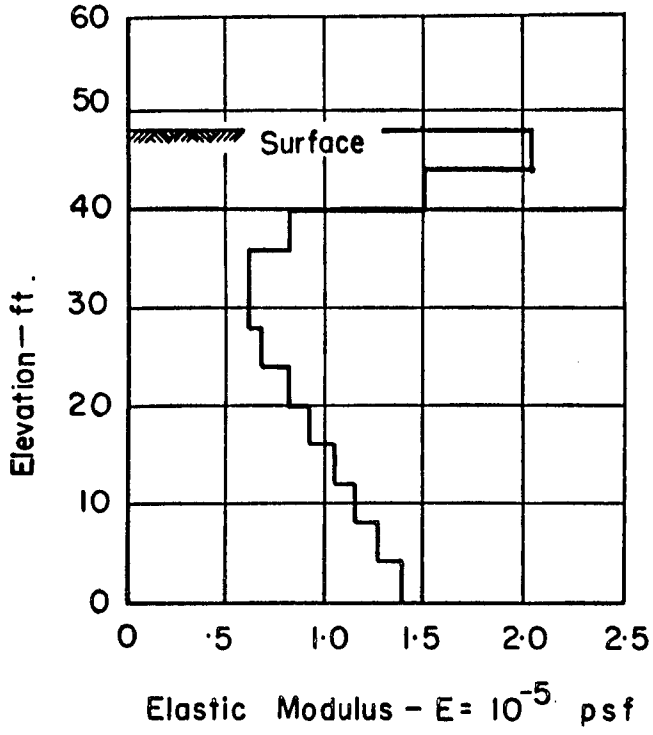

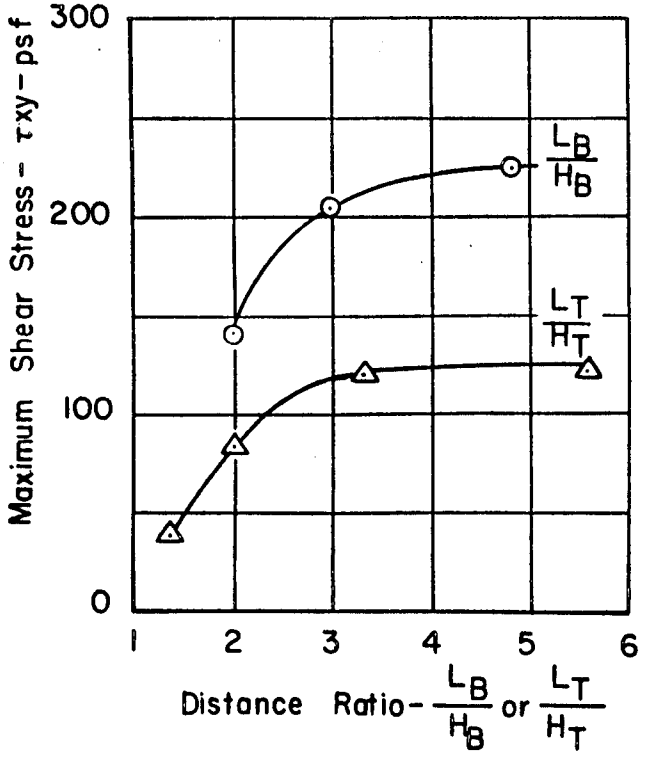

FIG. 77. MODULUS-DEPTH VARIATION AND INFLUENCE OF LATERAL BOUNDARY LOCATION ON THE SHEAR STRESS.

Table 10. Slopes Analyzed for Boundary Effects.

Slope Angle, i	18°, 90°
H_T/H	1.0, 1.7, 2.0, 3.0
L_B/H_B	1.0, 1.5, 2.0
L_T/H_T	0.5, 1.0, 2.0
Elastic Modulus, E	Constant, varied (Fig. 77(a))

In the studies to determine the influence of the location of the finite element mesh boundaries on the stresses, strains and displacements in the region of interest the value of Poisson's ratio was taken to be 0.475. The influence of the value of Poisson's ratio was not studied because for the total stress analysis of saturated clays for short term loading there is little volume change and therefore, if isotropic elasticity is assumed, the value of Poisson's ratio must necessarily approach one-half.

Element Size

It has previously been mentioned that the most efficient analyses require a minimum number of elements necessary for accurate representation of the system being studied. In certain problems it has been shown that it is necessary to include elements in the regions adjacent to the region of interest for the purpose of eliminating undesirable boundary effects from the region of interest. Because stresses, strains and displacements in these regions are of little interest, it is desirable to use as few elements as necessary. To determine criteria for the size of elements it is convenient to consider the element as a height and a shape factor, where the height is the layer thickness and the shape factor is defined as the ratio of the longest side to the shortest side for rectangles and the base to height ratio for triangles and trapezoids.

Layer Thickness

The effect of layer thickness on the accuracy of the finite element idealization has previously been studied for the static built-up embankment case by Clough and Woodward (1967).

Clough and Woodward considered a construction sequence for an embankment which consisted of the progressive placement of layers of soil until the final configuration was reached, each added layer applying only vertical normal stresses to the previously placed soil. Goodman and Brown (1963) have shown that such a construction procedure results in stresses, strains and displacements dependent upon the number of construction steps taken. Clough and Woodward (1967) concluded that a 7 step and a 14 step construction procedure produced practically the same results and therefore used a 10 step sequence for their studies.

Studies to determine the effect of layer thickness were performed on two vertical slopes composed of square elements with 8 and 16 layers. Because a direct comparison of stresses, strains and displacements over an area is difficult the stresses at four vertical sections are compared; Fig. 78 shows the horizontal, vertical and shear stress ratios at vertical sections 5 feet on either side of the vertical cut face; Fig. 79 shows the same stress ratios on vertical sections at 40 feet on either side of the vertical cut face. It may be noted that the stress ratios for the 8 and 16 layer configurations are essentially the same with the exception of the horizontal and vertical stresses in the region of the toe of the slope (Fig. 78), these being somewhat larger for the 8-layer representation; the shear stresses for the two analyses are virtually the same. Because the value of the normal stress is relatively unimportant for clays in undrained shear, and because stress concentrations at lesser slope angles are not as pronounced as for vertical slopes it would appear that an 8 layer configuration was adequate for most purposes. Studies of slopes constructed in materials with bi-linear elastic properties indicated that the stress changes occuring due to the incremental construction procedure in an 8 layer configuration were quite large, causing stresses to exceed the assigned material strengths by appreciable amounts. Subsequent analyses have been conducted on 10 or more layer configurations with better results.

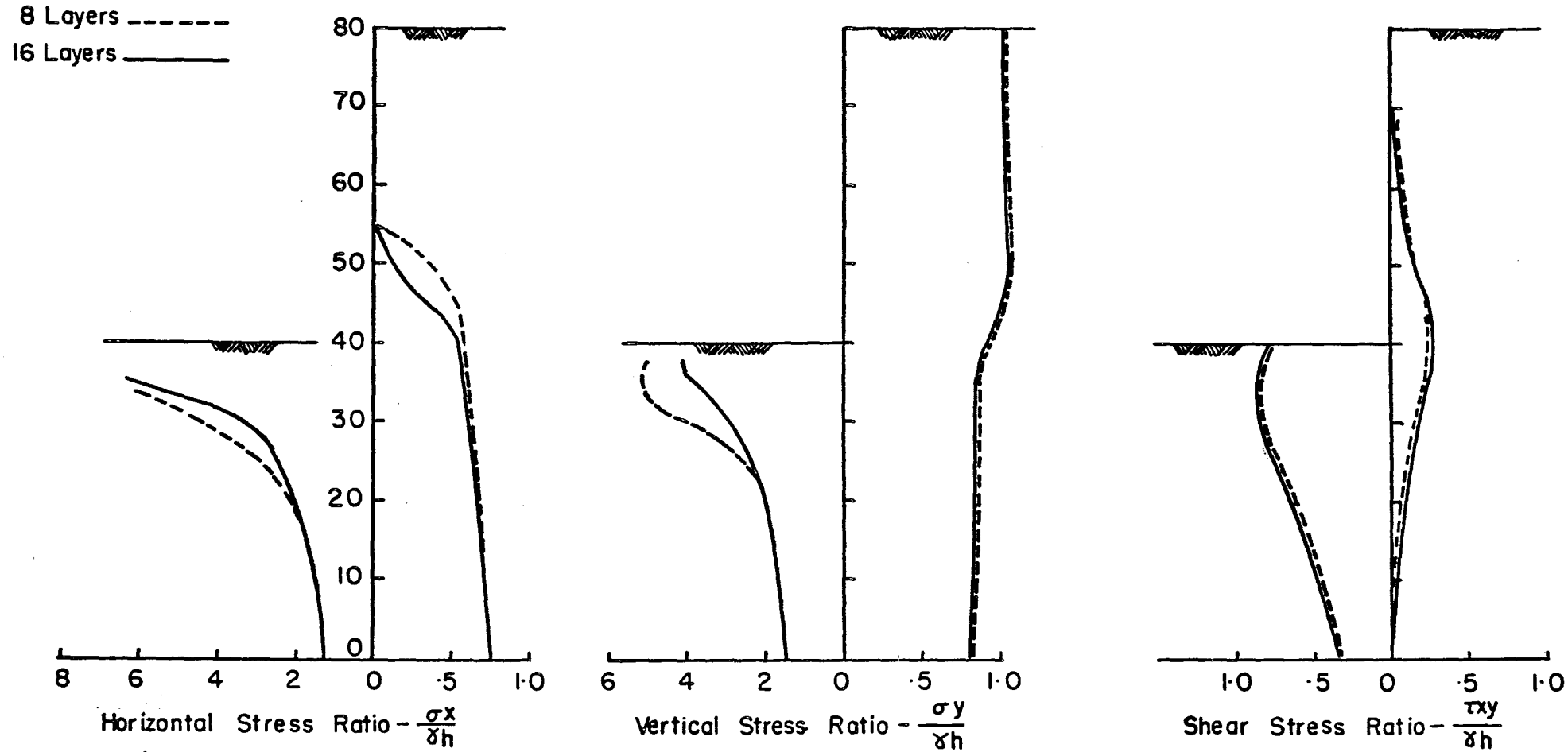

FIG. 78. THE EFFECT OF LAYER THICKNESS ON STRESSES AT 5 FT. ON EITHER SIDE OF A VERTICAL CUT.

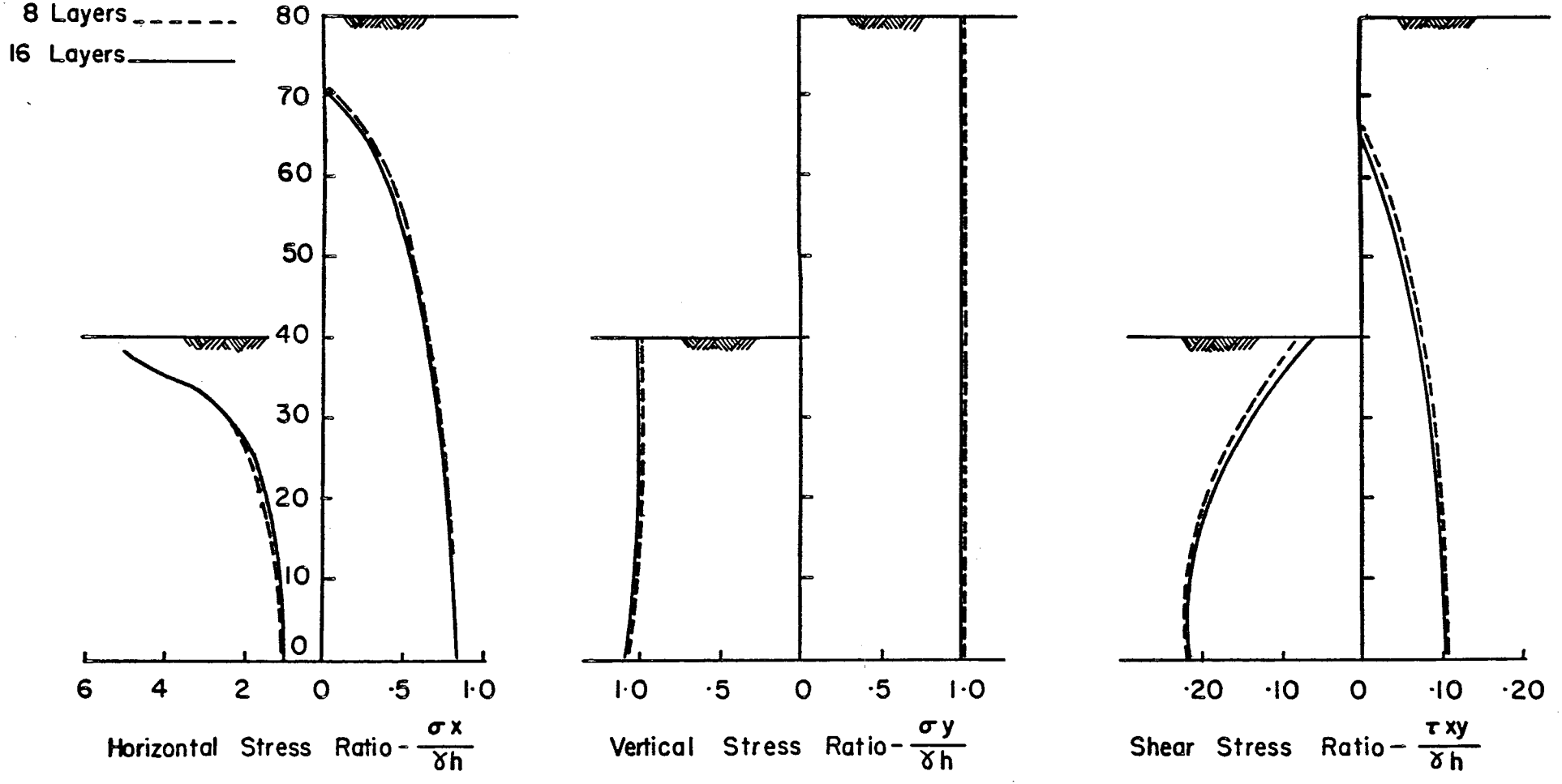

FIG. 79. THE EFFECT OF LAYER THICKNESS ON STRESSES AT 40 FT. ON EITHER SIDE OF A VERTICAL CUT .

Element Shapes

The effect of the element shape on the accuracy of stresses, strains and displacements of the system being analyzed probably depends largely upon the location of the element within the mesh configuration and the forces and/or displacements applied to it.

Idriss (1966), in studying the effect of triangular element shape on the response of earth banks subjected to earthquakes, concluded that triangular elements with base-to-height ratios of 5 or less had little effect on the results anywhere in the slope and ratios of 10 away from the slope had little effect on results in the slope region. For rectangular elements (composed of 4 triangular elements) these base-to-height ratios are equivalent to 2.5:1 and 5:1 respectively. Ratios used in the present study are within these limits and no systematic analyses were undertaken to develop limiting ratios. However, it was determined in the course of studying several vertical slopes that element side ratios of 5:1 outside the region of interest did not influence stresses within the region. In general for the slopes analyzed (1.5:1 and 3:1) and the finite element meshes used, the element length to height ratios within the region of interest did not exceed 1.5:1. Ratios greater than 5 were never used within a distance H_T or H_B of the boundary of the region of interest and a maximum length to height ratio used was 8, at a distance greater than $2H_T$ or $2H_B$ from the boundary of the region of interest.

APPENDIX B

CORRECTIONS FOR SIMPLE SHEAR TEST RESULTS

Recent studies have shown that the strength and stress-strain behavior of soft weak clays may be greatly influenced by the strength of rubber membranes, filter paper drains and various other factors related to equipment design. For tests on specimens of San Francisco Bay Mud, Duncan and Seed (1967) have shown that neglecting to correct for these effects may result in overestimating the soil strength by as much as 20% at low consolidation pressures. Since the simple shear tests are to be performed on Bay Mud specimens at low consolidation pressures, it is necessary to determine appropriate corrections for the strength and stress-strain curves.

Rubber Membrane Correction

The simple shear specimens are 6 cm square and approximately 2 cm. high. The rubber membranes used to enclose the specimens are approximately 5 percent smaller than the specimen and .010 in. in thickness. This difference in size will result in an initial prestress in the specimen. Because of the lateral support of the top and base plates only vertical prestress will occur in the specimen. This initial vertical stress due to the undersized rubber membrane may be determined as described in the following paragraphs.

In order to derive corrections for the rubber membrane in the simple shear test, the rubber is assumed to be an isotropic linear elastic material with the same properties in tension and compression and to have a Poisson's ratio of one-half. The governing equations may be written as

$$\begin{aligned} E_m \varepsilon_z &= \sigma_z - \nu\ (\sigma_p + \sigma_n) \\ E_m \varepsilon_p &= \sigma_p - \nu\ (\sigma_z + \sigma_n) \\ E_m \varepsilon_n &= \sigma_n - \nu\ (\sigma_z + \sigma_p) \end{aligned} \qquad \text{(B-1)}$$

in which E_m = the elastic modulus for the rubber membrane, ε_z = the vertical strain, ε_p = the perimetral strain, ε_n = the strain normal to the membrane surface, σ_z = the vertical stress, σ_p = the perimetral stress, σ_n = the stress in membrane normal to membrane surface and ν = the

Poisson's ratio. Duncan (1965) found that $E_m = 14\ kg/cm^2$ for pure latex rubber membranes, which were used for the simple shear tests.

The initial strain in the membrane is ε_{opm} and

$$\varepsilon_p = \varepsilon_{opm}$$
$$\varepsilon_z = \varepsilon_{opm}$$
$$\sigma_n = 0$$

By substituting these into Equations (B-1) the following expressions for stresses in the membrane may be determined.

$$\sigma_z = 2\ E_m\ \varepsilon_{opm}$$
$$\sigma_p = 2\ E_m\ \varepsilon_{opm}$$

Only the force corresponding to σ_z will act on the specimen since the force resulting from σ_p will be transferred to the top and bottom steel plates. Therefore the vertical stress during consolidation must be corrected.

The vertical force due to the membrane stress, σ_z may be expressed as

$$P_z = A_m \cdot 2\ E_m\ \varepsilon_{opm}$$

where $$A_m = t_m\ 4W_s$$

in which A_m = the membrane area and W_s = the width or length of the square specimen. Since t_m may be expressed in terms of initial thickness t_{om} and strains ε_{opm},

$$t_m = \frac{t_{om}}{(1-\varepsilon_{opm})^2}$$

and the specimen area is W_s^2, the following expression for initial stress in the specimen due to the membrane is obtained.

$$\Delta\sigma_{a_m} = \frac{8\ t_{om}\ E_m\ \varepsilon_{opm}}{(1-\varepsilon_{opm})^2\ W_s} \qquad \text{(B-2)}$$

During consolidation under the desired pressure strains will occur and produce further stress changes in the sample. For the consolidation process

$$\varepsilon_z = \varepsilon_{ac}$$

$$\varepsilon_p = 0$$

$$\sigma_n = 0$$

where ε_{ac} = the axial strain during consolidation. Again substituting into equations (B-1) results in

$$\sigma_z = \frac{4}{3} E_m \varepsilon_{ac}$$

$$\sigma_p = \frac{2}{3} E_m \varepsilon_{ac}$$

and the σ_p is again carried by the top and bottom plates. Proceeding in a similar manner to the above it may be seen that

$$\Delta\sigma_{a_m} = -\frac{16}{3} \frac{t_{om} E_m \varepsilon_{ac}}{(1-\varepsilon_{opm})^2 (1-\varepsilon_{ac}) W_s} \qquad \text{(B-3)}$$

The total vertical stress correction at the end of consolidation for the simple shear rubber membrane is therefore the sum of equations (B-2) and (B-3).

$$\Delta\sigma_{am} = -\frac{16}{3} \frac{t_{om} E_m \varepsilon_{ac}}{(1-\varepsilon_{opm})^2 (1-\varepsilon_{ac}) W_s} - \frac{8\, t_{om} E_m \varepsilon_{opm}}{(1-\varepsilon_{opm})^2 W_s} \qquad \text{(B-4)}$$

Since the initial strain ε_{opm} and the vertical strain during consolidation ε_{ac} are of opposite sign the two portions of the correction tend to cancel one another as a result the axial stress correction is usually less than .01 Kg/cm^2.

Because predominantly shear strains are induced during the simple shear test the stress-strain correction due to the deformation of the membrane may be calculated in the following manner. The shear strains cause a shear force

$$P_{xy} = 2W_s\, t_m\, G_m\, \gamma_{xy}$$

$$= \frac{2W_s \cdot t_{om}}{(1-\varepsilon_{opm})^2 (1-\varepsilon_{ac})} \frac{E_m}{2(1+\nu)} \gamma_{xy} \qquad \text{(B-5)}$$

in which G_m = the shear modulus of the membrane, γ_{xy} = the shear strain, and all other symbols are as previously defined, and the shear stress correction is, therefore,

$$\Delta\tau_{xy} = -\frac{2}{3}\frac{t_{om}\,E_m}{(1-\varepsilon_{opm})^2(1-\varepsilon_{ac})\,W_s}\cdot\gamma_{xy} \qquad \text{(B-5)}$$

This correction is less than .01 kg/cm^2 for strains up to 20 percent with the membranes used in the present study and therefore the correction was neglected.

Friction is present in the simple shear device as rolling and sliding friction. Because the steel sides of the simple shear box cannot deform in the same manner as the specimen there is relative motion between the rubber membrane and the box sides (Fig. 80). The magnitude of the friction force resulting from this relative motion depends upon the method of lubrication, the consolidation pressure acting on the specimen, the back pressure, the time of consolidation, the materials in contact and the construction of the simple shear box. Decreased friction results from increased viscosity, lower consolidation and back pressures, decreased consolidation time and smoother materials in contact.

Duncan and Dunlop (1968) have presented an experimental relationship for friction versus theoretical grease thickness between polished lucite and rubber with Dow Corning stop cock grease and high vacuum grease as lubricants. It is expected that this relationship should also be applicable to polished steel and rubber.

The simple shear box (Fig. 80) as constructed may be considered to represent an infinite strip contact between the rubber and steel. The relative motion between the rubber membrane and the shear box sides and "drainage paths" for the grease are shown in Fig. 80.

During consolidation the lateral pressure and pore pressure act on the rubber membrane and grease. This pressure will cause the grease to escape at locations A, B, and C since these points are at atmospheric pressure. (It would be better to have these points at a higher pressure, thereby reducing the pressure gradient in the grease.) Because of grease escape at point B, the one-half width of the infinite strip was estimated to be 0.75h.

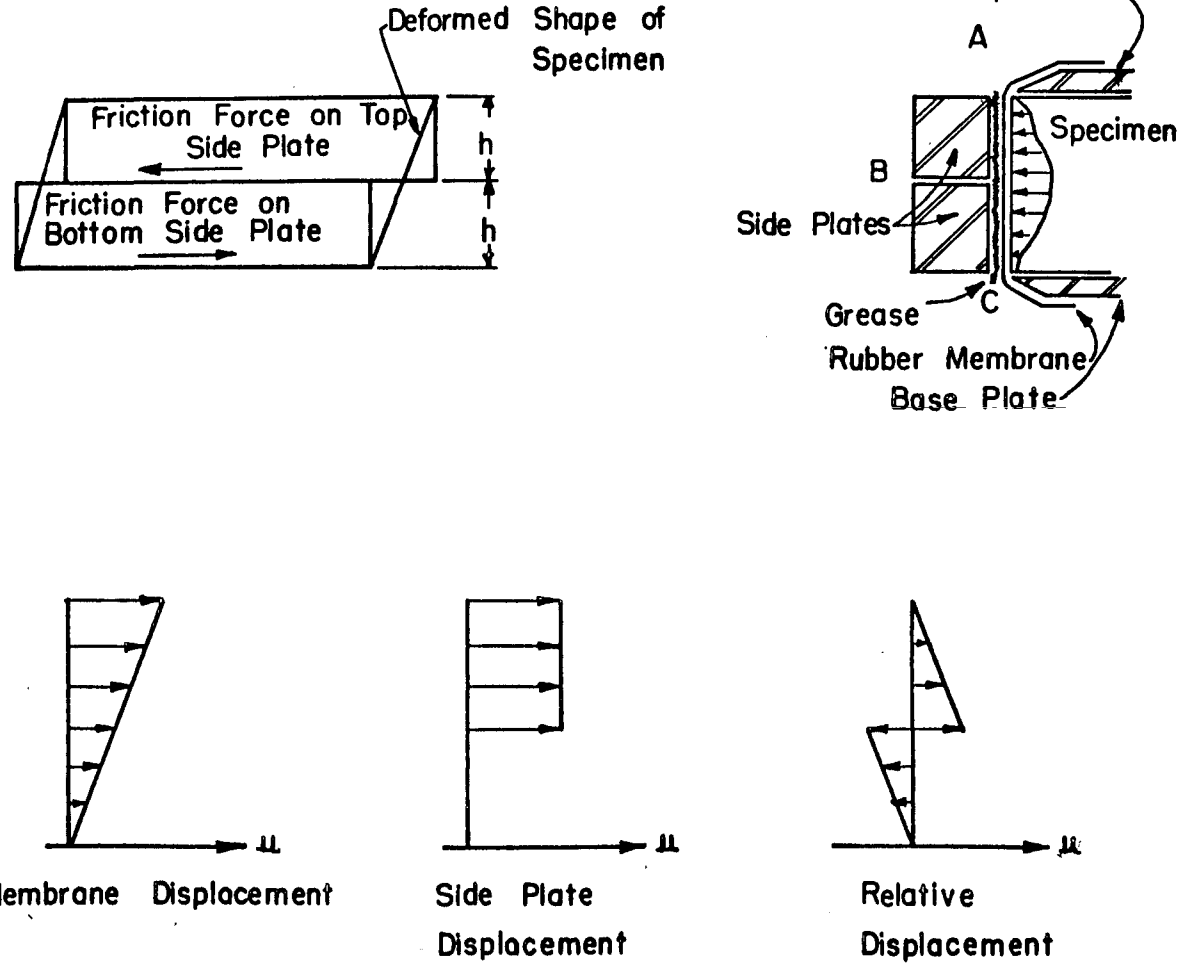

FIG. 80. SIMPLE SHEAR BOX RELATIVE DISPLACEMENTS AND LUBRICATION OF SIDES.

The theoretical thickness of grease between two rigid, perfectly smooth infinite strips is

$$h^2 = \frac{ho^2}{1 + \frac{1}{4}\frac{ho^2 \cdot F \cdot t}{\mu \cdot b^3}} \qquad \text{(B-6)}$$

F = the force per unit length forcing the strips together
b = the one-half width of the strip
μ = the viscosity of the separating lubricant
ho = the original grease thickness
t = time during which the pressure acted.

Using this relationship and the variation of sliding friction with grease thickness (h) determined by Duncan & Dunlop (1968) it is possible to estimate the friction between the simple shear box sides and the rubber membrane. Friction is also present in the form of rolling and sliding friction of the moving parts of the simple shear apparatus. The amount of friction due to both rolling and sliding was measured at various values of normal pressure using an aluminum specimen in the simple shear device. The displacements induced by applied shear loads under this test arrangement are shown in Fig. 81a. The shear load difference between the load and unload cycles at the same strain is expected to be double the friction force since this friction in each case opposes the shear motion. Figure 81b shows the variation of this friction for various total vertical stresses applied to the sample. This correction to the shear stress is applied by determining the friction force for the test procedure from Fig. 81b and dividing this by the sample area.

A friction calibration for simple shear box friction was also performed using a water-filled membrane, applying a pressure and, after some time, conducting a strain controlled test on the water "specimen". In this way the sliding, rolling, and other friction factors will approximate those factors acting during the tests on clay samples. The side friction for this water test is not truly equivalent to that for a soil specimen because the water sample pressure will be uniform, whereas the clay sample pressure may be nonuniform. A gradient causing grease flow requires nonuniform pressure, and it would therefore be expected that

more grease would be extruded and the friction forces would be somewhat higher for a clay sample.

Although the pressure distribution for the soil and water specimens are not the same, the two methods of correcting for friction result in corrections of almost exactly the same magnitude. In fact, the corrections estimated from the sliding, rolling and membrane friction and those estimated from the water specimen tests agree within approximately 5%. The total correction to the shear stress was of the order of .08 kg/cm^2 or about 15% of the applied shear stress for the pressures used in the present tests. Equation B-6 and Fig. 81b show that the total shear stress correction depends upon the consolidation pressure and the consolidation time as well as the thickness and viscosity of the lubricant.

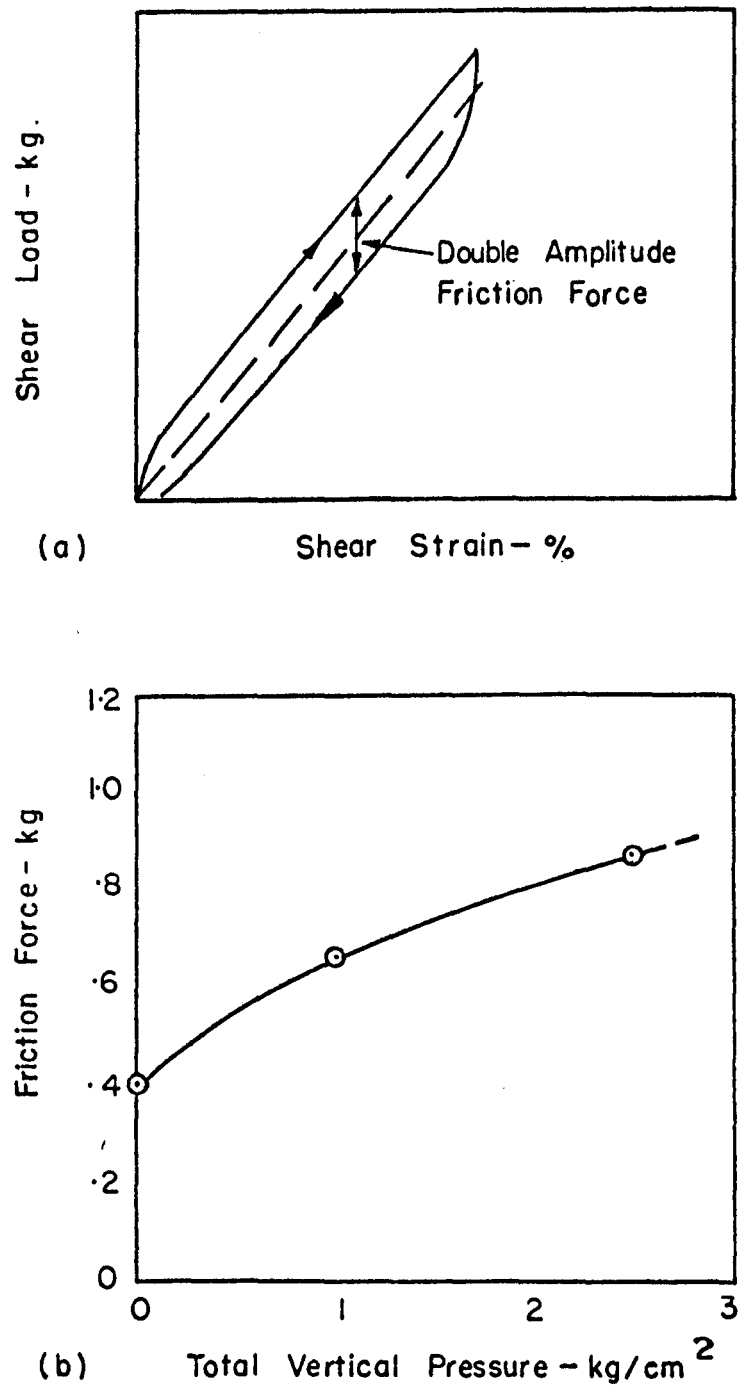

FIG. 81 . SLIDING AND ROLLING FRICTION IN THE SIMPLE SHEAR APPARATUS .

APPENDIX C

FINITE ELEMENT COMPUTER PROGRAM FOR EXCAVATED SLOPES

Identification

This program consists of a main program (MAIN) and seven subroutines (STIFF, QUAD, TRISTF, STRES, BANSOL, MODI, INIT).

Purpose

This program calculates stresses, strains and displacements for a cut slope composed of either homogeneous soils or horizontally layered soils. The program may be used for analysis of slopes in materials with linear, bilinear or multilinear stress-strain properties.

Input Data

IDENTIFICATION CARD: FORMAT (12A6)

Cols. 2-72 Identifying information to be printed with results.

SLOPE CONFIGURATION CARD: FORMAT (3I5, F10.2, 3I5)

Cols. 1-5 Number of layers of elements (NL $\leq$ 23)

6-10 Number of columns of elements (NI $\leq \frac{450-NT}{NL+1} - 1$)

11-15 Number of different materials (NUMMAT $\leq$ 20)

16-25 Vertical acceleration (ACELZ). This is 0.0 for this program; the initial stresses are generated by $\sigma_{vertical} = \gamma \cdot$ depth and $\sigma_{horizontal} = K \cdot \sigma_{vertical}$

26-30 Number of iterations in calculating elastic properties (NPP)

31-35 Number of the first column to the right of the slope top (NX)

36-40 Number of layers to be removed (NT). These layers are removed 1 at a time.

The inclination of the slope is determined by the spacing of verticals and horizontals in the slope (shaded region, Fig. 82) and must be uniform.

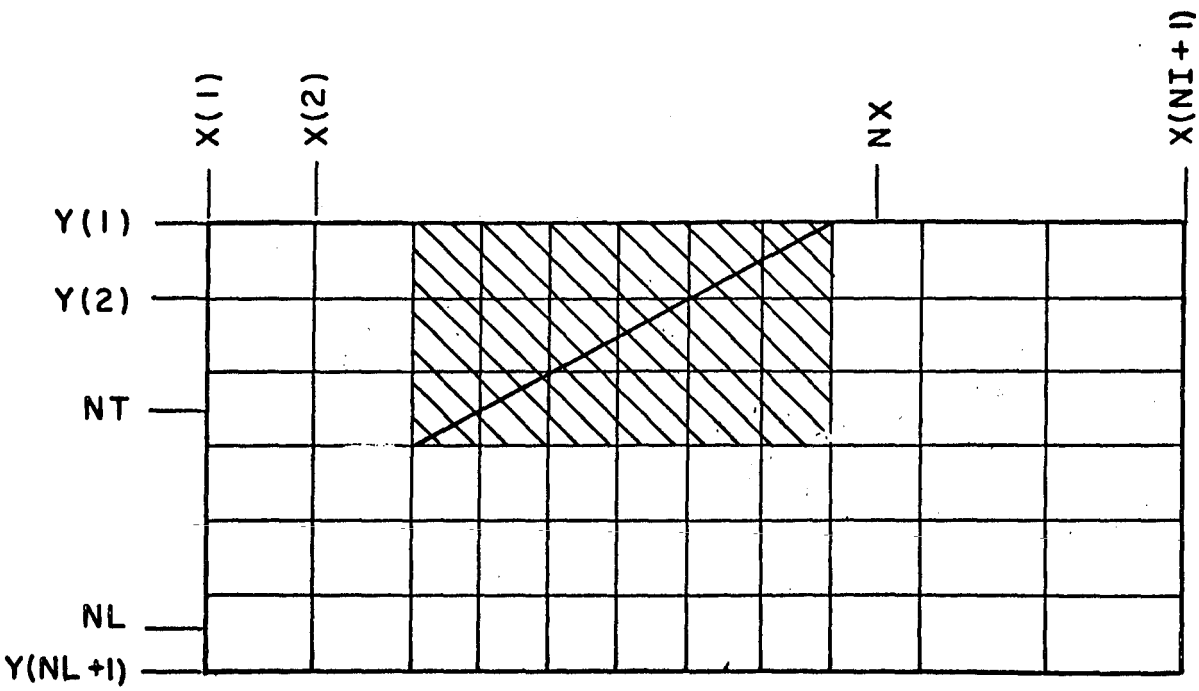

FIG. 82. CONFIGURATION OF GENERATED SLOPE.

MATERIAL PROPERTY CARD: FORMAT (1I0,4F10.2); NUMMAT cards; one for each material.

Cols. 1-10 Material type (MTYPE)

11-20 Material unit weight (RO(MTYPE))

21-30 Elastic modulus (E(1,MTYPE))

31-40 Poisson's ratio (E(2,MTYPE)); this is restricted to < .50 and should perhaps be ≤ .49 to give accurate results

41-50 Material shear strength (PRESS(MTYPE)).

51-60 Total stress coefficient of earth pressure (CAYO(MTYPE)).

The next-to-last card MTYPE(NUMMAT - 1), designates the properties assigned to the materials after failure; the unit weight and Poisson's ratio should be the same as before failure, but the modulus should be reduced. The last card, MTYPE (NUMMAT), is used to designate the properties assigned to the materials in elements which have been "removed"; the unit weight should be zero, modulus should be very small (typically 0.01), Poisson's ratio should be the same as before removal, and the strength may be entered as zero.

VERTICAL BOUNDARY LOCATION CARD: FORMAT (8F10.2)

Cols. 1-10 First vertical line, X(1); this represents the left boundary; see Fig. 82. These X values must be whole numbers because of slope generation, i.e., X = 10.0, 21.0, 57.0; values such as 10.3, 21.27, etc.... cannot be used for vertical boundaries between elements.

11-20 Second vertical line, X(2) which is the boundary between the first and second column of elements.

21-30 ....

Continue to X(number of columns + 1),X(NL+1) which is the right boundary.

HORIZONTAL BOUNDARY LOCATION CARD: FORMAT (8F10.2)

Cols. 1-10 First horizontal line Y(1); this represents the surface (must be whole numbers as for vertical boundaries).

11-20 Second horizontal line Y(2); this forms the boundary between the top layer and the second layer.

21-30 ....

Continue to Y (number of layers + 1),Y(NL+1); this is the bottom boundary.

LAYER MATERIAL TYPE CARD: FORMAT (1215)

Cols. 1-5 Material type for top layer MAT(1) = 1.

6-10 Material type for second layer MAT(2) = 1 or 2.

11-15 ....

Continue to number of layers MAT(NL). The material types must increase consecutively from the top down however, any one type can be repeated in adjacent layers.

Sequence of Operations

After the input data is read, the elements and nodal points are generated in the main program. The main program then calls subroutine INIT which calculates the initial stresses in the configuration. The stiffness of the removed elements is reduced and the main program calls subroutine STIFF (and QUAD and TRISTF) which assembles the stiffness and nodal point forces. BANSOL is next called to solve for the nodal point displacements and STRESS is called to calculate the element stresses and strains.

Output

The input data and the following quantities are printed.

(1) Nodal point displacements.

(2) Element stresses, strains and pore pressures.

Program Listing

The program has been coded in FORTRAN IV language and has been used on BC DCS IBM 7090 - 7094 and CDC 6400 computers. The listing of the program is presented in the following pages.

```
$IBFTC MAIN
C
C      BOUNDARY REVERSE CUT DOWN  POISSON,S RATIO RESTRICTED
C
       COMMON NUMNP,NUMEL,NUMMAT,ACELZ,NPP,N,VOL,MTYPE,NXX,NXP,
      1 NL,NT,HED(12),E(3,20),RO(20),R(500),Z(500),UR(500),
      2 UZ(500),CODE(500),SIG(10),NUMLAY,NUMIT
       COMMON /ARG/ RRR(5),ZZZ(5),S(10,10),P(10),TT(4),LM(4),
      1 DD(3,3),HH(6,10),RR(4),ZZ(4),C(4,4),H(6,10),D(6,6),
      2 F(6,10),TP(6),XI(10),EE(4),IX(450,5),STRESS(450,3),
      3 SU(20),NBACK(50),STREG(20),POREPR(450),STRAIN(450,3),
      4 GAMAX(450),BETAI(450)
       COMMON /SLP/ CAYO(30),TOPX,TOPY,TOEX,TOEY,N1,N2
       COMMON / BANARG / MBAND,NUMBLK,B(108),A(108,54)
       DIMENSION X(100),Y(30),MAT(30)
C
   50  READ(5,1006) HED,NL,NI,NUMMAT,ACELZ,NPP,NX,NT
       NUMNP=(NL+1)*(NI+1)+NT
       NUMEL=(NL)*(NI)+2*NT
       WRITE(6,2000)HED,NUMNP,NUMEL,NUMMAT,ACELZ,NPP,NX,NT
       NI1=NI+1
       NL1=NL+1
C
       WRITE (6,2011)
   56  DO 59 MM=1,NUMMAT
       READ (5,1001) MTYPE,RO(MTYPE),(E(I,MTYPE),I=1,2),
      1 STREG(MTYPE),CAYO(MTYPE)
       WRITE(6,2010) MTYPE,RO(MTYPE),(E(I,MTYPE),I=1,2),
      1 STREG(MTYPE),CAYO(MTYPE),MTYPE
   59  CONTINUE
C
C      READ AND PRINT OF NODAL POINT DATA
C
       READ(5,1007)  (X(I),I=1,NI1)
       READ(5,1007)  (Y(I),I=1,NL1)
       READ(5,1008)(MAT(I),I=1,NL)
       DO 31 N=1,NUMEL
       GAMAX(N) =0.
       BETAI(N) =0.
       DO 31 K=1,3
   31  STRAIN (N,K) =0.
       DO 32 K=1,NUMNP
       UR(K)=0.
   32  UZ(K)=0.
C
C**** LOCATE NODAL POINTS FOR SLOPE THREE
C
       NP=0
       NS=NL-NT
       NX2NL=NX-2*NT
       WRITE (6,2004)
       I=0
   75  I=I+1
       NL1=NL+1
       IF (I.LE.NX2NL.OR. I.GE.NX)       GO TO 66
```

```
      MMM=I-NX2NL+1
      NNN=MMM/2
      IF (MMM.NE.2*NNN)       GO TO 77
      NS=NS+1
      NL1=NL+2
   77 DO 27 J=1,NL1
      NP=NP+1
      IF (MMM.NE.2*NNN)       GO TO 24
      IF(J-(NL+2-NS))24,81,82
   81 Z(NP)=(Y(J-1)+Y(J))/2.
      GO TO 25
   82 Z(NP)=Y(J-1)
      GO TO 25
   24 Z(NP)=Y(J)
   25 CODE(NP)=0.
      IF(I.EQ.1.OR.I.EQ.NI1) CODE(NP)=1.0
      IF(Z(NP).EQ.Y(NL+1))   CODE(NP)=3.0
      R(NP)=X(I)
   27 WRITE(6,2002) NP,CODE(NP),R(NP),Z(NP),UR(NP),UZ(NP)
      IF(NUMNP-NP)100,76,75
   66 DO 6 J=1,NL1
      NP=NP+1
      Z(NP)=Y(J)
      CODE(NP)=0.
      IF(I.EQ.1.OR.I.EQ.NI1) CODE(NP)=1.0
      IF(Z(NP).EQ.Y(NL+1))   CODE(NP)=3.0
      R(NP)=X(I)
    6 WRITE(6,2002) NP,CODE(NP),R(NP),Z(NP),UR(NP),UZ(NP)
      IF(NUMNP-NP)100,76,75
  100 WRITE (6,2009) N
      CALL EXIT
C
C**** GENERATE ELEMENTS FOR SLOPE 3
C
   76 I=0
      WRITE (6,2001)
      NS=NL-NT
      NL1=NL+1
      NE=0
   70 I=I+1
      IF (I.GE.NX2NL.AND.I.LT.NX)       GO TO 39
      DO 10 J=1,NL
      IF (NE.GE.NUMEL)        GO TO 190
      NE=NE+1
      IX(NE,1)=NE+I-1
      IF(I.GE.NX) IX(NE,1)=IX(NE,1)+NS-NL
      IX(NE,2)=IX(NE,1)+1
      IX(NE,3)=IX(NE,2)+NL1
      IX(NE,4)=IX(NE,3)-1
      IX(NE,5)=MAT(J)
   10 WRITE(6,2003)  NE,(IX(NE,I),I=1,5)
      GO TO 70
   39 Q=((Y(1)-Y(NT+1))/(X(NX)-X(NX2NL)))*(X(I)-X(NX))+Y(1)+.001
   54 DO 11 J=1,NL
      NYJ1=Y(J+1)
```

```
      NYJ=Y(J)
      NQ=Q
      IF (NQ.GE.NYJ)          GO TO 49
      IF (NQ.GT.NYJ1)         GO TO 53
      P=I
      PP=NX2NL
      PPP=(P-PP)/2.+.6
      NNN=PPP
      NE=NE+1
      IX(NE,1)=NE+I-1-NNN
      IX(NE,2)=IX(NE,1)+1
      MP=(I-NX2NL)
      MP2=MP/2
      IF (MP.NE.2*MP2)        GO TO 57
      N22=NL1
      GO TO 58
   57 N22=NL1+1
   58 IX(NE,3)=IX(NE,2)+N22
      IX(NE,4)=IX(NE,3)-1
      IX(NE,5)=MAT(J)
      WRITE(6,2003)  NE,(IX(NE,I),I=1,5)
      IF (NQ.NE.NYJ1)         GO TO 11
      NE=NE+1
      IX(NE,1)=IX(NE-1,2)
      IX(NE,4)=IX(NE-1,3)
      IX(NE,3)=IX(NE,4)
      IX(NE,2)=IX(NE,3)+1
      IX(NE,5)=MAT(J)
      GO TO 12
   53 NE=NE+1
      IF (J.NE.1)             GO TO 104
      IX(NE,1)=IX(NE-1,2)+1
      IX(NE,2)=IX(NE,1)+1
      IX(NE,3)=IX(NE-1,3)+1
      IX(NE,4)=IX(NE,3)
      IX(NE,5)=MAT(J)
      GO TO 107
  104 IX(NE,1)=IX(NE-1,2)
      IX(NE,2)=IX(NE,1)+1
      IX(NE,3)=IX(NE-1,3)
      IX(NE,4)=IX(NE,3)
      IX(NE,5)=MAT(J)
  107 WRITE(6,2003)  NE,(IX(NE,I),I=1,5)
      NE=NE+1
      IX(NE,1)=IX(NE-1,2)
      IX(NE,2)=IX(NE,1)+1
      IX(NE,3)=IX(NE-1,3)+1
      IX(NE,4)=IX(NE,3)-1
      IX(NE,5)=MAT(J)
      GO TO 12
   49 NE=NE+1
      IF (NQ.EQ.NYJ)          GO TO 91
      IX(NE,1)=IX(NE-1,2)
      IX(NE,2)=IX(NE,1)+1
      IX(NE,4)=IX(NE-1,3)
```

```
      IX(NE,3)=IX(NE,4)+1
      IX(NE,5)=MAT(J)
      GO TO 12
   91 IX(NE,1)=IX(NE-1,1)
      IX(NE,4)=IX(NE-1,2)
      IX(NE,2)=IX(NE,1)+1
      IX(NE,3)=IX(NE,4)+1
      IX(NE,5)=MAT(J)
   12 WRITE(6,2003)  NE,(IX(NE,I),I=1,5)
   11 CONTINUE
      IF (NE.LT.NUMEL)        GO TO 70
  190 CONTINUE
C
C**** DETERMINE BAND WIDTH
C
      J=0
      DO 340 N=1,NUMEL
      DO 340 I=1,4
      DO 325 L=1,4
      KK=IABS(IX(N,I)-IX(N,L))
      IF (KK.GT.J)            J=KK
  325 CONTINUE
  340 CONTINUE
      MBAND=2*J+2
C
      CALL INIT
C
      DO 339 J=1,4
      DO 339 K=1,4
  339 C(J,K)=0.
      DO 341 I=1,50
  341  NBACK(I)=0.
C
C**** ALTER STIFFNESS
C
      NUMLAY=NL
      NXX=0
      NXP=NX+1
      GO TO 161
  163 DO 164 I=1,NUMNP
      UR(I)=0.
  164 UZ(I)=0.
  161 NXX=NXX+1
      TOPX   = X(NX)
      TOPY   = Y(1)
      NN   = NX-2*NXX
      TOEX   = X(NN)
      TOEY   = Y(NXX+1)
      WRITE (6,1009)
      NXP=NXP-2
      NNN=NXX-NUMLAY
      DO 162 I=1,NXP
      MNN=NUMLAY
      IF(I.GE.(NX2NL+1))  MNN=NUMLAY+1
      NNN=NNN+MNN
```

```
      NBACK(I)=NNN
      IX(NNN,5)=NUMMAT
  162 WRITE (6,1004) NNN,IX(NNN,5)
      IF (ACELZ.NE.0..AND.NXX.LT.NT)   GO TO 163
      IF (ACELZ.GT.1.)   READ (5,1010)M,(N,UR(N),UZ(N),NUM=1,M)
C
      DO 500 NUMIT=1,NPP
C
      CALL STIFF
C
      CALL BANSOL
C
      IF (NUMIT.LT.NPP)       GO TO 410
      WRITE (6,2006)
      WRITE (6,2005) (N,B(2*N-1),B(2*N),N=1,NUMNP)
  410 CONTINUE
C
      CALL STRES
C
  500 CONTINUE
      IF(NXX.LT.NT) GO TO 163
C
      GO TO 50
C
 1001 FORMAT (I10,5F10.2)
 1004 FORMAT (2I5,F10.0)
 1006 FORMAT (12A6/3I5,F10.2,3I5)
 1007 FORMAT(8F10.2)
 1008 FORMAT(12I5)
 1009 FORMAT ( // 35H    N  MTYPE  FOR REMOVED ELEMENTS      / )
 1010 FORMAT (I10/(I10,2F10.2))
 2000 FORMAT (1H1 12A6/
     1 30H0 NUMBER OF NODAL POINTS------ I3 /
     2 30H0 NUMBER OF ELEMENTS---------- I3 /
     3 30H0 NUMBER OF DIFF. MATERIALS--- I3 /
     5 30H0 Y ACCELERATION-------------  F12.4  /
     6 30H0 NUMBER OF APPROXIMATIONS---- I3/
     7 30H0 NX FIRST COLUMN------------- I3/
     8 30H0 NT NO. OF LAYERS REMOVED---- I3/ )
 2001 FORMAT (12H1ELEMENT NO.6X1HI5X1HJ5X1HK5X1HL4X8HMATERIAL)
 2002 FORMAT (I12,F12.2,2F12.3,2E24.7,F12.3)
 2003 FORMAT (1I13,4I6,1I12)
 2004 FORMAT (12H1NODAL POINT 8X 28HTYPE  X-ORDINATE  Y-ORDINATE
     1 2X 46H XLOAD OR DISPLACEMENT  Y LOAD OR DISPLACEMENT )
 2005 FORMAT ( I12,2F12.4)
 2006 FORMAT ( 12H1N.P.NUMBER  9X 3H UX 9X 3H UY      )
 2009 FORMAT (26HONODAL POINT CARD ERROR N= I5)
 2010 FORMAT ( I9,F8.2,F12.2,F10.5,F13.2,F9.4,I3/)
 2011 FORMAT ( 9H1MATERIAL 8H  WEIGHT 4X 7HMODULUS 4X 7HPOISSON
     1 5X  8HSTRENGTH  5X 4HCAYO //)
C
      END
```

```
$IBFTC STIF
      SUBROUTINE STIFF
C
      COMMON NUMNP,NUMEL,NUMMAT,ACELZ,NPP,N,VOL,MTYPE,NXX,NXP,
     1 NL,NT,HED(12),E(3,20),RO(20),R(500),Z(500),UR(500),
     2 UZ(500),CODE(500),SIG(10),NUMLAY,NUMIT
      COMMON /ARG/ RRR(5),ZZZ(5),S(10,10),P(10),TT(4),LM(4),
     1 DD(3,3),HH(6,10),RR(4),ZZ(4),C(4,4),H(6,10),D(6,6),
     2 F(6,10),TP(6),XI(10),EE(4),IX(450,5),STRESS(450,3),
     3 SU(20),NBACK(50),STREG(20),POREPR(450),STRAIN(450,3),
     4 GAMAX(450),BETAI(450)
      COMMON / BANARG / MBAND,NUMBLK,B(108),A(108,54)
C
      REWIND 2
      NB=27
      ND=2*NB
      ND2=2*ND
      STOP=0.0
      NUMBLK=0
      IF (ACELZ.NE.0..OR.NUMIT.NE.1)   GO TO 38
C
C**** REVERSE BOUNDARY STRESSES
C
  163 DO 162 II=1,NXP
      N=NBACK(II)
  161 I=IX(N,2)
      J=IX(N,3)
      DR = R(J) - R(I)
      DZ = Z(J) - Z(I)
      IF(II.GE.(NXP-3))  GO TO 164
  168 SIGRY=(STRESS(N,2)+STRESS(N+1,2))/2.
      SIGRX=(STRESS(N,1)+STRESS(N+1,1))/2.
      SIGRT=(STRESS(N,3)+STRESS(N+1,3))/2.
      UR(I) = UR(I)+SIGRT*DR*.5
      UR(J) = UR(J)+SIGRT*DR*.5
      UZ(I) = UZ(I)+SIGRY*DR*.5
      UZ(J) = UZ(J)+SIGRY*DR*.5
      IF(II.EQ.1)  UR(I)=0.0
      GO TO 167
  164 IF(II.GT.1)  NN=NBACK(II-1)
      MM=NBACK(II+1)
      NPX=(II-(NXP-4))
      GO TO (151,153,153,152),NPX
  152 SIGGN=SGGRN
      SIGGT=SGGRT
      SGGRN=0.
      SGGRT=0.
      GO TO 156
  151 IF(NXX.EQ.NT) GO TO 168
      SIGLY=(STRESS(N,2)+STRESS(NN+1,2))/2.
      SIGLT=(STRESS(N,3)+STRESS(NN+1,3))/2.
      GO TO 154
  153 SIGLY=SIGRY
      SIGLX=SIGRX
      SIGLT=SIGRT
```

```
  154 K=N+1
      M=MM+1
      IF(NPX.EQ.1.OR.NPX.EQ.2)  M=M+1
      IF(NXX.EQ.NT.AND.NPX.EQ.1) M=M-1
      IF(NPX.EQ.2)  K=K+1
      IF(NXX.EQ.NT.AND.NPX.EQ.2)  GO TO 158
      GO TO 157
  158 M=MM+2
      SIGRY=(STRESS(N,2)+STRESS( M,2))/2.
      SIGRX=(STRESS(N,1)+STRESS( M,2))/2.
      SIGRT=(STRESS(N,3)+STRESS( M,3))/2.
      GO TO 10
  157 SIGRY=(STRESS(N,2)+STRESS(K,2)+STRESS(MM,2)+STRESS(M,2))/4.
      SIGRX=(STRESS(N,1)+STRESS(K,1)+STRESS(MM,1)+STRESS(M,1))/4.
      SIGRT=(STRESS(N,3)+STRESS(K,3)+STRESS(MM,3)+STRESS(M,3))/4.
      IF (DZ.GT.0.)           GO TO 155
   10 SIGGN=SIGLY
      SIGGT=SIGLT
      SGGRN=SIGRY
      SGGRT=SIGRT
      GO TO 156
  155 ALPHA=ATAN2(DZ,DR)
      CC=COS(ALPHA)
      SS=SIN(ALPHA)
      SIGGN=SIGLY*CC*CC+SIGLX*SS*SS-2.*SIGLT*SS*CC
      SIGGT=(SIGLY-SIGLX)*SS*CC+SIGLT*(CC*CC-SS*SS)
      SGGRN=SIGRY*CC*CC+SIGRX*SS*SS-2.*SIGRT*SS*CC
      SGGRT=(SIGRY-SIGRX)*SS*CC+SIGRT*(CC*CC-SS*SS)
  156 UR(I) = UR(I)+DR*(2.*SIGGT+SGGRT)/6.-DZ*(2.*SIGGN+SGGRN)/6.
      UR(J) = UR(J)+DR*(2.*SGGRT+SIGGT)/6.-DZ*(2.*SGGRN+SIGGN)/6.
      UZ(I) = UZ(I)+DR*(2.*SIGGN+SGGRN)/6.+DZ*(2.*SIGGT+SGGRT)/6.
      UZ(J) = UZ(J)+DR*(2.*SGGRN+SIGGN)/6.+DZ*(2.*SGGRT+SIGGT)/6.
  167 DO 159 I=1,3
  159 STRESS(N,I)=0.
      POREPR(N)=0.
  162 CONTINUE
C
   38 WRITE (6,3000)
      DO 40 N=1,NUMNP
      IF (UR(N).EQ.0..AND.UZ(N).EQ.0.) GO TO 40
      WRITE (6,2900) N,UR(N),UZ(N)
   40 CONTINUE
C
   49 DO 50 N=1,ND2
      B(N)=0.0
      DO 50 M=1,ND
   50 A(N,M)=0.0
      NBN=1
C
C**** FORM STIFFNESS MATRIX IN BLOCKS
C
   60 NUMBLK=NUMBLK+1
      NH=NB*(NUMBLK+1)
      NM=NH-NB
      NL=NM-NB+1
```

```
      KSHIFT=2*NL-2
C
      DO 210 N=NBN,NUMEL
C
      INDEX=N
      KMIN=MIN0(IX(N,1),IX(N,2),IX(N,3),IX(N,4))
      IF (KMIN.LT.NL)          GO TO 210
      IF (KMIN.GT.NM)          GO TO 211
   90 CALL QUAD
C
      IF (VOL.GT.0.)           GO TO 144
      WRITE (6,2003) N
      STOP=1.0
  144 IF (IX(N,3).EQ.IX(N,4))      GO TO 165
      DO 150 II=1,9
      CC=S(II,10)/S(10,10)
      P(II)=P(II)-CC*P(10)
      DO 150 JJ=1,9
  150 S(II,JJ)=S(II,JJ)-CC*S(10,JJ)
C
      DO 160 II=1,8
      CC=S(II,9)/S(9,9)
      P(II)=P(II)-CC*P(9)
      DO 160 JJ=1,8
  160 S(II,JJ)=S(II,JJ)-CC*S(9,JJ)
C
C**** ADD ELEMENT STIFFNESS TO TOTAL STIFFNESS
C
  165 DO 166 I=1,4
  166 LM(I)=2*IX(N,I)-2
C
      DO 200 I=1,4
      DO 200 K=1,2
      II=LM(I)+K-KSHIFT
      KK=2*I-2+K
      B(II)=B(II)+P(KK)
      DO 200 J=1,4
      DO 200 L=1,2
      JJ=LM(J)+L-II+1-KSHIFT
      LL=2*J-2+L
      IF (JJ.LE.0)             GO TO 200
      IF (ND.GE.JJ)            GO TO 195
      WRITE (6,2004) N
      STOP=1.0
      GO TO 210
  195 A(II,JJ)=A(II,JJ)+S(KK,LL)
  200 CONTINUE
  210 CONTINUE
  211 CONTINUE
      NBN =INDEX
```

```
C
C**** ADD CONCENTRATED FORCES WITHIN BLOCK
C
      DO 250 N=NL,NM
      K=2*N-KSHIFT
      B(K)=B(K)+UZ(N)
  250 B(K-1)=B(K-1)+UR(N)
C
C**** DISPLACEMENT BOUNDARY CONDITIONS
C
  310 DO 400 M=NL,NH
      IF (M.GT.NUMNP)          GO TO 400
      U=UR(M)
      N=2*M-1-KSHIFT
      IF (CODE(M).LT.0.)       GO TO 390
      IF (CODE(M).EQ.0.)       GO TO 400
      IF (CODE(M).EQ.1.)       GO TO 370
      IF (CODE(M).EQ.2.)       GO TO 390
      IF (CODE(M).EQ.3.)       GO TO 380
  370 CALL MODIFY(A,B,ND2,MBAND,N,U)
      GO TO 400
  380 CALL MODIFY(A,B,ND2,MBAND,N,U)
  390 U=UZ(M)
      N=N+1
      CALL MODIFY(A,B,ND2,MBAND,N,U)
  400 CONTINUE
C
C**** WRITE BLOCK OF EQUATIONS ON TAPE AND SHIFT UP LOWER BLOCK
C
      WRITE (2) (B(N),(A(N,M),M=1,MBAND),N=1,ND)
C
      DO 420 N=1,ND
      K=N+ND
      B(N)=B(K)
      B(K)=0.0
      DO 420 M=1,ND
      A(N,M)=A(K,M)
  420 A(K,M)=0.0
C
C**** CHECK FOR LAST BLOCK
C
      IF (NM.LT.NUMNP)         GO TO 60
      IF (STOP.NE.0.)          CALL EXIT
  500 RETURN
C
 2003 FORMAT (26HONEGATIVE AREA ELEMENT NO. I4)
 2004 FORMAT (29HOBAND WIDTH EXCEEDS ALLOWABLE I4)
 2900 FORMAT (I10,2F15.2)
 3000 FORMAT (1HO 18HNODAL POINT FORCES // 8X 2HNP 5X
     1 10HHORIZONTAL 7X 8HVERTICAL //)
C
      END
```

```
$IBFTC QUADF
      SUBROUTINE QUAD
C
      COMMON NUMNP,NUMEL,NUMMAT,ACELZ,NPP,N,VOL,MTYPE,NXX,NXP,
     1 NL,NT,HED(12),E(3,20),RO(20),R(500),Z(500),UR(500),
     2 UZ(500),CODE(500),SIG(10),NUMLAY,NUMIT
      COMMON /ARG/ RRR(5),ZZZ(5),S(10,10),P(10),TT(4),LM(4),
     1 DD(3,3),HH(6,10),RR(4),ZZ(4),C(4,4),H(6,10),D(6,6),
     2 F(6,10),TP(6),XI(10),EE(4),IX(450,5),STRESS(450,3),
     3 SU(20),NBACK(50),STREG(20),POREPR(450),STRAIN(450,3),
     4 GAMAX(450),BETAI(450)
      COMMON / BANARG / ND,NUMBLK,B(108),A(108,54)
      COMMON /SLP/ CAYO(30),TOPX,TOPY,TOEX,TOEY,N1,N2
C
      I=IX(N,1)
      J=IX(N,2)
      K=IX(N,3)
      L=IX(N,4)
      MTYPE=IX(N,5)
   10 EE(1) = E(1,MTYPE)
      EE(2) = E(2,MTYPE)
C
C**** FORM STRESS-STRAIN RELATIONSHIP
C
      COMM=EE(1)/((1.-2.*EE(2))*(1.+EE(2)))
      C(1,1)=COMM*(1.-EE(2))
      C(1,2)=COMM*EE(2)
      C(2,1)=C(1,2)
      C(2,2)=C(1,1)
      C(4,4)=.5*EE(1)/(1.+EE(2))
C
C**** FORM QUADRILATERAL STIFFNESS MATRIX
C
  151 RRR(5)=(R(I)+R(J)+R(K)+R(L))/4.
      ZZZ(5)=(Z(I)+Z(J)+Z(K)+Z(L))/4.0
      DO 94 M=1,4
      MM=IX(N,M)
   93 RRR(M)=R(MM)
   94 ZZZ(M)=Z(MM)
C
      DO 100 II=1,10
      P(II)=0.0
      DO 95 JJ=1,6
   95 HH(JJ,II)=0.0
      DO 100 JJ=1,10
  100 S(II,JJ)=0.0
C
      IF (K.NE.L)              GO TO 125
      CALL TRISTF(1,2,3)
      RRR(5)=(RRR(1)+RRR(2)+RRR(3))/3.0
      ZZZ(5)=(ZZZ(1)+ZZZ(2)+ZZZ(3))/3.0
       VOL=XI(1)
      GO TO 130
  125 VOL=0.0
      CALL TRISTF(4,1,5)
```

```
      CALL TRISTF(1,2,5)
      CALL TRISTF(2,3,5)
      CALL TRISTF(3,4,5)
C
  131 DO 140 II=1,6
      DO 140 JJ=1,10
  140 HH(II,JJ)=HH(II,JJ)/4.
C
  130 RETURN
 1000 FORMAT (I5,6F10.3,F15.3,F10.3)
C
      END
```

```
$IBFTC TRIST
      SUBROUTINE TRISTF(II,JJ,KK)
C
      COMMON NUMNP,NUMEL,NUMMAT,ACELZ,NPP,N,VOL,MTYPE,NXX,NXP,
     1 NL,NT,HED(12),E(3,20),RO(20),R(500),Z(500),UR(500),
     2 UZ(500),CODE(500),SIG(10),NUMLAY,NUMIT
      COMMON /ARG/ RRR(5),ZZZ(5),S(10,10),P(10),TT(4),LM(4),
     1 DD(3,3),HH(6,10),RR(4),ZZ(4),C(4,4),H(6,10),D(6,6),
     2 F(6,10),TP(6),XI(10),EE(4),IX(450,5),STRESS(450,3),
     3 SU(20),NBACK(50),STREG(20),POREPR(450),STRAIN(450,3),
     4 GAMAX(450),BETAI(450)
      COMMON / BANARG / ND,NUMBLK,B(108),A(108,54)
C
      LM(1)=II
      LM(2)=JJ
      LM(3)=KK
C
      RR(1)=RRR(II)
      RR(2)=RRR(JJ)
      RR(3)=RRR(KK)
      ZZ(1)=ZZZ(II)
      ZZ(2)=ZZZ(JJ)
      ZZ(3)=ZZZ(KK)
C
   85 DO 100 I=1,6
      DO 90 J=1,10
      F(I,J)=0.0
   90 H(I,J)=0.0
      DO 100 J=1,6
  100 D(I,J)=0.0
C
      COMM=RR(2)*(ZZ(3)-ZZ(1))+RR(1)*(ZZ(2)-ZZ(3))+
     1 RR(3)*(ZZ(1)-ZZ(2))
      XI(1)=COMM/2.0
      VOL=VOL+XI(1)
C
      D(2,2)=XI(1)*C(1,1)
      D(2,6)=XI(1)*C(1,2)
      D(3,3)=XI(1)*C(4,4)
      D(3,5)=D(3,3)
      D(5,5)=D(3,3)
      D(6,6)=XI(1)*C(2,2)
C
  108 DO 110 I=1,6
      DO 110 J=I,6
  110 D(J,I)=D(I,J)
C
C**** FORM DISPLACEMENT TRANSFORMATION MATRIX
C
      DD(1,1)=(RR(2)*ZZ(3)-RR(3)*ZZ(2))/COMM
      DD(1,2)=(RR(3)*ZZ(1)-RR(1)*ZZ(3))/COMM
      DD(1,3)=(RR(1)*ZZ(2)-RR(2)*ZZ(1))/COMM
      DD(2,1)=(ZZ(2)-ZZ(3))/COMM
      DD(2,2)=(ZZ(3)-ZZ(1))/COMM
      DD(2,3)=(ZZ(1)-ZZ(2))/COMM
```

```
      DD(3,1)=(RR(3)-RR(2))/COMM
      DD(3,2)=(RR(1)-RR(3))/COMM
      DD(3,3)=(RR(2)-RR(1))/COMM
C
      DO 120 I=1,3
      J=2*LM(I)-1
      H(1,J)=DD(1,I)
      H(2,J)=DD(2,I)
      H(3,J)=DD(3,I)
      H(4,J+1)=DD(1,I)
      H(5,J+1)=DD(2,I)
  120 H(6,J+1)=DD(3,I)
C
C**** FORM ELEMENT STIFFNESS MATRIX
C
      DO 130 J=1,10
      DO 130 K=1,6
      IF (H(K,J).EQ.0.)       GO TO 130
      DO 129 I=1,6
  129 F(I,J)=F(I,J)+D(I,K)*H(K,J)
  130 CONTINUE
C
      DO 140 I=1,10
      DO 140 K=1,6
      IF (H(K,I).EQ.0.)       GO TO 140
      DO 139 J=1,10
  139 S(I,J)=S(I,J)+H(K,I)*F(K,J)
  140 CONTINUE
      IF (ACELZ.NE.1.)        GO TO 400
C
C**** GRAVITY LOADS
C
      COMM  = RO(MTYPE)*XI(1)/3.
      DO 170 I=1,3
      J  = 2*LM(I)-1
  170 P(J+1) = P(J+1)-ACELZ*COMM
C
C**** FORM STRAIN TRANSFORMATION MATRIX
C
  400 DO 410 I=1,6
      DO 410 J=1,10
  410 HH(I,J)=HH(I,J)+H(I,J)
C
      RETURN
C
      END
```

```
$IBFTC MODI
      SUBROUTINE MODIFY(A,B,NEQ,MBAND,N,U)
C
      DIMENSION A(108,54),B(108)
C
      DO 250 M=2,MBAND
      K=N-M+1
      IF (K.LE.0)                GO TO 235
      B(K)=B(K)-A(K,M)*U
      A(K,M)=0.0
  235 K=N+M-1
      IF (NEQ.LT.K)              GO TO 250
      B(K)=B(K)-A(N,M)*U
      A(N,M)=0.0
  250 CONTINUE
      A(N,1)=1.0
      B(N)=U
      RETURN
C
      END
```

```
$IBFTC BANS
      SUBROUTINE BANSOL
C
      COMMON /BANARG/ MM,NUMBLK,B(108),AA(108,54)
      DIMENSION A(54,108)
      EQUIVALENCE (A,AA)
C
      DIMENSION NAB(34)
      NN=54
      NCOUNT = NN*NN
      JUMPA = NCOUNT/460  +  1
      JUMPB = NN/460 + 1
      NTRACK=1
      NL=NN+1
      NH=NN+NN
      REWIND 2
      NB=0
      GO TO 150
C
C**** REDUCE EQUATIONS BY BLOCKS
C
  100 NB=NB+1
      DO 125 N=1,NN
      NM=NN+N
      B(N)=B(NM)
      B(NM)=0.0
      DO 125 M=1,MM
      A(M,N) = A(M,NM)
  125 A(M,NM) = 0.0
C
C**** READ NEXT BLOCK OF EQUATIONS INTO CORE
C
      IF (NUMBLK.EQ.NB)       GO TO 200
  150 READ (2) (B(N),(A(M  ,N), M = 1, MM), N = NL, NH )
      IF (NB.EQ.0)            GO TO 100
C
C**** REDUCE BLOCK OF EQUATIONS
C
  200 DO 300 N=1,NN
      IF ( A(1,N) )                  225,  300,  225
  225 B(N) = B(N) / A(1,N)
      DO 275 L=2,MM
      IF ( A(L,N) )                  230,  275,  230
  230 C = A(L,N) / A(1,N)
      I=N+L-1
      J=0
      DO 250 K=L,MM
      J=J+1
  250 A(J,I) = A(J,I) - C * A(K,N)
      B(I) = B(I) - A(L,N) * B(N)
      A(L,N) = C
  275 CONTINUE
  300 CONTINUE
```

```
C
C**** WRITE BLOCK OF REDUCED EQUATIONS ON DISK
C
      IF (NUMBLK.EQ.NB)       GO TO 400
  375 IF(NCOUNT+NN.GT.(39-MOD(NTRACK,40))*460)
     1  NTRACK=(NTRACK/40)*40+40
      NAB(NB) = NTRACK
      CALL WRDISK ( NTRACK, A, NCOUNT )
      NTRACK = NTRACK + JUMPA
      CALL WRDISK ( NTRACK, B, NN )
      NTRACK = NTRACK + JUMPB
      GO TO 100
C
C**** BACK-SUBSTITUTION
C
  400 DO 450 M=1,NN
      N=NN+1-M
      DO 425 K=2,MM
      L=N+K-1
  425 B(N) = B(N) - A(K,N) * B(L)
      NM=N+NN
      B(NM)=B(N)
  450 A(NB,NM) = B(N)
      NB=NB-1
      IF (NB.EQ.0)            GO TO 500
  475 NTRACK = NAB(NB)
      CALL RDDISK ( NTRACK, A, NCOUNT )
      NTRACK = NTRACK + JUMPA
      CALL RDDISK ( NTRACK, B, NN )
      GO TO 400
C
C**** ORDER UNKNOWNS IN B ARRAY
C
  500 K=0
      DO 600 NB=1,NUMBLK
      DO 600 N=1,NN
      NM=N+NN
      K=K+1
  600 B(K) = A(NB, NM)
C
      RETURN
C
      END
```

```
$IBFTC STRS
      SUBROUTINE STRES
C
      COMMON NUMNP,NUMEL,NUMMAT,ACELZ,NPP,N,VOL,MTYPE,NXX,NXP,
     1 NL,NT,HED(12),E(3,20),RO(20),R(500),Z(500),UR(500),
     2 UZ(500),CODE(500),SIG(10),NUMLAY,NUMIT
      COMMON /ARG/ RRR(5),ZZZ(5),S(10,10),P(10),TT(4),LM(4),
     1 DD(3,3),HH(6,10),RR(4),ZZ(4),C(4,4),H(6,10),D(6,6),
     2 F(6,10),TP(6),XI(10),EE(4),IX(450,5),STRESS(450,3),
     3 SU(20),NBACK(50),STREG(20),POREPR(450),STRAIN(450,3),
     4 GAMAX(450),BETAI(450)
      COMMON /SLP/ CAYO(30),TOPX,TOPY,TOEX,TOEY,N1,N2
      COMMON / BANARG / ND,NUMBLK,B(108),A(108,54)
C
C**** COMPUTE ELEMENT STRESSES
C
      N1 = 2
      MPRINT=0
C
      DO 300 N=1,NUMEL
      MTYPE=IX(N,5)
      IF (MTYPE.EQ.NUMMAT)   GO TO 300
C
      CALL QUAD
C
      DO 120 I=1,4
      II=2*I
      JJ=2*IX(N,I)
      P(II-1)=B(JJ-1)
  120 P(II)=B(JJ)
  122 DO 150 I=1,2
      RR(I)=P(I+8)
      DO 150 K=1,8
  150 RR(I)=RR(I)-S(I+8,K)*P(K)
C
      COMM=S(9,9)*S(10,10)-S(9,10)*S(10,9)
      IF (COMM.EQ.0.)          GO TO 160
      P(9)=(S(10,10)*RR(1)-S(9,10)*RR(2))/COMM
      P(10)=(-S(10,9)*RR(1)+S(9,9)*RR(2))/COMM
C
  160 DO 170 I=1,6
      TP(I)=0.0
      DO 170 K=1,10
  170 TP(I)=TP(I)+HH(I,K)*P(K)
C
      RR(1)=TP(2)
      RR(2)=TP(6)
      RR(3)=0.0
      RR(4)=TP(3)+TP(5)
C
  176 DO 180 I=1,4
      SIG(I)=0.
      DO 180 K=1,4
  180 SIG(I)=SIG(I)-C(I,K)*RR(K)
      SIG(3)=SIG(4)
```

```
      BETAI(N) = .5*ATAN2(2.*SIG(3),SIG(1)-SIG(2))
      BTAI   = 57.296*BETAI(N)
      GAMAX(N) = SQRT ((STRAIN(N,2)+RR(2)-STRAIN(N,1)-
     1 RR(1))**2+(STRAIN(N,3)+RR(4))**2)
C
      IF (NUMIT.LT.NPP)       GO TO 300
C
C**** INCREMENT STRESSES
C
      STRESS(N,1) = STRESS(N,1)+SIG(1)
      STRESS(N,2) = STRESS(N,2)+SIG(2)
      STRESS(N,3) = STRESS(N,3)+SIG(3)
      STRAIN(N,1) = STRAIN(N,1)-RR(1)
      STRAIN(N,2) = STRAIN(N,2)-RR(2)
      STRAIN(N,3) = STRAIN(N,3)-RR(4)
      CC = .5*(STRESS(N,2)+STRESS(N,1))
      BB = .5*(STRESS(N,2)-STRESS(N,1))
      CR=SQRT(BB*BB+ STRESS(N,3)**2)
      SIG(4)=CC+CR
      SIG(5)=CC-CR
      BETA   =.5*ATAN2(STRESS(N,3),-BB)
      SIG(6) = 57.296*BETA
      CC = ABS(BETA)
C
C**** CHECK STRENGTH
C
      IF (CR.LT.STREG(MTYPE))GO TO 190
      MTYPE = NUMMAT-1
      WRITE (6,2003)N
C
  190 CONTINUE
C
  104 IF (MPRINT) 110,105,110
  105 WRITE (6,2000)
      MPRINT=50
  110 MPRINT=MPRINT-1
C
C**** STEP PORE PRESSURE
C
      TOP   = TOEY
      IF (RRR(5).GT.TOEX.AND.RRR(5).LT.TOPX) TOP =TOEY+(RRR(5)
     1 -TOEX)*(TOPY-TOEY)/(TOPX-TOEX)
      IF (RRR(5).GT.TOPX)     TOP =TOPY
      GAMH   = RO(MTYPE)*(TOP-ZZZ(5))
      BETTA = ABS(BETAI(N))
      ABAR=1.08
      BB   = 0.5*(SIG(2)-SIG(1))
      CC   = 0.5*(SIG(2)+SIG(1))
      CRR  = SQRT(BB*BB+SIG(3)**2)
      DSIG3 = CC-CRR
      DPORE = DSIG3+2.*ABAR*CRR
      POREPR(N)=POREPR(N)+DPORE
      RU   = POREPR(N)/GAMH
```

```
C
  305 WRITE (6,2001) N,RRR(5),ZZZ(5),(STRESS(N,I),I=1,3),
     1 (SIG(I),I=4,6),CR,(STRAIN(N,I),I=1,3),GAMAX(N),
     2 (SIG(I),I=1,3),ABAR,DPORE,BTAI,POREPR(N),RU
  300 CONTINUE
C
      N1 = 1
  320 RETURN
C
 2000 FORMAT (7H1EL.NO.  7X 1HX  7X 1HY 4X 8HX-STRESS 3X
     1 8HY-STRESS 3X 9HXY-STRESS 3X 3HMAX 9X 3HMIN 4X 4HBETA
     2 3X 6HRADIUS 25H    EX    EY   GAM  GAMAX/ 27X 6HDELTAX
     3 5X 6HDELTAY 5X 7HDELTAXY 5X 4HABAR 7X 5HDPORE 3X
     4 5HBETAI 2X 6HPOREPR 4X 2HRU /)
 2001 FORMAT (I7,2F8.2,5F11.2,F7.2,F9.2,F7.3,2F6.3,F7.4/ 23X
     2 5F11.2,F7.2,F9.2,F7.3 )
 2003 FORMAT ( 17H FAILED ELEMENT=  I4)
 2004 FORMAT(23X,5F11.2,F7.2,F9.2,F7.3/56X,2F11.2,7X,F9.2,F7.3)
 2005 FORMAT (I7,3F10.3)
C
      END
```

DISTRIBUTION LIST

Address	No. of Copies
Office, Chief of Engineers ATTN: ENGCW-ES Library Washington, D. C. 20315	 4 2
Each Corps of Engineers Division ATTN: Chief, Geology, Soils, and Materials Branch, Engineering Division	 2 ea
Each Corps of Engineers District ATTN: Chief, Foundation and Materials Branch, Engineering Division	 1 ea
Director, Nuclear Cratering Group U. S. Army Corps of Engineers ATTN: NCG-ES Lawrence Radiation Laboratory P. O. Box 808 Livermore, Calif. 94550	2
District Engineer U. S. Army Engineer District, Jacksonville ATTN: SAJGI Jacksonville, Fla. 32201	2
Mr. George E. Bertram 4701 Kenmore Avenue, Apartment 819 Alexandria, Va. 22304	1
Mr. Stanley D. Wilson 1105 North 38th Street Seattle, Wash. 98103	1
Prof. Arthur Casagrande Pierce Hall, Harvard University Cambridge, Mass. 02138	1
Mr. John Lowe III Tippetts-Abbett-McCarthy-Stratton 375 Park Avenue New York, N. Y. 10022	1
Prof. Ralph B. Peck Department of Civil Engineering, University of Illinois Urbana, Ill. 61801	1

Address	No. of Copies
Prof. Steve J. Poulos Pierce Hall, Harvard University Cambridge, Mass. 02138	1
Prof. Ronald C. Hirschfield Room 1-330 Massachusetts Institute of Technology Cambridge, Mass. 02139	1
Prof. H. Bolton Seed Department of Civil Engineering, University of California Berkeley, Calif. 94720	1
Prof. James Michael Duncan Department of Civil Engineering, University of California Berkeley, Calif. 94720	25
Defense Documentation Center ATTN: Mr. Meyer Kahn Cameron Station Alexandria, Va. 22314	20

Unclassified

Security Classification

DOCUMENT CONTROL DATA - R & D

(Security classification of title, body of abstract and indexing annotation must be entered when the overall report is classified)

1. ORIGINATING ACTIVITY (Corporate author)	2a. REPORT SECURITY CLASSIFICATION
College of Engineering, Office of Research Services University of California Berkeley, California	Unclassified
	2b. GROUP

3. REPORT TITLE

FINITE ELEMENT ANALYSES OF SLOPES IN SOIL

4. DESCRIPTIVE NOTES (Type of report and inclusive dates)

Final report

5. AUTHOR(S) (First name, middle initial, last name)

Peter Dunlop
James M. Duncan
H. Bolton Seed

6. REPORT DATE	7a. TOTAL NO. OF PAGES	7b. NO. OF REFS
May 1968	226	48

8a. CONTRACT OR GRANT NO.	9a. ORIGINATOR'S REPORT NUMBER(S)
DA-22-079-CIVENG-62-47	
b. PROJECT NO.	TE 68-3
c.	9b. OTHER REPORT NO(S) (Any other numbers that may be assigned this report) U. S. Army Engineer Waterways Experiment Station Contract Report S-68-6
d.	

10. DISTRIBUTION STATEMENT

This document has been approved for public release and sale; its distribution is unlimited.

11. SUPPLEMENTARY NOTES	12. SPONSORING MILITARY ACTIVITY
Prepared under Contract for U. S. Army Engineer Waterways Experiment Station, CE, Vicksburg, Miss.	Office, Chief of Engineers U. S. Army

13. ABSTRACT The study described in this report was conducted to investigate the behavior of excavated slopes and embankments using the finite element method of analysis. The aspects of slope behavior considered include stresses, strains, displacements, pore pressures, and progressive development of failure zones. Analyses have been performed using nonlinear stress-strain characteristics as well as linear elastic stress-strain behavior. A method has been developed for simulating analytically the excavation of a slope in a clay layer with arbitrary initial stress conditions. Analyses performed using this procedure have shown that the behavior of an excavated slope depends on the initial horizontal stresses in the soil layer and the variation of strength with depth. Analyses performed using initial stresses and strength profiles representative of normally consolidated clays indicate behavior which is compatible with the results of short-term ($\phi = 0$) stability analyses; the failure zones determined strongly suggest development of a curved surface of sliding, and the factors of safety calculated by the $\phi = 0$ method were close to unity at the final stage of the analysis when the failure zone encompassed a large zone between the crest and the toe of the slope. Similar analyses performed using initial stresses and strength profiles representative of overconsolidated clays indicated quite different behavior; failure zones developed which intersected the bottom of the excavations and the lower portions of the slopes while the factors of safety were still about 2. These failure zones did not resemble the usual curved failure surfaces used in equilibrium analyses of slope stability, but instead suggest the development of the condition of "loss of ground" wherein the soil in the bottom of the excavation bulges up slowly as additional soil is excavated. Detailed consideration was given to the stress-strain characteristics of soft, (Continued)

DD FORM 1 NOV 65 1473 REPLACES DD FORM 1473, 1 JAN 64, WHICH IS OBSOLETE FOR ARMY USE.

Unclassified

Security Classification

Unclassified

Security Classification

14. KEY WORDS	LINK A		LINK B		LINK C	
	ROLE	WT	ROLE	WT	ROLE	WT
Embankments						
Finite element method						
Slopes						

13. ABSTRACT (Continued)
saturated clays under undrained loading conditions. Using the results of horizontal and vertical plane strain tests on San Francisco Bay Mud, an empirical stress-strain relationship was developed for this material. The relationship developed was nonlinear, anisotropic, and dependent on the consolidation pressure. In spite of its complexity, the relationship can be represented in a reasonably simple form and could be conveniently employed in finite element analyses. Using this relationship, analyses were performed to predict the behavior of San Francisco Bay Mud under simple shear loading conditions, and the predicted behavior was found to agree quite well with experimental results. Analyses were performed to calculate pore pressures around excavated slopes and in embankment foundations using a variety of possible assumptions regarding the stress-strain behavior and the pore pressure coefficients of clay soils. The most significant factor affecting the calculated distributions were found to be anisotropy with respect to both stress-strain behavior and development of pore-water pressures. Using the finite element method it is possible to include realistic soil properties in analyses of slope performance. Nonlinear, anisotropic stress-strain relationships and anisotropic pore pressure coefficients may be incorporated in analyses in a logical and straight-forward manner, providing a means of making more accurate evaluations of stress distribution and pore pressure distributions in soil masses.

Unclassified

Security Classification